National Library of Canada
Canadian Theses Service
Ottawa, Canada
K1A 0N4

Bibliothèque nationale du Canada
Services des thèses canadiennes

CANADIAN THESES

THÈSES CANADIENNES

NOTICE

The quality of this microfiche is heavily dependent upon the quality of the original thesis submitted for microfilming. Every effort has been made to ensure the highest quality of reproduction possible.

If pages are missing, contact the university which granted the degree.

Some pages may have indistinct print especially if the original pages were typed with a poor typewriter ribbon or if the university sent us an inferior photocopy.

Previously copyrighted materials (journal articles, published tests, etc.) are not filmed.

Reproduction in full or in part of this film is governed by the Canadian Copyright Act, R.S.C. 1970, c. C-30. Please read the authorization forms which accompany this thesis.

AVIS

La qualité de cette microfiche dépend grandement de la qualité de la thèse soumise au microfilmage. Nous avons tout fait pour assurer une qualité supérieure de reproduction.

S'il manque des pages, veuillez communiquer avec l'université qui a conféré le grade.

La qualité d'impression de certaines pages peut laisser à désirer, surtout si les pages originales ont été dactylographiées à l'aide d'un ruban usé ou si l'université nous a fait parvenir une photocopie de qualité inférieure.

Les documents qui font déjà l'objet d'un droit d'auteur (articles de revue, examens publiés, etc.) ne sont pas microfilmés.

La reproduction, même partielle, de ce microfilm est soumise à la Loi canadienne sur le droit d'auteur, SRC 1970, c. C-30. Veuillez prendre connaissance des formules d'autorisation qui accompagnent cette thèse.

THIS DISSERTATION
HAS BEEN MICROFILMED
EXACTLY AS RECEIVED

LA THÈSE A ÉTÉ
MICROFILMÉE TELLE QUE
NOUS L'AVONS REÇUE

NL 339 (r. 86/01)

Canada

52

0-315-23250-1

National Library of Canada | Bibliothèque nationale du Canada

Canadian Theses Division | Division des thèses canadiennes

Ottawa, Canada
K1A 0N4

PERMISSION TO MICROFILM — AUTORISATION DE MICROFILMER

• Please print or type — Ecrire en lettres moulées ou dactylographier

Full Name of Author — Nom complet de l'auteur

SHANTHINI WALGAMA

Date of Birth — Date de naissance	Country of Birth — Lieu de naissance
23 Feb. 1957	SRI LANKA

Permanent Address — Residence fixe

F-2, Gaverment Flats
Colombo-4, SRI LANKA

Title of Thesis — Titre de la these

BIFURCATION PHENOMENA OF GENERALIZED NEWTONIAN FLUIDS IN CURVED RECTANGULAR DUCTS

University — Université

University of ALBERTA

Degree for which thesis was presented — Grade pour lequel cette these fut presentee

M Sc. in Chemical Engineering

Year this degree conferred — Annee d'obtention de ce grade	Name of Supervisor — Nom du directeur de thèse
1985	Dr. K. NANDAKUMAR

Permission is hereby granted to the NATIONAL LIBRARY OF CANADA to microfilm this thesis and to lend or sell copies of the film.

The author reserves other publication rights, and neither the thesis nor extensive extracts from it may be printed or otherwise reproduced without the author's written permission.

L'autorisation est, par la présente, accordée à la BIBLIOTHÈQUE NATIONALE DU CANADA de microfilmer cette thèse et de prêter ou de vendre des exemplaires du film.

L'auteur se réserve les autres droits de publication; ni la thèse ni de longs extraits de celle-ci ne doivent être imprimés ou autrement reproduits sans l'autorisation écrite de l'auteur.

Date	Signature
~~Aug 02' 85~~ Aug 02' 85	R Shanthini

NL-91 (4/77)

THE UNIVERSITY OF ALBERTA

Bifurcation Phenomena of Generalized Newtonian Fluids in Curved Rectangular Ducts

by

(C) Shanthini Walgama

A THESIS

SUBMITTED TO THE FACULTY OF GRADUATE STUDIES AND RESEARCH

IN PARTIAL FULFILMENT OF THE REQUIREMENTS FOR THE DEGREE

OF Master of Science

Chemical Engineering

EDMONTON, ALBERTA

FALL 1985

THE UNIVERSITY OF ALBERTA

RELEASE FORM

NAME OF AUTHOR Shanthini Walgama

TITLE OF THESIS Bifurcation Phenomena of Generalized Newtonian Fluids in Curved Rectangular Ducts

DEGREE FOR WHICH THESIS WAS PRESENTED Master of Science

YEAR THIS DEGREE GRANTED FALL 1985

Permission is hereby granted to THE UNIVERSITY OF ALBERTA LIBRARY to reproduce single copies of this thesis and to lend or sell such copies for private, scholarly or scientific research purposes only.

The author reserves other publication rights, and neither the thesis nor extensive extracts from it may be printed or otherwise reproduced without the author's written permission.

(SIGNED) ...S. Shanthini...

PERMANENT ADDRESS:

...F2...Govt...Flats.

...Colombo 4.....

...SRI LANKA.....

DATED ...August 22....1985

THE UNIVERSITY OF ALBERTA

FACULTY OF GRADUATE STUDIES AND RESEARCH

The undersigned certify that they have read, and recommend to the Faculty of Graduate Studies and Research, for acceptance, a thesis entitled Bifurcation Phenomena of Generalized Newtonian Fluids in Curved Rectangular Ducts submitted by Shanthini Walgama in partial fulfilment of the requirements for the degree of Master of Science.

.....

Supervisor

.....

.....

.....

Date.....

ABSTRACT

The bifurcation phenomenon in flow through curved rectangular pipe is investigated in this study. The non-linear equations of motion governing the steady, fully developed laminar flow of an incompressible generalized Newtonian fluid were solved numerically over a wide range of parameters. Extensive results have been generated in an effort to map the regions of multiple solution in the parameter space of Dean number, Dn, aspect ratio, γ, power-law index, n, and radius of curvature, r. For a Newtonian fluid (n=1), at a fixed curvature (r=100), the transition between symmetric 2 and 4 vortex solutions appears to follow a tilted cusp. The extent of the stable symmetric 2-cell solution surface is critically influenced by the length scale γ. The repetitive nature of the state locus at almost regular intervals of γ might serve as a key to the understanding of the stability characteristics of curved flow. In the non-Newtonian case, at a fixed aspect ratio (γ=1) and a fixed curvature (r=100), the flow transition follows that of a fold catastrophe. The influence of the curvature is reasonably well accounted for in Dn. The bifurcation set determined in the Dn-γ space remains qualitatively the same at any value of n or r. These parameters merely shift and/or stretch the equilibrium surface determined by Dn and γ.

TABLE OF CONTENTS

CHAPTER		PAGE
1.	INTRODUCTION	1
2.	BACKGROUND	3
	2.1 Early Recognition and Explanation of Curved Flows	3
	2.2 Newtonian Fluids	5
	2.2.1 Circular Cross-section	5
	2.2.2 Non-Circular Cross-sections	7
	2.3 Dual Solutions	12
	2.4 Stability of Multiple Solutions	13
	2.5 Non-Newtonian Fluids	21
	2.5.1 Behaviour and Modelling	21
	2.5.2 Available Literature	24
3.	PROBLEM FORMULATION AND SOLUTION	28
	3.1 Governing Equations	28
	3.2 Finite Difference Formulation	44
	3.3 Method and Accuracy of the Numerical Solution	54
	3.3.1 Method of Solution	55
	3.3.2 Accuracy of Solution	58
4.	RESULTS AND DISCUSSION PART I - NEWTONIAN FLUIDS	74
	4.1 Influence of the Centrifugal Force	75
	4.2 End Effects on the Flow	81
	4.3 Modelling	100
	4.4 Curvature Effects	110
5.	RESULTS AND DISCUSSION PART II - POWER-LAW FLUIDS	114

5.1 Dual Solutions.....115

5.1.1 Influence of the Centrifugal Force ... 115

5.1.2 Influence of the Power-Law Index n ... 121

5.2 Modelling 121

5.3 Curvature Effects 129

5.4 The Frictional Resistance 129

6. CONCLUSIONS 141

BIBLIOGRAPHY..... 143

APPENDIX A. The source code of the computer program . 152

APPENDIX B. The numerical results for Newtonian Fluids 165

APPENDIX C. The numerical results for power-law fluids 187

LIST OF TABLES

Table	Description	Page
2.1	Friction factor correlations for Newtonian fluids in curved rectangular pipes	9
2.2	Friction factor correlations for power-law fluids in curved circular pipes	26
3.1	The f-Re results for Newtonian fluids in straight rectangular pipes and comparison with the results of Shah & London(1978)	59
3.2	The f-Re results for power-law fluids in straight square pipes and comparison with the available results	60
3.3	Comparison of the f-Re results for curved square pipes of different curvatures with Cheng et al.(1976)	68
3.4	Comparison of the f-Re results for curved pipes of γ=2.0, 5.0 & 0.5 with Cheng et al.(1976)	69
4.1	The critical Dn for Newtonian fluids at r=100	105
4.2	The critical Dn for Newtonian fluids in square pipes at different curvatures	113
5.1	The critical Dn for power-law fluids in square pipes of r=100	128

LIST OF FIGURES

Figure		Page
2.1	The tilted cusp-catastrophe representing the 2-4 cell transition in the bounded Taylor problem	15
2.2	The five characteristic properties of the cusp-catastrophe model	17
2.3	The experimentally determined bifurcation set in Re-γ space for 2-4 cell transition in bounded Taylor problem	18
2.4	The state loci corresponding to Figure 2.3	19
3.1	Geometry and Coordinate systems	29
3.2	Numerical grid used	45
3.3	Axial velocity distribution at y=0 for power-law fluids in straight square pipe	62
3.4a	Dimensionless viscosity profile for power-law fluids in straight square pipe at y=0.0 and y=0.025	63
3.4b	Dimensionless viscosity profile for power-law fluids in straight square pipe at y=0.5 and y=0.475	64
3.5	The 3-dimensional profiles of the viscosity of a power-law fluid across the entire cross-sectional plane of a square pipe	66
3.6	Friction factor results for Newtonian fluids in square pipes compared with available results	67
3.7a	Axial velocity distribution at y=0, compared with the experimental results of Mori et al.(1971)	71
3.7b	Axial Velocity distribution at x=0, compared with the experimental results of Mori et al.(1971)	72
3.8	The contours of ψ and w of a Newtonian fluid in a square pipe of r=10	73

4.1a Contour plots showing the 2-vortex flow at different Dn for γ=1 & r=100 76

4.1b Contour plots showing the 4-vortex flow at different Dn for γ=1 & r=100 77

4.2 u at y=0 for n=1, γ=1 & r=100 78

4.3 u at x=0.4 & y=0 for n=1, γ=1 & r=100 80

4.4 Friction factor results for n=1, γ=1 & r=100 82

4.5a Contour plots showing the distribution of ψ in 2-vortex flows at different γ 83

4.5b Contour plots showing the flow area occupied by the additional vortices at different γ 84

4.6 The Dn_{4-2} locus at n=1 & r=100 86

4.7 The Dn_{2-4} locus at n=1 & r=100 87

4.8a The discontinuity in the Δp_{2-4} locus at n=1 & r=100 89

4.8b The discontinuity in the Dn_{2-4} locus at n=1 & r=100 90

4.9a Friction factor results for n=1, γ=1.35 & r=100 92

4.9b u at x=0.4 & y=0 for n=1, γ=1.35 & r=100 93

4.10 u at x=0.4 & y=0 at various aspect ratios for n=1 & r=100 95

4.10 continued 96

4.10 continued 97

4.10 continued 98

4.11 The loci of limit points at n=1 and r=100 101

4.12 The state loci at different γ for n=1 & r=100 103

4.13 The extent of the stable 2-cell solution surface 107

4.14 u at x=0.4 & y=0 for γ=2.4 & γ=3.0 at r=100 109

4.15 Friction factor results for square pipes of r=100, 10 & 4 with n=1 111

4.16 u at x=0.4 & y=0 for square pipes of r=100, 10 & 4 with n=1 112

5.1a Contour plots showing the 2-vortex flow at different Dn for n=0.7, γ=1 & r=100 116

5.1b Contour plots showing the 4-vortex flow at different Dn for n=0.7, γ=1 & r=100 117

5.2 Axial Velocity distribution at y=0 for n=0.7, γ=1 & r=100 118

5.3 u at y=0 for n=0.7, γ=1 & r=100 119

5.4 u at x=0.3 & y=0 for n=0.7, γ=1 & r=100 120

5.5 Contour plots showing the flow area occupied by the additional vortices dt different n 122

5.5 continued 123

5.6 u at x=0.3 & y=0 for various n at γ=1 & r=100 124

5.6 continued 125

5.7a The loci of limit points in the Δp-n plane at γ=1 & r=100 126

5.7b The loci of limit points in Dn-n plane at γ=1 & r=100 127

5.8 Friction factor results for n=0.7 & γ=1 at r=100, 10 & 4 130

5.9 u at x=0.4 & y=0 for n=0.7 & γ=1 at r=100, 10 & 4 131

5.10 The mean axial velocity of power-law fluids under the influence of imposed pressure gradient in square pipes of r=100 132

5.11 Friction factor results for power-law fluids in square pipes of r=100 134

5.12a The dimensionless viscosity profile at the line of symmetry (y=0) 135

5.12b The dimensionless viscosity profile at the top wall (y=0.5) 136

5.12c The dimensionless viscosity profile at the inner wall (x=-0.5) 137

5.12d The dimensionless viscosity profile at the outer wall (x=0.5) 138

NOMENCLATURE

a	the width of the rectangular cross-section (Figure 3.1) or the spacing between two concentric cylinders
b	the height of the rectangular cross-section (Figure 3.1)
C	the parameter defined by Equation 3.51
$\underline{\underline{D}}$	the dimensionless rate of strain tensor (Equations 3.21 & 3.30)
$\underline{\underline{D}}'$	the rate of strain tensor (Equations 3.11 & 3.13)
D_{kl}	the components of the dimensionless rate of strain tensor.
D'_{kl}	the components of the rate of strain tensor
De	the equivalent hydraulic diameter (Equation 3.47)
Dn	the Dean number (Equation 3.52)
Dn^{+}	the modified Dean number (Equation 3.53)
Dn_{2-4}	the critical Dean number at which the 2-vortex solution jump to the 4-vortex solution
Dn_{4-2}	the critical Dean number at which the 4-vortex solution jump to the 2-vortex solution
$\underline{\underline{F}}$	the dimensionless stress tensor (Equations 3.20 & 3.29)
$\underline{\underline{F}}'$	the stress tensor (Equation 3.10)
F_{kl}	the components of the dimensionless stress tensor
F'_{kl}	the components of the stress tensor
$\bar{F}_{kl}$	a dimensionless quantity defined by Equations 3.31 & 3.34
$\langle F_{wall} \rangle$	the average stress experienced by the fluid at the pipe wall (Equations 3.39 & 3.44)
f	the friction factor (Equation 3.38)
f_1	the friction factor f evaluated from a macroscopic force balance (Equations 3.40 & 3.41)

f_2	the friction factor f evaluated from the axial velocity gradients at the wall (Equation 3.45)
f-Re	the product of friction factor and Reynolds number, represented by f_1-Re in the discussion
K	the consistency constant (Equation 3.14)
M	the dimensionless viscosity (Equations 3.19 & 3.37)
NX	the number of grid points in X-direction (Figure 3.2)
NY	the number of grid points in Y-direction (Figure 3.2)
n	the power-law index (Equation 3.14)
P	the pressure
p	the dimensionless pressure (Equation 3.18)
pgrad	Δp
R	the radius of curvature of the pipe (Figure 3.1)
r	the dimensionless radius of curvature of the pipe (Equation 3.16)
R_1	the radius of the inner cylinder
Re	the Reynolds number (Equations 3.46, 3.48 & 3.49)
Re^+	the modified Reynolds number (Equation 3.50)
U,V,W	the velocity components in X, Y & θ directions, respectively (Figure 3.1)
u,v,w	the dimensionless velocity components in X', Y & θ directions, respectively (Equation 3.17)
$\underline{V}$	the local velocity vector of the flow having U, V & W as the components
X',Y',Z'	the Cartesian coordinates (Figure 3.1)
X,Y	the toroidal rectangular coordinates along the cross-sectional plane (Figure 3.1)
x,y	the dimensionless toroidal rectangular coordinates along the cross-sectional plane(Equation 3.16)

Greek symbols

β the friction factor ratio

$$= \frac{f\text{-}Re_c}{f\text{-}Re_s} = \frac{f\text{-}Re^+_c}{f\text{-}Re^+_s} = \frac{Q_s}{Q_c} = \frac{\langle W \rangle_s}{\langle W \rangle_c}$$

β_1 (f_1-Re) in curved pipe/(f_1-Re) in straight pipe

β_2 (f_2-Re) in curved pipe/(f_2-Re) in straight pipe

γ the aspect ratio b/a

δ a small difference

θ one of the toroidal rectangular coordinates (Figure 3.1)

μ the apparent viscosity(Equation 3.14)

μ_o the reference viscosity (Equation 3.36)

ρ the density

ψ the dimensionless stream function (Equations 3.22 & 3.23)

Ω the dimensionless vorticity function (Equation 3.24)

χ the dummy variable used in Equation 3.54

Special symbols

%df the percentage difference between f_1-Re and f_2-Re defined as

$$[\{f_1\text{-}Re - f_2\text{-}Re\}/f_1\text{-}Re]*100$$

$\%df^+$ replace Re by Re^+ in the definition of %df

$\%d\beta$ the percentage difference between β_1 and β_2 defined as

$$[\{\beta_1 - \beta_2\}/\beta_1]*100$$

$\Delta x, \Delta y$ the grid sizes in X & Y directions, respectively (Figure 3.2 & Equations 3.56a & b)

$\Delta x^2, \Delta y^2$ squares of Δx & Δy, respectively (Equations 3.56a & b)

Δp	the dimensionless pressure gradient in θ direction, $(-\partial p/\partial \theta)$
$< >$	denotes mean values
$_$	denotes vectors
$=$	denotes tensors
∇	the 'Del' operator

Subscripts

c,s	values referring to the curved and straight pipe, respectively
i,j	the space subscripts of a grid point in X & Y directions, respectively
k,l	the dummy indices referring a particular component in a tensor, which take x,y or θ
x,y,θ	the indices used to refer a tensor component in terms of the toroidal rectangular coordinates X, Y & θ

CHAPTER 1

INTRODUCTION

Curved sections arise in numerous piping systems. Curved configurations such as helical coils and spiral coils are frequently used in heat exchangers, chemical reactors, rocket engines and other geometries requiring a large area to volume ratio.

The special features of curvature-induced flow when compared to the Poiseuille flow can be summarized as follows:

- Increased flow resistance
- Delayed onset of turbulence
- Increased residence time distribution of a fluid element
- Better circulation of the fluid along the cross-sectional plane of the pipe even in the absence of external mixing agents

The consequences are interesting. Increased flow resistance results in higher pumping power. Increased residence time is a favourable feature in some continuous chemical

reactors. Better circulation of the fluid results in enhanced mass and heat transfer. Therefore a knowledge of the magnitude of these effects is important in designing curved configurations. Hence this type of flow has been the subject of extensive research for more than a century. Yet certain intricate features of these flows are beginning to be understood only in the last decade (Masliyah 1980, Dennis and Ng 1982, Nandakumar and Masliyah 1982).

Steady, fully developed, incompressible, laminar flow of generalized Newtonian fluids in curved pipes of rectangular cross-section under imposed constant axial pressure gradient is examined in this study.

The equations governing the curved flow are highly non-linear under high flow conditions, because of the presence of intense secondary flow. Non-unique solutions are possible for non-linear problems. Catastrophical changes in the stability of the flow seem to be inherent to hydrodynamic problems with external body forces (Benjamin 1976,1978a,b,c). An attempt is made in this study, to map the surface of stable solutions and thereby to be able to identify this particular hydrodynamic stability problem with the existing models in Catastrophe theory (Zeeman 1977). This theory deals with the shapes of all possible equilibrium surfaces for processes where smooth and continuous changes in behaviour do not always exist.

CHAPTER 2

BACKGROUND

2.1 Early Recognition and Explanation of Curved Flows

Thompson(1876) first examined the influence of the centrifugal force field on the flow in curved geometry in an attempt to understand the behaviour of the flow in river bends. Williams et al.(1902) observed that the location of the maximum axial velocity was shifted towards the outer wall of curved circular pipe. Eustice(1910,1911,1925) observed that for a given pressure gradient, the volumetric flow of water through a curved pipe was less than that of a straight pipe of equal length. His flow visualization experiments in curved pipes of both circular and rectangular cross-sections demonstrated the flow to be helical in nature and not parabolic as in straight pipes.

The axial velocity component in a pipe flow, often generated by an imposed pressure gradient, keeps changing its direction as it passes through a curved pipe. Hence the flow is subjected to the influence of the centrifugal force field, which increases with increasing axial velocity component of the flow and with increasing curvature of the coiled pipe. Under the condition of a non-uniform axial velocity distribution, the centrifugal forces acting on the

fluid particles within the cross-section of the pipe are clearly of different magnitudes. As a result a pressure gradient develops across the plane perpendicular to the flow direction (sometimes known as the diametrical pressure drop) in order to balance the centrifugal force. The pressure is the greatest at the outer wall and the least at the inner wall. Because of the the frictional resistances at the pipe boundaries, the viscous flow near the top and the bottom of the wall is slower than that in the central core. Hence the diametrical pressure gradient required to balance the centrifugal force is smaller at the upper and the lower walls than at the midplane. Consequently a secondary flow occurs in which the fluid near the central core moves outwards and the fluid near the top and the bottom walls moves inwards, towards the center of the curvature. Superimposing the secondary velocity vector on the axial velocity, one can construct the image of the velocity field as a double helix, symmetrically placed about the horizontal plane.

Because of the presence of the diametrical pressure gradient, a greater axial pressure gradient would be required to pump the same amount of fluid in a curved pipe when compared to a straight pipe. It results in increased flow resistance. In viscous flow through straight pipe, the inertial forces should overcome the viscous forces in order to enter turbulence region. In case of a curved pipe, viscous forces as well as the centrifugal forces should be

overcome for the flow to become turbulent. Hence the onset of turbulence is delayed with the increasing strength of the curvature induced secondary flow.

2.2 Newtonian Fluids

2.2.1 Circular Cross-section

Dean(1927,1928a), for the first time, theoretically analyzed the viscous flow of a Newtonian fluid through a curved pipe of circular cross-section, using the method of successive approximation. He assumed that the radius of curvature of the pipe is large in comparison with the radius of cross-section of the pipe. This is known as the loose coiling approximation. Successive approximation is based on a perturbation expansion of the solution about Poiseuille flow and hence is valid only when the effect of the centrifugal force field is small. The remarkable contribution of his work is the introduction of a parameter, a combination of Reynolds number and the radius of curvature of the pipe, which accounts for the centrifugal force experienced by the fluid. This parameter is now known as the Dean number, although several definitions of this quantity are in current use. The Dean number, Dn, used in this study is defined by Equation 3.52. Dean's original work was later expanded by Topakoglu(1967), Larrain and Bonila(1970), Sankaraiah and Rao(1973) and Van Dyke(1978).

Adler(1934) used helical coils of different curvature and measured the axial velocity field very precisely for both laminar and turbulent flows. After obtaining experimental data on the nature of the flow in the central core, Adler analyzed the laminar flow in curved pipes at large values of Dean number by making use of the Prantl boundary layer theory. This analysis divides the flow into two parts; an inviscid core where only centrifugal forces and pressure forces are considered to be dominant and a thin boundary layer close to the wall where viscous forces are dominant. Barua(1963), Mori and Nakayama(1965), Itō(1969) and Nunge and Lin(1973) analyzed the curved flow using the above approach. Hawthorne(1951) and Detra(1953) analyzed the curved flow using inviscid fluid theory over the entire flow domain.

McConalogue and Srivastava(1968) reduced the governing partial differential equations to ordinary differential equations and solved the resulting equations numerically. Their solution is valid for loosely coiled pipes in the intermediate range of Dean numbers. Truesdell and Adler(1970) employed a finite difference technique to solve the governing partial differential equations. They introduced a stream function in terms of the secondary velocity components. Their analysis is valid over a broader range of Dean numbers. Akiyama and Cheng(1971) introduced a vorticity function in the governing equations and thereby assured faster convergence. Greenspan(1973), Austin and

Seader(1973), Collins and Dennis(1975) and Dennis(1980) studied the various aspects of the numerical solutions of the curved flow. Manlapaz and Churchill(1980) numerically analyzed the effect of the pitch on the curved flow.

Grindly and Gibson(1908), White(1929), Taylor(1929), Kerlegan and Berj(1937), Ito(1959,1969), Kubair and Varrier(1961/62), Srinivasan et al.(1970) and Mishra and Gupta(1979a) carried out extensive experimental studies on the nature of the flow in helical pipes. The resistance law proposed by White is still in use. The delayed appearance of turbulence was clearly demonstrated by Taylor. The effects of pitch was studied in detail by Mishra and Gupta.

2.2.2 Non-Circular Cross-sections

Square and elliptic cross-sections, possessing low degree of geometric symmetry, were theoretically analyzed first by Ito(1951), using perturbation analysis. His solution described the familiar double-helical motion. The series analysis of Cuming(1952) showed the secondary flow in square section was more intense than the secondary flow in circular section. Dean and Hurst(1959) analyzed the flow in curved pipes of rectangular and circular cross-sections by replacing the actual secondary flow by a uniform stream. Masliyah and Nandakumar(1979) numerically analyzed the flow in semicircular cross-section having the curved surface as the outer wall. Pipes of triangular cross-section were

analyzed by Collins and Dennis(1976a,b). Tabbarrok and Lin(1978) introduced a simple triangular finite element as an alternative to the inflexibility of the mesh in the finite difference scheme. They were able to solve the flow equations for any arbitrary cross-section.

Ludwieg(1951) studied the laminar flow in a curved square pipe using the boundary layer approach. The theoretical correlations of Mori et al.(1971) well bracketed the experimental data of Ludwieg for stationary square pipe of r=5.67, up to about Dn=3000. Beyond this, turbulence was observed to occur. These correlations, given in Table 2.1, were obtained from the first and second approximations of the boundary layer approximation method and valid for large Dean numbers only. The experimental friction factor correlation (see Table 2.1) proposed by Baylis(1971) is valid for curved square pipes of r=17.5 in the range $500<Dn<2000$.

Cheng and Akiyama(1970) numerically analyzed the flow in a rectangular section using a finite difference method. At sufficiently high Dean numbers, they observed the secondary flow pattern changing from the regular two vortices (or cells) to four vortices without destroying the symmetry. The additional two vortices were located near the central part of the outer wall. The numerical studies of Joseph et al.(1925) and Cheng et al.(1976) also showed the abrupt transition from 2-cell flow to 4-cell flow around

Table 2.1 Friction factor correlations for flow of Newtonian fluids in curved pipes of rectangular cross-sections.

1. Cheng and Akiyama(1970)

numerical

$$\beta = 0.225\ Dn^{0.39}$$

$100<Dn<1500$

for square pipes

2. Baylis(1971)

experimental

$$\beta = 0.107\ \sqrt{Dn}$$

$500<Dn<2000$

$r=17.5$

for square pipes

3. Mori et al.(1971)

theoretical

$$\beta = 0.09378\ \sqrt{Dn}$$ (First Approximation)

$$\beta = \frac{0.09378\ \sqrt{Dn}}{[1 - (7.126/\sqrt{Dn})]}$$ (Second Approximation)

large Dn

for square pipes

Table 2.1(Contd.)

4. Cheng et al.(1976)

numerical

$$\beta = C_0 \, Dn^{0.5} \left[1 + \frac{C_1}{Dn^{0.5}} + \frac{C_2}{Dn} + \frac{C_3}{Dn^{1.5}} + \frac{C_4}{Dn^2} \right]$$

where

γ	C_0	C_1	C_2	C_3	C_4
0.5	0.0880	4.832	-16.36	178.6	-273.9
1	0.1278	-0.257	0.669	187.7	-512.2
2	0.2188	-23.06	281.6	-1974.0	2046.0
5	0.0915	-4.592	80.9	-138.3	0

Dn≅150 in curved square pipes. Both these analyses reported the additional vortices to be smaller than the normal vortices, but equally as strong in terms of velocities. The experiments of Joseph et al.(1975) and Cheng et al.(1977) confirmed the existence of the 4-vortex flow in rectangular pipes.

The axial velocity component of the double helical flow in curved pipe increases and then decreases towards the outer concave wall, giving rise to a centrifugal force field whose intensity is lesser at the outer wall than at the region away from the outer wall. Consequently, centrifugal instability can develop in the region closer to the outer wall (Drazin and Reid 1981). This may be the reason for the birth of these additional cells.

The symmetric nature of the predicted 4-cell flow can be clearly seen in the photographs of Cheng et al.(1977). Such patterns were observed at Dn=176.1 and at 305.2 in a pipe of γ=1 and at Dn=164.3 and 258.3 in a pipe of γ=2. Both these pipes were of r=5. The flow pattern was found to become complex when Dn was increased further. However the numerical study of Cheng et al.(1976) revealed the reappearance of the symmetric 2-cell flow at Dn=520 for a square pipe of r=4.

2.3 Dual Solutions

Masliyah(1980) numerically and experimentally established the stable existence of *both* 2-vortex and 4-vortex flows beyond a critical Dean number in curved semicircular pipes with flat outer wall.

Dennis and Ng(1982) and Nandakumar and Masliyah(1982) observed this dual pattern in curved circular pipes using different numerical schemes. Nandakumar and Masliyah gradually changed the semicircular section having flat outer wall, through several moon shaped configurations, a full circle and finally to a semicircle with curved outer wall. Dual solutions were observed in all cases, revealing the fact that the shape of the outer wall does not play a crucial role in determining the type of solution even though it is easier to obtain the 4-vortex solution when the outer surface is nearly flat.

The existence of the symmetric 4-vortex solutions in circular and semicircular sections was confirmed by the flow visualization experiments of Masliyah(1980) and Cheng et al.(1983). However, at high Dean numbers, a secondary vortex oscillation with loss of symmetry was observed in both these works. Cheng et al. suggested that it may be due to the imperfect geometrical shape.

Dual solutions to curved flow problems are not surprising because the equations describing the flow are

non-linear. The regions of the stable existence of a particular solution for the flow in curved rectangular pipes are the focus of the present study.

2.4 Stability of Multiple Solutions

Dean(1928b) analyzed the streaming tangential pressure-driven flow in the annulus of two infinitely long concentric cylinders (now known as the Dean problem), using the linear stability analysis. This analysis is based on introducing the slightly perturbed basic solution into the flow equations and then analyzing the behaviour of the solution of the linearised disturbed flow equations. He simplified this analysis by assuming a, the spacing between the cylinders, is very small when compared to R_1, the radius of the inner cylinder. He showed that when the parameter $Re\sqrt{a/R_1}$ exceeds 36, the streaming tangential flow becomes unstable. This instability gives rise to a stable cellular laminar flow. This type of analysis was first carried out by Taylor(1923). He studied the stability of the flow in a similar geometry but the flow was driven by rotating the inner cylinder where the outer cylinder was held stationary (now known as the Taylor problem). Taylor also arrived at similar stability characteristics. The Dean problem was also studied by Yih and Sangster(1957) and Reid(1958). Sparrow(1964) extended the earlier analysis by relaxing the restriction on the spacing between the cylinders.

In the above mentioned linear stability analysis, the primary flow is two dimensional because of the infinite extent of fluid in all but one direction. An extension of this analysis to a three dimensional primary flow, such as the double helical motion of the fluid in curved pipe of *finite* cross-section, is difficult since the components of velocities of the stream line motion are coefficients in the differential equations of the disturbed flow. Hence the study of stability of the flow in curved pipes had remained untouched.

An attempt is made in this study to analyze the existence of dual solutions in bounded Dean problem and their relative stability using the elementary models of Catastrophe theory (Zeeman 1977) as tools. The advantage of these tools lie in the fact that a satisfactory account of the exact problem can be obtained with or without solving the problem in the full domain of interest.

Benjamin(1978b) experimentally analyzed the transition between 2-cell and 4-cell modes arising in the Taylor problem in a short annulus. He showed that this transition is controlled by the Reynolds number, Re, and the aspect ratio, γ, and can be described by the "cusp-catastrophe" model shown in Figure 2.1 (not drawn to scale). This model results when *a state* of a process is controlled by *two* conflicting parameters. The charecteristic properties of the cusp-catastrophe model are illustarated by the simplest

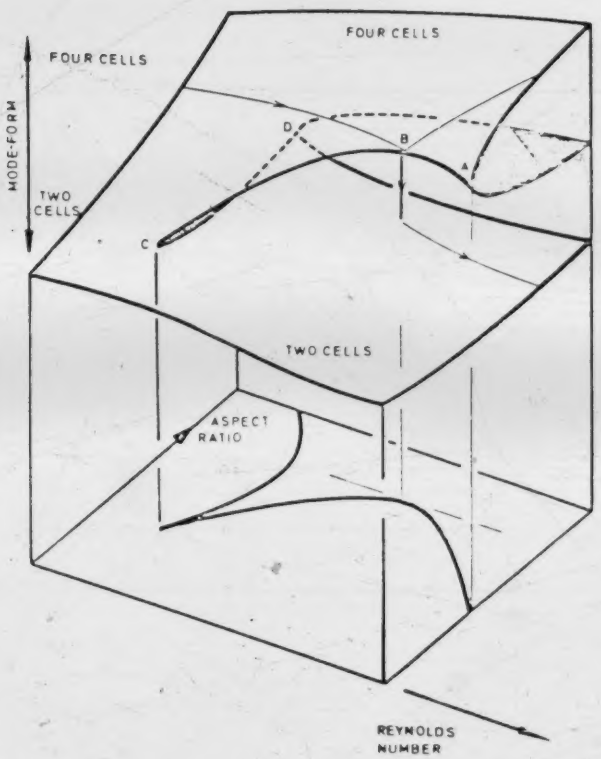

Fig. 2.1 The tilted cusp–catastrophe representing the transition between 2–vortex and 4–vortex modes in the bounded Taylor problem (not drawn to scale).

form of this model in Figure 2.2. In the words of Zeeman(1977), the state is always *bimodal* in some range, and *catastropic jumps* are observed between one mode of state and the other. The jump from the top sheet (in Figure 2.2) to the bottom sheet does not take place at the same position as the jump from the bottom sheet to the top one, an effect called *hysteresis*. Between the top and bottom sheets there is an *inaccessible zone* on the state axis. In the vicinity of the cusp point, *divergence* of the state is possible. These features can also be observed in the tilted cusp of Figure 2.1. The upper surface of Figure 2.1 corresponds to the stable 4-cell solution and the lower surface to the stable 2-cell solution. The middle surface, corresponding to the unstable solution of the flow equations, is inaccessible in reality. This tilted cusp is completely analogous to that suggested by Zeeman(1977) in developmental biology.

Since the interest of the present study is the transition between 2-cell and 4-cell, though in a slightly different system, it is useful to take a closer look at the cusp located by Benjamin(1978b). The projection of this cusp model on the Re-γ control space is reproduced in Figure 2.3. The successive developments of the state loci are given in (a) through (e) of Figure 2.4. The solid curves of these state loci represent the stable solutions and the dotted curves represent the unstable solutions. Below

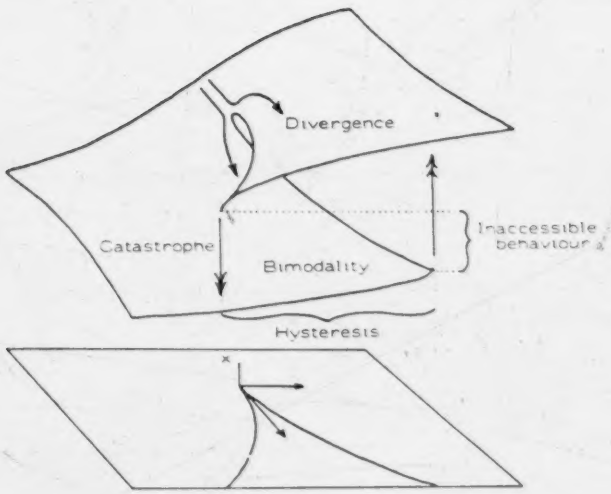

Fig. 2.2 The five characteristic properties of the cusp-catastrophe model.

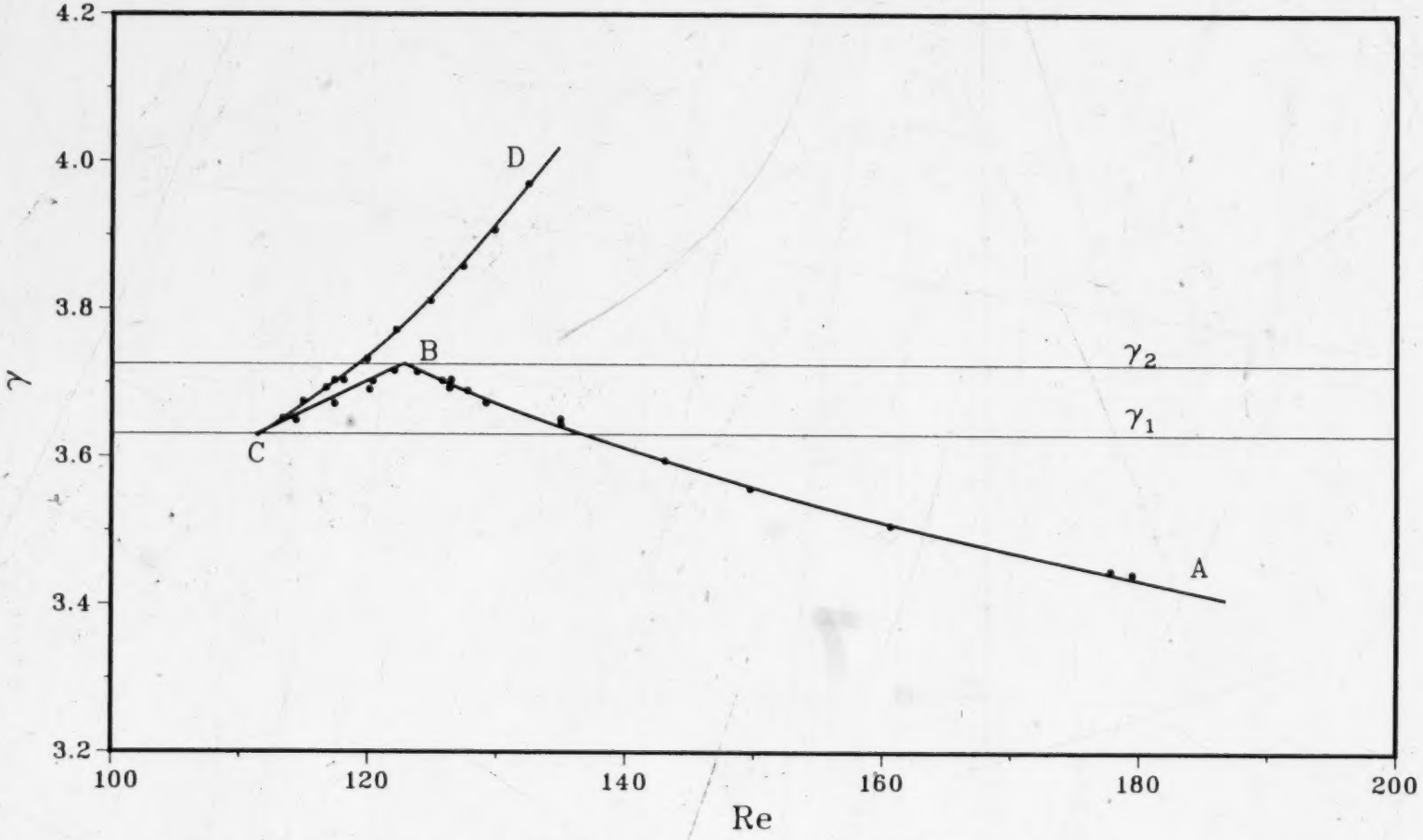

Fig. 2.3 The experimentally determined (Benjamin (1978b)) bifurcation set in the Re–γ space for the 2–4 vortex transition in the bounded Taylor problem.

(a) $\gamma < \gamma_1$

(b) $\gamma = \gamma_1$

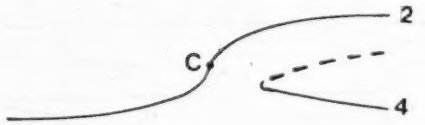

One-sided bifurcation

(c) $\gamma_1 < \gamma < \gamma_2$

(d) $\gamma = \gamma_2 = 3.72$

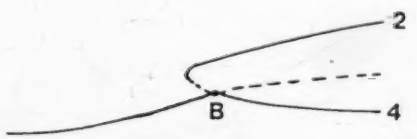

Transcritical bifurcation

(e) $\gamma > \gamma_2$

Fig. 2.4 The state loci corresponding to Figure 2.3.

level γ_1, the primary mode is 2-cell flow. Above level γ_2, the primary mode is 4-cell flow. Within level γ_1 and γ_2, a 2-cell flow with embryonic 4-cell feature is evolved continuously up to the curve CB (Figure 2.3), at which the abrupt transition to a clear 2-cell structure takes place. In this region the primary locus is folded showing hysteresis (Figure 2.4(c)). The primary mode mutuates at point B (Figure 2.3) via transcritical bifurcation (Figure 2.4(d)). The cusp point C (Figure 2.3) is given by the one sided bifurcation (Figure 2.4(b)) which predominates as a practical possibility requiring in general no special symmetry for its existence. Benjamin(1976,1978a,b,c) has pointed out that the idealized Taylor problem can be represented by the supercritical bifurcation whose symmetry is necessarily destroyed in the real world of experimental situations. Mullin(1982) experimentally analyzed the crucial role of the end effects on the flow in bounded Taylor problem. He recognized that the tilted cusp can also well account for the 4-6, 6-8, 8-10 and 10-12 cell transitions. Even though the direction of the tilt of these cusps cannot be predicted beforehand, the orientation of all these cusps towards the γ-axis is not surprising since divergence of the flow behaviour is observable in the region of low Re with changing γ.

Nandakumar et al.(1985) investigated a related problem of instability in buoyancy induced flow in a straight rectangular pipe. The range of aspect ratios of interest,

distributed around $\gamma=1$, was much lower than the range considered by either Benjamin or Mullin, where the minimum γ was greater than 3. The orientation of the cusp predicted by Nandakumar et al. is very different from those discussed earlier for good reasons. The results of the present study, discussed in Chapter 4, are somewhat similar to that of Nandakumar et al.

The analysis of Winters and Brindly(1984) using finite element method is another work which is closely related to the present study. Because of the similarity between both of these studies, their results will be critically discussed in Chapter 4.

2.5 Non-Newtonian Fluids

2.5.1 Behaviour and Modelling

Newtonian fluids exhibit a direct proportionality between the shear stress and the shear rate. The proportionality constant, known as viscosity, is a function of temperature and pressure only; and is independent of shear rate. There are a number of fluids, frequently encountered in processing industries and elsewhere, that behave quite differently. The differences in behaviour are not merely of a small quantitative nature; they are major qualitative ones.

Shear rate dependent viscosity and normal stresses are characteristic features of non-Newtonian fluids. Interestingly some of them exhibit memory effects. The purely viscous fluids with almost no memory effects are classified into two major categories; pseudoplastic fluids and dilatant fluids. The apparent viscosity of pseudoplastic fluids decreases with increasing shear rate. Consequently the pressure gradient required to generate a certain volumetric flow is lower than that of the corresponding Newtonian fluid; this is known as shear thinning. Dilatant fluids exhibit the opposite phenomenon, shear thickening. Almost all polymer melts and solutions that exhibit a shear rate dependent viscosity are pseudoplastic. Fairly concentrated suspensions of very small particles are dilatant. Secondary flows of pseudoplastic and dilatant fluids in finite curved geometry are analyzed in this study.

The stress ($\underline{\underline{F}}'$) of a purely viscous incompressible fluid is a function only of the instantaneous rate of strain ($\underline{\underline{D}}'$) and can be modelled as follows (Bird et al. 1977):

$$\underline{\underline{F}}' = \phi_1 \underline{\underline{D}}' + \phi_2 (\underline{\underline{D}}' . \underline{\underline{D}}') \qquad (2.1)$$

where ϕ_1 and ϕ_2 are functions of two of the three principal invariants of $\underline{\underline{D}}'$.

The above model, known as the Reiner-Rivlin model, suffers from the basic deficiency of not modelling the first normal

stress difference.

The power-law model of Ostwald and de Waele is a special case of the Reiner-Rivlin model and can be written as

$$\underline{\underline{F}}' = \phi_1 \underline{\underline{D}}' \qquad (2.2)$$

where $\phi_2 = 0$ and ϕ_1 , sometimes known as apparent viscosity μ , is defined as (Bird et al. 1977)

$$\phi_1 = \mu \equiv K \{(D'_{kl}:D'_{kl})/2\}^{(n-1)/2} \qquad (2.3)$$

The consistency constant, K, and the power-law index, n, are the two adjustable parameters. Despite its inability to account for normal stress differences, elastic effects and memory effects, power-law model is the most widely used model in non-Newtonian fluid mechanics. It is appealing for its simplicity. Calculations of flow rates and shearing forces in steady state shear flows are best done using the power-law model. Having an empirical basis, it provides no limiting values on the apparent viscosity, μ, at small and large values of shear rates. Hence the ability of the power-law model to describe the stress-strain relationship of a real fluid over a wide stress range is limited. Further discussion on its applicability is given in Subsection 2.5.2 and in Section 3.1.

The Caireau model (Bird et al. 1977) provides limiting values on the apparent viscosity but it involves four

adjustable parameters. The Ellis model (Bird et al. 1977) has three adjustable parameters. These and several other models, listed in Bird et al.(1977) and Skelland(1967), are best used for specific applications.

2.5.2 Available Literature

Following the work of Dean(1927,1928a), Jones(1960) theoretically analyzed the laminar flow of a visco-inelastic fluid in a loosely coiled circular pipe using successive approximation. Jones solution described the familiar double helical motion. He used the Reiner-Rivlin model in his analysis.

Mashelkar and Devarajan(1976a) analyzed the laminar flow of a power-law fluid using the boundary layer approach. The friction factor correlation proposed (given in Table 2.2) in this work is in good agreement with their subsequent experimental results(1976b).

The experiments of Rajasekaran et al.(1964,1966) and Mashelkar and Devarajan(1977) revealed the delay in onset of turbulence with increasing curvature and decreasing power-law index. The dependence of friction factor and heat transfer coefficient on the curvature and the power-law index was verified in the experiments of Rajasekaran et al.(1970a,b) and Gupta and Mishra(1975) (see Table 2.2).

The experimental results of Mujawar and Rao(1978) are in satisfactory agreement with the predicted correlation of Mashelkar and Devarajan(1976a); 20 to 30% lower than the values predicted by the correlation of Gupta and Mishra(1975); and in fairly large disagreement with the results of Rajasekaran et al.(1970b). Mujawar and Rao introduced a new dimensionless number as given in Table 2.2. Mishra and Gupta(1979b) represented their experimental friction factor results by defining a Reynolds number in terms of a pseudo shear viscosity (see Table 2.2).

Hsu and Patankar(1982) analyzed the curved flow of power-law fluids using a finite difference technique. The friction factor results obtained in this study are valid over a wider range of Dean numbers and are in good agreement with the correlations of Meshalkar and Devarajan(1976a) and Mujawar and Rao(1978). The analysis of Hsu and Patankar is best applied to curved pipes of $r>5$, since they neglect the secondary velocity gradients in the expression for apparent viscosity.

The present study is, in a way, extending the analysis of Hsu and Patankar to curved pipes of square cross-section. Since the secondary velocities are taken into account in expressing the apparent viscosity, this analysis is claimed to be valid even for a highly curved pipe.

Table 2.2 Friction factor correlations for flow of power-law fluids in curved pipes of circular cross-section.

1. Rajesekaran et al.(1970b)

experimental

$$\beta = 1.23\left[Dn_1\right]^{0.3}$$

where

$$Dn_1 = \frac{\rho\, a^n \langle w\rangle^{2-n}}{K\, 8^{n-1}} \sqrt{a/2R}$$

2. Gupta and Mishra(1975)

experimental

$$\beta = 0.288\ \left[Dn_1\right]^{0.675}$$

3. Mashelkar and Devarajan(1976a)

theoretical

$$f = [9.069-9.438n+4.374n^2]\ [\sqrt{a/2R}]\ [Dn_1]^{(0.122n-0.768)}$$

$70 \le Dn_1 \le 400$

$3.7 \le (R/a) \le 50$

$0.35 \le n \le 1$

Table 2.2(contd.)

4. Mujawar and Rao(1978)

experimental

$$f = 16 / M$$

where

$$M = \frac{\rho\, a^{nc} \langle W \rangle^{2-nc}}{Kc\ 8^{nc-1}} \left[\frac{2R}{a}\right]^{mc}$$

$$Kc = 3.13530 \times 10^{-6} + 4.10459 \times 10^{-1}\ Ks - 4.00427 \times 10\ Ks^2 + 9.55172 \times 10^{4}\ Ks^3$$

$$\frac{2-nc}{2-ns} = 1.515 - 0.875\ ns$$

$$mc = 0.4375\ ns - 0.2575$$

ns and Ks refers to the n and K obtained from a straight pipe flow.

5. Mishra and Gupta(1979b)

experimental

$$\frac{f}{f_s} = 1 + 0.033 \left[\log Dn_2\right]^4$$

where

$$f_s = 16 / Re_2$$

$$Dn_2 = Re_2 \sqrt{a/2R}$$

$$Re_2 = \rho a \langle W \rangle / \mu_2$$

$$\mu_2 = K_2 \left[\langle F \rangle_{wall} / K_2\right]^{(n-1)/n}$$

$$K_2 = K \left[(3n+1)/4n\right]^n$$

CHAPTER 3

PROBLEM FORMULATION AND SOLUTION

3.1 Governing Equations

Steady, fully developed laminar flow of an incompressible generalized Newtonian fluid through a uniformly curved pipe of rectangular cross-section is theoretically analyzed in this study. The toroidal rectangular coordinate system (X,Y,θ) shown in Figure 3.1, is best suited for this geometry. The flow is solely driven by a constant pressure gradient imposed along the axial direction of the torus.

The continuity equation and the stress equations of motion describing the flow were initially written in Cartesian coordinates (X',Y',Z') and were then transformed to toroidal rectangular coordinates (X,Y,θ). These two orthogonal coordinate systems are related to each other as given by the equations below:

$$X' = (R+X)\cos\theta \tag{3.1}$$

$$Y' = Y \tag{3.2}$$

$$Z' = (R+X)\sin\theta \tag{3.3}$$

The above mentioned coordinate transformation was carried out using the metrical coefficients 1, 1 and $1/(R+X)$ respectively. The resulting equations are as follows:

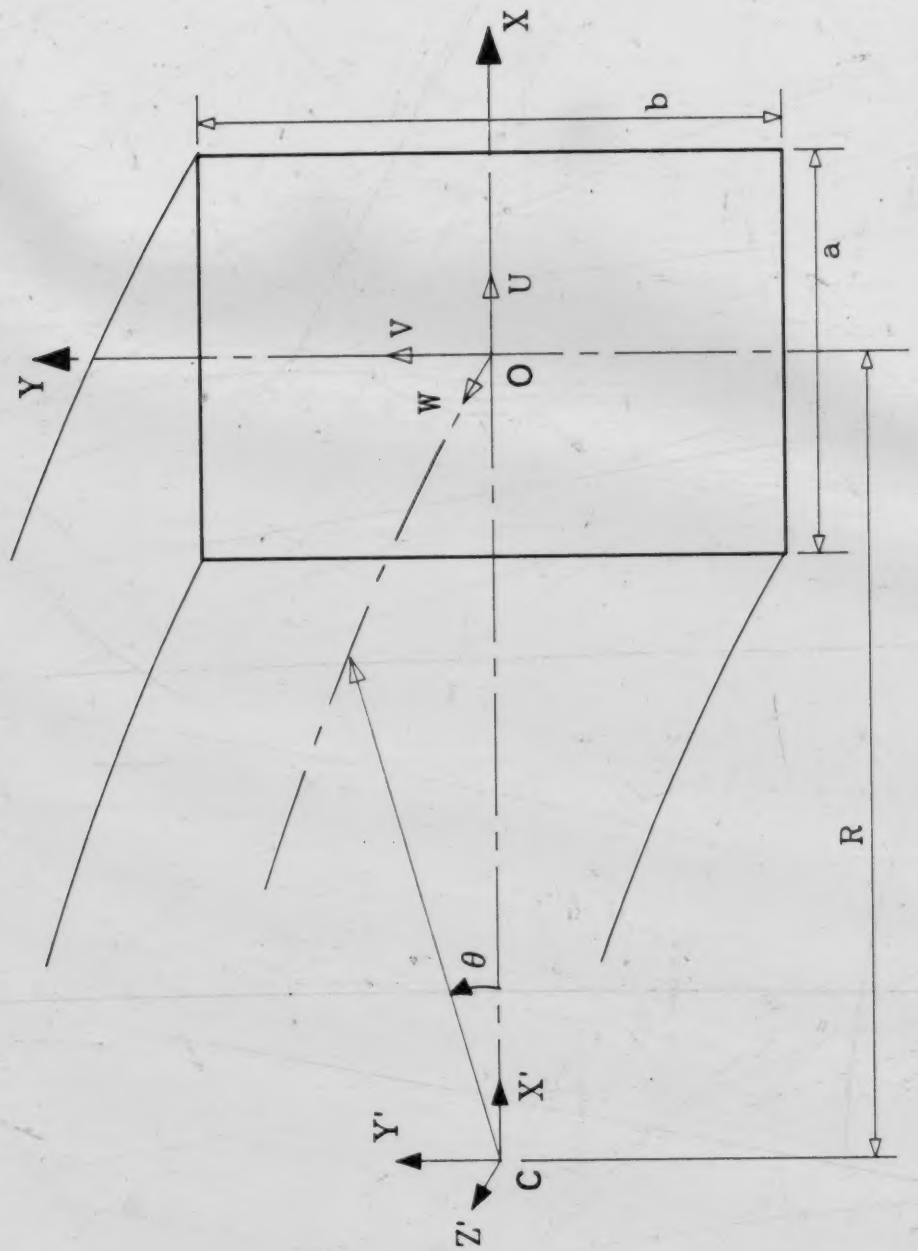

Fig. 3.1 Geometry and Coordinate Systems

the continuity equation,

$$\frac{\partial U}{\partial X} + \frac{\partial V}{\partial Y} + \frac{U}{R+X} = 0 \tag{3.4}$$

the stress equation in X-direction,

$$U \frac{\partial U}{\partial X} + V \frac{\partial U}{\partial Y} - \frac{W^2}{R+X} = -\frac{1}{\rho}\frac{\partial P}{\partial X} + \frac{1}{\rho}\left[\frac{\partial F'_{xx}}{\partial X} + \frac{\partial F'_{xy}}{\partial Y} + \frac{F'_{xx}}{R+X} - \frac{F'_{\theta\theta}}{R+X} \right] \tag{3.5}$$

the stress equation in Y-direction,

$$U \frac{\partial V}{\partial X} + V \frac{\partial V}{\partial Y} = -\frac{1}{\rho}\frac{\partial P}{\partial Y} + \frac{1}{\rho}\left[\frac{\partial F'_{xy}}{\partial X} + \frac{\partial F'_{yy}}{\partial Y} + \frac{F'_{xy}}{R+X} \right] \tag{3.6}$$

the stress equation in θ-direction,

$$U \frac{\partial W}{\partial X} + V \frac{\partial W}{\partial Y} + \frac{UW}{R+X} = -\frac{1}{\rho}\frac{1}{R+X}\frac{\partial P}{\partial \theta} + \frac{1}{\rho}\left[\frac{\partial F'_{x\theta}}{\partial X} + \frac{\partial F'_{y\theta}}{\partial Y} + 2\frac{F'_{x\theta}}{R+X} \right] \tag{3.7}$$

with the following boundary conditions:

imposing no-slip condition at the wall,

$$U = V = W = 0 \tag{3.8}$$

and symmetry along the horizontal center line (Y=0).

$$V = \frac{\partial U}{\partial Y} = \frac{\partial W}{\partial Y} = 0 \tag{3.9}$$

The stress Tensor $\underline{\underline{F}}'$ and the apparent viscosity μ

The Ostwald-de Waele power-law model, expressed by Equations 2.2 and 2.3, is used in this study to describe the relation between the stress tensor $\underline{\underline{F}}'$ and the rate of strain tensor $\underline{\underline{D}}'$.

$$\underline{\underline{F}}' = \mu \, \underline{\underline{D}}' \tag{3.10}$$

where $\underline{\underline{D}}'$ is given by,

$$\underline{\underline{D}}' = \left[(\nabla \underline{V}) + (\nabla \underline{V})^T \right] \tag{3.11}$$

The dyadic product $\nabla \underline{V}$, in the toroidal rectangular coordinate system, under fully developed conditions, can be expressed as follows:

$$\nabla \underline{V} = \begin{bmatrix} \frac{\partial U}{\partial X} & \frac{\partial V}{\partial X} & \frac{\partial W}{\partial X} \\ \frac{\partial U}{\partial Y} & \frac{\partial V}{\partial Y} & \frac{\partial W}{\partial Y} \\ \frac{-W}{R+X} & 0 & \frac{U}{R+X} \end{bmatrix} \tag{3.12}$$

Therefore the rate of strain tensor $\underline{\underline{D}}'$ is as follows:

$$\underline{\underline{D}}' = \begin{bmatrix} 2\frac{\partial U}{\partial X} & \frac{\partial V}{\partial X}+\frac{\partial U}{\partial Y} & \frac{\partial W}{\partial X}-\frac{W}{R+X} \\ \frac{\partial V}{\partial X}+\frac{\partial U}{\partial Y} & 2\frac{\partial V}{\partial Y} & \frac{\partial W}{\partial Y} \\ \frac{\partial W}{\partial X}-\frac{W}{R+X} & \frac{\partial W}{\partial Y} & 2\frac{U}{R+X} \end{bmatrix} \tag{3.13}$$

It can be seen that the rate of strain tensor $\underline{\underline{D}}'$ is symmetric and it gives rise to the symmetric stress tensor $\underline{\underline{F}}'$. The components of these tensors will be referred to as D'_{kl} and F'_{kl}, respectively, in the following discussion, where k and l take x,y, or θ.

The apparent viscosity μ defined by Equation 2.3 is

$$\mu = K \left[(D'_{kl}:D'_{kl})/2\right]^{(n-1)/2} \qquad (3.14)$$

Equation 3.14 can be expanded as:

$$\mu = K \left[(D'^{2}_{xx} + D'^{2}_{yy} + D'^{2}_{\theta\theta} + 2\,D'^{2}_{xy} + 2\,D'^{2}_{x\theta} + 2\,D'^{2}_{y\theta}) / 2\right]^{(n-1)/2} \qquad (3.15)$$

D'_{kl} are expressed in terms of appropriate velocity gradients in Equation 3.13.

As discussed in Subsection 2.5.1, the power-law model has a serious theoretical defect of predicting infinitely large and vanishingly small values of μ. However it has been proven to be adequate to describe the double helical flow in curved circular pipe by Hsu and Patankar(1982) and several others(see Subsection 2.5.2 for details). Wheeler and Wissler(1965) used the power-law model to describe the flow through a straight pipe of rectangular cross-section. They obtained good agreement between the calculated and

measured values of friction factors. Careful experimental observations of Wheeler and Wissler revealed no secondary flow in straight square pipe. Secondary flow can develop in a straight pipe as a result of normal stresses which the power-law model is incapable of modelling. No experimental study of non-Newtonian fluid flow through curved pipes of rectangular cross-section has been reported to the author's knowledge.

Dimensionless Variables

For the sake of generality, the variables are non-dimensionalized using the following scheme:

Coordinates and radius of curvature,

$$x = \frac{X}{a} \quad , \quad y = \frac{Y}{a} \quad , \quad r = \frac{R}{a} \tag{3.16}$$

velocity components,

$$u = \frac{a\rho U}{\mu_o} \quad , \quad v = \frac{a\rho V}{\mu_o} \quad , \quad w = \frac{a\rho W}{\mu_o} \tag{3.17}$$

pressure,

$$p = \frac{a^2 \rho P}{\mu_o^2} \tag{3.18}$$

viscosity,

$$M = \frac{\mu}{\mu_o} \tag{3.19}$$

It follows from the primary scaling that the stress

components and the rate of strain components can be scaled as follows:

$$F_{kl} = F'_{kl} \frac{a^2\rho}{\mu_o^2} \tag{3.20}$$

$$D_{kl} = D'_{kl} \frac{a^2\rho}{\mu_o} \tag{3.21}$$

It is also convenient to express the dimensionless secondary velocity components, u and v, in terms of a dimensionless stream function ψ as

$$u = \frac{1}{r+x} \frac{\partial\psi}{\partial y} \tag{3.22}$$

$$v = - \frac{1}{r+x} \frac{\partial\psi}{\partial x} \tag{3.23}$$

The pressure terms are conveniently eliminated from the secondary flow Equations 3.5 and 3.6 by introducing a dimensionless vorticity function Ω defined as

$$\Omega = \frac{\partial v}{\partial x} - \frac{\partial u}{\partial y} \tag{3.24}$$

The governing equations of the flow (3.4 through 3.7) can be rewritten in dimensionless form as follows:

stream function-vorticity equation,

$$\frac{\partial^2\psi}{\partial x^2} + \frac{\partial^2\psi}{\partial y^2} - \frac{1}{r+x} \frac{\partial\psi}{\partial x} = - (r+x)\Omega \tag{3.25}$$

vorticity transport equation,

$$u \frac{\partial \Omega}{\partial x} + v \frac{\partial \Omega}{\partial y} - \frac{u\Omega}{r+x} + \frac{2w}{r+x} \frac{\partial w}{\partial y}$$

$$= \frac{\partial^2 F_{xy}}{\partial x^2} - \frac{\partial^2 F_{xy}}{\partial y^2} - \frac{\partial^2 F_{xx}}{\partial x \partial y} + \frac{\partial^2 F_{yy}}{\partial x \partial y} - \frac{F_{xy}}{(r+x)^2}$$

$$+ \frac{1}{r+x} \frac{\partial F_{xy}}{\partial x} - \frac{1}{r+x} \frac{\partial F_{xx}}{\partial y} + \frac{1}{r+x} \frac{\partial F_{\theta\theta}}{\partial y} \qquad (3.26)$$

axial momentum equation,

$$u \frac{\partial w}{\partial x} + v \frac{\partial w}{\partial y} + \frac{uw}{r+x}$$

$$= - \frac{1}{r+x} \frac{\partial p}{\partial \theta} + \frac{\partial F_{x\theta}}{\partial x} + \frac{\partial F_{y\theta}}{\partial y} + 2 \frac{F_{x\theta}}{r+x} \qquad (3.27)$$

where u and v are defined by Equations 3.22 and 3.23, respectively.

The boundary conditions (Equations 3.8 and 3.9) are restated as:

at all the walls,

$$\psi = w = u = v = 0 \qquad (3.28a)$$

at the top wall,

$$\Omega = - \frac{1}{r+x} \frac{\partial^2 \psi}{\partial y^2} \qquad (3.28b)$$

at the inner wall,

$$\Omega = -\frac{1}{r-0.5}\frac{\partial^2\psi}{\partial x^2} \tag{3.28c}$$

at the outer wall,

$$\Omega = -\frac{1}{r+0.5}\frac{\partial^2\psi}{\partial x^2} \tag{3.28d}$$

and at y=0 (line of symmetry).

$$\psi = \Omega = \frac{\partial w}{\partial y} = v = \frac{\partial u}{\partial y} = 0 \tag{3.28e}$$

The stress-strain relation (Equation 3.10) in dimensionless form is

$$F_{kl} = M\, D_{kl} \tag{3.29}$$

where

$$\underline{D} = \begin{bmatrix} 2\frac{\partial u}{\partial x} & \frac{\partial v}{\partial x}+\frac{\partial u}{\partial y} & \frac{\partial w}{\partial x}-\frac{w}{r+x} \\ \frac{\partial v}{\partial x}+\frac{\partial u}{\partial y} & 2\frac{\partial v}{\partial y} & \frac{\partial w}{\partial y} \\ \frac{\partial w}{\partial x}-\frac{w}{r+x} & \frac{\partial w}{\partial y} & 2\frac{u}{r+x} \end{bmatrix} \tag{3.30}$$

The stream function-vorticity equation (3.25) is in the familiar elliptic form. In order to recover the elliptic nature of the equivalent equations in Newtonian fluid mechanics, the following substitution is made in the vorticity transport equation (3.26) and in the axial momentum equation (3.27) (Davis et al. 1979)

$$F_{kl} = \bar{F}_{kl} + D_{kl} \tag{3.31}$$

Thus, the vorticity transport equation (3.26) becomes

$$u \frac{\partial \Omega}{\partial x} + v \frac{\partial \Omega}{\partial y} - \frac{u\Omega}{r+x}$$

$$= - \frac{2w}{r+x} \frac{\partial w}{\partial y} + \frac{\partial^2 \Omega}{\partial x^2} + \frac{\partial^2 \Omega}{\partial y^2} + \frac{1}{r+x} \frac{\partial \Omega}{\partial x} - \frac{\Omega}{(r+x)^2}$$

$$+ \frac{\partial^2 \bar{F}_{xy}}{\partial x^2} - \frac{\partial^2 \bar{F}_{xy}}{\partial y^2} - \frac{\partial^2 \bar{F}_{xx}}{\partial x \partial y} + \frac{\partial^2 \bar{F}_{yy}}{\partial x \partial y} - \frac{\bar{F}_{xy}}{(r+x)^2}$$

$$+ \frac{1}{r+x} \frac{\partial \bar{F}_{xy}}{\partial x} - \frac{1}{r+x} \frac{\partial \bar{F}_{xx}}{\partial y} + \frac{1}{r+x} \frac{\partial \bar{F}_{\theta\theta}}{\partial y} \tag{3.32}$$

and the axial momentum equation (3.27) becomes

$$u \frac{\partial w}{\partial x} + v \frac{\partial w}{\partial y} + \frac{uw}{r+x}$$

$$= - \frac{1}{r+x} \frac{\partial p}{\partial \theta} + \frac{\partial^2 w}{\partial x^2} + \frac{\partial^2 w}{\partial y^2} + \frac{1}{r+x} \frac{\partial w}{\partial x} - \frac{w}{(r+x)^2}$$

$$+ \frac{\partial \bar{F}_{x\theta}}{\partial x} + \frac{\partial \bar{F}_{y\theta}}{\partial y} + 2 \frac{\bar{F}_{x\theta}}{r+x} \tag{3.33}$$

From Equations 3.29 and 3.31, it can be shown that the new stress component $\bar{F}_{kl}$ can be expressed as,

$$\bar{F}_{kl} = (M-1) D_{kl} \tag{3.34}$$

where, from Equation 3.30, the individual components of the strain tensor are given by,

$$D_{xx} = 2 \frac{\partial u}{\partial x} \tag{3.35a}$$

$$D_{yy} = 2 \frac{\partial v}{\partial y} \tag{3.35b}$$

$$D_{\theta\theta} = 2 \frac{u}{r+x} \tag{3.35c}$$

$$D_{xy} = \frac{\partial v}{\partial x} + \frac{\partial u}{\partial y} \tag{3.35d}$$

$$D_{x\theta} = \frac{\partial w}{\partial x} - \frac{w}{r+x} \tag{3.35e}$$

$$D_{y\theta} = \frac{\partial w}{\partial y} \tag{3.35f}$$

By defining the reference viscosity, μ_o, as

$$\mu_o = K \{<W>/a\}^{(n-1)} \tag{3.36}$$

the dimensionless viscosity,M, can be stated as

$$M = \left[\{D_{xx}^2 + D_{yy}^2 + D_{\theta\theta}^2 + 2 D_{xy}^2 + 2 D_{x\theta}^2 + 2 D_{y\theta}^2\} / \{2 <w>^2\}\right]^{(n-1)/2} \tag{3.37}$$

It can be noted that the governing equations for Newtonian fluid can be easily recovered by setting the power-law index,n, to unity.

Friction Factor

In problems of flow in pipes, it is important to know the relation between the axial pressure drop and the volumetric flow rate. It is accomplished by evaluating the frictional resistance experienced by the flow and thus a friction factor,f, is defined as the ratio of the average

stress experienced by the fluid at the pipe wall, $\langle F_{wall} \rangle$, to the kinetic energy per unit mass of fluid, $\frac{1}{2} \rho \langle W \rangle^2$,

$$f = 2 \langle F_{wall} \rangle / (\rho \langle W \rangle^2) \qquad (3.38)$$

The average stress, $\langle F_{wall} \rangle$, can be evaluated in two different ways as discussed below:

Method 1:

A macroscopic force balance over a volume element of differential axial length, $(R+X)\delta\theta$, in the direction of main flow yields the following expression for $\langle F_{wall} \rangle$.

$$\langle F_{wall} \rangle = - \frac{ab}{2(a+b)} \frac{1}{R} \frac{\partial P}{\partial \theta} \qquad (3.39)$$

Thus the friction factor, denoted by f_1, is,

$$f_1 = - \frac{ab}{a+b} \frac{1}{R} \frac{1}{\rho \langle W \rangle^2} \frac{\partial P}{\partial \theta} \qquad (3.40)$$

In terms of dimensionless variables, f_1 can be expressed as follows

$$f_1 = - \frac{\gamma}{(1+\gamma)} \frac{1}{\langle w \rangle^2} \frac{1}{r} \frac{\partial p}{\partial \theta} \qquad (3.41)$$

f_1 is a measure of the average axial velocity and it is insensitive to the fine details of the axial velocity profile. Hence, any discrepancy in the axial velocity

profile may not be revealed by f_1.

Method 2:

The total force experienced by the fluid at the wall surface of differential axial length $(R+X)\delta\theta$ can be evaluated by considering the wall shear stress, and hence the axial velocity gradients along the pipe wall, as follows (refer figure 3.1):

$$\text{Total Force} = 2\,\delta\theta \int_{-a/2}^{a/2} \left[(R+X)\,\mu\,\left(-\frac{\partial W}{\partial Y}\right)' \right] dX + (R-0.5a)\,\delta\theta \int_{-b/2}^{b/2} \left[\mu\,\left(\frac{\partial W}{\partial X}\right) \right] dY + (R+0.5a)\,\delta\theta \int_{-b/2}^{b/2} \left[\mu\,\left(-\frac{\partial W}{\partial X}\right) \right] dY \qquad (3.42)$$

The area on which this total force acts is given by,

$$\text{Total Area} = 2\,(a+b)\,R\,\delta\theta \qquad (3.43)$$

The average wall stress, $\langle F_{wall} \rangle$, is

$$\langle F_{wall} \rangle = \frac{\text{Total force}}{\text{Total Area}} \qquad (3.44)$$

Thus, the friction factor, denoted by f_2, can be expressed in dimensionless form as follows:

$$f_2 = \frac{2}{r(1+\gamma)\langle w\rangle^2}\left[\int_{-0.5}^{0.5}\left[(r-x)\,M\left(-\frac{\partial w}{\partial y}\right)\right]dx + (r-0.5)\int_{0}^{\gamma/2}\left[M\left(\frac{\partial w}{\partial x}\right)\right]dy + (r+0.5)\int_{0}^{\gamma/2}\left[M\left(-\frac{\partial w}{\partial x}\right)\right]dy\right] \qquad (3.45)$$

The agreement between the numerical values of f_1 and f_2 can be a measure of the accuracy of the axial velocity profile, and hence the accuracy of the solution, as will be discussed in Section 3.3.

Dimensionless groups

Since it is customary to represent the flow behaviour in terms of dimensionless groups, such as Reynolds number and Dean number, appropriate definitions of the dimensionless groups should be searched for. For power-law fluids in straight pipe of circular section, it can be

analytically shown that the product of friction factor and the Reynolds number can be made equal to a constant for any value of power-law index,n, provided the Reynolds number is defined appropriately (see Hsu and Patankar 1982). Pipes with rectangular cross-section, having lesser degree of geometric symmetry than pipes with circular cross-section, cannot be investigated analytically and thus choosing a suitable Reynolds number becomes a difficult task. In this study the Reynolds Number Re is chosen as

$$Re = \rho \, De^{(n)} \, \langle W \rangle^{(2-n)} \, / \, K \qquad (3.46)$$

where the characteristic length scale of the geometry is chosen as the equivalent hydraulic diameter, De, and is defined as,

$$De = \frac{4(ab)}{2(a+b)} = \frac{2a\gamma}{(1+\gamma)} \qquad (3.47)$$

By substituting for the consistancy constant K, from Equation 3.36, Re becomes

$$Re = \left[\frac{2\gamma}{1+\gamma} \right]^{(n)} \frac{\rho a \langle W \rangle}{\mu_o} = \left[\frac{2\gamma}{1+\gamma} \right]^{(n)} \langle w \rangle \qquad (3.48)$$

when the power-law index n is unity, as in the case of Newtonian fluid, the Re defined above takes the following familiar form:

$$Re = \frac{\rho De \langle W \rangle}{\mu_o} = \frac{2\gamma}{(1+\gamma)} \langle w \rangle \qquad (3.49)$$

The above defined Re can be modified as follows

$$Re^+ = Re / C \qquad (3.50)$$

where

$$C = 8^{(n-1)} \left[\frac{1+3n}{4n} \right]^{(n)} \qquad (3.51)$$

The above expression for C can be analytically obtained for pipe with circular section. However introducing C into the definition of Reynolds number for rectangular pipes is found to bring the product of friction factor-Reynolds number for the power-law fluids in straight rectangular pipes closer to the corresponding Newtonion fluid values (as will be seen in Table 3.2).

Having defined the dimensionless groups that account for the flow in a straight pipe, the Dean Number Dn, which represents the centrifugal force field experienced by the fluid, is defined as follows:

$$Dn = Re \sqrt{(a/R)} = Re / \sqrt{r} \qquad (3.52)$$

The modified Dean Number, Dn^+, is,

$$Dn^+ = Re^+ / \sqrt{r} \qquad (3.53)$$

3.2 Finite Difference Formulation

The three elliptic type simultaneous, second-order, partial differential equations (3.25, 3.32 and 3.33) describing the flow, must be solved using a numerical scheme in order to obtain solutions over a wide range of flow parameters. Central difference method is chosen for this purpose. The numerical grid system used is shown in Figure 3.2. The symmetric nature of the flow will be exploited in the solution procedure. Using the 3-point central difference approximation for the derivatives, each of the above mentioned Equation can be transformed into a set of non-linear algebraic equations in the following form.

$$A_1 \chi_{i,j} = A_2 \chi_{i+1,j} + A_3 \chi_{i-1,j} + A_4 \chi_{i,j+1} + A_5 \chi_{i,j-1} + A_6 \qquad (3.54)$$

where $i = 2, 3, 4, \ldots\ldots, (NX-1)$

$j = 2, 3, 4, \ldots\ldots, (NY-1)$

In Equation 3.54, χ is a dummy varaible which stands for ψ, Ω or w, and A_1 to A_6 are the coefficients as expressed below.

For the stream function-vorticity equation (3.25), $\chi = \psi$ and

$$A_1 = \frac{2}{\Delta x^2} + \frac{2}{\Delta y^2} \qquad (3.55a)$$

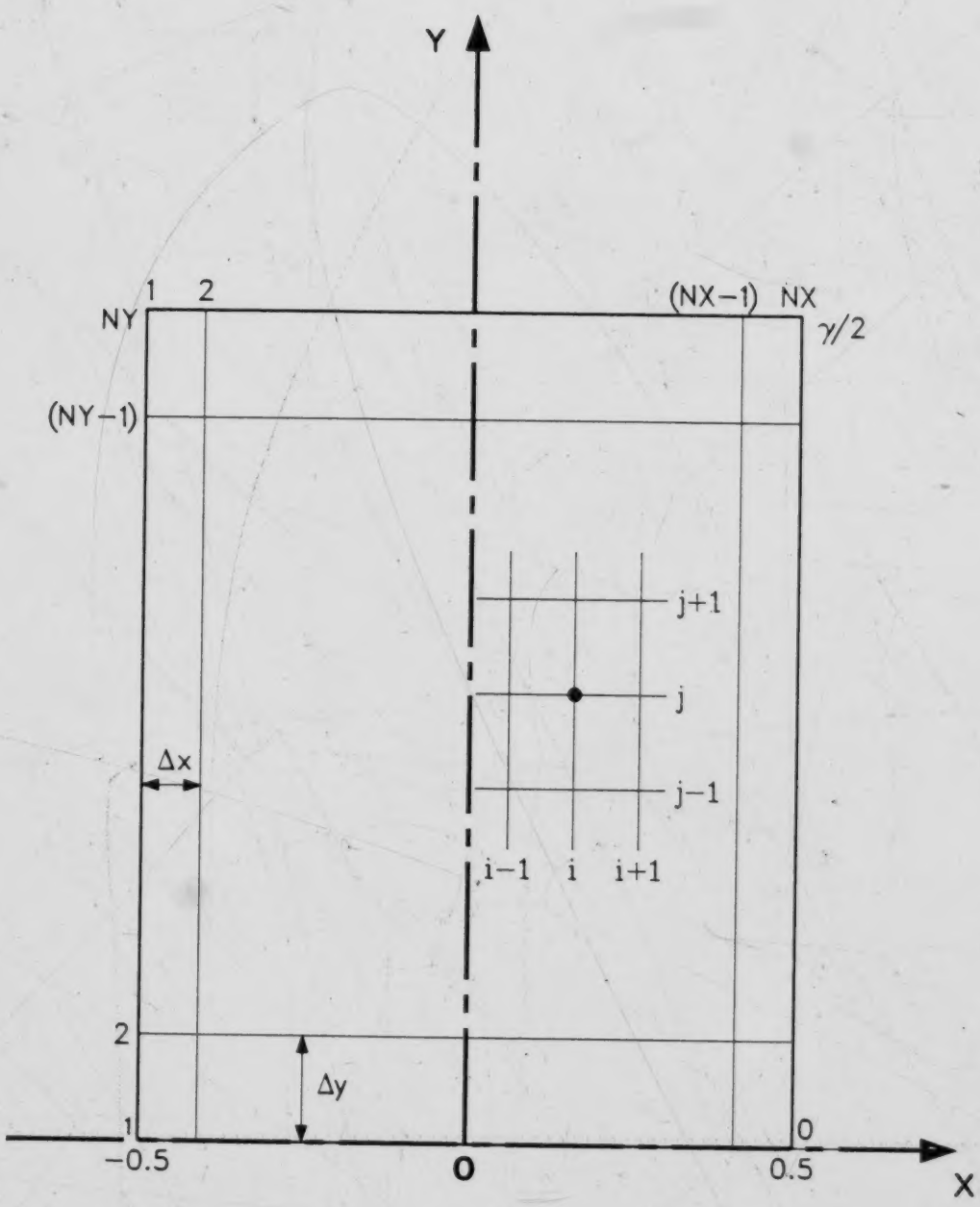

Fig. 3.2 Numerical Grid used; The top half of the cross-sectional plane with scaled dimensions is shown.

$$A_2 = \frac{1}{\Delta x^2} - \frac{1}{2\Delta x(r+x_i)} \qquad (3.55b)$$

$$A_3 = \frac{1}{\Delta x^2} + \frac{1}{2\Delta x(r+x_i)} \qquad (3.55c)$$

$$A_4 = \frac{1}{\Delta y^2} \qquad (3.55d)$$

$$A_5 = \frac{1}{\Delta y^2} \qquad (3.55e)$$

$$A_6 = (r+x_i)\ \Omega_{i,j} \qquad (3.55f)$$

where,

$$\Delta x = \frac{1}{(NX-1)} \quad \& \quad \Delta x^2 = (\Delta x)^2 \qquad (3.56a)$$

$$\Delta y = \frac{1}{(NY-1)} \quad \& \quad \Delta y^2 = (\Delta y)^2 \qquad (3.56b)$$

For the vorticity transport equation (3.32), $\chi = \Omega$ and

$$A_1 = \frac{2}{\Delta x^2} + \frac{2}{\Delta y^2} + \frac{1}{(r+x_i)^2} - \frac{u_{i,j}}{(r+x_i)} \qquad (3.57a)$$

$$A_2 = \frac{1}{\Delta x^2} + \frac{1}{2\Delta x(r+x_i)} - \frac{u_{i,j}}{2\Delta x} \qquad (3.57b)$$

$$A_3 = \frac{1}{\Delta x^2} - \frac{1}{2\Delta x(r+x_i)} + \frac{u_{i,j}}{2\Delta x} \qquad (3.57c)$$

$$A_4 = \frac{1}{\Delta y^2} - \frac{v_{i,j}}{2\Delta y} \qquad (3.57d)$$

$$A_5 = \frac{1}{\Delta y^2} + \frac{v_{i,j}}{2\Delta y} \qquad (3.57e)$$

$$A_6 = - \frac{w_{i,j}}{\Delta y (r+x_i)} \left[w_{i,j+1} - w_{i,j-1} \right]$$

$$+ \frac{1}{\Delta x^2} \left[\bar{F}_{xy_{i+1,j}} - 2 \bar{F}_{xy_{i,j}} + \bar{F}_{xy_{i-1,j}} \right]$$

$$- \frac{1}{\Delta y^2} \left[\bar{F}_{xy_{i,j+1}} - 2 \bar{F}_{xy_{i,j}} + \bar{F}_{xy_{i,j-1}} \right]$$

$$- \frac{1}{4\Delta x \Delta y} \left[\bar{F}_{xx_{i+1,j+1}} + \bar{F}_{xx_{i-1,j-1}} - \bar{F}_{xx_{i+1,j-1}} - \bar{F}_{xx_{i-1,j+1}} \right]$$

$$+ \frac{1}{4\Delta x \Delta y} \left[\bar{F}_{yy_{i+1,j+1}} + \bar{F}_{yy_{i-1,j-1}} - \bar{F}_{yy_{i+1,j-1}} - \bar{F}_{yy_{i-1,j+1}} \right]$$

$$+ \frac{1}{2\Delta x (r+x_i)} \left[\bar{F}_{xy_{i+1,j}} - \bar{F}_{xy_{i-1,j}} \right]$$

$$- \frac{1}{2\Delta y (r+x_i)} \left[\bar{F}_{xx_{i,j+1}} - \bar{F}_{xx_{i,j-1}} \right]$$

$$+ \frac{1}{2\Delta y (r+x_i)} \left[\bar{F}_{\theta\theta_{i,j+1}} - \bar{F}_{\theta\theta_{i,j-1}} \right]$$

$$- \frac{1}{(r+x_i)^2} \bar{F}_{xy_{i,j}} \qquad (3.57f)$$

For the axial momentum equation (3.33), $\chi = w$ and

$$A_1 = \frac{2}{\Delta x^2} + \frac{2}{\Delta y^2} + \frac{1}{(r+x_i)^2} + \frac{u_{i,j}}{(r+x_i)} \qquad (3.58a)$$

A_2, A_3, A_4 and A_5 are as in Equations 3.57b, 3.57c, 3.57d and 3.57e respectively

$$A_6 = - \frac{1}{(r+x_i)} \frac{\partial p}{\partial \theta} + \frac{1}{2\Delta x} \left[\bar{F}_{x\theta_{i+1,j}} - \bar{F}_{x\theta_{i-1,j}} \right] + \frac{1}{2\Delta y} \left[\bar{F}_{y\theta_{i,j+1}} - \bar{F}_{y\theta_{i,j-1}} \right] + \frac{2}{(r+x_i)} \bar{F}_{x\theta_{i,j}} \qquad (3.58b)$$

The secondary velocity components, u and v, at the interior grid points, (i = 2, 3,....., (NX-1) & j = 2, 3,....., (NY-1)), are computed using

$$u_{i,j} = \frac{\psi_{i,j+1} - \psi_{i,j-1}}{2 \Delta y \ (r+x_i)} \qquad (3.59)$$

$$v_{i,j} = - \frac{\psi_{i+1,j} - \psi_{i-1,j}}{2 \Delta x \ (r+x_i)} \qquad (3.60)$$

The stress components, $\bar{F}_{kl}$, at all i and j are computed in the following manner.

$$\bar{F}_{kl_{i,j}} = (M_{i,j} - 1) \ D_{kl_{i,j}} \qquad (3.61)$$

where $M_{i,j}$ is given by

$$M_{i,j} = (SUM)^{(n-1)/2} \tag{3.62}$$

and

$$SUM = \frac{1}{2<w>^2} \left[D_{xx}{}_{ij}^2 + D_{yy}{}_{ij}^2 + D_{\theta\theta}{}_{ij}^2 + 2\, D_{xy}{}_{ij}^2 + 2\, D_{x\theta}{}_{ij}^2 + 2\, D_{y\theta}{}_{ij}^2 \right] \tag{3.63}$$

The rate of strain components, D_{kl}, at the interior grid points, (i = 2, 3,....., (NX-1) & j = 2, 3,....., (NY-1)), are expressed as follows

$$D_{xx}{}_{i,j} = \frac{u_{i+1,j} - u_{i-1,j}}{\Delta x} \tag{3.64a}$$

$$D_{yy}{}_{i,j} = \frac{v_{i,j+1} - v_{i,j-1}}{\Delta y} \tag{3.64b}$$

$$D_{\theta\theta}{}_{i,j} = 2\,\frac{u_{i,j}}{(r+x_i)} \tag{3.64c}$$

$$D_{xy}{}_{i,j} = \frac{v_{i+1,j} - v_{i-1,j}}{2\,\Delta x} + \frac{u_{i,j+1} - u_{i,j-1}}{2\,\Delta y} \tag{3.64d}$$

$$D_{x\theta}{}_{i,j} = \frac{w_{i+1,j} - w_{i-1,j}}{2\,\Delta x} - \frac{w_{i,j}}{(r+x_i)} \tag{3.64e}$$

$$D_{y\theta}{}_{i,j} = \frac{w_{i,j+1} - w_{i,j-1}}{2\,\Delta y} \tag{3.64f}$$

Central difference method cannot be effectively used at the boundaries. Therefore numerical schemes with comparable

order of accuracy, such as Taylor's series expansion and 3-point forward or backward difference formulation, are used to handle the boundaries. The results are listed as follows:

at the top wall ($y = \gamma/2$),
where $i = 1, 2, \ldots, NX$ and $j = NY$

$$\psi_{i,NY} = w_{i,NY} = u_{i,NY} = v_{i,NY} = 0 \tag{3.65a}$$

$$\Omega_{i,NY} = -\frac{1}{(r+x_i)}\left[\frac{\partial^2\psi}{\partial y^2}\right]_{i,NY}$$

$$= \frac{\psi_{i,NY-2} - 8\psi_{i,NY-1}}{2(r+x_i)\Delta y^2} \tag{3.65b}$$

$$D_{xy_{i,NY}} = \frac{-4u_{i,NY-1} + u_{i,NY-2}}{2\Delta y} \tag{3.65c}$$

$$D_{yy_{i,NY}} = \frac{-4v_{i,NY-1} + v_{i,NY-2}}{\Delta y} \tag{3.65d}$$

$$D_{y\theta_{i,NY}} = \frac{-4w_{i,NY-1} + w_{i,NY-2}}{2\Delta y} \tag{3.65e}$$

$$D_{xx_{i,NY}} = D_{x\theta_{i,NY}} = D_{\theta\theta_{i,NY}} = 0 \tag{3.65f}$$

at the inner wall ($x = -0.5$),
where $i = 1$ and $j = 1, 2, \ldots, NY$

$$\psi_{1,j} = w_{1,j} = u_{1,j} = v_{1,j} = 0 \tag{3.66a}$$

$$\Omega_{1,j} = -\frac{1}{(r-0.5)}\left[\frac{\partial^2\psi}{\partial x^2}\right]_{1,j}$$

$$= \frac{\psi_{3,j} - 8\psi_{2,j}}{2(r-0.5)\Delta x^2} \qquad (3.66b)$$

$$D_{xx_{1,j}} = \frac{4u_{2,j} - u_{3,j}}{\Delta x} \qquad (3.66c)$$

$$D_{xy_{1,j}} = \frac{4v_{2,j} - v_{3,j}}{2\Delta x} \qquad (3.66d)$$

$$D_{x\theta_{1,j}} = \frac{4w_{2,j} - w_{3,j}}{2\Delta x} \qquad (3.66e)$$

$$D_{yy_{1,j}} = D_{y\theta_{1,j}} = D_{\theta\theta_{1,j}} = 0 \qquad (3.66f)$$

at the outer wall (x = 0.5),

where i = NX and j = 1, 2,...., NY

$$\psi_{NX,j} = w_{NX,j} = u_{NX,j} = v_{NX,j} = 0 \qquad (3.67a)$$

$$\Omega_{NX,j} = -\frac{1}{(r+0.5)}\left[\frac{\partial^2\psi}{\partial x^2}\right]_{NX,j}$$

$$= \frac{\psi_{NX-2,j} - 8\psi_{NX-1,j}}{2(r+0.5)\Delta x^2} \qquad (3.67b)$$

$$D_{xx_{NX,j}} = \frac{-4u_{NX-1,j} + u_{NX-2,j}}{\Delta x} \qquad (3.67c)$$

$$D_{xy_{NX,j}} = \frac{-4v_{NX-1,j} + v_{NX-2,j}}{2\Delta x} \qquad (3.67d)$$

$$D_{x\theta}{}_{NX,j} = \frac{-4w_{NX-1,j} + w_{NX-2,j}}{2\Delta x} \qquad (3.67e)$$

$$D_{yy}{}_{NX,j} = D_{y\theta}{}_{NX,j} = D_{\theta\theta}{}_{NX,j} = 0 \qquad (3.67f)$$

at the line of symmetry (y=0),

where i = 2, 3,....., (NX-1) and j = 1

$$\psi_{i,1} = \Omega_{i,1} = v_{i,1} = 0 \qquad (3.68a)$$

$$u_{i,1} = \frac{4\psi_{i,2} - \psi_{i,3}}{2\Delta y(r+x_i)} \qquad (3.68b)$$

$w_{i,1}$ is computed using Equations 3.54, 3.58a, 3.57b, 3.57c, 3.57d, 3.57e and 3.58b, considering the symmetry across the line y=0.

$$D_{xx}{}_{i,1} = \frac{u_{i+1,1} - u_{i-1,1}}{\Delta x} \qquad (3.68c)$$

$$D_{yy}{}_{i,1} = \frac{4v_{i,2} - v_{i,3}}{\Delta y} \qquad (3.68d)$$

$$D_{\theta\theta}{}_{i,1} = 2\,\frac{u_{i,1}}{(r+x_i)} \qquad (3.68e)$$

$$D_{x\theta}{}_{i,1} = \frac{w_{i+1,1} - w_{i-1,1}}{2\,\Delta x} - \frac{w_{i,1}}{(r+x_i)} \qquad (3.68f)$$

$$D_{xy}{}_{i,1} = D_{y\theta}{}_{i,1} = 0 \qquad (3.68g)$$

The sets of algebraic equations together with the boundary conditions are solved on an Array Processor in the following manner:

1. For a given power-law index n, radius of curvature r, aspect ratio γ, and axial pressure gradient $(\partial p/\partial\theta)$, the initial values of ψ, Ω, w and $\langle w \rangle$ are provided.

2. Stream function ψ at the interior points is updated using the Gauss-Siedel point iterative procedure with a relaxation factor. Three iterative cycles are performed in order to smooth ψ.

3. Boundary vorticity and the secondary velocity components, u and v, are computed using the updated stream function.

4. With the known velocity components, u,v and w, the rate of strain tensor component D_{kl} are computed. The dimensionless viscosity M is computed using Equations 3.62 and 3.63. When $n<1$, if SUM given by Equation 3.63 is less than 10^{-6} then SUM is reset to 10^{-6} in order to avoid comparatively large values of M. This singularity occurs only at certain points and its influence is localized as will be shown in Subsection 3.3.2. Knowing M and D_{kl}, the stress tensor components are computed using Equation 3.61. In case of a Newtonian fluid, where $n=1$, this step

is skipped and M is set equal to unity and $\bar{F}_{kl}$ is set equal to zero.

5. The axial velocity component w and the vorticity Ω are updated using the Gauss-Siedel point iterative procedure with relaxation.

6. From the known axial velocity profile, the average axial velocity <w> is computed using Simpson's 1/3 rule for integration.

This completes one cycle of outer iteration. This cycle is repeated until a specified number of outer iterations are exceeded. Upon completion of iterative cycles, the Reynolds numbers, the Dean Numbers and the friction factors are computed. The computer program used is given in Appendix A.

3.3 Method and Accuracy of the Numerical Solution

Stability, rate of convergence and accuracy of the numerical solutions are sensitive to grid size, relaxation factors and initial guesses. Several numerical experiments, conducted to establish the grid size and relaxation factors, revealed that different regions of solutions have to be treated differently. The solution procedure, in general, is discussed in Subsection 3.3.1. Few specific cases which deviates from the general procedure are given in Chapters 4 and 5, where it is appropriate. The accuracy of the

numerical solutions is discussed in Subsection 3.3.2.

3.3.1 Method of Solution

Newtonian Fluids

The power-law index n is unity for Newtonian fluids. The aspect ratio γ was varied between 0.3 and 2.0. First, the curvature effects on the flow were suppressed by choosing a large enough radius of curvature, r=10,000, and a comparable pressure gradient, $\Delta p=(-\partial p/\partial\theta)=10,000$. This is referred to as the straight pipe approximation. Parabolic profiles, obtained using zero initial guesses, were the solutions under the above conditions. Then r was set to 100 and Δp was so chosen that 2-vortex secondary flow with low Dn could be obtained. Parabolic profiles served as initial guesses. The solution procedure was continued by taking finite steps in Δp with the previously converged solutions as initial guesses. Up to about Dn≅70 or 80, the solutions converged easily with relaxation factors of unity. As Dn was increased, the solution did not converge, instead oscillated. A new set of relaxation factors (typically 0.8,0.1 and 0.8 for ψ, Ω and w respectively) overcame this difficulty and converged solutions were obtained easily. It should be emphasized here, it was the vorticity Ω which created problem most of the time and hence it needed a relatively small relaxation factor. In this region there was a tendency for the solution with 2 vortices to switch to

one with 4 vortices. This was avoided by taking small enough step in Δp (and hence Dn) until a critical Dn was reached; where the solution catastrophically jumped from 2-cell flow to a 4-cell flow. These sudden jumps were verified with fine grids. Moving forward with smaller relaxation factors were also carried out when further confirmation of the jump was needed. Considerable amount of computing time was spent in locating these jumps within the accuracy of ±1 in Dn.

Due to the small step in Δp, the small relaxation factors and the closeness of the initial guess to the solution (except at the point of sudden jumps), the solution was at times misleading. The 'residuals' stayed as low as the order of 10^{-3} when going from one Dn to another. Residuals were evaluated for all three main variables ψ, Ω and w independently by averaging the difference between the old and the new values of these variables over the number of grid points. For a converged solution, these residuals should be lower or equal to the order of 10^{-5}. Printing out these residuals and other parameters, such as Dn, f_1-Re, f_2-Re etc., for every specified number of outer iteration cycles (600 to 1,000) served as a better convergence criterian than a built-in algorithm. The outer iteration cycles were repeated until the residuals became equal to or lesser than 10^{-5} and the parameters remained constant at least up to the third decimal place. This criterian was

obtained after working with the problem in different regions of the solutions.

Once the 4-vortex solution was established, the procedure was continued in both increasing and decreasing directions of Δp. Decreasing direction of Δp encountered a sudden jump back to the 2-vortex solution. Hence care was exercised in this region. By marching along constant γ lines in the increasing Δp direction, only 4-vortex solutions were obtained within the range of Δp investigated. Some interesting features of the solution in this region is discussed in Chapter 4. Further increase in Δp led to oscillating results which were left unexplored.

Power-law Fluids

In order to keep the computational effort at a modest level, but still explore the interesting features, the power-law index was varied between 0.6 and 1.4; the Dn was varied up to about 300; but the aspect ratio and the radius of curvature were kept constant at 1 and 100 respectively.

The solution procedure was the same as for Newtonian fluids. Sudden jumps from 2 to 4 vortices were observed. Oscillating results at high Dn were left unexplored. Outside the range n=0.6 to 1.4, relaxation factors less than unity were needed even to obtain the parabolic profiles. In addition, solutions for $n<0.6$ required a finer grid and thus were left unexplored.

3.3.2 Accuracy of solution

The difference between f_1-Re and f_2-Re provides a mean of assessing the accuracy of the solutions. This difference can be attributed partly to the inaccuracy of the finite difference approximation, particularly forward and backward difference methods, in representing steeper velocity gradients. Even though this difference can be reduced by employing a finer grid size, computing time sets the lower limit on the grid size. Nevertheless the solutions obtained in this study show less than a 2% difference in most cases and up to a 5% difference in few cases.

The f-Re results of this study for a straight pipe limit are listed in Tables 3.1 and 3.2, along with the f-Re values from literature. It should be pointed out that the straight pipe approximation always introduces a small error. As the grid points are increased, the difference between f_1-Re and f_2-Re decreases and the f_1-Re values of this study approaches those given in the literature. This demonstrates the influence of the grid size on the accuracy of the numerical solution. Table 3.1 shows that the f_1-Re values for 0.5 and 2.0 are very close. It is due to the fact that the flow in the straight pipe is only sensitive to the geometry and the cross-sectional area, not to the orientation of the geometry. The small deviations observed are partly due to the different grid sizes used. In Table 3.2, the difference between f_1-Re and f_2-Re also increases

Table 3.1 The f-Re results for Newtonian fluids in straight rectangular pipes and comparison with the f-Re values of Shah & London(1978).

Aspect ratio Y	Shah & London (1978)	Present Study			
		f_1-Re	f_2-Re	%df	Grid NX×NY
0.3	17.51209	17.525	17.409	0.66	41×25
		17.527	17.392	0.77	41×13
		17.537	17.334	1.16	41×7
0.4	16.36810	16.380	16.275	0.64	41×17
		16.387	16.229	0.96	41×9
0.5	15.54806	15.557	15.472	0.55	41×21
		15.563	15.434	0.83	41×11
0.6	14.97996	14.988	14.916	0.48	41×25
		14.993	14.884	0.73	41×13
0.75	14.47570	14.485	14.401	0.58	41×17
0.8	14.37780	14.388	14.303	0.59	41×17
1.0	14.22708	14.235	14.166	0.48	41×21
		14.258	14.034	1.57	21×11
1.2	17.32808	14.340	14.243	0.68	31×19
1.35	----	14.503	14.451	0.36	41×29
1.4	14.56482	14.576	14.478	0.67	31×19
1.5	14.71184	14.720	14.644	0.52	31×25
1.6	----	14.879	14.802	0.52	31×25
1.7	----	15.044	14.967	0.51	31×25
1.8	----	15.212	15.148	0.42	31×31
2.0	15.54806	15.552	15.512	0.26	41×41
		15.555	15.490	0.42	31×31
2.4	----	16.217	16.160	0.35	31×37
3.0	17.08967	17.095	17.042	0.31	31×41
5.0	19.07050	19.076	19.013	0.33	21×51
		19.080	18.988	0.48	17×41

Table 3.2 The f-Re' results for Power-law fluids in straight square pipes and comparison with available results

Power-law index n	Wheeler & Wissler (1965)	Tomcej & Nandakumar (1984)	Present study			
			f_1-Re'	f_2-Re'	%df'	Grid NX×NY
1.5	----	----	14.061	14.031	0.21	41×21
1.4	----	----	14.094	14.060	0.24	41×21
1.25	----	14.140	14.147	14.102	0.32	41×21
1.2	----	----	14.152	14.138	0.10	81×41
			14.163	14.115	0.34	41×21
1.0	14.23	14.235	14.235	14.166	0.48	41×21
0.9	14.30	14.277	14.270	14.186	0.59	41×21
0.8	14.32	14.323	14.312	14.280	0.22	81×41
			14.304	14.201	0.72	41×21
0.7	14.37	----	14.355	14.313	0.29	81×41
			14.333	14.207	0.88	41×21
0.6	14.41	----	14.381	14.338	0.30	81×41
			14.356	14.200	1.09	41×21
0.5	14.48	----	14.430	14.364	0.46	81×41
			14.366	14.173	1.34	41×21
0.4	14.54	----	14.436	14.365	0.49	81×41
			14.358	14.119	1.66	41×21

as the power-law index n decreases. It may be due to the steeper velocity gradients closer to the wall at lower values of n, as can be seen in Figure 3.3. The f-Re values of this study also deviate from those of Wheeler and Wissler(1965) as n decreases. These deviations can be significantly reduced by using a finer grid size, as shown in the Table 3.2. It should be noted that Wheeler and Wissler did not use an equivalent grid finer than 41x21. However they employed a 5-point central difference approximation, which yields significantly more accurate results for a given grid size when compared to the 3-point central difference method. In addition, they solved a single non-linear partial differential equation for a straight pipe with only 4 non-zero stress components.

Tables 3.1 and 3.2 show that the numerical values f_1-Re are always closer to the literature values than the numerical values f_2-Re are. Therefore f_1-Re is considered to represent the friction factor-Reynolds number relation more accurately. Hence the values represented by f-Re, in this thesis, refer to f_1-Re.

The axial velocity profiles shown in Figure 3.3 and the viscosity profiles shown in Figures 3.4a and 3.4b were in good agreement with the predicted behaviour of the power-law fluids. When confronted with zero strain rate, the power-law model predicts infinitely large values of viscosity when $n<1$. It is handled by the approximation

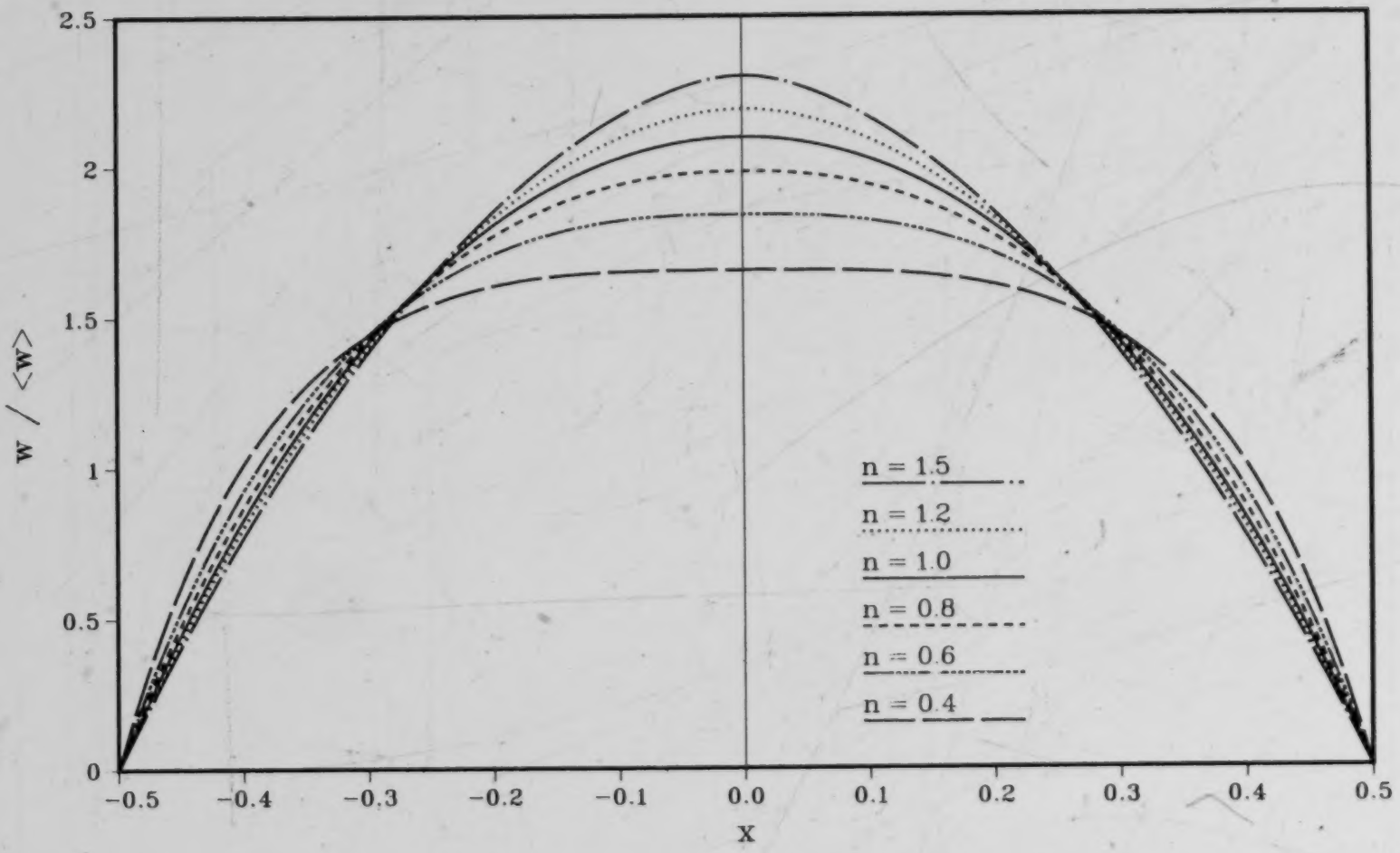

Fig. 3.3 Axial Velocity distribution at y = 0 for Power−law fluids in straight square channel

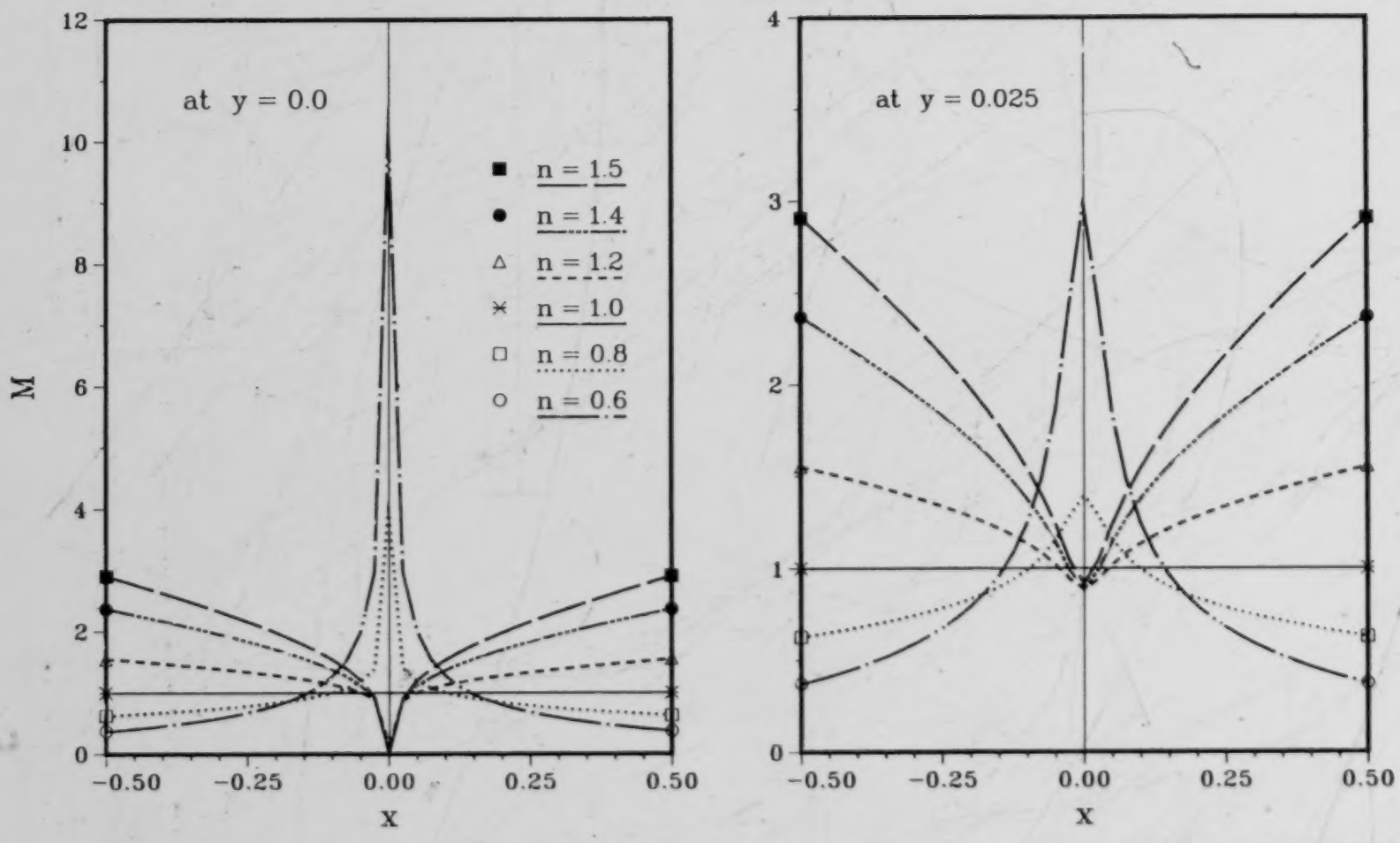

Fig. 3.4a Dimensionless Viscosity (M) profile for Power–law fluids in straight square channel

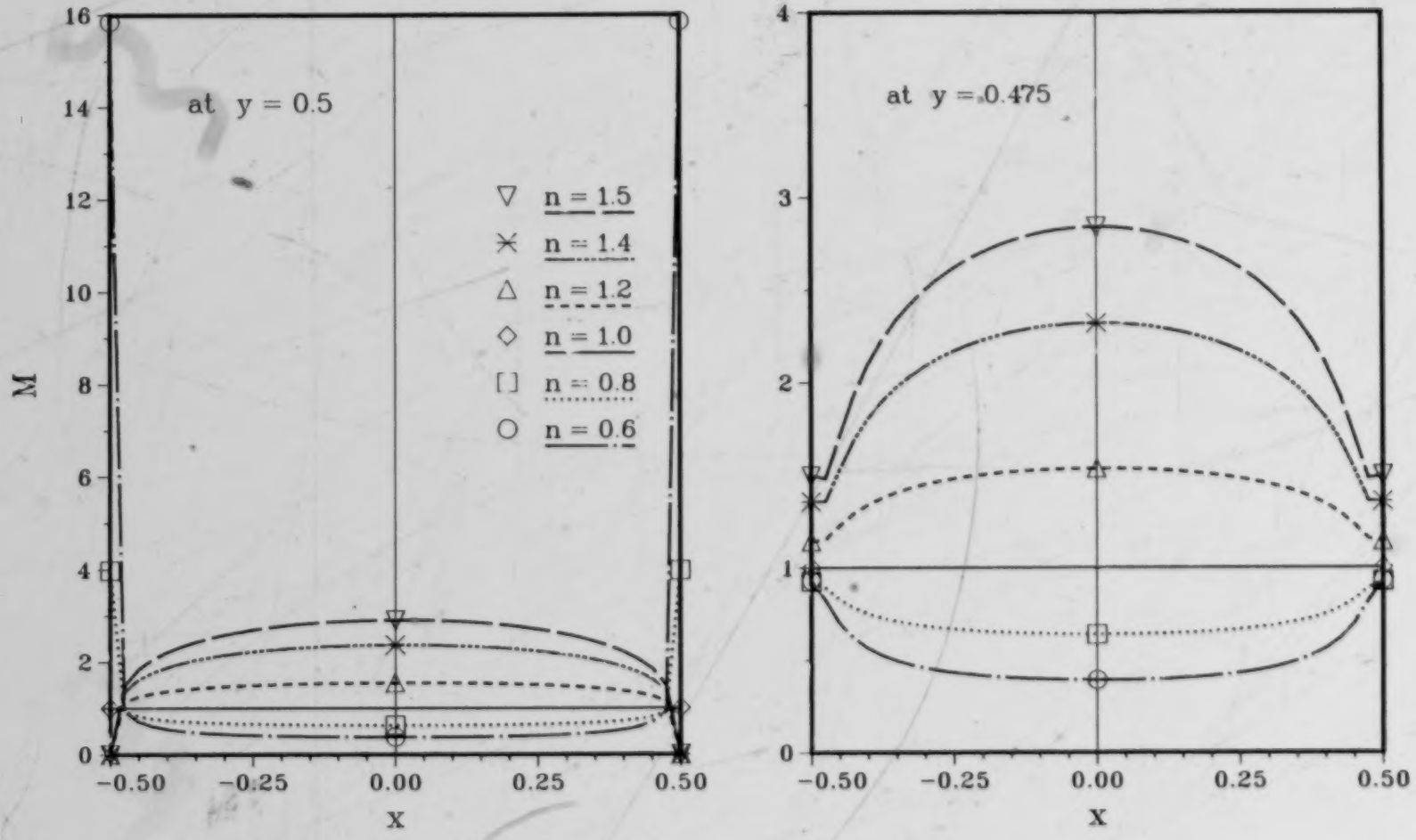

Fig. 3.4b Dimensionless Viscosity (M) profile for Power–law fluids in straight square channel

discussed in Section 3.2, step 4 of the computer algorithm. Zero strain rate occurs at the corners and at the center of straight rectangular pipes. The double helical flow in a curved rectangular pipe removes the existence of the zero strain rates from the center but not from the corners. Figures 3.5(a) and (b) well illustrate that the effect of this approximation is localized. This can also be seen in Figures 3.4a and 3.4b. In order to confirm this fact, a different approximation was attempted at the corners, which have zero strain rates even when the pipe is curved. The strain rates at the corners were set equal to the average of the strain rates at the adjacent points along the wall. The results obtained by both methods, for the few cases investigated, were the same except at the points of zero strain rates. Hence the theoretical defect of the power-law model is insignificant in this study.

The f-Re results for Newtonian fluids in curved square pipes are compared with available theoretical, numerical and experimental results in Figure 3.6. Good agreement is observed with the experimental results of Ludwieg(1951) and Baylis(1971). A detailed account of these available results is given in Subsection 2.2.2. Results of this study are compared with that of Cheng et al.(1976) in Tables 3.3 and 3.4. It can be seen that the numerical accuracy has been improved using finer grid.

(a) Straight pipe

(approximated)

(b) Curved pipe

(r = 100 ; Dn = 102.4)

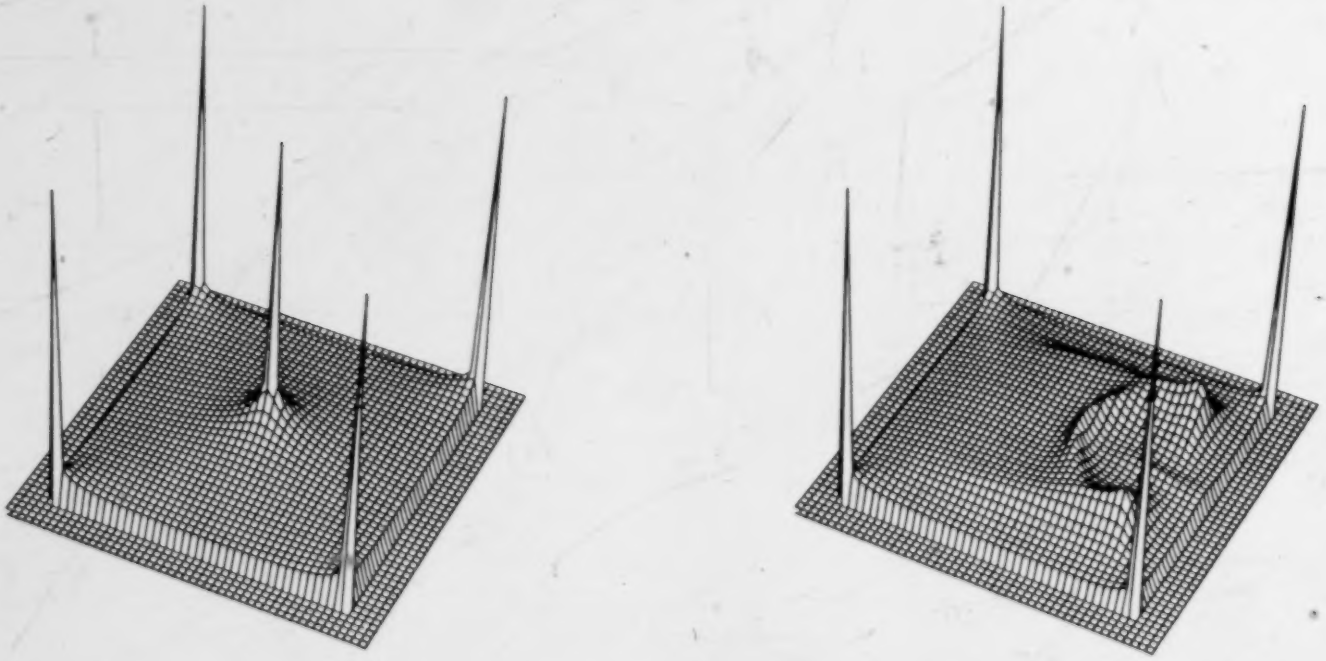

Fig. 3.5 The 3-dimensional profiles of the viscosity(M) of a power-law fluid (n = 0.7) across the entire cross-sectional plane of a square pipe.

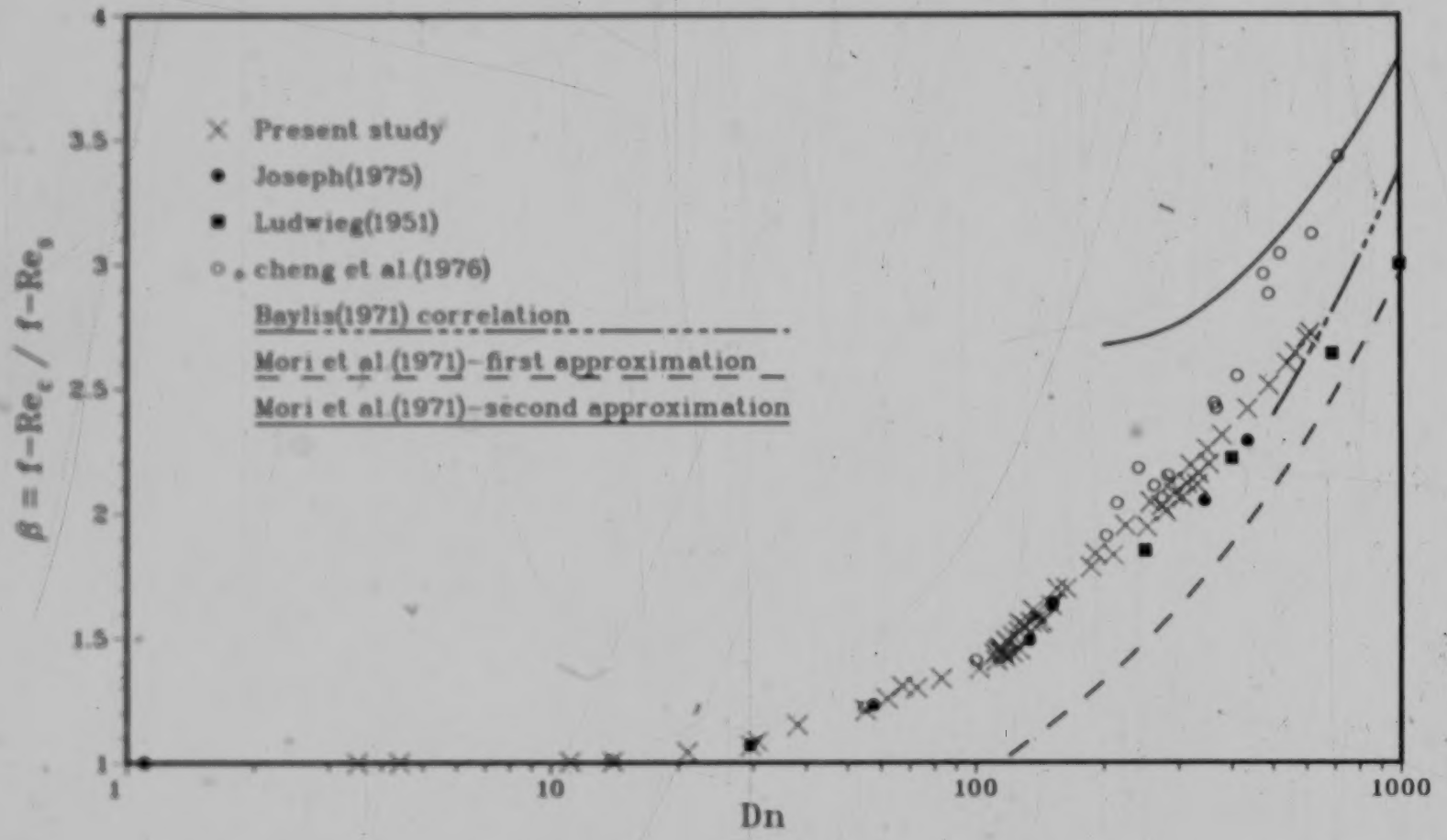

Fig 3.6 Friction factor results for Newtonian fluids in square channel ($\gamma = 1$) at various radii of curvature (r) compared with available theoretical, numerical and experimental results

Table 3.3 Comparisons of the f-Re results for curved square pipes with Cheng et al (1976)

pgrad	r	Cheng et al (1976)						Present study					
		Dn	β_1	β_2	%dβ	Grid NX×NY	No of cells	Dn	β_1	β_2	%dβ	Grid NX×NY	No of cells
60,000	100	13.94	1.007	1.000	0.70	21×11	2	13.97	1.006	1.006	0.00	41×21	2
90,000	100	29.53	1.071	1.055	1.49	21×11	2	29.57	1.069	1.069	0.00	41×21	2
190,000	100	54.82	1.218	1.212	0.49	21×11	2	54.89	1.214	1.224	0.82	21×11	2
								55.14	1.210	1.211	0.08	41×21	2
400,000	100	100.0	1.406	1.416	0.71	21×11	2	101.1	1.387	1.414	1.95	21×11	2
								101.9	1.378	1.380	0.15	41×21	2
700,000	100	151.1	1.629	1.667	2.33	21×11	2	147.9	1.660	1.756	5.78	21×11	4
								150.9	1.630	1.643	0.80	41×21	4
1900,000	100	202.6	1.909	2.177	14.1	21×11	4	210.7	1.834	1.860	1.42	41×21	4
5600,000	100	274.3	2.060	2.620	27.2	21×11	4	280.0	2.007	2.045	1.89	41×21	4
50,000	10	262.7	2.112	2.561	21.2	21×11		273.6	2.030	2.037	0.34	41×21	4
55,000	10	263.4	2.154	2.521	17.0	21×11		294.3	2.076	2.086	0.48	41×21	4
60,000	4	214.8	2.042	2.136	4.6	21×11		225.0	1.951	1.908	2.20	41×21	4
12,000	4	241.2	2.180	2.300	5.5	21×11		257.7	2.045	2.002	2.10	41×21	4
24,000	4	411.9	2.550	3.090	21.2	21×11		435.8	2.418	2.386	1.32	41×21	4
32,000	4	475.3	2.957	2.882	2.54	41×21		540.4	2.600	2.581	0.73	41×21	4
		488.4	2.880	3.216	29.4	21×11							
36,000	4	520.2	3.04	3.03	0.33	21×11	2	589.2	2.683	2.673	0.37	41×21	4

Table 3.4 Comparison of the f-Re results for curved pipes of aspect ratios γ=2.0, 5.0 & 0.5 with Cheng et al (1976)

pgrad	r	Cheng et al (1976)						Present study					
		Dn	β_1	β_2	%dβ	Grid NX×NY	No of cells	Dn	β_1	β_2	%dβ	Grid NX×NY	No of cells
Aspect ratio γ=2.0													
281,250	133.33	15.90	1.014	1.000	1.38	17×17	2	16.02	1.003	1.003	0.00	31×31	2
562,500		31.50	1.027	1.022	0.49	17×17	2	31.23	1.029	1.029	0.00	31×31	2
1462,500		72.15	1.165	1.160	0.43	17×17	2	72.83	1.148	1.148	0.00	31×31	2
2250,000		103.5	1.249	1.252	0.24	17×17	2	105.0	1.225	1.226	0.08	31×31	2
3375,000		143.8	1.350	1.362	0.89	17×17	2	146.9	1.313	1.315	0.15	31×31	2
Aspect ratio γ=5.0													
288,000	166.67	20.82	1.001	1.000	0.10	13×31	2	20.96	1.000	1.000	0.00	17×41	2
504,000		36.00	1.020	1.001	1.86	13×31	2	36.61	1.002	1.002	0.00	17×41	2
1080,000		76.90	1.024	1.019	0.49	13×31	4	77.07	1.020	1.020	0.00	17×41	2
Aspect ratio γ=0.5													
1125,000	66.67	16.00	1.010	1.000	0.99	33×9	2	16.02	1.003	1.003	0.00	41×11	2
2250,000		31.10	1.039	1.028	1.06	33×9	2	31.13	1.032	1.032	0.00	41×11	2
5850,000		68.09	1.235	1.238	0.24	33×9	2	68.58	1.218	1.223	0.41	41×11	2
11250,000		112.6	1.436	1.463	1.88	33×9	2	114.6	1.402	1.419	1.21	41×11	2
20250,000		176.6	1.648	1.729	4.90	33×9	2	181.7	1.591	1.630	2.45	41×11	2
24750,000		200.7	1.772	1.942	9.60	33×9	4	207.6	1.702	1.765	3.70	41×11	4

The experimental axial velocity measurements of Mori et al.(1971) under the zero wall heat flux condition are presented with the axial velocity profiles obtained in this numerical study, in Figures 3.7a and 3.7b. Fair agreement is obtained only for low Dn flows. Significant disagreement is observed as Dn increases. The profiles of Mori et al.(1971) clearly show the outward shift of the location of the maximum axial velocity. The profiles of this study show two distinct characteristics. At Dn=30.7,61.9 and 115.5, the profiles are similar to that of Mori et al.(1971). At Dn=186.7 and 353.9, the location of the maximum axial velocity along y=0 is closer to the mid plane of the flow. It should be noted that the first three profiles of this study posses the normal secondary flow with two vortices as shown in Figure 3.8(a). The last two profiles posses two additional counter rotating vortices near the center of the outer wall as shown in Figure 3.8(b). Similar discrepancy was also reported by Cheng et al.(1976). There is a possibility that flows with only two cells were experienced in the experiments of Mori et al.(1971), even at Dean numbers as high as 251. Cheng et al.(1976) and Winters and Brindley(1984) have reported the reappearance of 2-cell flow at high Dean numbers. This phenomenon is discussed in detail in Chapter 4.

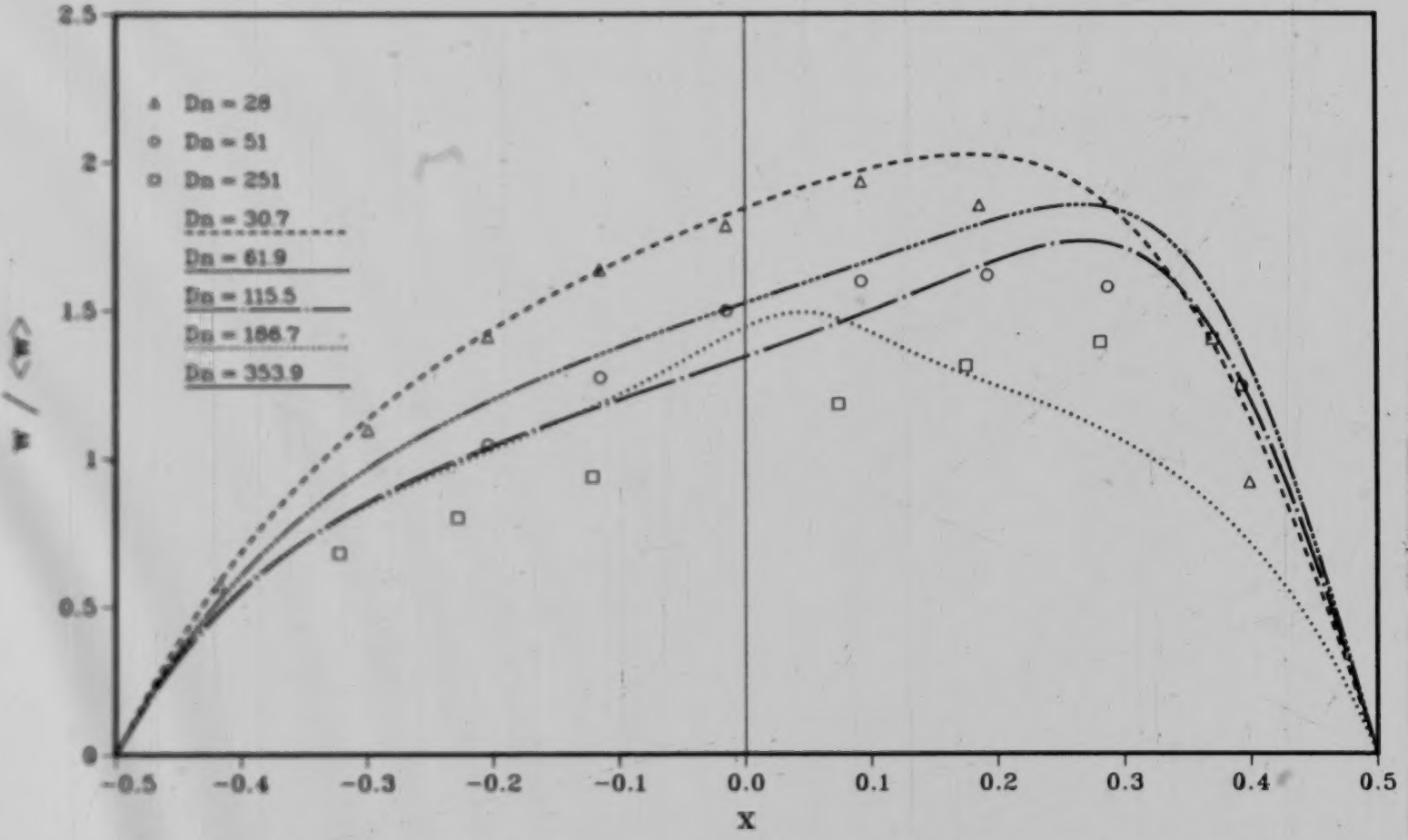

Fig. 3.7a Axial Velocity distribution at y = 0 for Newtonian fluids in square channel. Scattered points represent the experimental data of Mori et al.(1971) at r = 14. Curves represent the results of present study at r = 10.

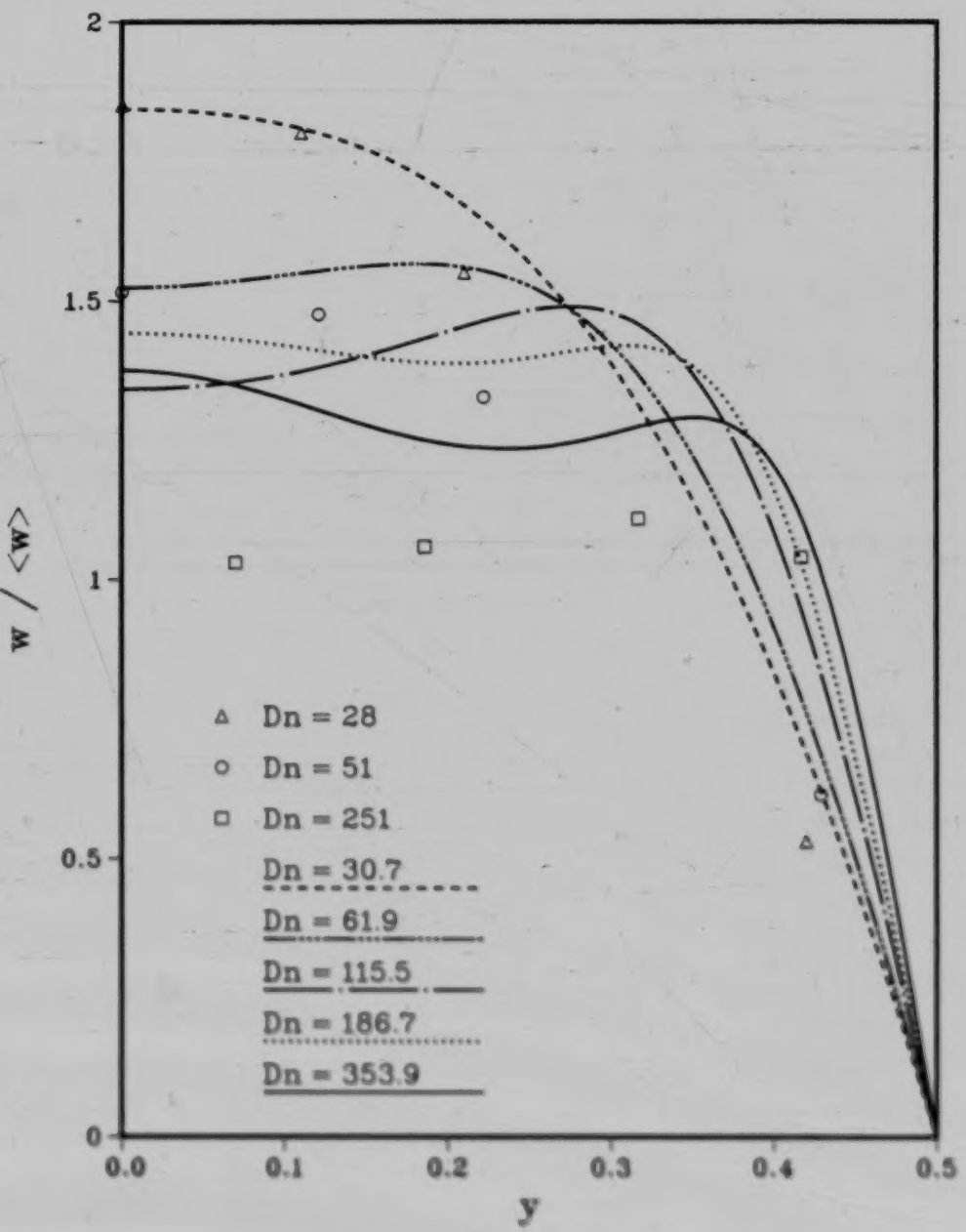

Fig. 3.7b Axial Velocity distribution at x = 0 for Newtonian fluids in square channel. Scattered points represent the experimental data of Mori et al (1971) at r =14. curves represent the results of present study at r = 10

(a) 2–vortex flow

(Dn = 54.5)

(b) 4–vortex flow

(Dn = 294.3)

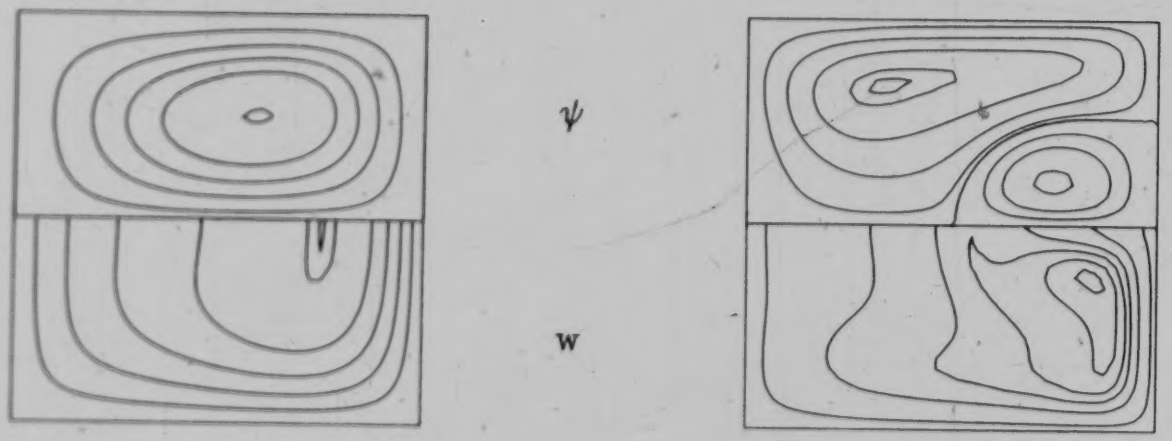

Fig. 3.8 The contours of the stream function (ψ) and the axial velocity (w) of a Newtonian fluid in a square pipe of r = 10

CHAPTER 4

RESULTS AND DISCUSSION

PART I - NEWTONIAN FLUIDS

The influence of the centrifugal force field(Dn) and the end effects(γ) on the solution structure under constant curvature condition (r=100) are discussed in Sections 4.1 and 4.2 respectively. The state of the solution is measured by one or both of the means stated below:

- u at x=0.4 and y=0
  - the secondary velocity component at a point.
- $\beta = \frac{Q_s}{Q_c} = \frac{\langle W \rangle_s}{\langle W \rangle_c} = \frac{f\text{-}Re_c}{f\text{-}Re_s}$
  - a measure of the increase in resistance to flow when the pipe is curved.

A unified view of the solution, in the Dn-γ space investigated, is attempted in Section 4.3 with the aid of the elementary models in Catastrophe theory. The influence of the curvature of the pipe on the solution surface is discussed in Section 4.4.

A detailed account of the numerical results obtained in this study by changing Δp at different γ with n=1 and r=100 are presented in Appendix B. The results for square pipes

of r=10 and 4 are also presented in this Appendix.

4.1 Influence of the Centrifugal Force

The Dean number, defined as $Dn=Re/\sqrt{r}$, is a measure of the intensity of the centrifugal force field acting on the flow. Unfortunately this Dn cannot be changed directly and has to be manipulated via Δp. The centrifugal force effect is demonstrated first for a square section.

Figures 4.1a and 4.1b show the spectacular changes of the contours ψ and w with increasing Dn. In Figure 4.1a, the axial velocity peak moves well away from the center of the pipe towards the outer wall along the central plane of the pipe, whilst the center of the circulation exhibits a clockwise motion about the origin and then reversed to one which is anticlockwise. Further increases in Dn cause the axial velocity peak to move away from the central plane and the stream function to reverse its direction in that region (Figure 4.1b).

Figure 4.2 shows the influence of Dn on the secondary velocity component u along the line of symmetry (y=0). The negative values of u represent the presence of the additional vortices. Along the line x=0,4 of Figure 4.2, u changes its sign indicating the change of flow pattern from 2-vortex to 4-vortex. Thus u at (0.4,0.0) is chosen to discriminate between both types of flow patterns. The

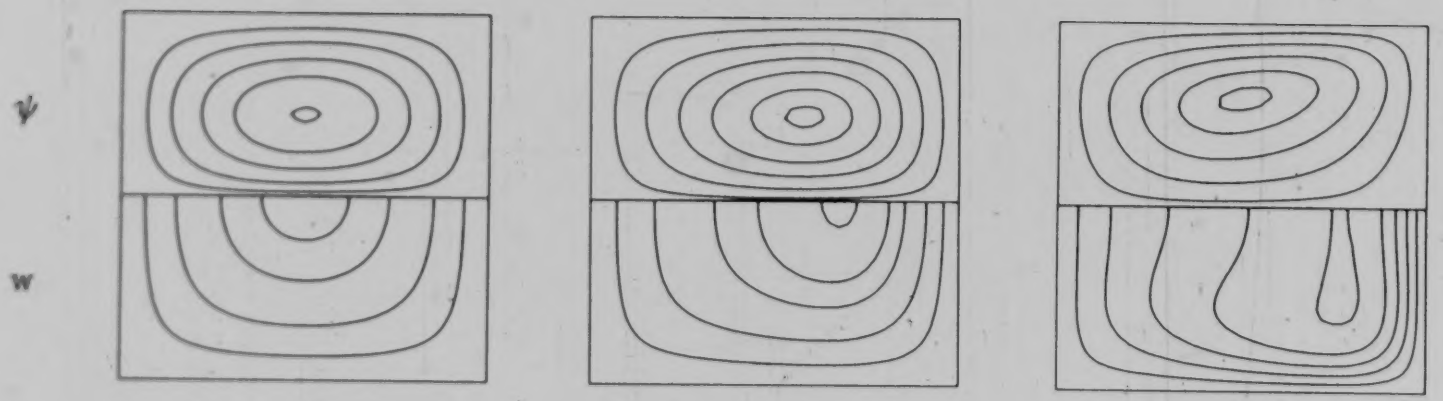

Fig. 4.1a Contour plots showing the 2–vortex flow at different Dn for $\gamma = 1$ & $r = 100$

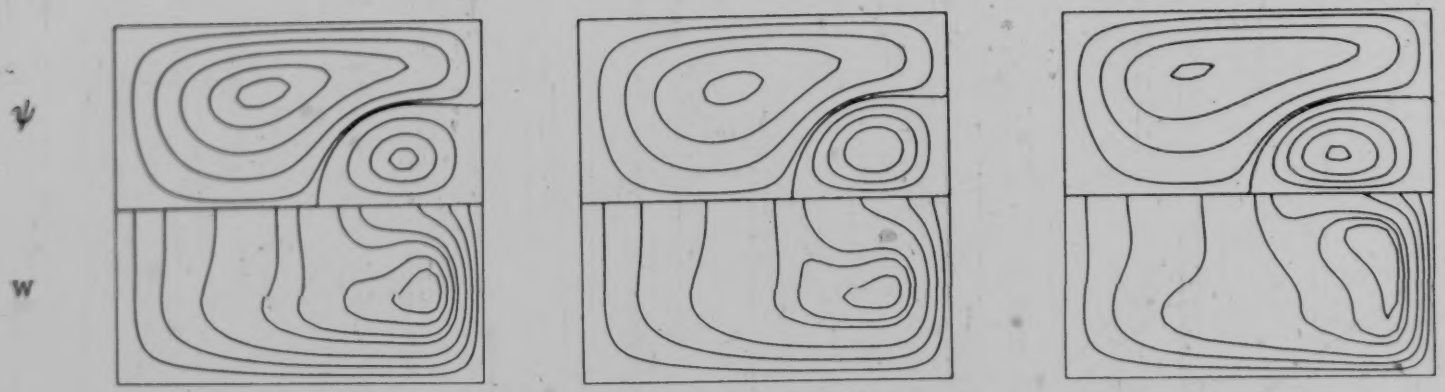

Dn = 130.7 Dn = 150.8 Dn = 279.9

Fig. 4.1b Contour plots showing the 4–vortex flow at different Dn for $\gamma = 1$ & $r = 100$

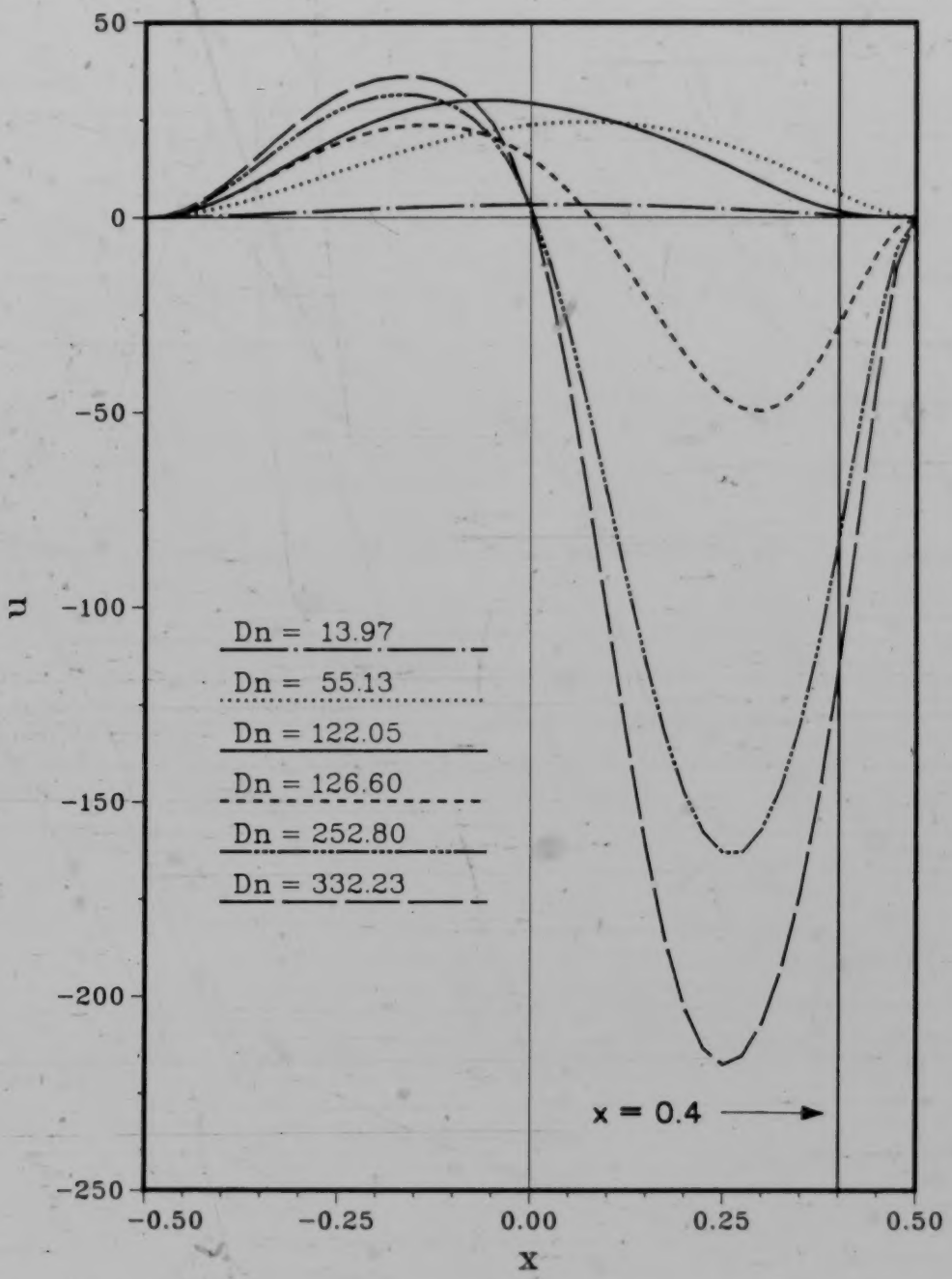

Fig. 4.2 u at y = 0 for $\gamma = 1$ & r = 100

evolution of u(0.4,0.0) is plotted against Dn in Figure 4.3. The procedure to obtain such solutions is outlined in Subsection 3.3.1. The interesting features of Figure 4.3 are as follows:

- Discontinuity

  The branch representing the stable 2-cell flow evolves continuously from the trival solution at $\Delta p=0$. It will be called the primary branch. The branch representing the stable 4-cell flow caused by the centrifugal instability will be referred as the secondary branch. These two branches are disconnected from each other.

- Sudden Jumps

  The flow pattern changes from 2 vortices to 4 vortices and from 4 vortices to 2 vortices via sudden jumps.

- Hysteresis

  The Dn (or Δp) associated with the above mentioned jumps are different from each other.

- Bimodality

  There exists a range of Dn (or Δp) within which both 2-vortex and 4-vortex flows are possible.

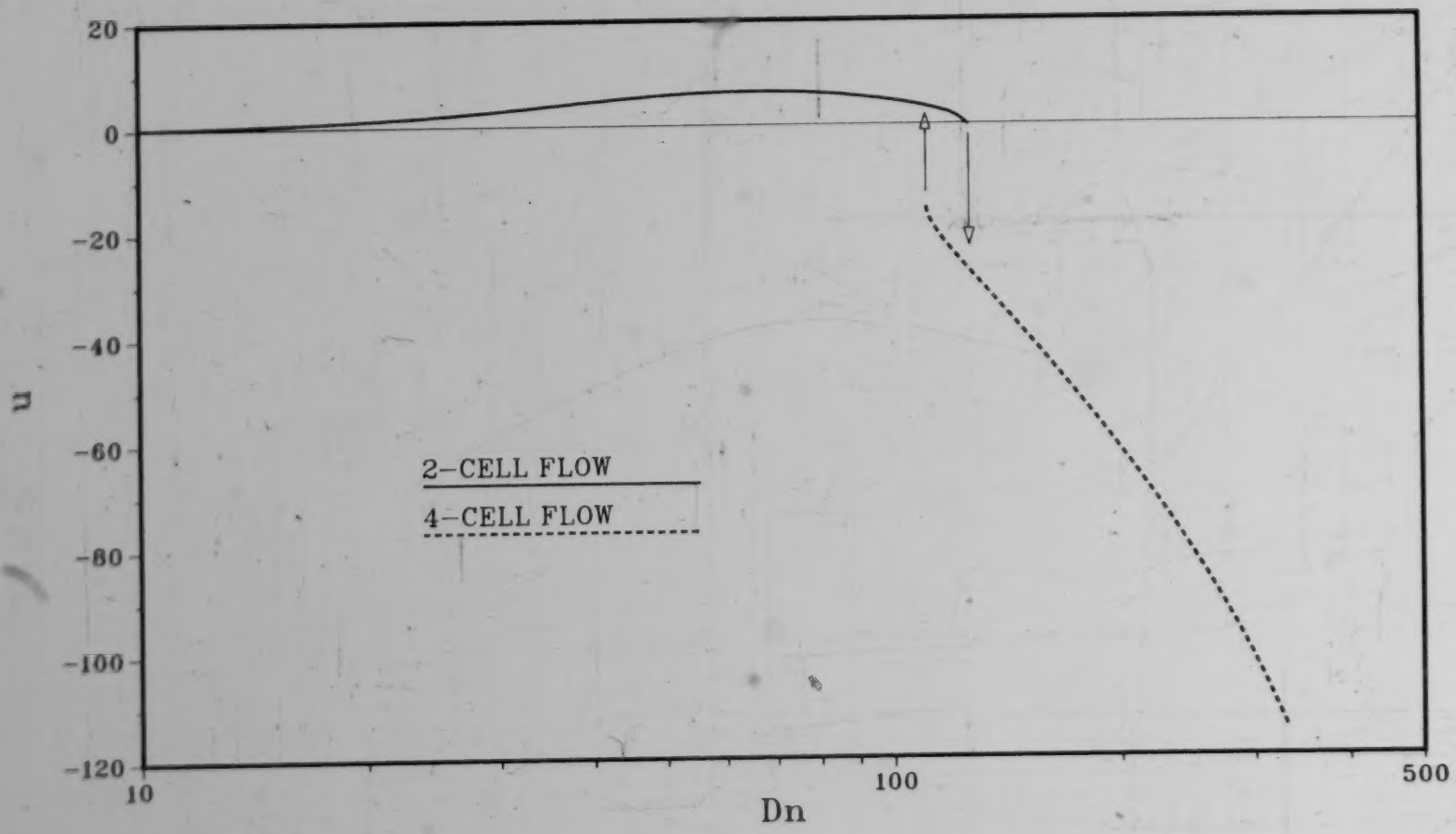

Fig. 4.3 u at $x = 0.4$ & $y = 0$ for $\gamma = 1$ & $r = 100$

- The magnitude of u reaches a maximum along the primary branch and then decreases. This is due to the behaviour of the core of the stream line contours shown in Figure 4.1a.

The first four features of Figure 4.3, listed above, are also revealed by Figure 4.4 which makes use of the more practical quantity, β, as the state function.

4.2 End Effects on the Flow

The driving force in the vorticity transport equation (3.32) consists of the axial velocity gradient in the Y-direction. This gradient is always present near the ends of a pipe of finite aspect ratio. Hence there is always a solution with helical motion near the ends. As γ decreases these end vortices dominate the whole flow area. This phenomenon can be observed in the series of stream line contour plots at different γ shown in Figure 4.5a. In this figure, the contours representing 0.0,0.2,0.4,0.6,0.8 and 0.99 are drawn. The actual stream function and the axial velocity values of these contours are normalized with respect to the corresponding maximum values.

The flow area, which the additional vortices can possibly occupy under the influence of the end effects, is shown in the series of contour plots of Figure 4.5b. The additional vortices can occupy the whole width of the pipe

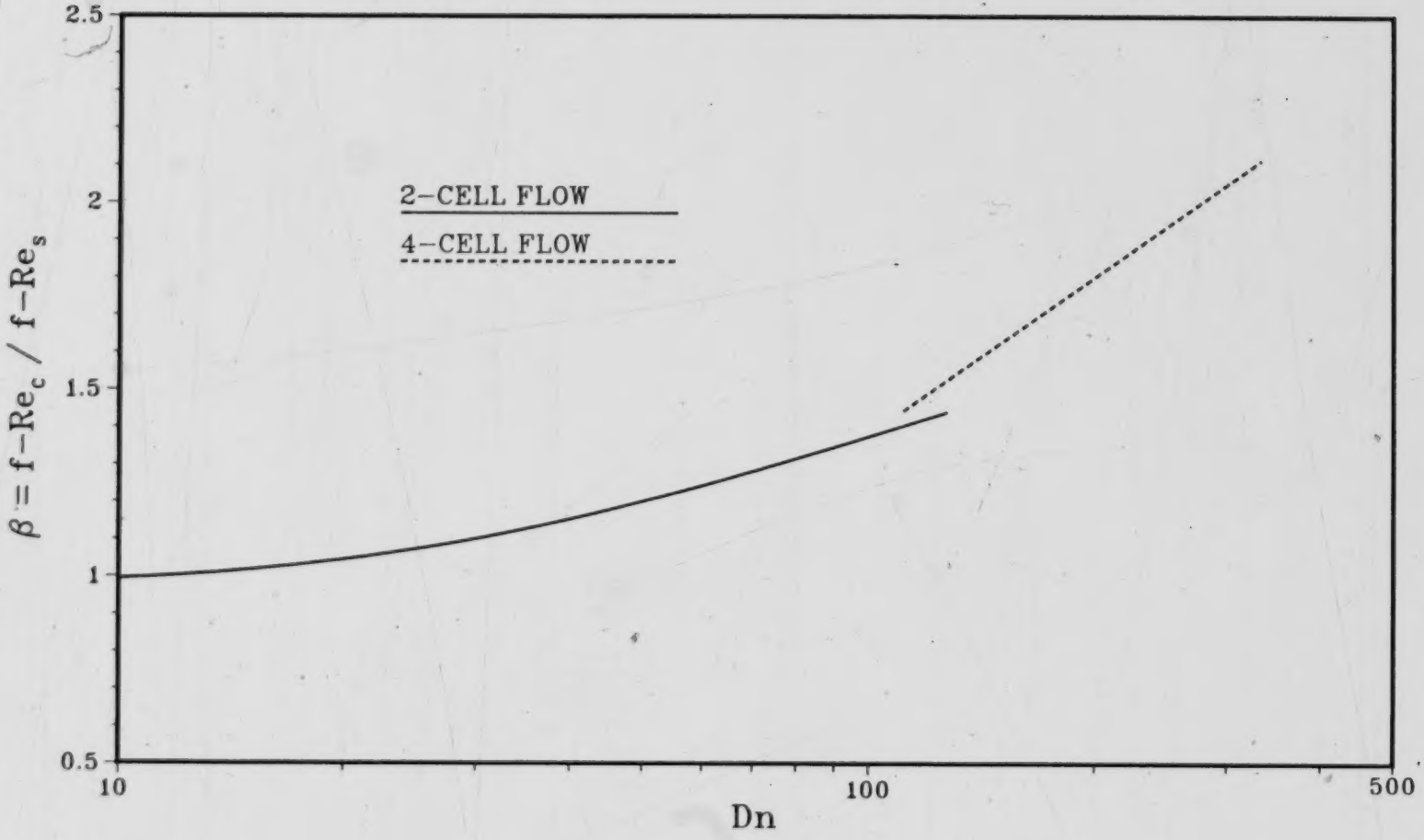

Fig. 4.4 Friction factor results for $\gamma = 1$ & $r = 100$

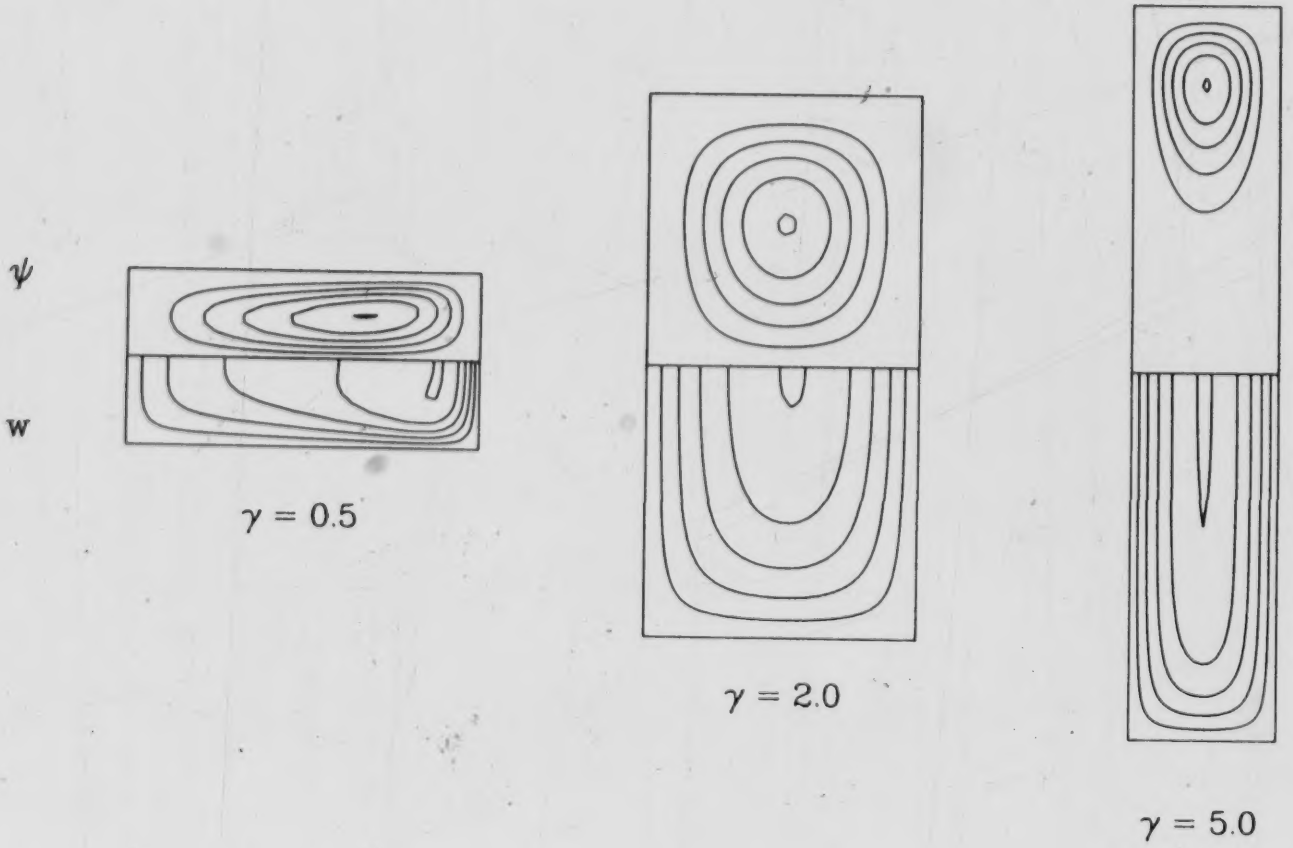

Fig. 4.5a Contour plots showing the distribution of ψ in 2–vortex flows at different γ.

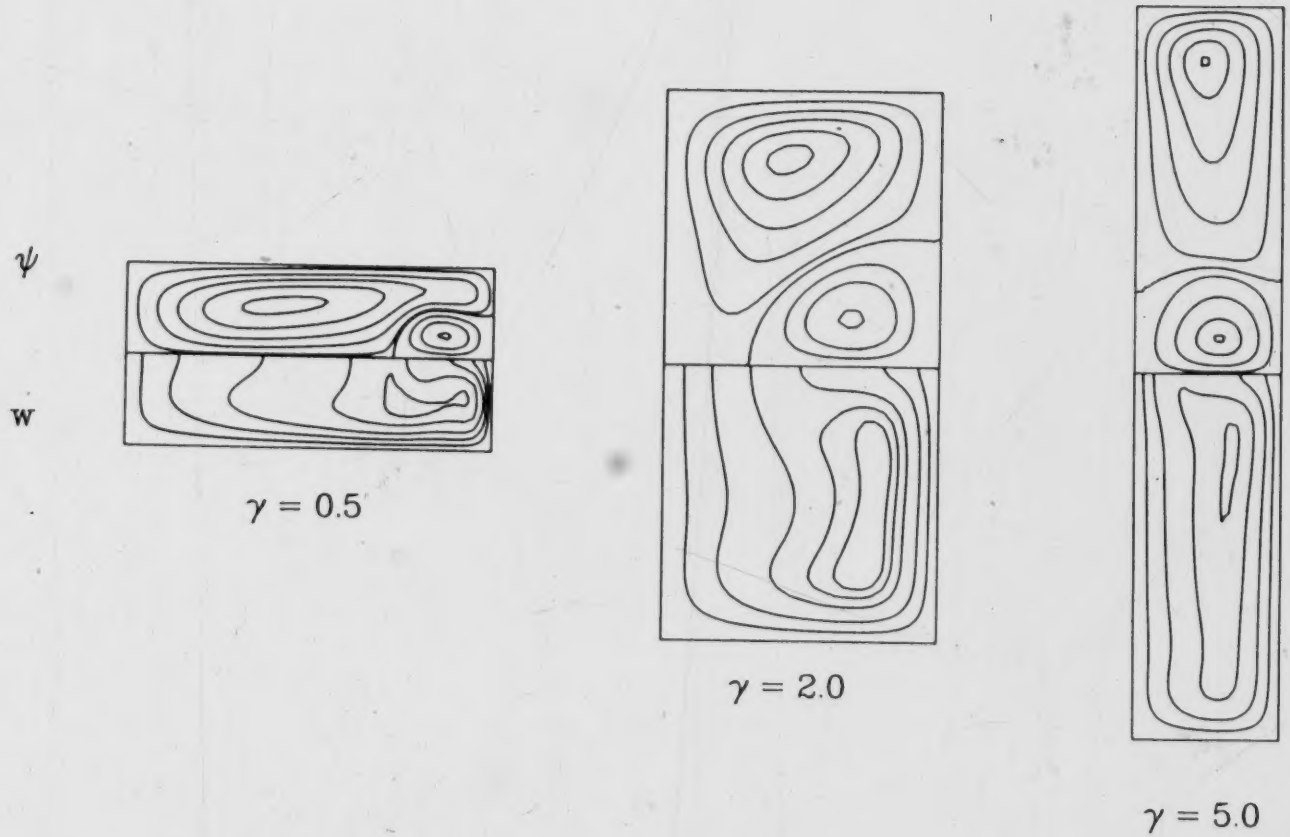

Fig. 4.5b Contour plots showing the flow area which the additional vortices could possibly occupy at different γ.

at γ=5.0, whereas they are restricted to a relatively small flow area at γ=0.5.

Figure 4.6 shows the locus of the critical Dn below which these additional pair of vortices cannot be sustained. This critical value will be referred to as Dn_{4-2}. The prolonged existence of the 2-cell flow as the unique solution at low γ may be due to the increasing strength of viscous forces as the ends are brought closer to each other.

Figure 4.7 shows the locus of the critical Dn where the 2-cell solution suddenly jumps to the 4-cell solution when Δp is slowly increased from zero along constant γ lines. This critical Dn will be referred to as Dn_{2-4}. The Dn_{2-4} locus is discontinuous! It is pertinent to mention the experimental investigations of Cheng et al.(1977) where they observed a discontinuity in the critical Dn locus. Their locus marked the onset of centrifugal instability in a rectangular pipe of r=5. However no comparison between these two studies is made since it is not clear in the work of Cheng et al. whether this locus belong to Dn_{4-2} or Dn_{2-4}.

When computations were carried out by starting at well converged 2-cell solutions at γ=1.5 and then by *slowly* decreasing the aspect ratio (typically by 0.1 or 0.2) along constant Δp lines. Stable 2-cell solutions were obtained for $\gamma \leq 1.4$ at Dn (or Δp) greater than the corresponding Dn_{2-4} (or Δp_{2-4}). Starting from these 2-cell solutions, computations were carried out in either direction of Δp

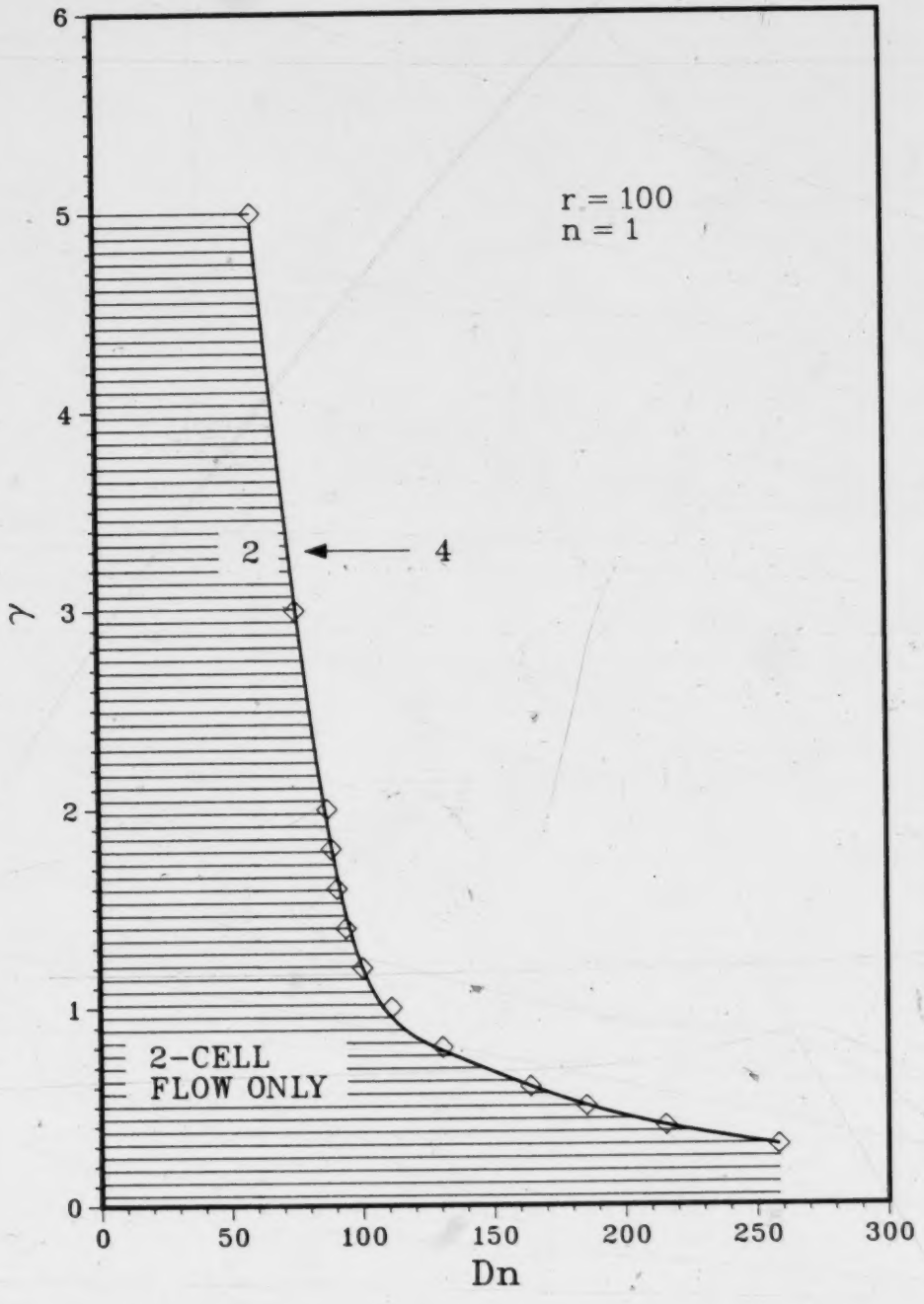

Fig. 4.6 The Dn_{4-2} locus.

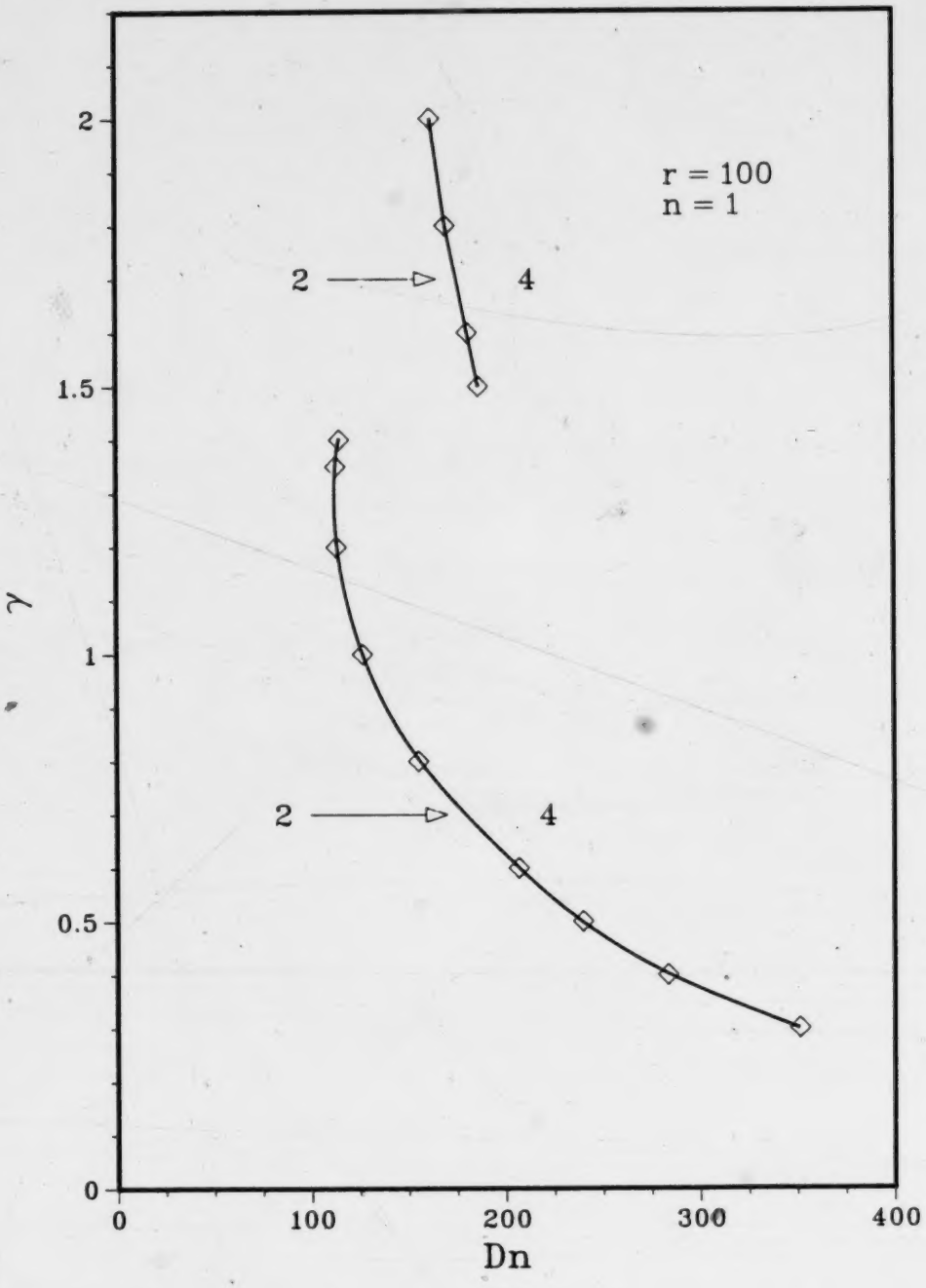

Fig. 4.7 The Dn_{2-4} locus.

along constant γ lines, thereby establishing the Dn_{2-4} locus as shown in Figures 4.8a and 4.8b. This critical locus exhibits a turning point slightly above $\gamma=1.4$. Great care was exercised in the decreasing direction of Δp in order to avoid premature jumps to 4-cell solutions. The increasing direction of Δp demanded a very small step in Dn (typically 2 to 4); oscillating results were set up otherwise. Every such point explored in this direction required 20,000 to 30,000 outer iteration cycles before some conclusions could be drawn about the nature of the solution; let alone the convergence. However, well converged solutions *were* obtained in this region. The state u(0.4,0.0) of these isolated 2-cell solutions increased with increasing Dn up to a certain Dn. These Dn are marked by the circles in Figures 4.8a and 4.8b. Beyond these Dn, the results first showed a tendency to converge *very* slowly. The residuals were of the order of 10^{-3} to 10^{-4} and the percentage decrease of these residuals over 1,000 outer iteration cycles was of the order of 0.05. When Dn was increased a little further, the results neither converged nor diverged, no matter how many iteration cycles were carried out. The residuals oscillated slightly around 10^{-3} and 10^{-4}, but the percentage difference between f_1-Re and f_2-Re stayed as low as 10^{-1}. The results exhibited very slow divergence with further increase in Dn. Eventually they jumped to the 4-cell solution. The corresponding Dn values are marked by the triangles in Figures 4.8a and 4.8b. The critical Dn_{2-4} should lie in the

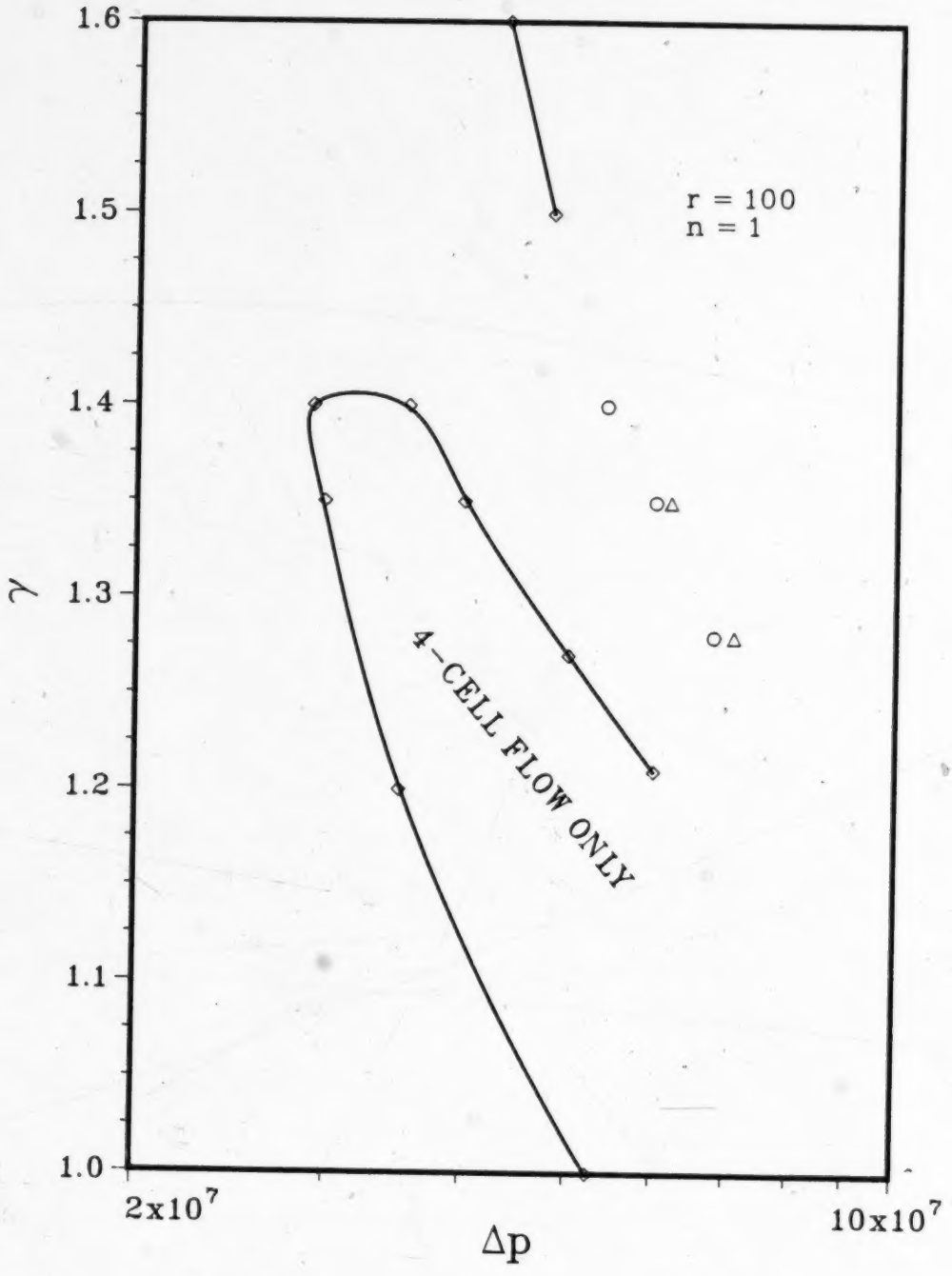

Fig. 4.8a The discontinuity in the Δp_{2-4} locus.

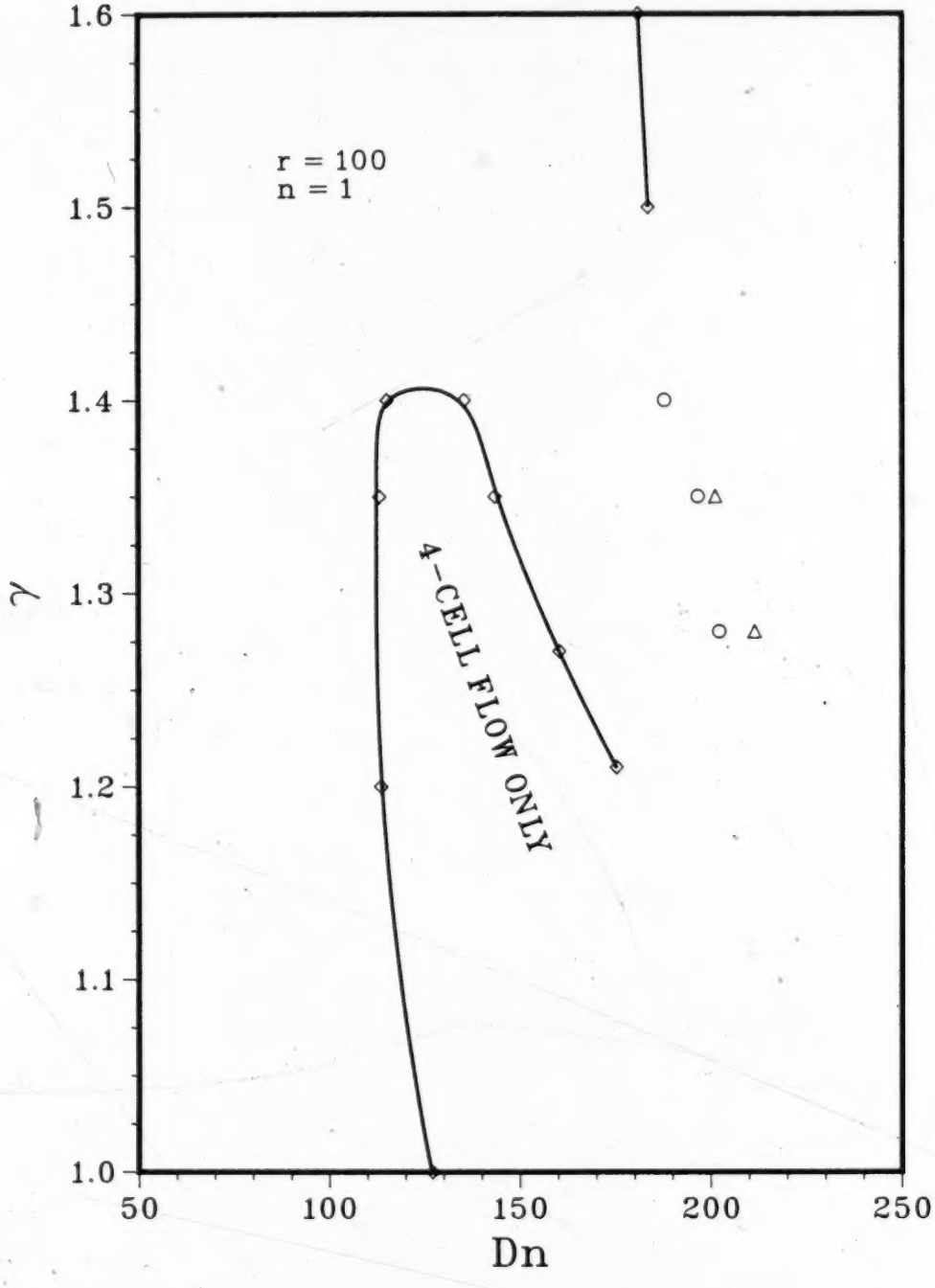

Fig. 4.8b The discontinuity in the Dn_{2-4} locus.

region limited by these circles and triangles. The 3-point central difference scheme as used in this study is incapable of locating the Dn_{2-4} precisely in this region.

The Moore and Spence algorithm used by Winters and Brindly(1984) can locate the limit points (Dn_{2-4} and/or Dn_{4-2}) precisely. However it is also limited by the fact that a very good initial guess is needed in order for the algorithm to converge to the precise limit points.

It is noteworthy that Nandakumar et al.(1985) has also observed a similar behaviour of the critical locus corresponding to the 2-cell to 4-cell transition around $\gamma=1.4$ in buoyancy-induced secondary flow in horizontally placed straight rectangular pipe.

A set of computations was carried out at $\gamma=1.35$ in order to make sure that the jumps occur at the points predicted by the critical loci. A high order grid of 41x29 was used and small steps in Δp were taken. The jumps did occur as predicted.

Figures 4.9a and 4.9b show all three branches of the stable solutions at $\gamma=1.35$, as located in this study. The hysteresis shown in these figures are already explained. The isolated branch of stable 2-cell solutions at high Dn is inaccessible if Δp is *slowly* increased from the trivial solution at constant γ. Figure 4.9a, having β as the state function, may be misleading for it seems to suggest that the

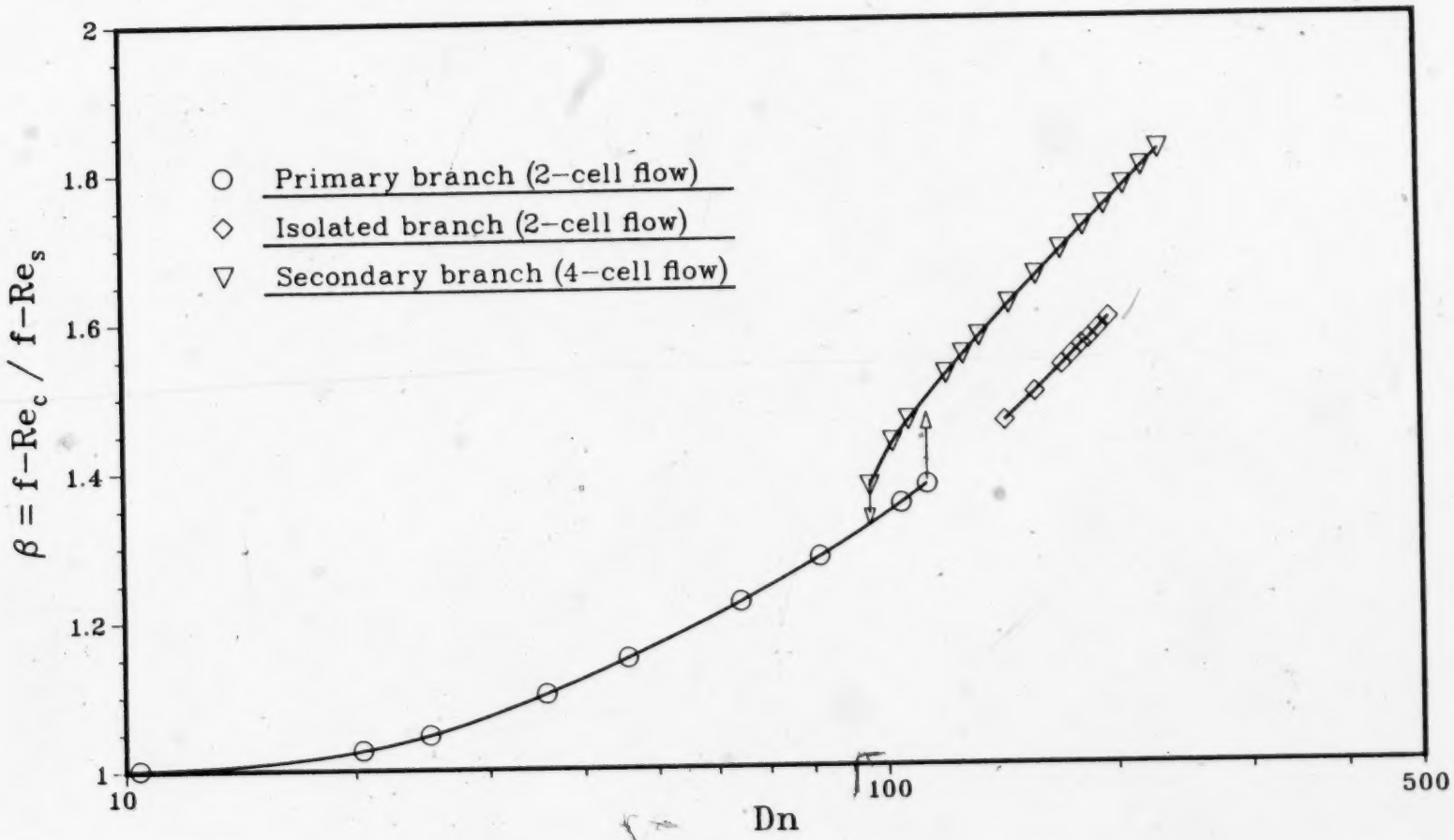

Fig. 4.9a Friction factor results for $\gamma = 1.35$ & $r = 100$

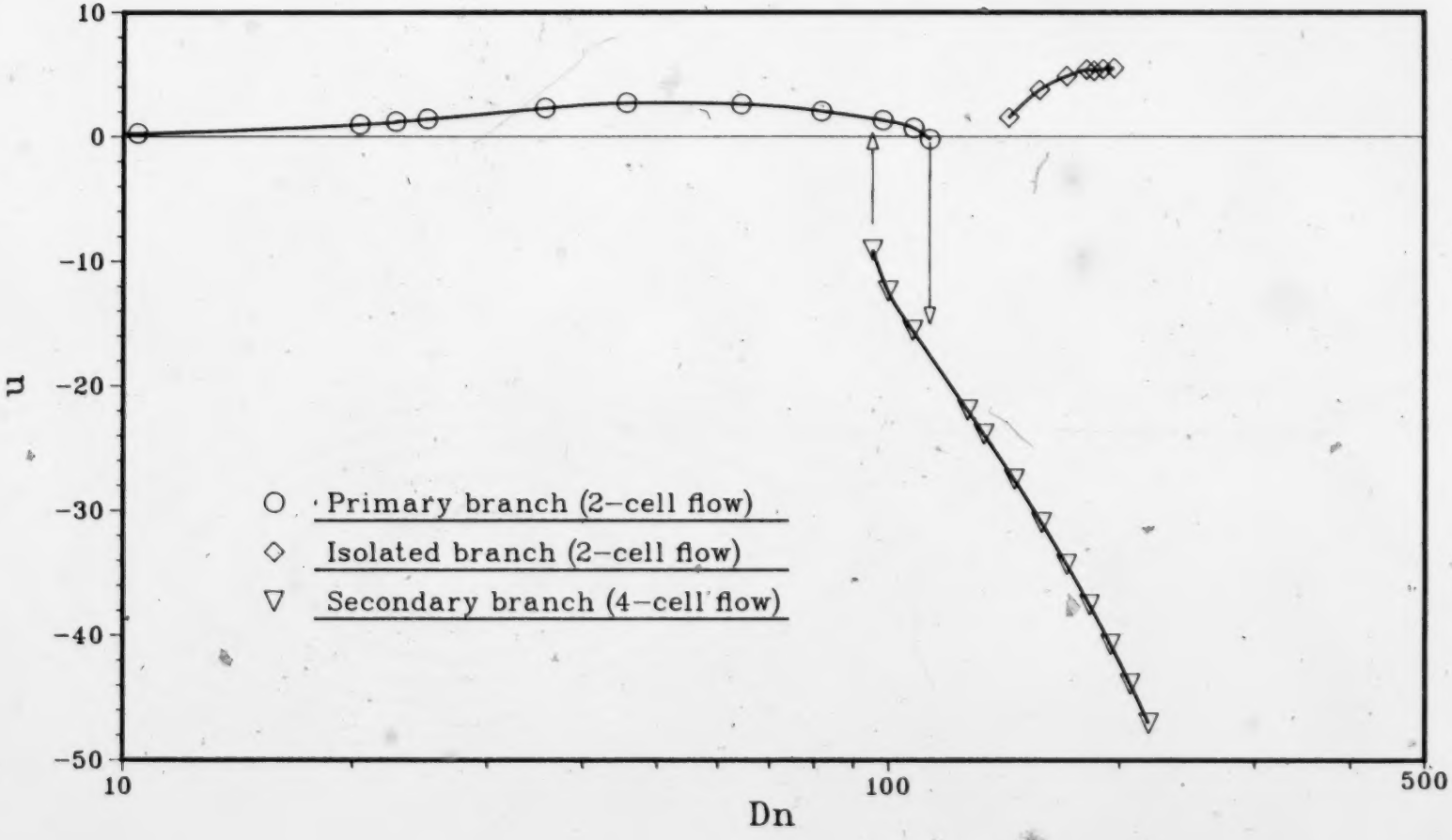

Fig. 4.9b u at x = 0.4 & y = 0 for $\gamma = 1.35$ & r = 100

isolated branch of 2-cell solution can be a part of the primary branch of 2-cell solution. Figure 4.9b, having u(0.4,0.0) as the state function, is an excellent representation of the solution behaviour. It shows that all three branches are *distinctly different* from each other.

The evolution of u(0.4,0.0) along the primary and/or the isolated branches is illustrated in (a) through (h) of Figure 4.10, for various aspect ratios. The end points of the primary branches mark the critical Dn_{2-4}. The arrows drawn mark the critical Dn_{4-2}. The isolated branches are shown in Figures 4.10(d) and (e) for γ=1.35 and 1.4, respectively. The fact that the isolated branch is not shown in other aspect ratios does not necessarily mean that it does not exist. The primary and the isolated branches move towards each other when γ is raised from 1.35 to 1.4 (Figures 4.10(d) and (e)) and they merge into one somewhere in between γ=1.4 and 1.5. This is the same range of γ where the discontinuity in the Dn_{2-4} locus was first located (Figure 4.7). Consequently the primary branch exhibits a local minimum at γ=1.5 (Figure 4.10(f)) in addition to the maximum which it so far experienced. The existing maximum losses it's uniqueness at γ=1.6 with the birth of a new maximum (Figure 4.10(g)), the embryo of which can be observed in the locus at γ=1.5 itself (Figure 4.10(f)). The end points which mark the critical Dn_{2-4} at γ=1.5 are found to be very close to the maximum of the u(0.4,0.0) locus. It is interesting to note that the numerical evaluation of the

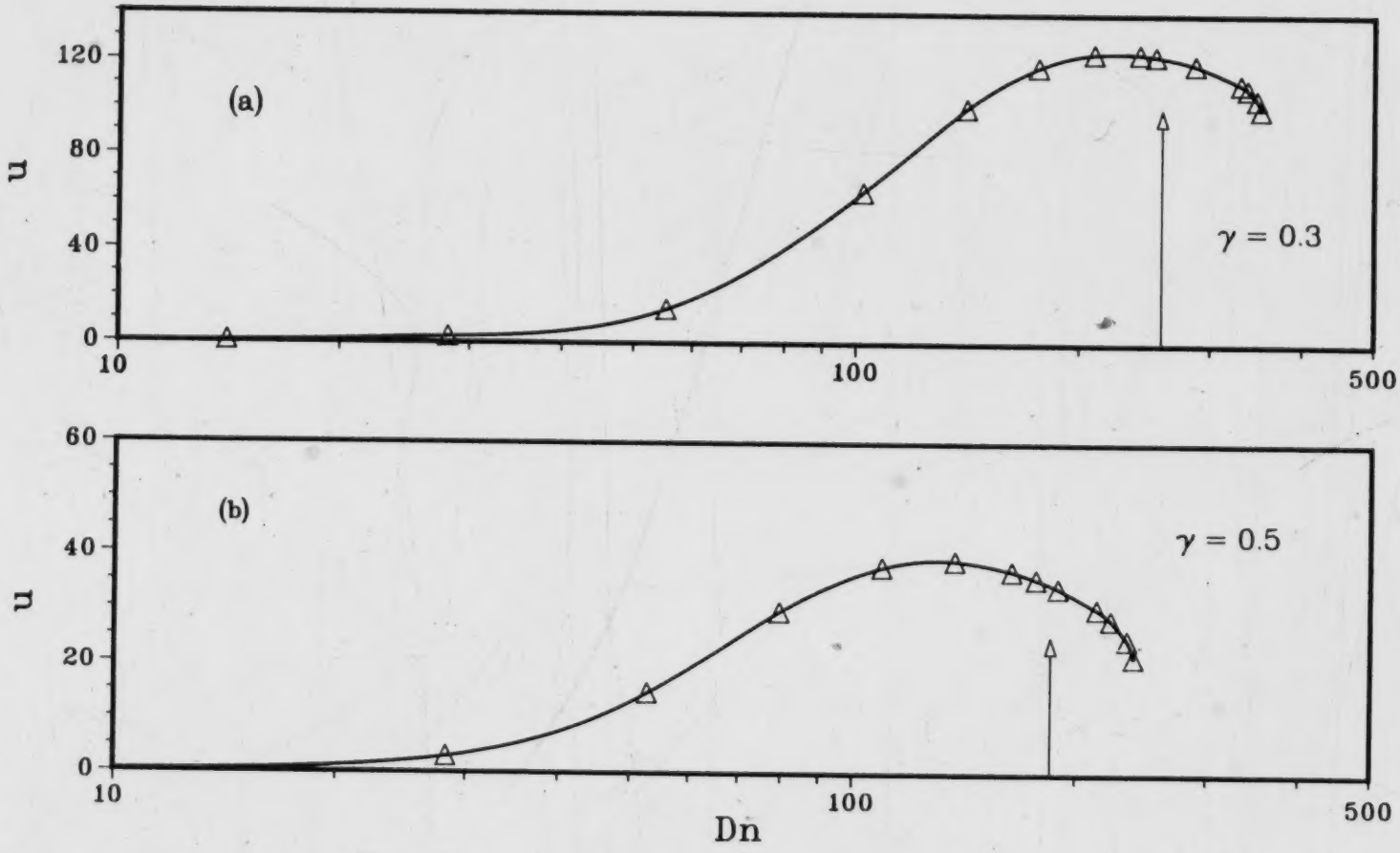

Fig. 4.10 u at x = 0.4 & y = 0 for various aspect ratios at r = 100

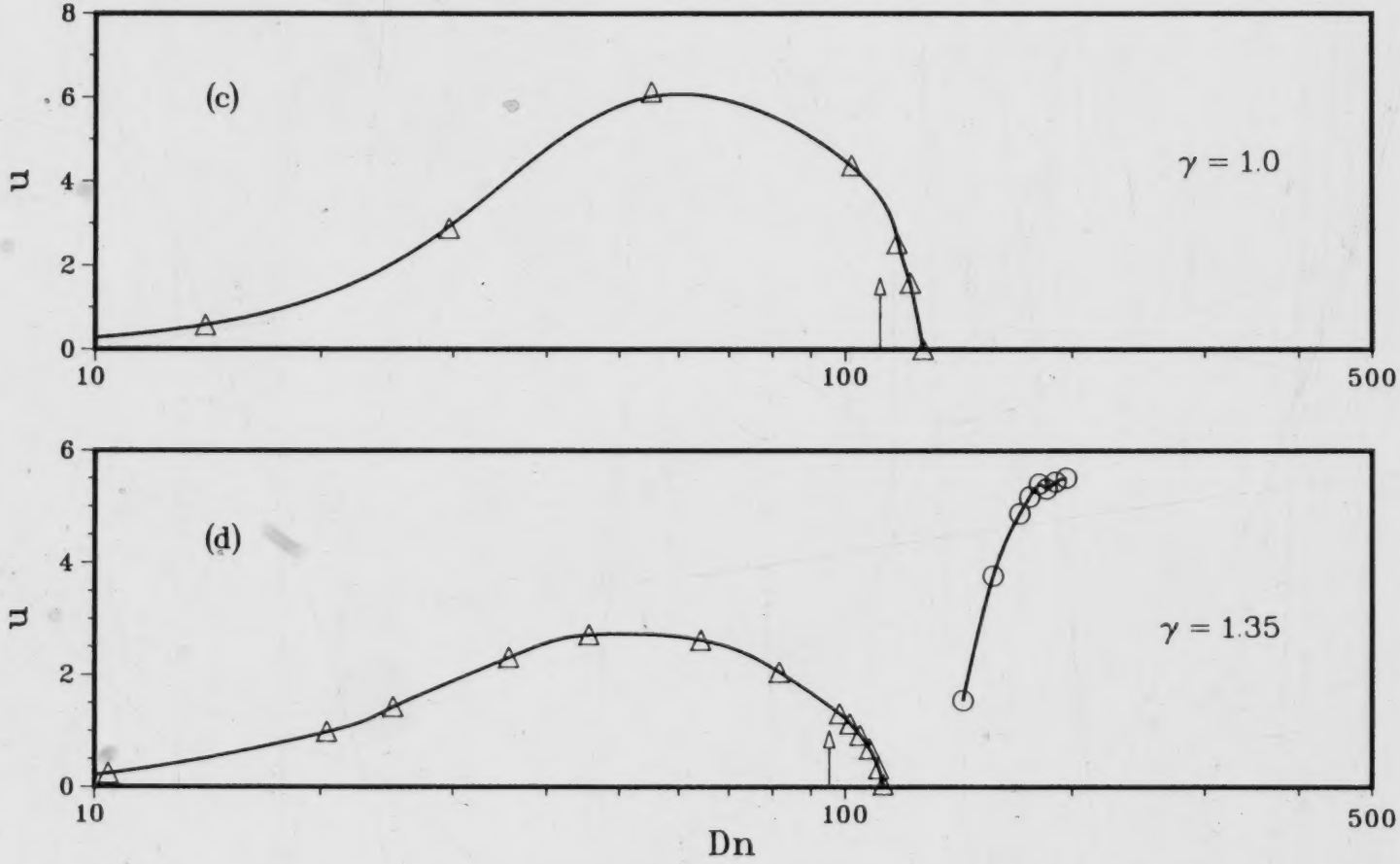

Fig. 4.10(contd.) u at x = 0.4 & y = 0 for various aspect ratios at r = 100
(Triangles – Primary branch ; Circles – Isolated branch)

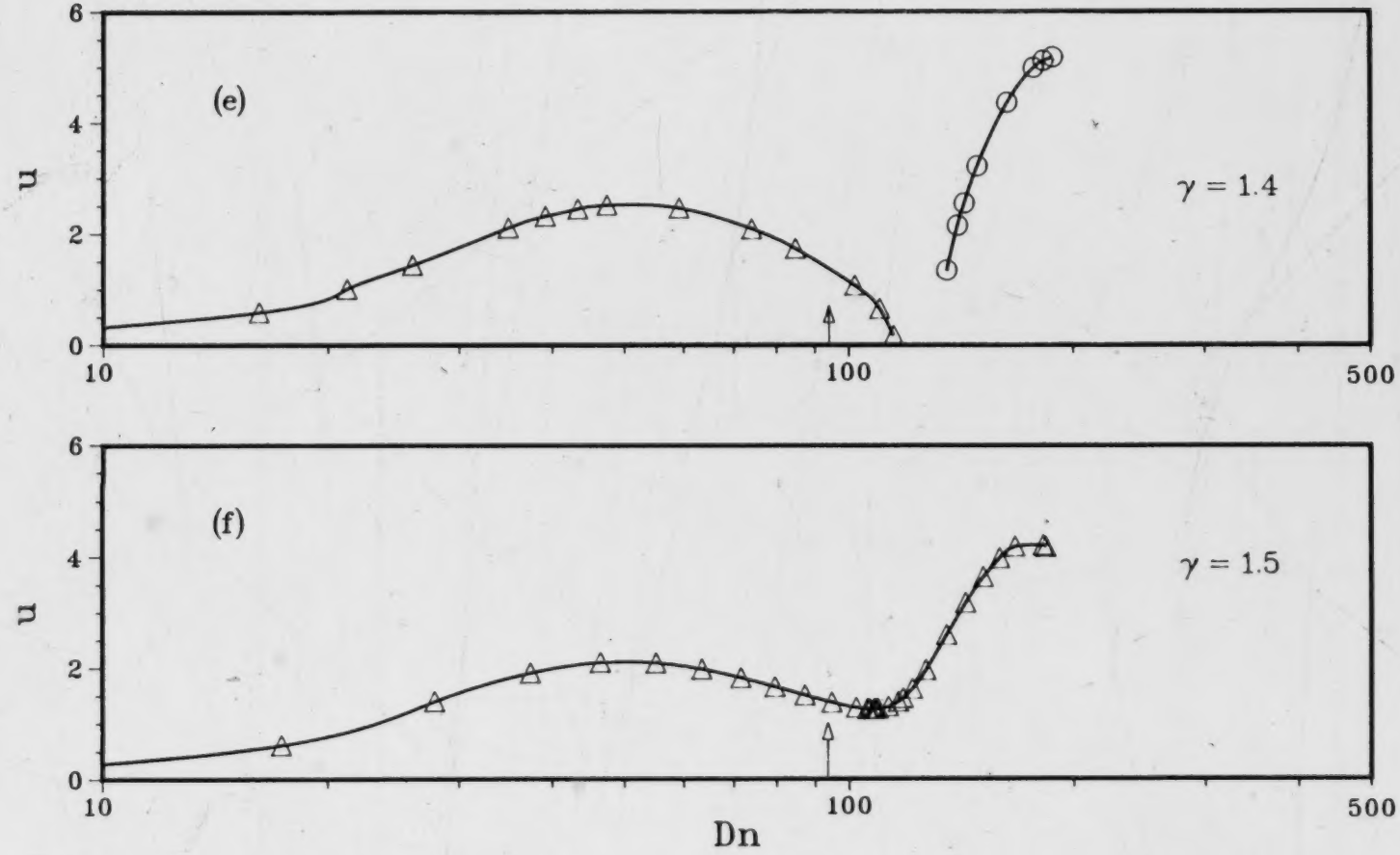

Fig. 4.10(contd.) u at x = 0.4 & y = 0 for various aspect ratios at r = 100
(Triangles – Primary branch ; Circles – Isolated branch)

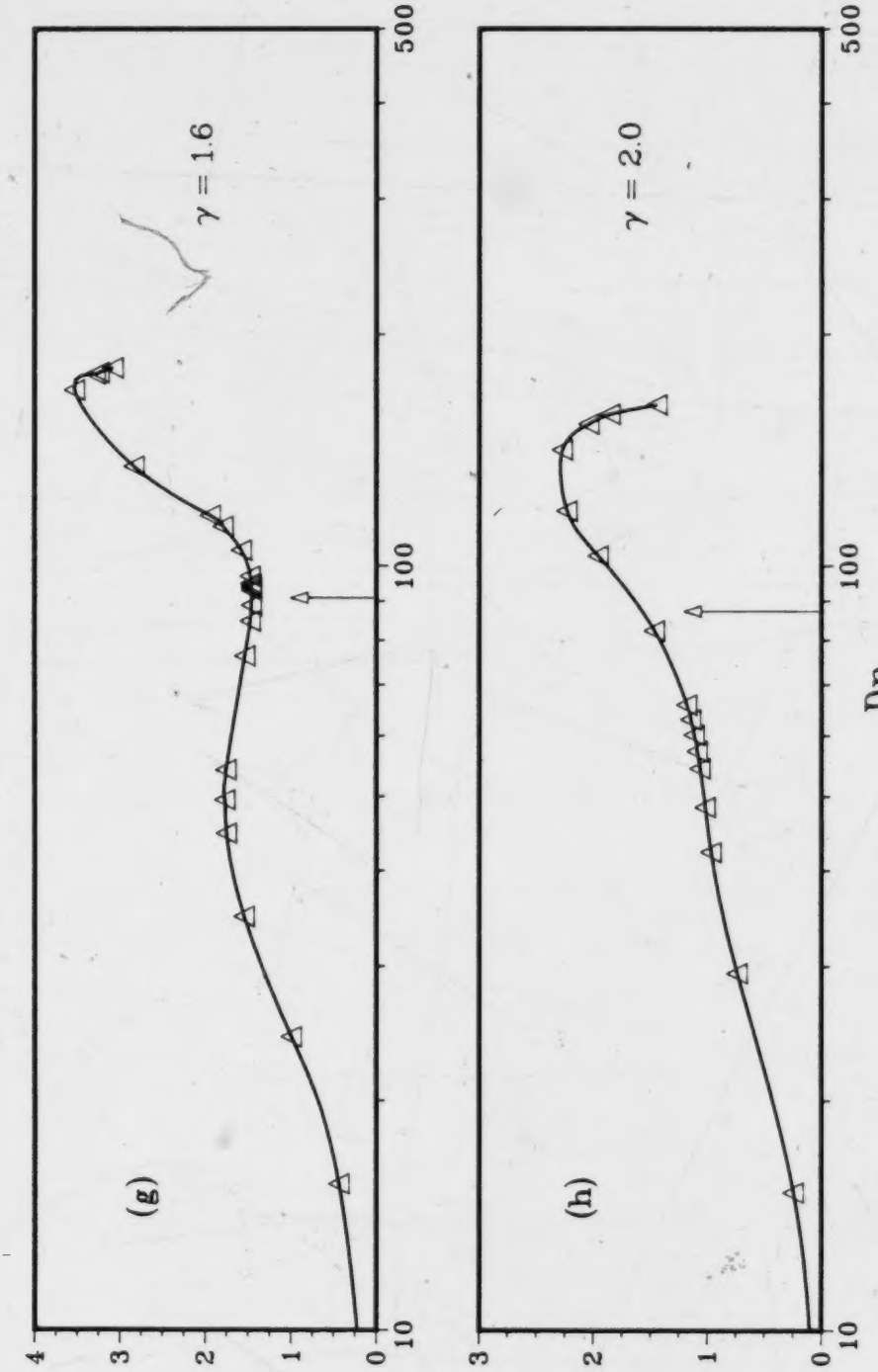

Fig. 4.10(contd.) u at x = 0.4 & y = 0 for various aspect ratios at r = 100

Dn_{2-4} at γ=1.5 was comparatively difficult. As γ is raised further the older maximum and minimum tend to even out and the new maximum is strengthened (Figure 4.10(h)). Just above γ=2.0, once again the primary branch might exhibit only *a maximum* as in the cases of $\gamma \leq 1.4$.

The above established isolated 2-cell solution branch may 'explain' the earlier observations of Cheng et al.(1976) and Winters and Brindly(1984) regarding the reappearance of the 2-cell solution at high Dn. Cheng et al. observed it at Dn=520 for square pipe of r=4; Winters and Brindly for square pipe of r=25. However these researchers have reported such phenomenon occurring when marching along constant γ lines. As illustrated in the state diagrams of Figures 4.3 and 4.9b, the u(0.4,0.0) along the 4-cell branch increases rapidly with increasing Dn. This denies the possibility of the 4-cell solution jumping back to the 2-cell solution when Dn is *slowly* increased along constant γ lines. Nevertheless bigger steps in Δp (or Dn) along constant γ can result in a greater perturbation of the solution algorithm causing one type of solution to switch to the other. In order to clarify this fact, bigger steps in Δp along γ=1 for a pipe of r=4 were attempted at high Dn. The solution algorithm diverged. Whereas smaller steps in γ resulted in well converged 4-cell solutions even up to Dn=610, beyond which oscillating results were observed.

At high values of Dn, the 3-point central difference scheme coupled with the Gauss-Siedel point iterative procedure seems to require a very good initial guess for ψ, Ω and w. It avoids high perturbation of the solution algorithm. The line iterative method and the Gaussian elimination method coupled with the 3-point central difference scheme as Cheng et al.(1976) used or the finite element method of solution as Winters and Brindly(1984) employed might allow such perturbations (meaning larger step in Δp at high Dn). However firm conclusions regarding these solution procedures cannot be drawn without closely examining such methods.

4.3 Modelling

Having confirmed the above mentioned features of the pressure-driven curved flow, the next and the important step is to give, a unified view of the behaviour of the solution in the range of Dn and γ investigated at constant curvature (r=100).

Bimodality, sudden jumps and hysteresis are few of the many features of the elementary models of Catastrophe theory (Zeeman 1977). With u(0.4,0.0) as the state function and Dn and γ as the control parameters, a folded surface that is typical of the elementary catastrophe models can be obtained. The critical Dn loci (Dn_{2-4} and Dn_{4-2}), reproduced in Figure 4.11, can be thought of mapping the

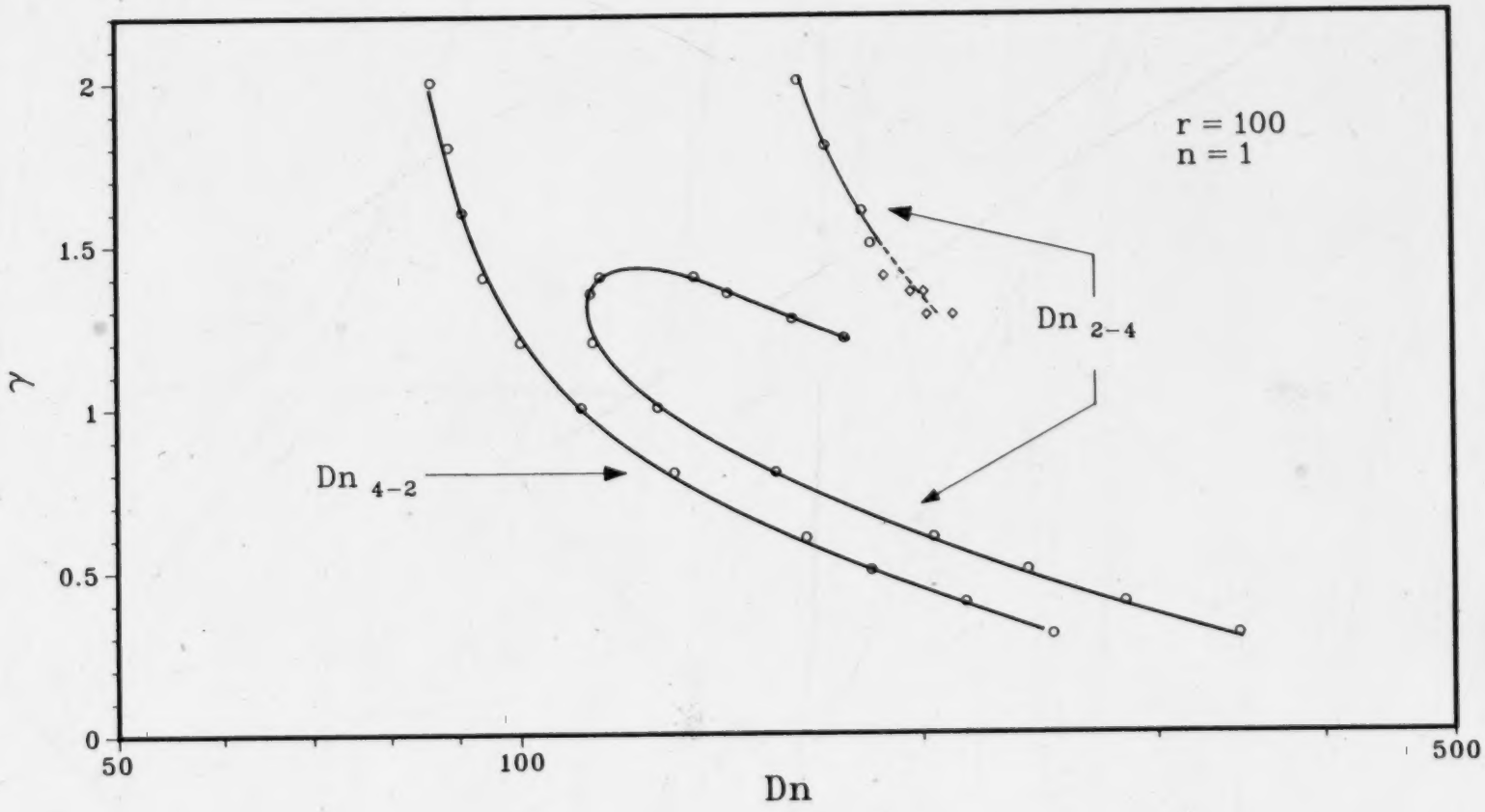

Fig. 4.11 The loci of limit points. Solid curves are of (±)1 accuracy in Dn; Dotted curve is approximate.

boundaries of the fold on such a surface. The series of state loci shown in (a) through (e) of Figure 4.12 clearly demonstrate this folded surface, speculated in this study. These loci are drawn with the guidance of Figures 4.10 and 4.11 and the numerical results tabulated in Appendix B, but they are not drawn to scale.

The solid curves of Figure 4.12 represent the stable solutions obtained in this study. The dotted curves corresponding to the middle sheet of the folded surface should be representing the 'unstable' solutions of the flow equations. The numerical scheme of this study is incapable of locating these unstable solutions and thus the existence of which is subjected to further verification in future. If the portions of these state loci representing the stable solutions are denoted by +1 and the 'unstable' solutions by -1 (the Leray-Schauder index), they also satisfy the generic properties of bounded flows stated by Benjamin(1976,1978a,b). According to Benjamin, except at critical points of the state loci, the number k of possible flows is odd and at least $\frac{1}{2}(k-1)$ of them are unstable. The bounded shape of the isolated branch (the limit point D) shown in Figure 4.12(b) and (c) needs to be confirmed in future.

This folded surface cannot definitely describe a fold-catastrophe model (see Section 5.2 for details) since it is well established that the state is indeed critically

(a) $\gamma = 1.0$

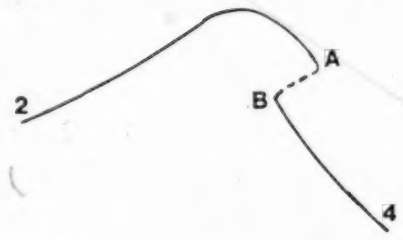

(b) $\gamma = 1.35$

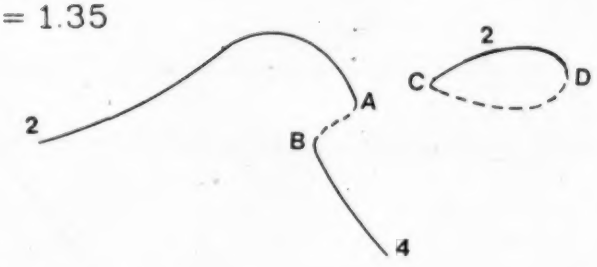

(c) $1.4 < \gamma < 1.5$

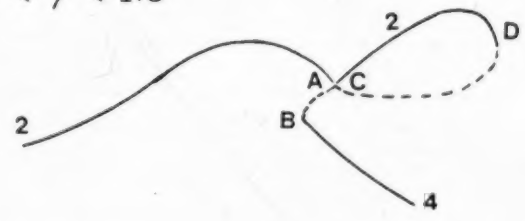

Transcritical bifurcation

(d) $\gamma = 1.6$

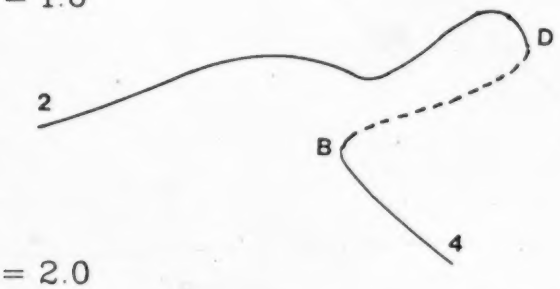

(e) $\gamma = 2.0$

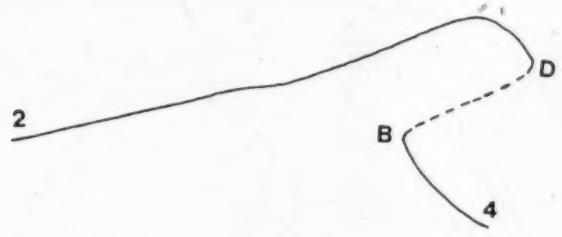

Fig. 4.12 The state loci u at (x=0.4,y=0) Vs Dn at different γ (not drawn to scale).

controlled by both Dn and γ. In order for this surface to represent the cusp-catastrophe model it misses one important feature, the 'cusp point'. Figure 4.11 seems to suggest that the cusp point can possibly be located at the lower range of $\gamma(<0.3)$ and at high Dn(>350). However it was extremely difficult to obtain meaningful numerical results in this region without employing a very high grid since the gradient are very steep at low values of γ. Computing time prohibited such exploration. Therefore it is necessary to analyze the merits and demerits of the results in order for them to fit a cusp-catastrophe model.

Firstly it is well known that the cusp point can exist only in the region where divergence in the state behaviour is feasible. Within the range of γ=0.3 to 2.0, low values of Dn always support clear 2-cell solutions only. That is why the orientation of the folded surface of Figure 4.11 is very different from those of Benjamin and Mullin (see Section 2.4). The region of low γ and high Dn, as Figure 4.11 shows, may allow the flow to settle into a 4-cell pattern as γ is increased slowly from very small values(!). This will lead to divergence and hence the cusp point. However there is a possibility for the critical Dn at low γ to grow so high that the flow might even leave the laminar region without answering whether there is a cusp point or not.

Figure 4.11 and Table 4.1 clearly shows that the difference between the critical values of Dn increases as γ decreases below 1.4. It may deny the possibility of speculating a cusp point at the region of low γ.

Table 4.1 The critical Dn for Newtonian fluids, located with ±1 accuracy.

γ	Dn_{2-4}	Dn_{4-2}
1.4	115	94
1.2	114	100
1.0	127	111
0.8	155	131
0.6	204	164
0.5	240	183
0.4	284	215
0.3	351	258

There is a possibility for the 4-cell flow to become the primary flow at low Dn region at large enough γ. This is an ideal situation to realize the divergence of state behaviour and hence the cusp point. Benjamin(1978b) in the bounded Taylor problem (see Section 2.4) and Fung et al.(1985) in the buoyancy-induced secondary flow problem have observed cusp point belong to 2-4 transition in this region of γ. Multiple cusps in a 2-control parameter space

is not unusual in catastrophe theory. The pair of cusp-catastrophes revealed by the Duffing equation is one example (Zeeman 1977).

Another interesting feature of this study is the boundary of the stable 2-cell solution surface. This boundary is incompletely mapped by the Dn_{2-4} locus in Figure 4.11. As stated in Section 4.2, the numerical scheme used in this study is incapable of mapping the Dn_{2-4} locus efficiently in this region. The performance of this scheme was also inferior when the Dn_{2-4} search was carried out in the region above γ=2.0. Even though well converged 2-cell solutions were easily observed in the region bounded by γ=2.2 and 3.0, locating the critical Dn_{2-4} precisely was a difficult task. The squares in Figure 4.13 mark the Dn up to which well converged 2-cell (primary) solutions were *easily* observed. Beyond which, very small steps in Dn was needed ; oscillations were set up otherwise. Due to the excessive computing effort involved, not many computations were carried out in this region. The region above γ=3.0 was also not explored except for the few results obtained at γ=5.0.

Figure 4.13 shows that the 2-cell (primary) solutions in the region bounded by γ=2.0 to 3.0 extend beyond the critical Dn_{2-4} at γ=2.0. This points out that the Dn_{2-4} locus may be facing another discontinuity in this region. This possibility is strengthened by the state loci of

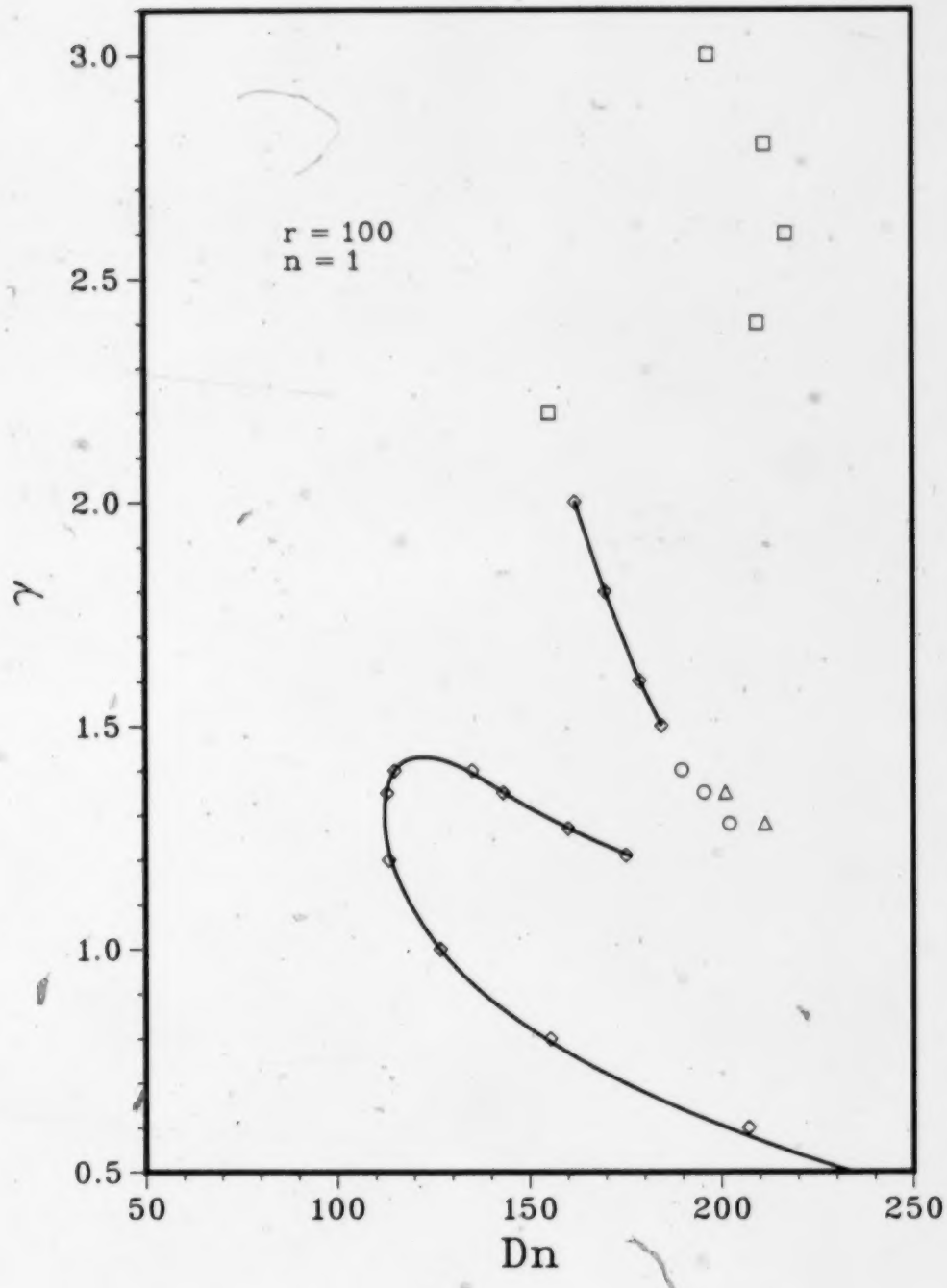

Fig. 4.13 An indication to the extent of the stable 2-cell solution surface.

Figure 4.14.

Figures 4.14(a) and (b) show the u(0.4,0.0) loci at γ=2.4 and 3.0 respectively. They are incomplete in the sense that the end points of these loci do not represent the boundary of the primary 2-cell solution surface precisely. The state locus of γ=2.4 (Figure 4.14(a)) exhibits a local minimum as in the cases of γ=1.5 and 1.6 (Figures 4.10(f) and (g)). Beyond this point the u(0.4,0.0) increases sharply. This locus reveals the fact that somewhere in between γ=2.0 and 2.4, the locus representing the primary 2-cell flow merges with the locus representing the isolated 2-cell flow (Transcritical bifurcation). The state locus at γ=3.0 (Figure 4.14(b)) resembles the state locus at γ=2.0 (Figure 4.10(h)). The evaluation of the critical Dn_{2-4} was also comparatively easier at γ=3.0 than at γ=2.4. These observations confirm the recurrence of the series of events illustrated by Figure 4.10 in the range of γ=2.0 to 3.0, and hence another turning point in the Dn_{2-4} locus associated with the isolated 2-cell solution.

At this point it was confirmed that the influence of the length scale on the stability charecteristics of the flow is not only crucial but also repetitive. This repetitve feature has to be researched further for it might answer the question of why the length scale influences the flow stability in the way it does. The oscillating nature of the results often encounted in the neighbourhood of the

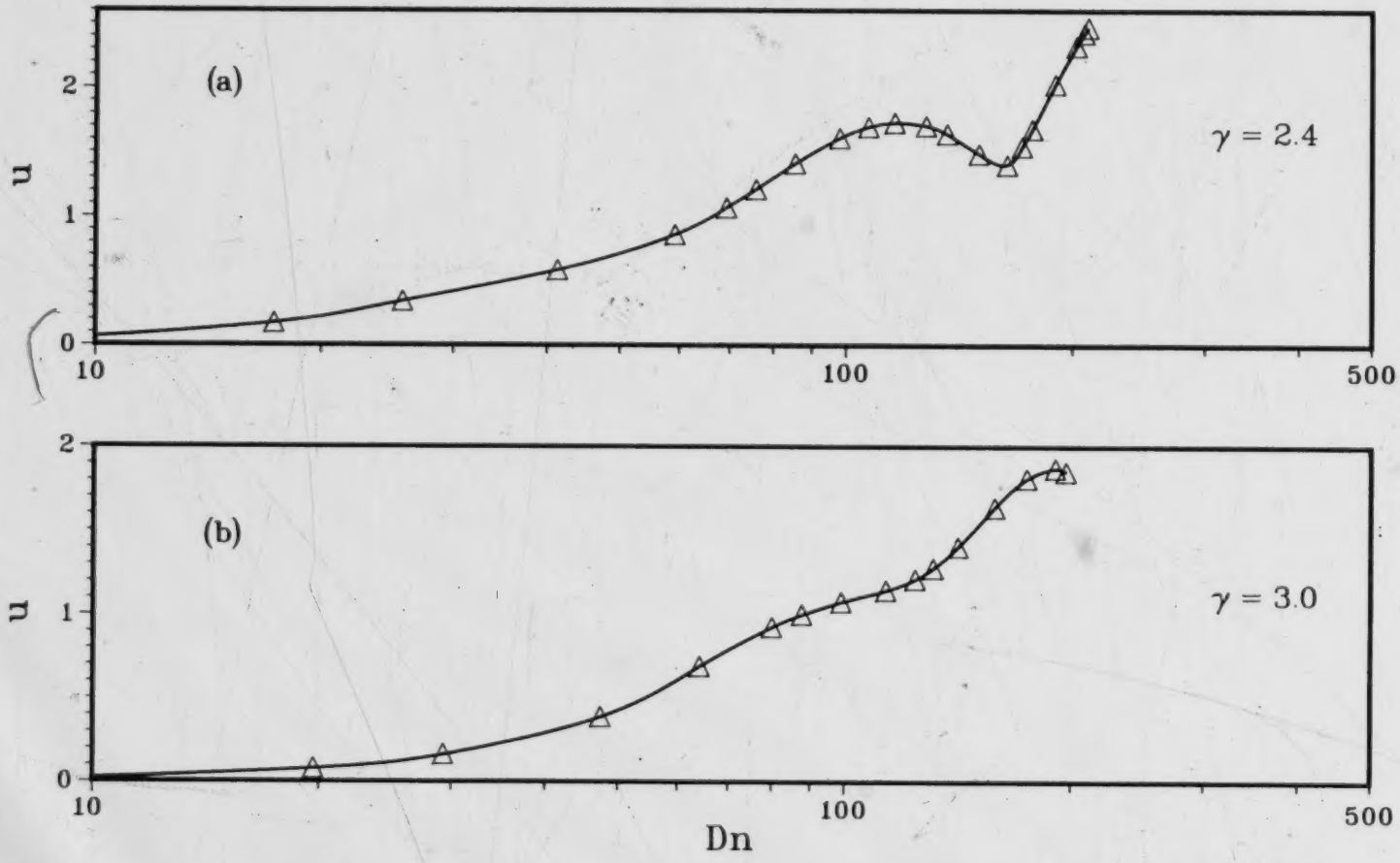

Fig. 4.14 u at x = 0.4 & y = 0 for $\gamma = 2.4$ & 3.0 at r = 100

2-cell solution surface boundary suggests, perhaps, the flow equations be formulated including the transient terms for further research. That might bring about more interesting features of the solution structure, marginally stable solutions for example, of the curvature induced secondary flow in finite sections.

4.4 Curvature Effects

The curvature of the pipe certainly influences the strength of the centrifugal force field experienced by the fluid. The control parameter Dn, defined as $Re/\sqrt{r}$, incorporates the curvature effects in it to a certain extent. This is shown by the state loci of Figures 4.15 and 4.16. The state is β in Figure 4.15 and u(0.4,0.0) in Figure 4.16. The results at r=100, 10 and 4 for square pipes are presented in these figures by the solid, dotted and dashed curves respectively. These curves exhibit a *slight* shift in the increasing direction of Dn when the curvature is increased. This shift is *comparatively* larger at high curvatures and shows that the function of Dn in accounting for the curvature effects is inferior for highly curved pipes, even though not critical.

The critical Dn values for square pipes of different curvatures are listed in Table 4.2. The critical Dn at r=25 is of Winters and Brindly(1985) and has been located precisely. The rest are obtained in this study within ±1

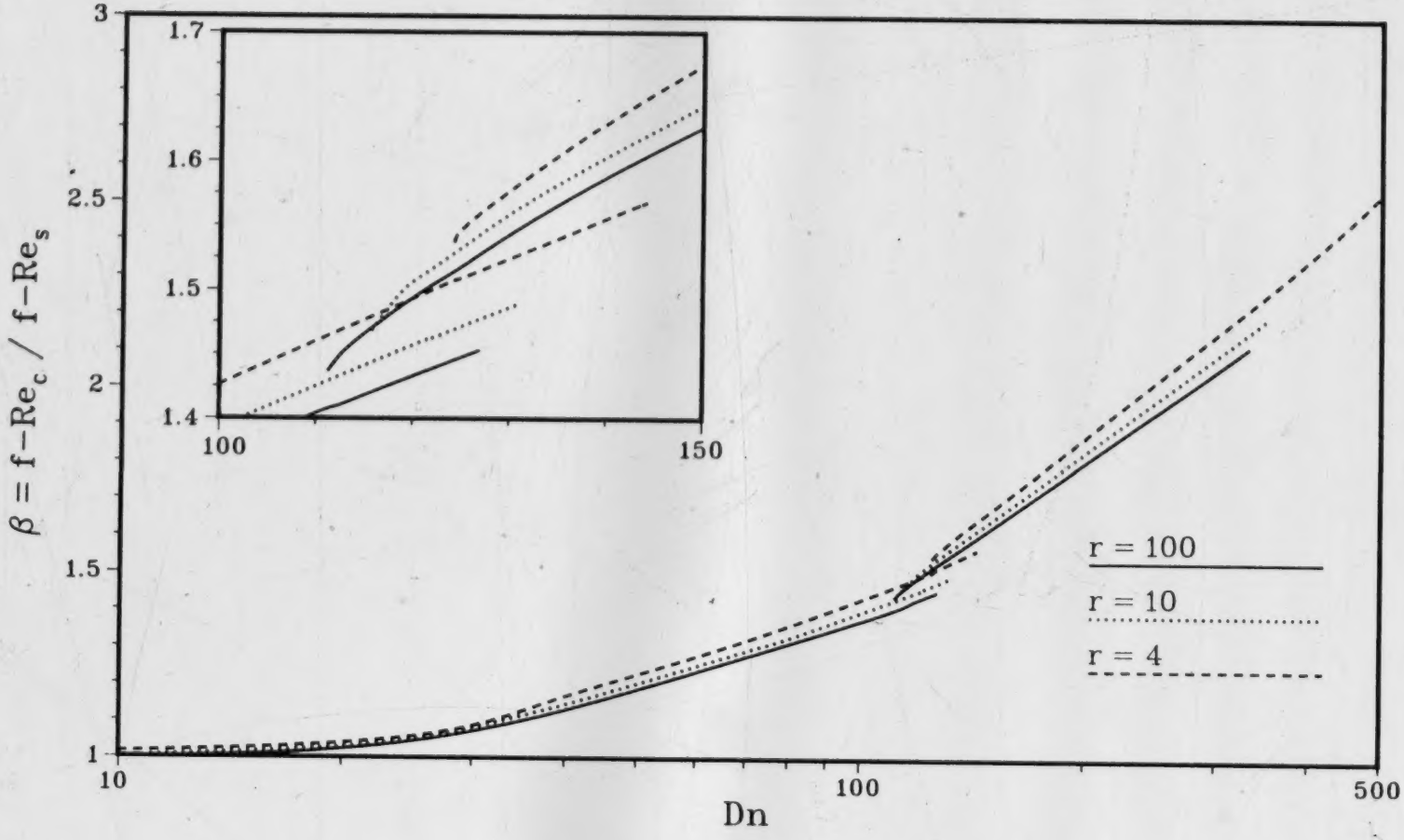

Fig. 4.15 Friction factor results for square pipes of r = 100, 10 & 4

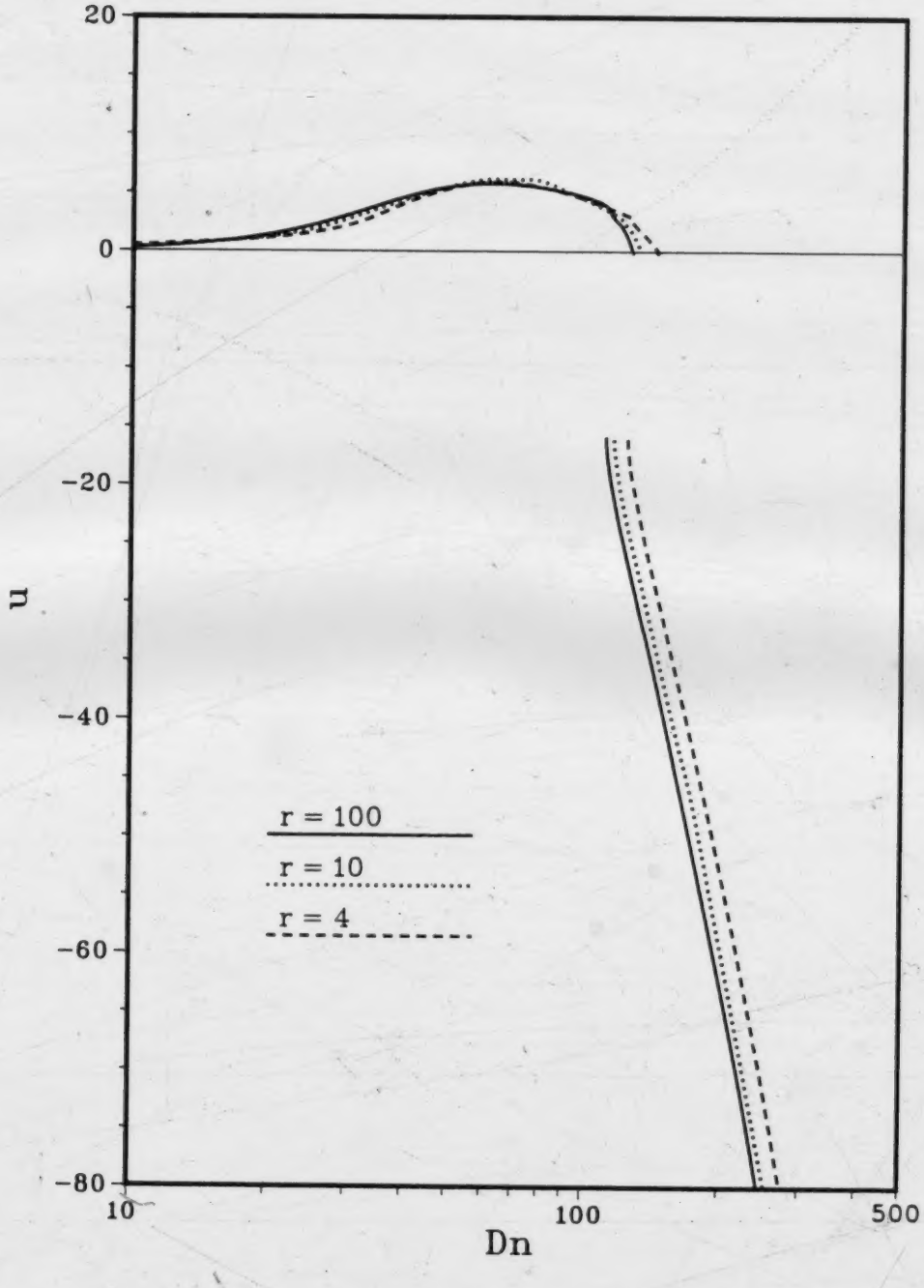

Fig. 4.16 u at x = 0.4 & y = 0 for square pipes of r = 100, 10 & 4

accuracy. The critical Dn are shifted to the increasing direction of Dn with increasing curvature as is the cases of Figures 4.15 and 4.16. Once again, this shift is large when the pipe is highly curved.

From the results discussed above one can conclude that the radius of curvature may not have a critical influence on the solution surface established in Section 4.3. However a slight shift of the critical loci in the Dn-γ space will be unavoidable with the changing curvature.

Table 4.2 The critical Dn for square pipes of different curvatures

r	Dn_{2-4}	Dn_{4-2}
100	127	111
25	-	113.24
10	133	115
4	144	124

CHAPTER 5

RESULTS AND DISCUSSION
PART II - POWER-LAW FLUIDS

The model for the flow of power-law fluids varies from that of Newtonian fluids only in one aspect. The viscosity is now a non-linear function of the velocity gradients, not a constant (see Section 3.1). This introduces an additional non-linearity into the equations governing the helical motion of the fluid as in Equations 3.32 and 3.33. The degree of this additional non-linearity is determined by the power-law index, n, and it vanishes altogether when n is unity (for Newtonian fluids). The influence of the index n on the stability characteristics of the solution (established in Chapter 4) is analyzed in Sections 5.1, 5.2 and 5.3, within the range of n=0.6 to 1.4. A square pipe is chosen for this purpose.

The frictional resistance experienced by the power-law fluids in the curved square pipe is discussed in Section 5.4 since it is the first time such results have been obtained to the author's knowledge.

5.1 Dual Solutions

5.1.1 Influence of the Centrifugal Force

The influence of the centrifugal force (measured by Dn) on the solution structure of the power-law fluid is first demonstrated using a fluid of index n=0.7 in a square pipe of r=100. The characteristics of the stream function-axial velocity contour plots shown in Figures 5.1a and 5.1b are very similar to those of Newtonian fluid in square pipe of r=100 (see Figures 4.1a and 4.1b). The outward shift of the maximum axial velocity with increasing Dn, demonstrated by Figure 5.1a, can also be clearly seen in Figure 5.2. This figure consists of the axial velocity profiles along the line of symmetry y=0. The profiles of Dn=6.1,45.4 and 92.2 belong to the 2-cell solutions; those of Dn=102.4 and 176.5 belong to the 4-cell solution (see also Figure 3.6).

The profiles of the secondary velocity component u at y=0, given in Figure 5.3, are also very similar to the corresponding profiles of Newtonian fluid given in Figure 4.2.

The state locus, chosen to be represented by u(0.3,0.0) is shown in Figure 5.4. The qualitative nature of this locus is comparable with that of Figure 4.3 (Newtonian fluids). The features such as discontinuity, catastrophic jumps, hysteresis and bimodality (see Section 4.1 for details) are also revealed by the power-law fluid of n=0.7.

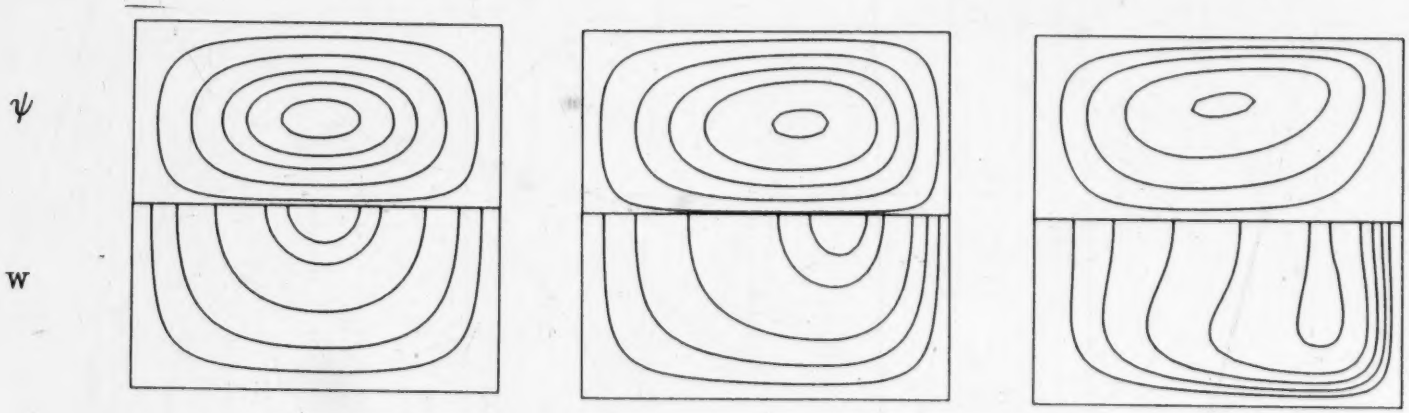

Fig. 5.1a Contour plots showing the 2–vortex flow at different Dn for $n = 0.7$, $\gamma = 1$ & $r = 100$

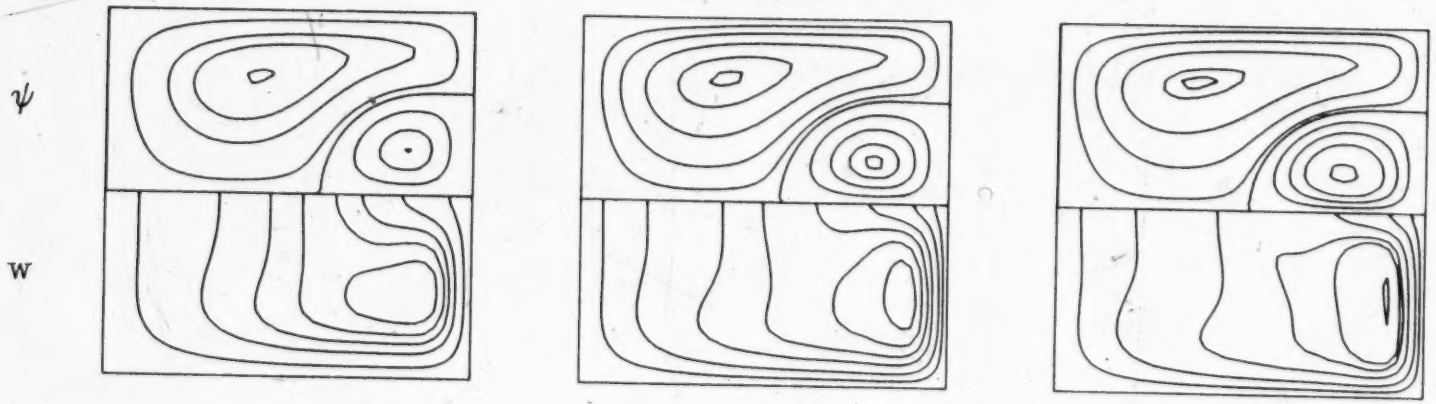

Fig. 5.1b Contour plots showing the 4–vortex flow at different Dn for $n = 0.7$, $\gamma = 1$ & $r = 100$

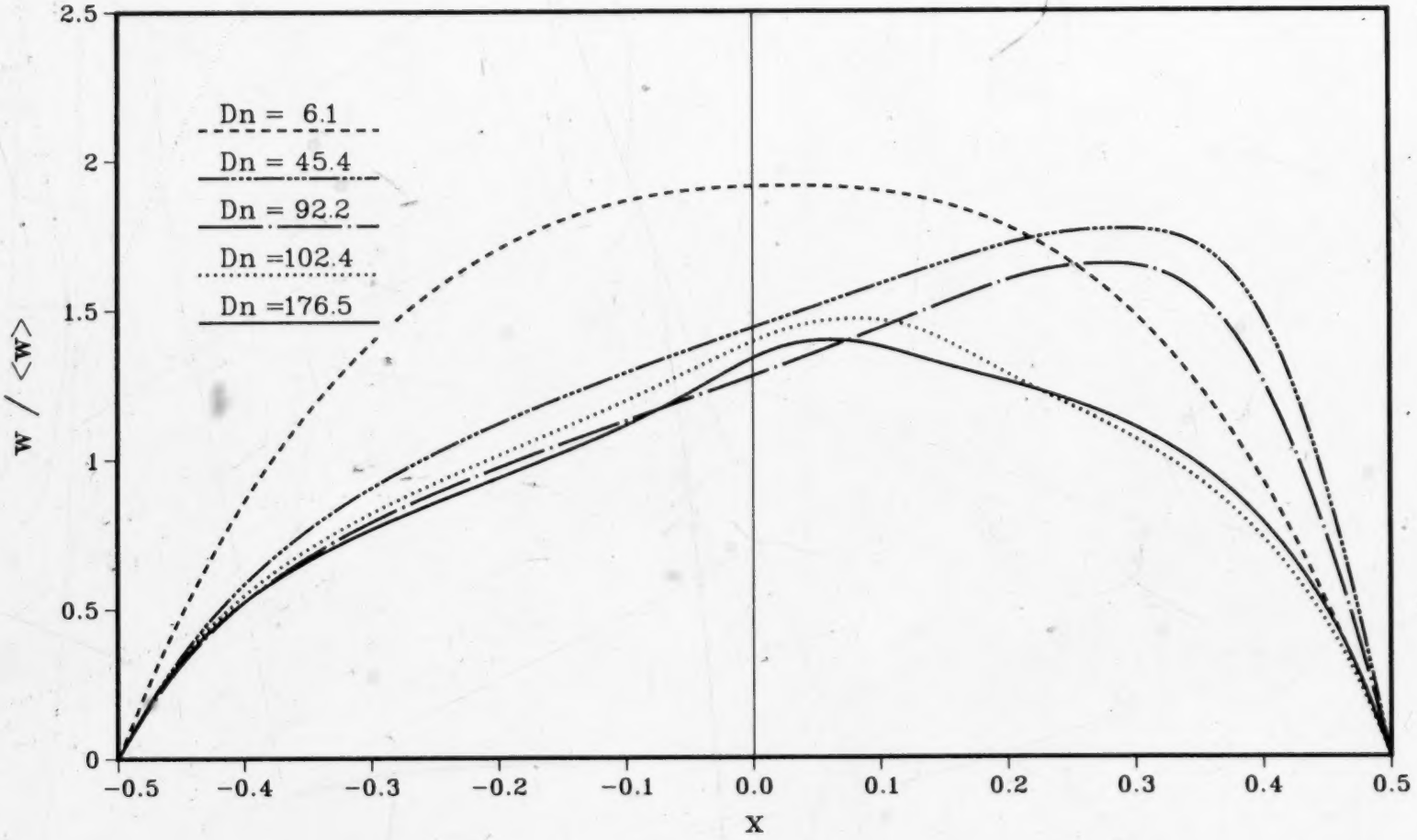

Fig. 5.2 Axial Velocity distribution at y = 0 for power−law fluid of n = 0.7 in square pipe of r = 100.

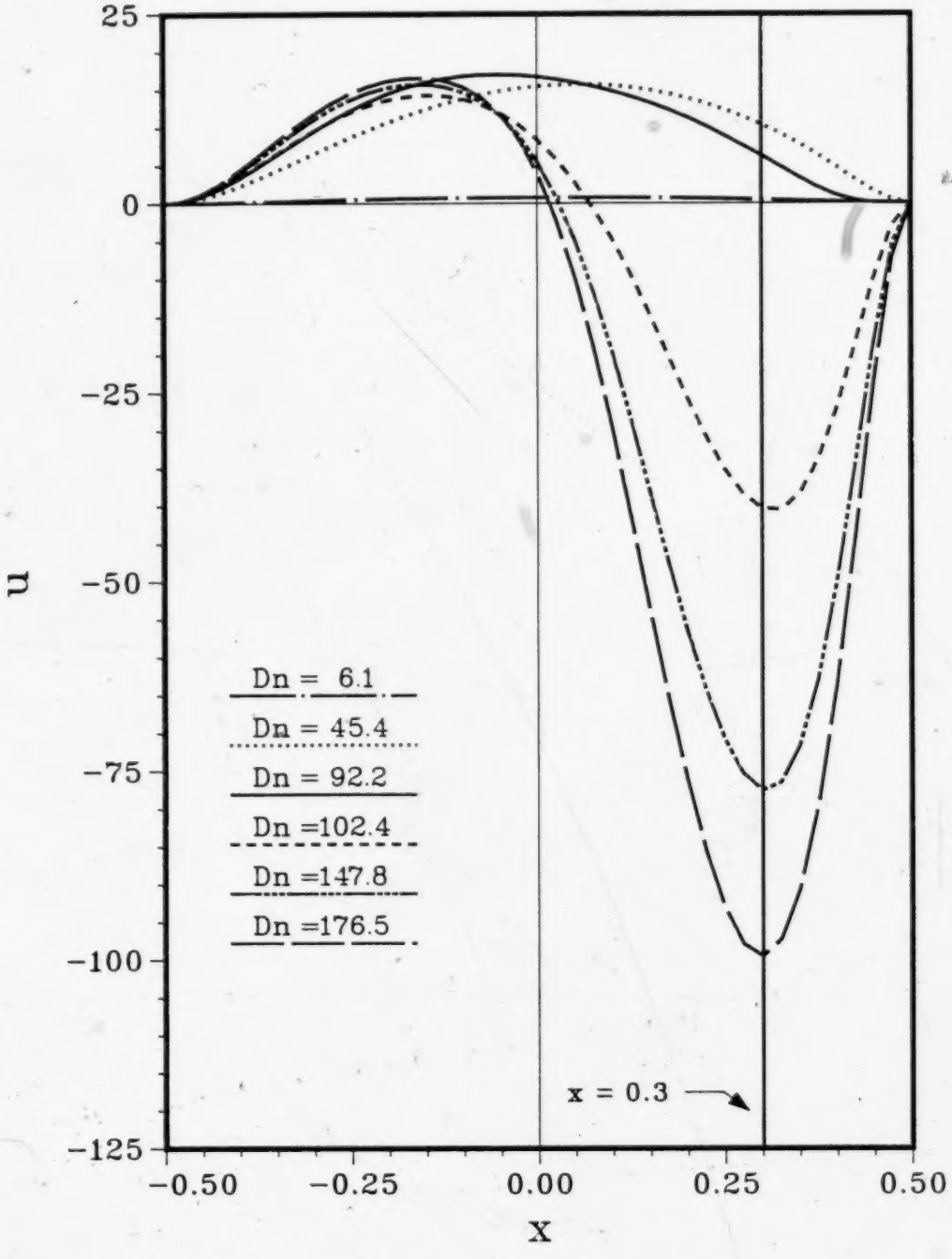

Fig. 5.3 u at y = 0 for a power-law fluid of n = 0.7 in a square pipe of r = 100

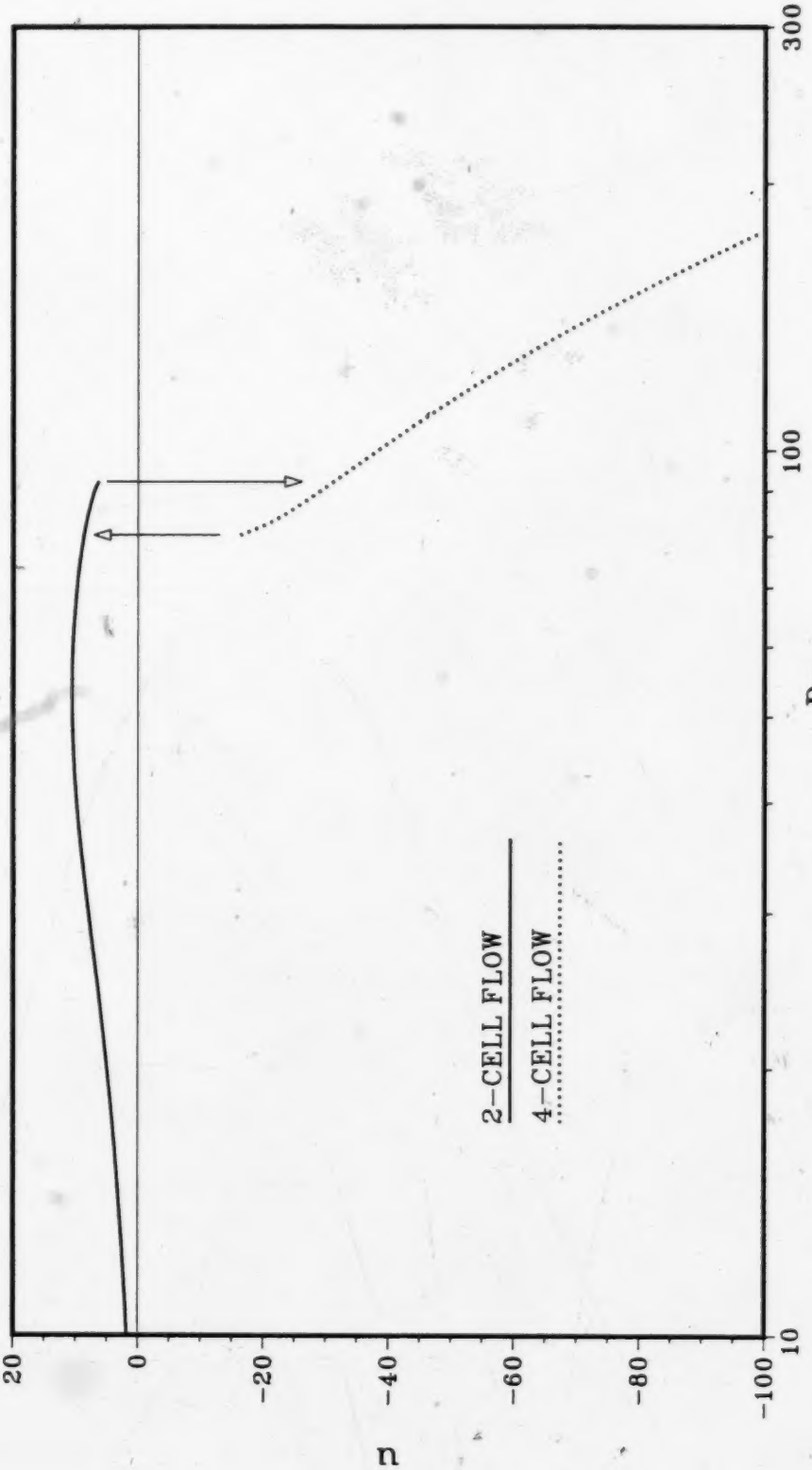

Fig. 5.4 u at x = 0.3 & y = 0.0 for n = 0.7 , $\gamma = 1$ & r = 100

5.1.2 Influence of the Power-law Index n

The series of stream function-axial velocity contour plots of Figure 5.5 at different values of n show the flow area that the additional vortices could possibly occupy. They are similar to each other, except for the axial velocity gradients close to the wall. In contrast, the additional vortices occupy distinctly different flow areas when γ is changed (see Figure 4.5).

The loci of the state function u(0.3,0.0) representing the 2-cell solution (primary) branch at different values of n are given in (a) through (d) of Figure 5.6. These plots do not significantly differ from each other as in the case of changing aspect ratio (see Figure 4.10).

The above established facts suggest that the non-linearity introduced by the power-law fluid, and hence the power-law index n, might not play a crucial role in determining the stability characteristics of the solutions to curved flow.

5.2 Modelling

The loci of the critical points, which mark the catastrophic jumps from one stable solution to the other, are drawn in Figures 5.7a and 5.7b. The critical axial pressure gradients are represented by Figure 5.7a and the

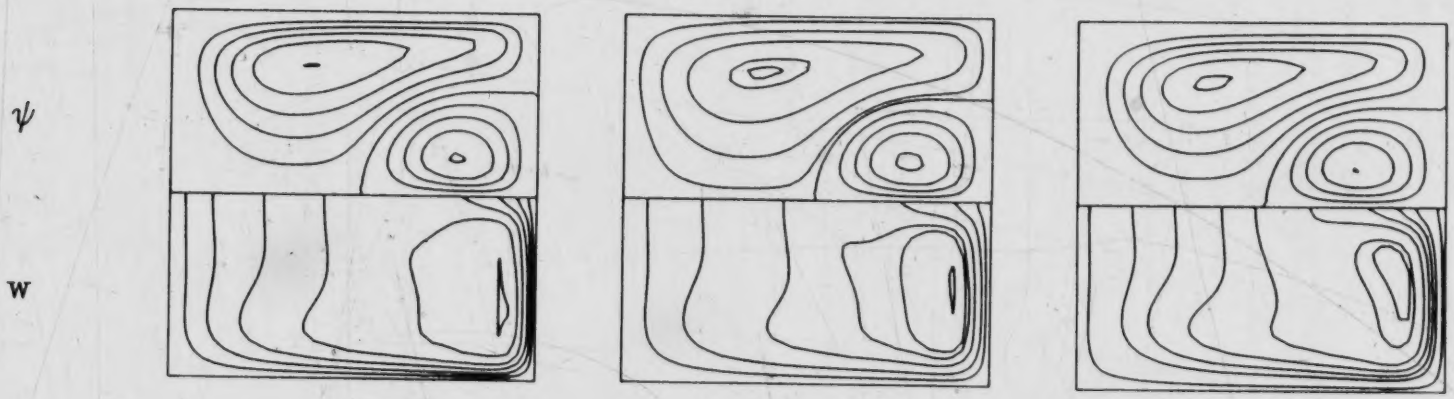

Fig. 5.5 Contour plots showing the flow area which the additional vortices could possibly occupy at different index n.

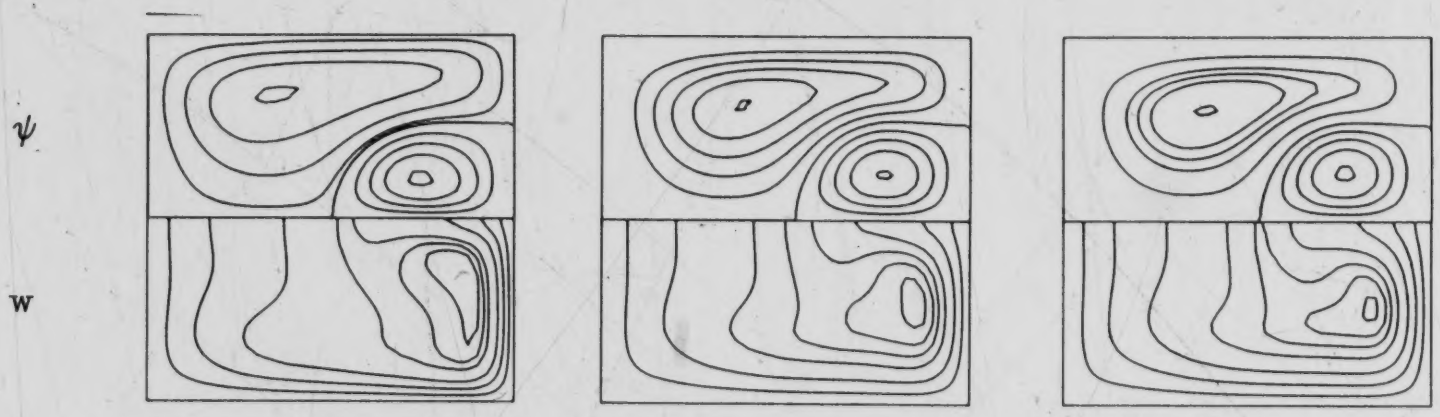

Fig. 5.5(contd.) Contour plots showing the flow area which the additional vortices could possibly occupy at different index n.

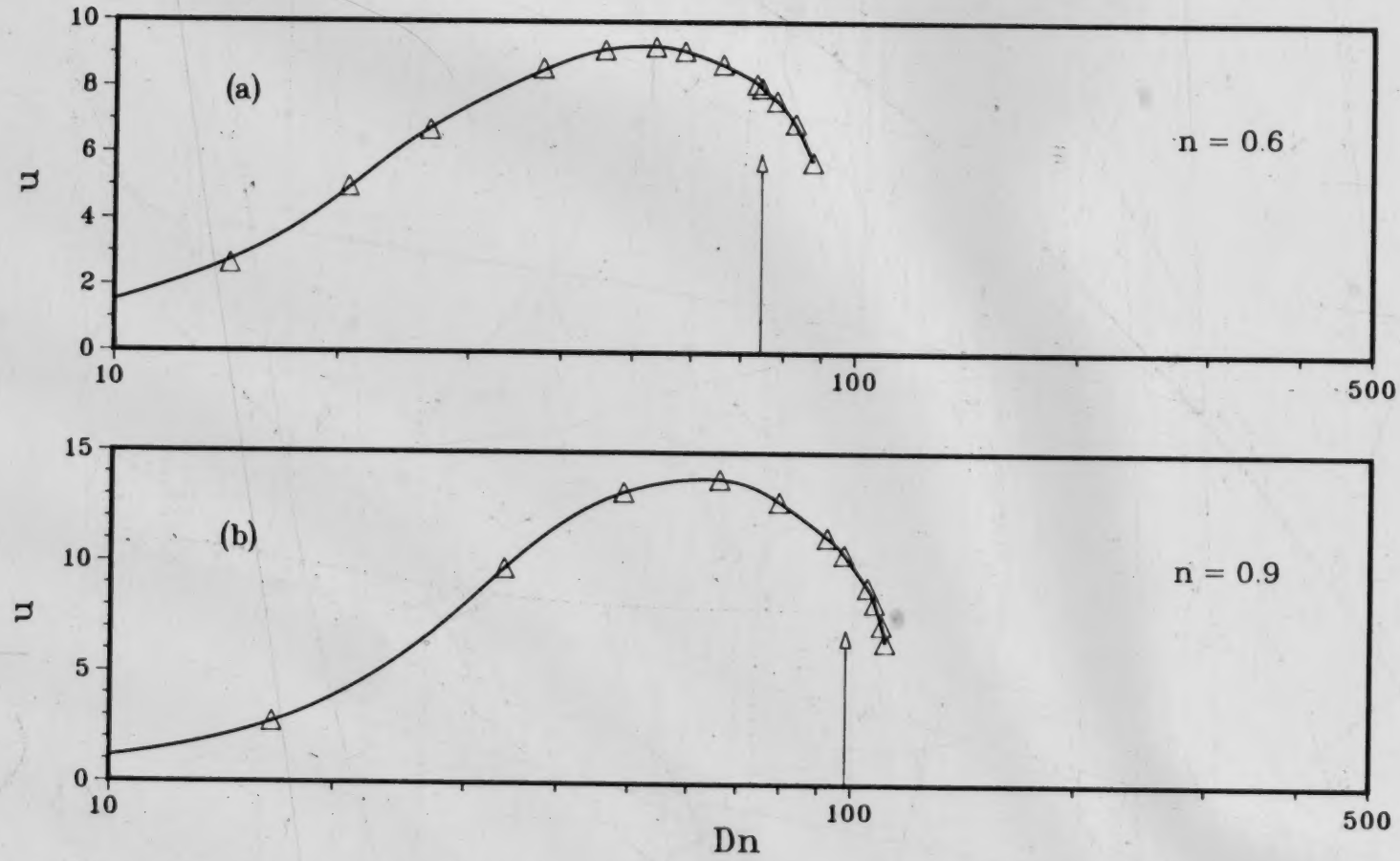

Fig. 5.6 u at x = 0.3 & y = 0 for various power–law indices at $\gamma = 1.0$ & r = 100

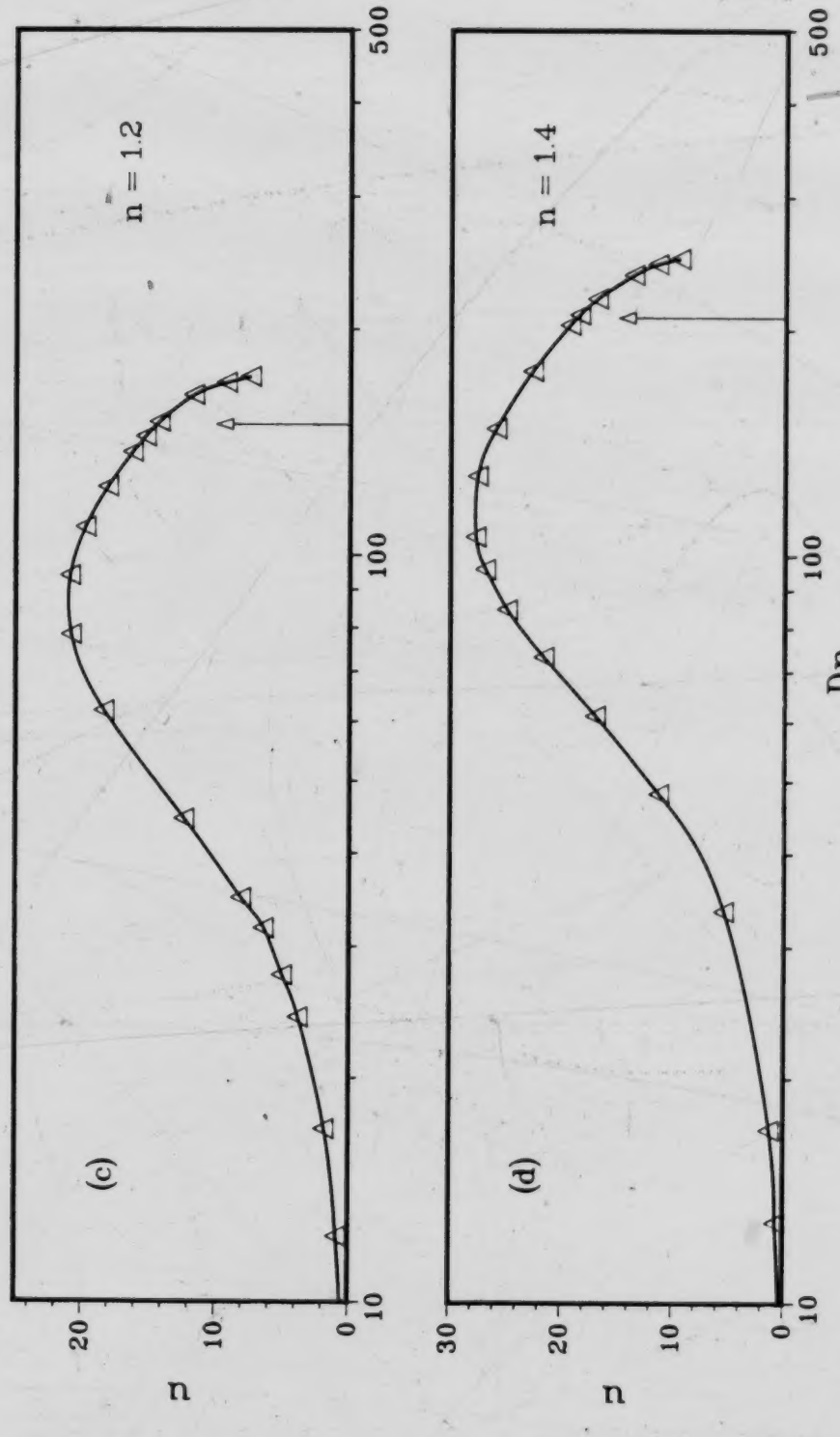

Fig. 5.6(contd.) u at x = 0.3 & y = 0 for various power–law indices at $\gamma = 1.0$ & r = 100

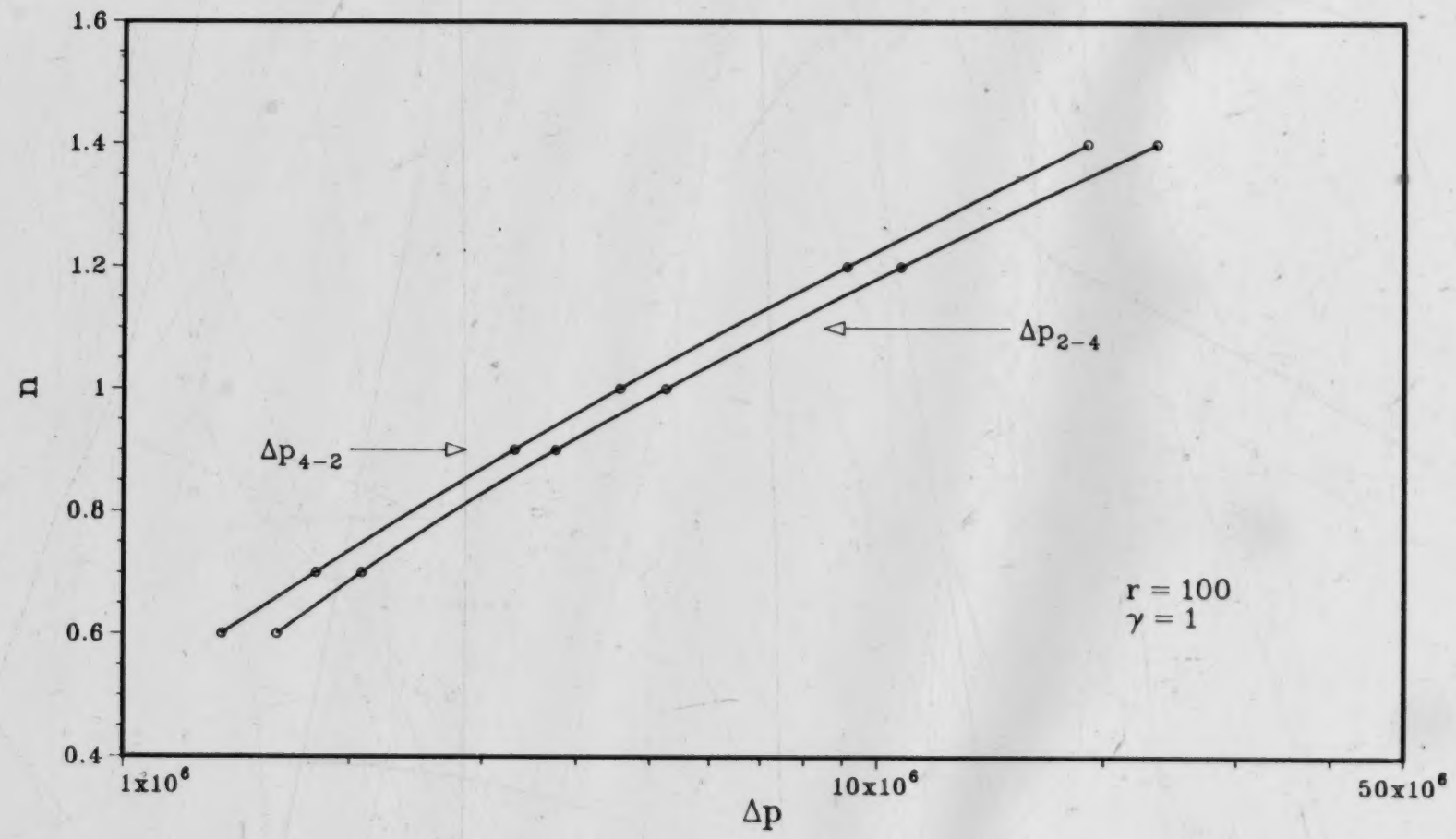

Fig. 5.7a The loci of limit points.

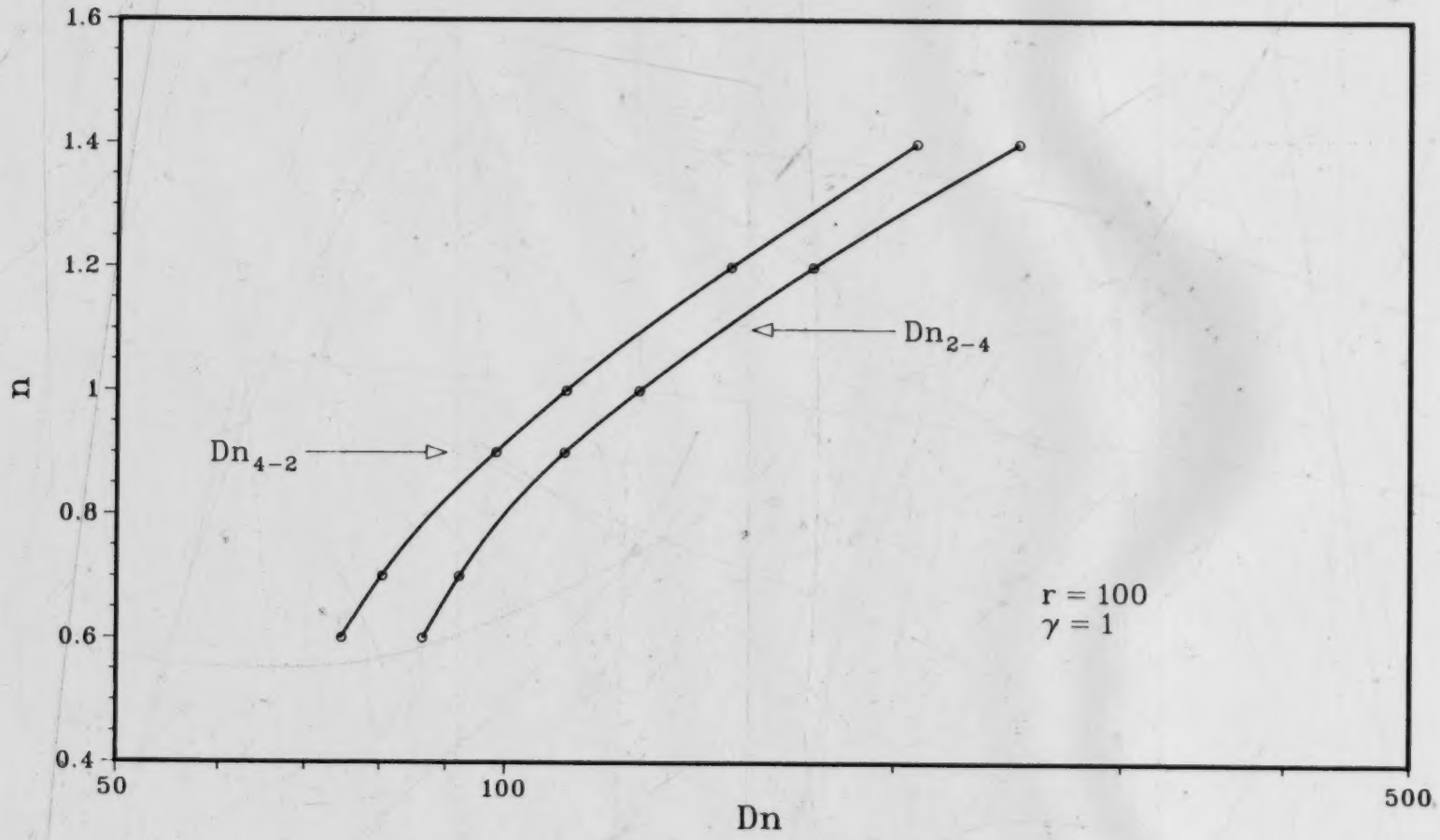

Fig. 5.7b The loci of limit points.

critical Dn by Figure 5.7b. The numerical values of these critical Dn are given in Table 5.1 below:

Table 5.1 The critical Dn for power-law fluids, located with ±1 accuracy.

n	Dn_{2-4}	Dn_{4-2}
1.4	249	207
1.2	173	149
1.0	127	111
0.9	111	98
0.7	92	80
0.6	86	75

These loci of Figure 5.7b can be thought of mapping the boundaries of the fold on a folded surface obtained with u(0.3,0.0) as the state function and Dn and n as the parameters. The folded surface can be identified with the simplest model of the Catastrophe theory , the 'fold-Catastrophe'. It is realisable when the state is controlled by only one parameter. In the present case, the control parameter is the Dn which represents the centrifugal force. The index n merely shifts the locations of the critical points in the Dn-n space. This is consistant with the results of Section 5.1.

5.3 Curvature Effects

The state loci of power-law fluid of index n=0.7 in square pipes of different curvatures are given in Figures 5.8 and 5.9. The solid and dashed curves represent the results for r=100 and 4 respectively. The scattered points represent the results for r=10.

For the square pipe of r=100, the critical Dn_{2-4} is 92(±1) and the critical Dn_{4-2} is 80(±1). For r=4, these critical values are 101(±1) and 86(±1) respectively.

The above results exhibit a slight shift in the increasing direction of Dn with increasing curvature. The close similarities between these results and the curvature effects on Newtonian fluids, discussed in Section 4.4, confirm the following fact; the radius of curvature r does not play any crucial role in determining the equilibrium solution surface provided Dn ($=Re/\sqrt{r}$) is chosen as one control parameter.

5.4 The Frictional Resistance

The axial pressure gradient required to generate a certain flow increases with increasing power-law index n as shown in Figure 5.10. In other words, the axial frictional resistance experienced by the fluids of different power-law indices are different when subjected to the similar external

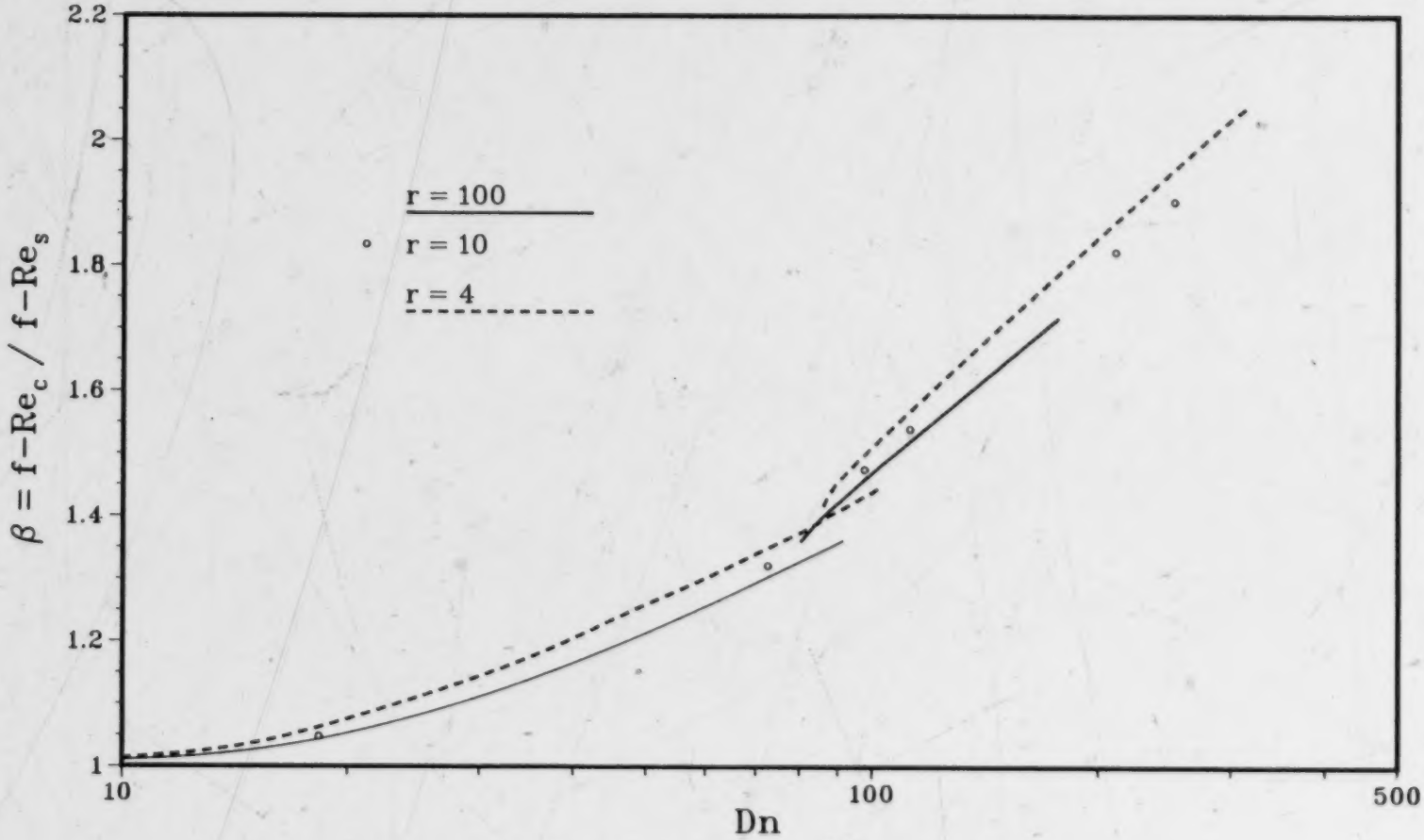

Fig. 5.8 Friction factor results for a power–law fluid (n = 0.7) in square pipes of r = 100, 10 & 4

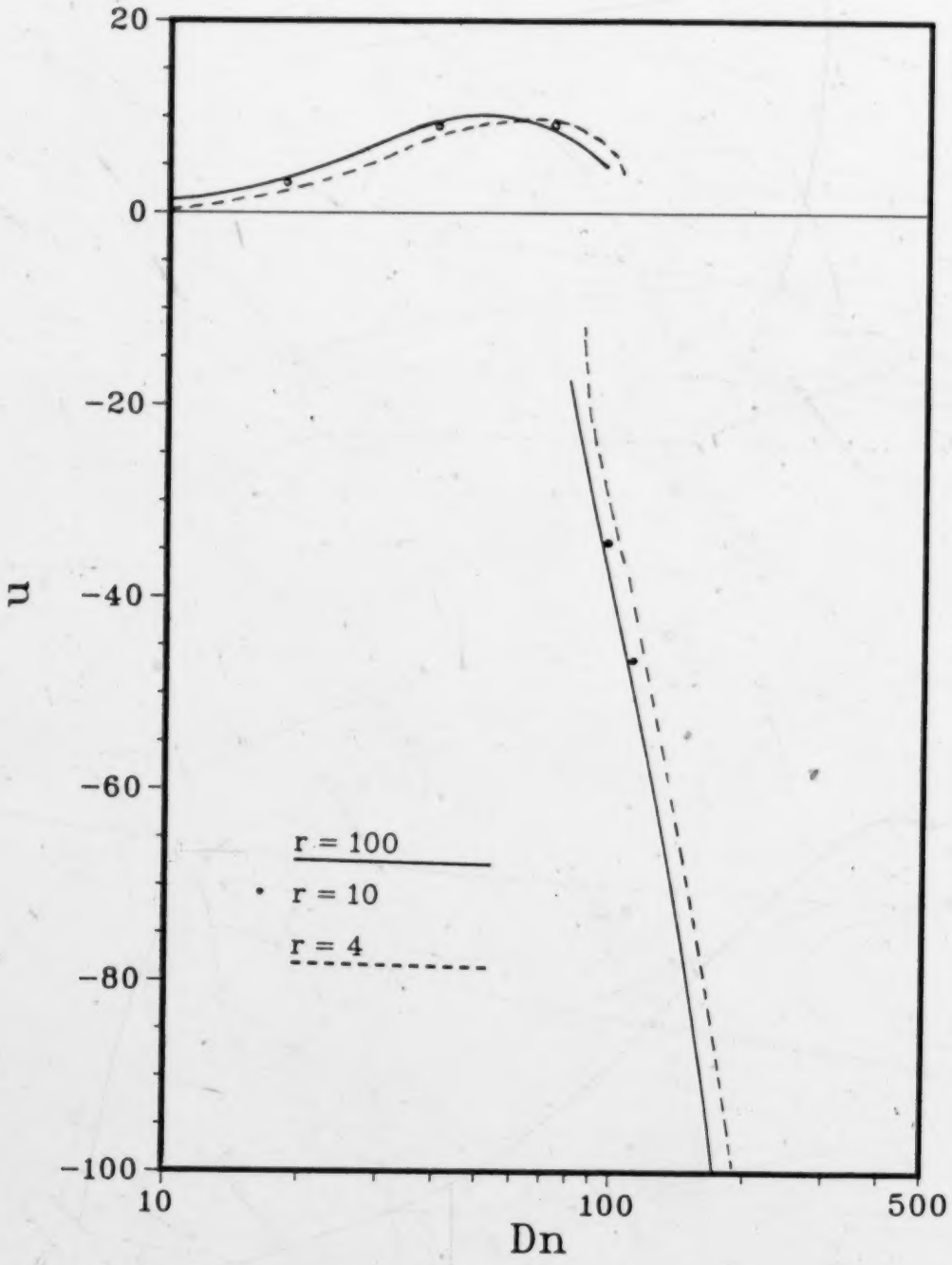

Fig. 5.9 u at x = 0.4 & y = 0 for a power-law fluid (n = 0.7) in square pipes of r = 100, 10 & 4

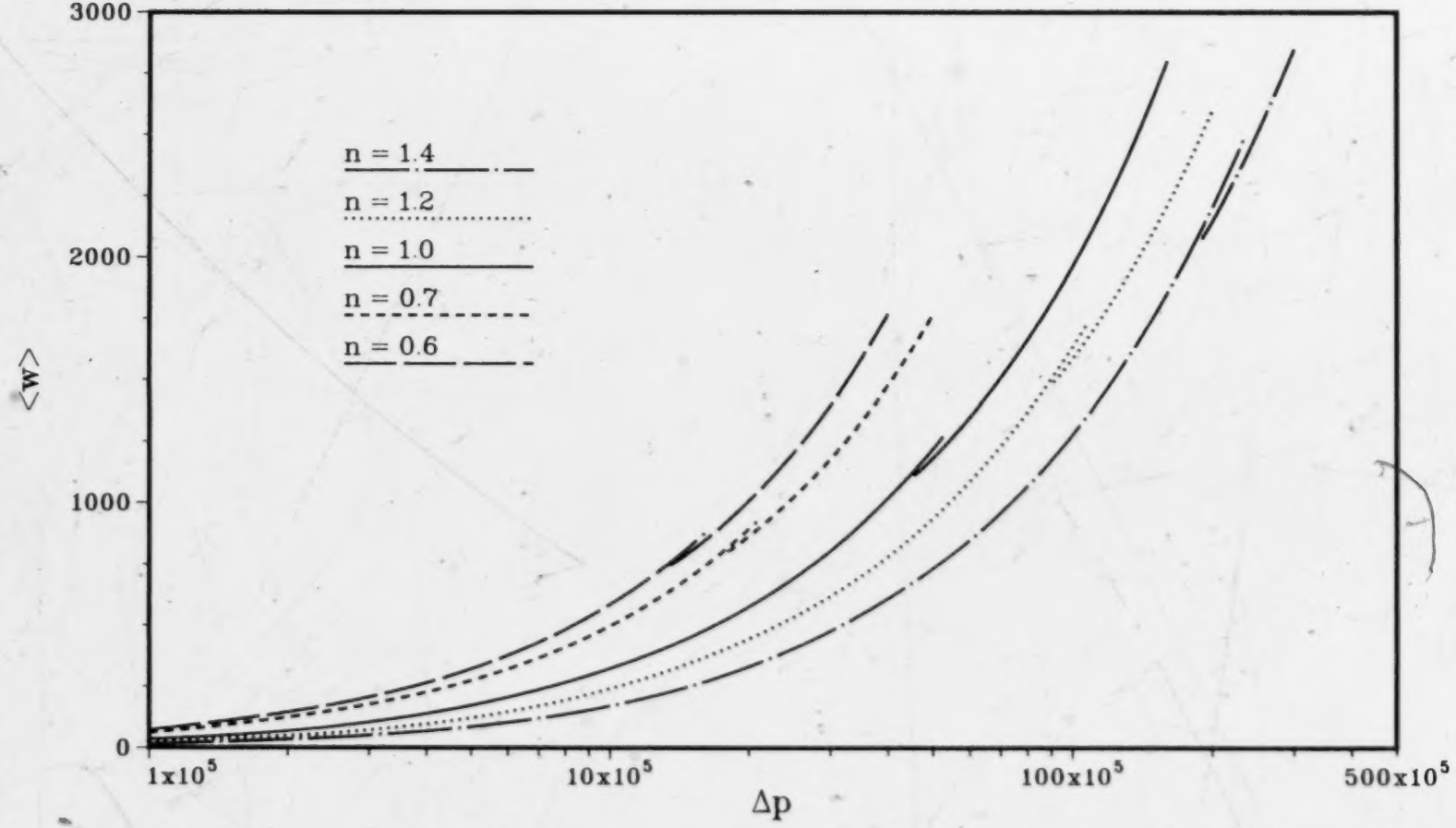

Fig. 5.10 The mean axial velocity (<w>) of Power-law fluids under the influence of imposed pressure gradient (Δp) in square pipes of r = 100

conditions. This feature is well illustrated in Figure 5.11 where one of the coordinates is represented by the modified Dean number $Dn^+(=Re^+/\sqrt{r})$.

The $f\text{-}Re^+$ of the dilatant fluids increases rapidly with increasing intensity of the secondary flow (or Dn). The $f\text{-}Re^+$ of the pseudoplastic fluids show a very slight departure from the $f\text{-}Re^+$ of the corresponding Poiseulle flow even up to about $Dn^+=60$. In both Figures 5.10 and 5.11, the pseudoplastic and the dilatant fluids lie on either side of the Newtonian fluid.

In case of a Newtonian fluid, the intensity of the secondary flow is the sole contributor toward the increase in the frictional resistance (see also Section 2.1). In the case of power-law fluids, the changing local apparent viscosities (see Subsection 2.5.1) also have their contributions towards the frictional resistance. As revealed by Equations 3.13 and 3.15, the velocity components and their gradients influences the local apparent viscosity μ and hence M. Few examples of these viscosity profiles at different Dn^+ are given in Figures 5.12a, 5.12b, 5.12c and 5.12d. The pseudoplastic fluid of n=0.6 and the dilatant fluid of n=1.4 in square pipe of r=100 are chosen for this purpose. The corresponding viscosity profile for the Newtonian fluids is always given by M=1. In these figures, the viscosity of the dilatant fluid is mostly greater than the viscosity of the Newtonian fluid. Therefore it

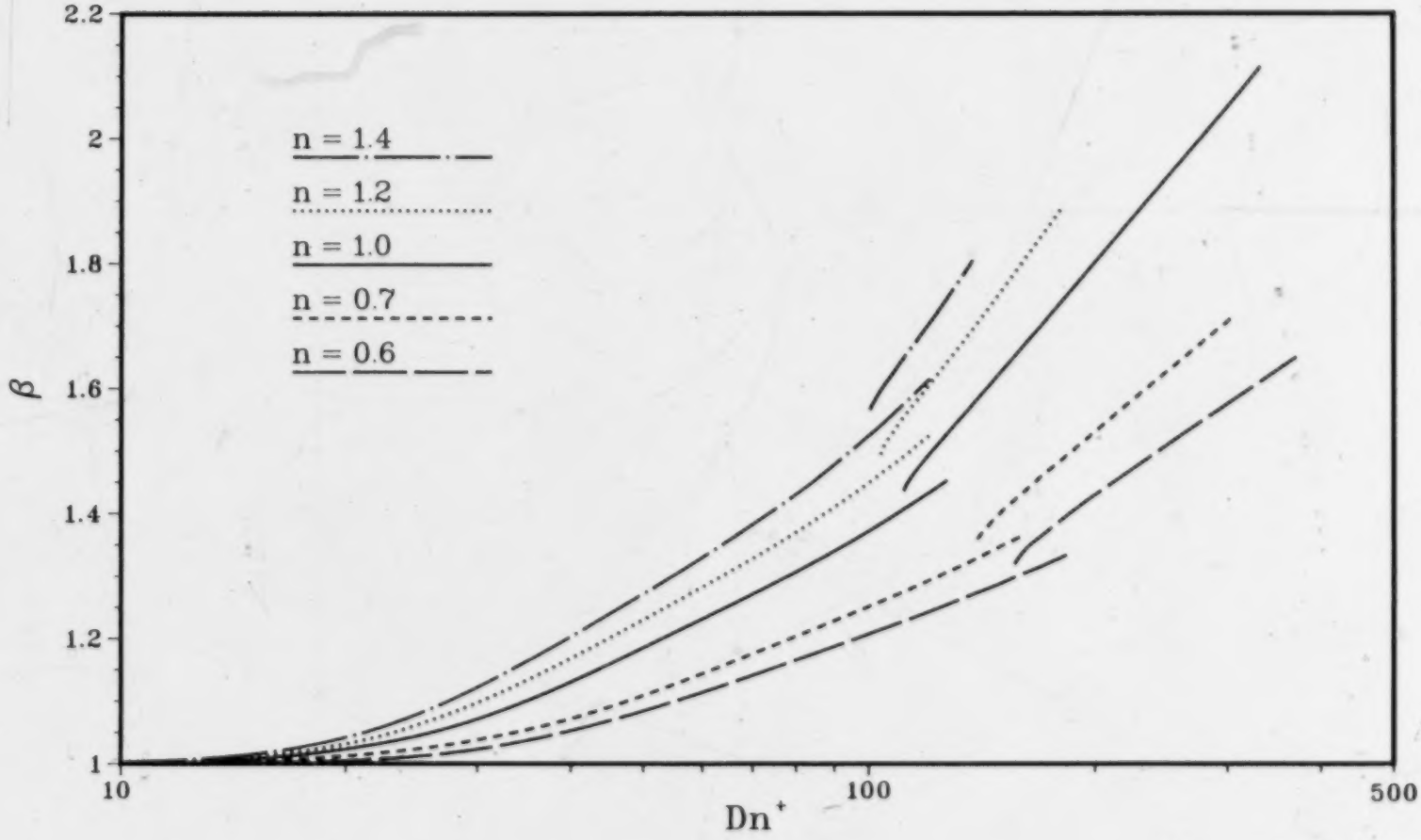

Fig. 5.11 Friction factor results for Power–law fluids in square pipes of r = 100

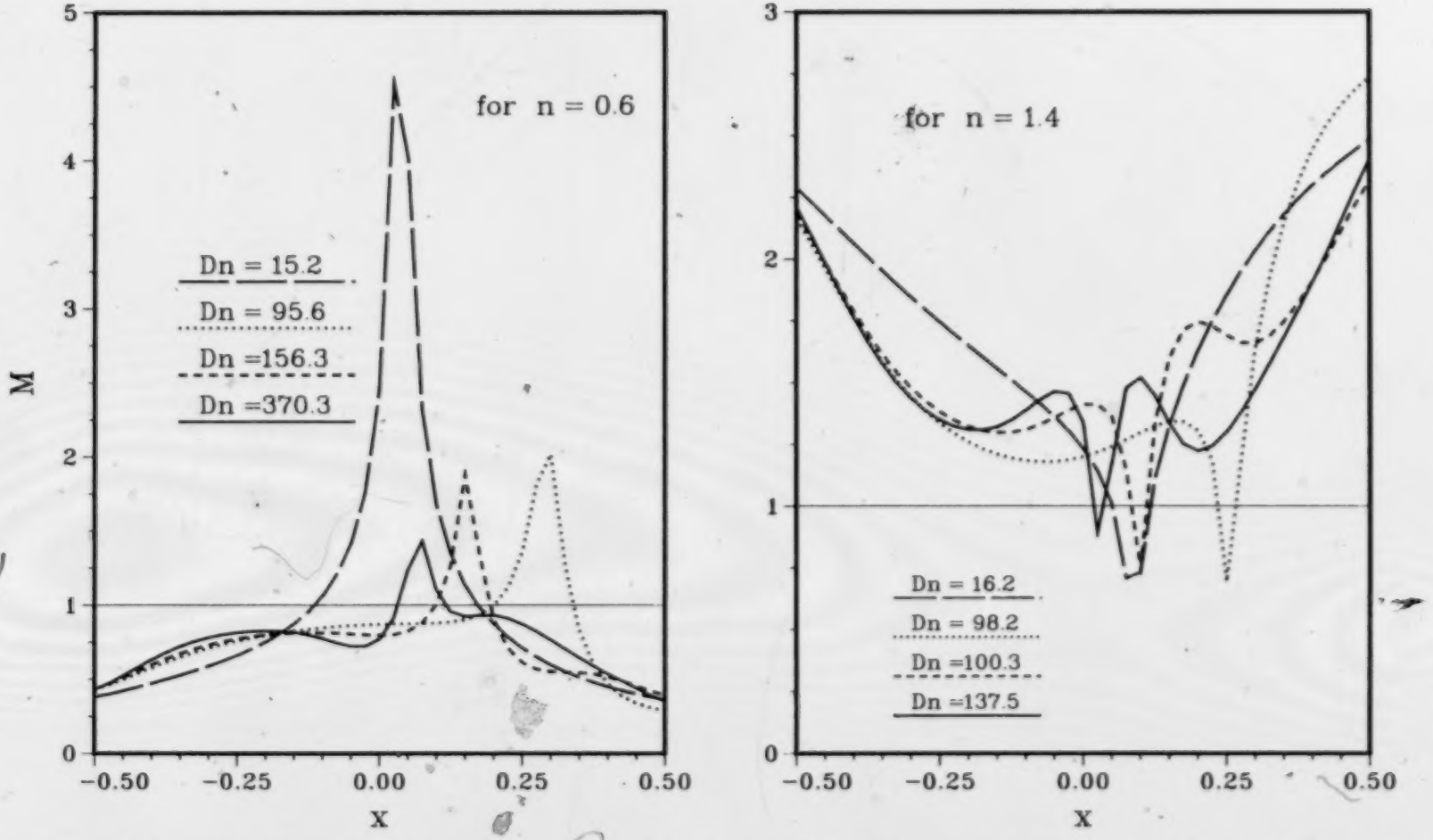

Fig. 5.12a The dimensionless viscosity (M) at the line of symmetry (y = 0) for $\gamma = 1$ & r = 100

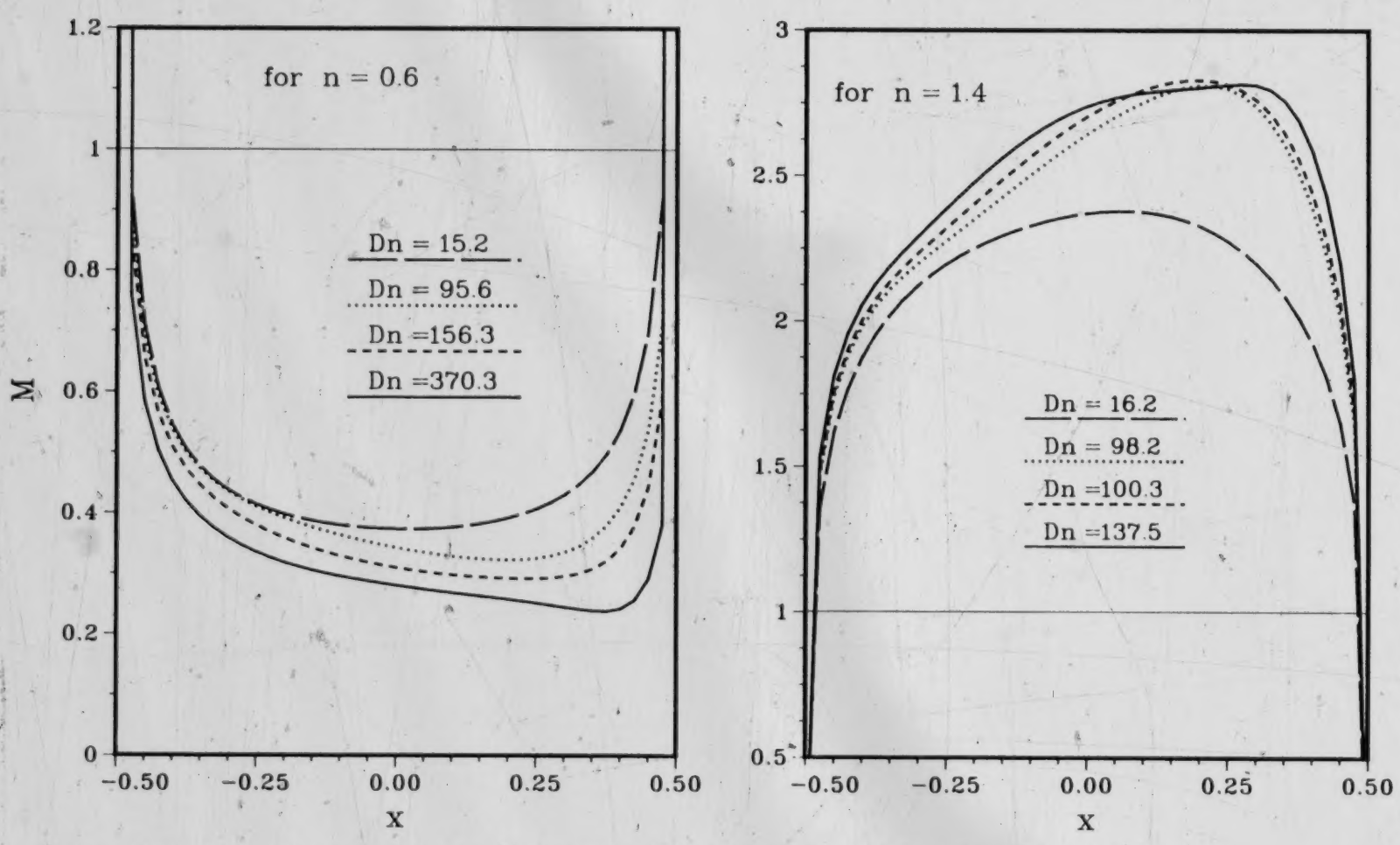

Fig. 5.12b The dimensionless viscosity (M) at the top wall (y = 0.5) for $\gamma = 1$ & r = 100

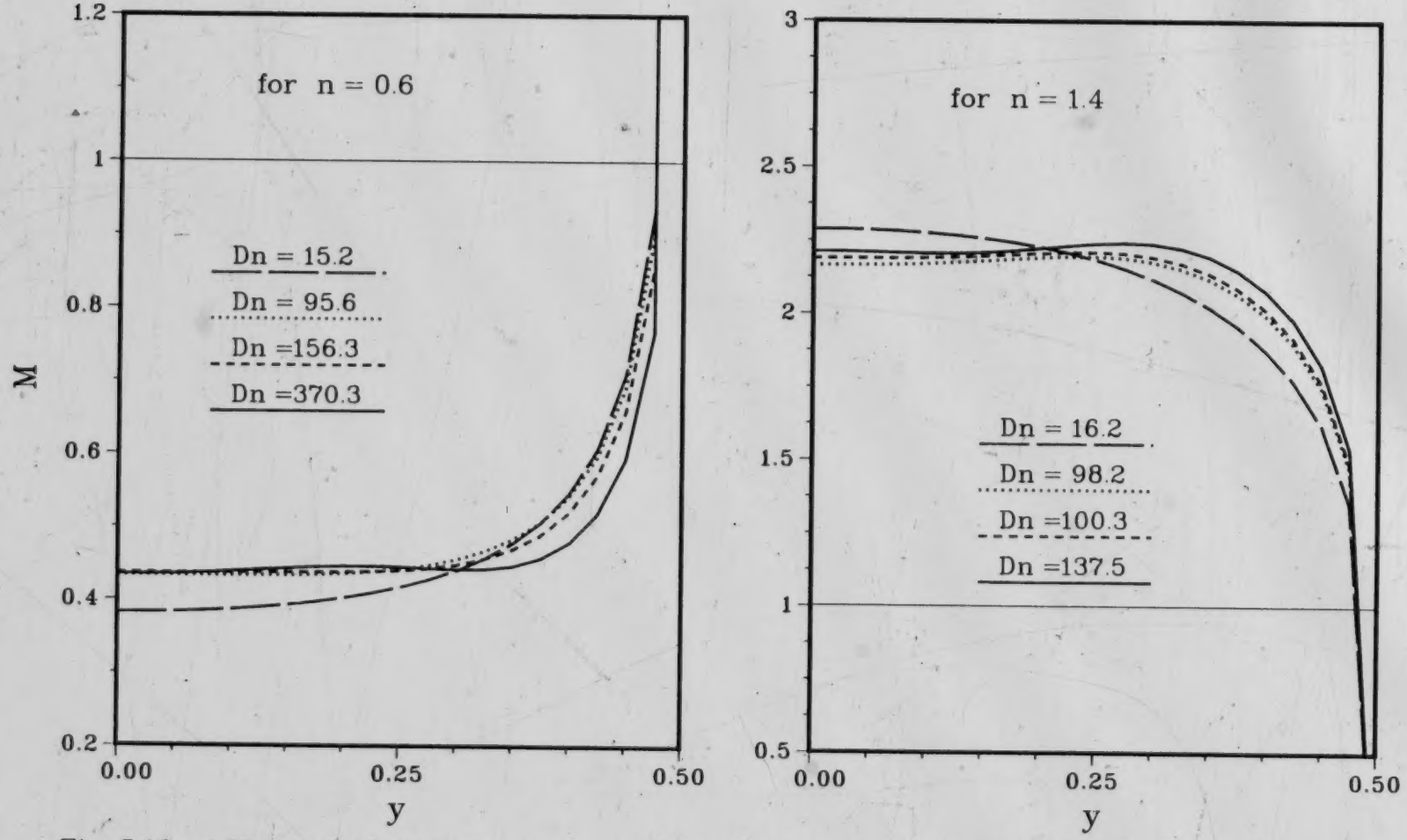

Fig. 5.12c The dimensionless viscosity (M) at the inner wall (x = −0.5) for $\gamma = 1$ & r = 100

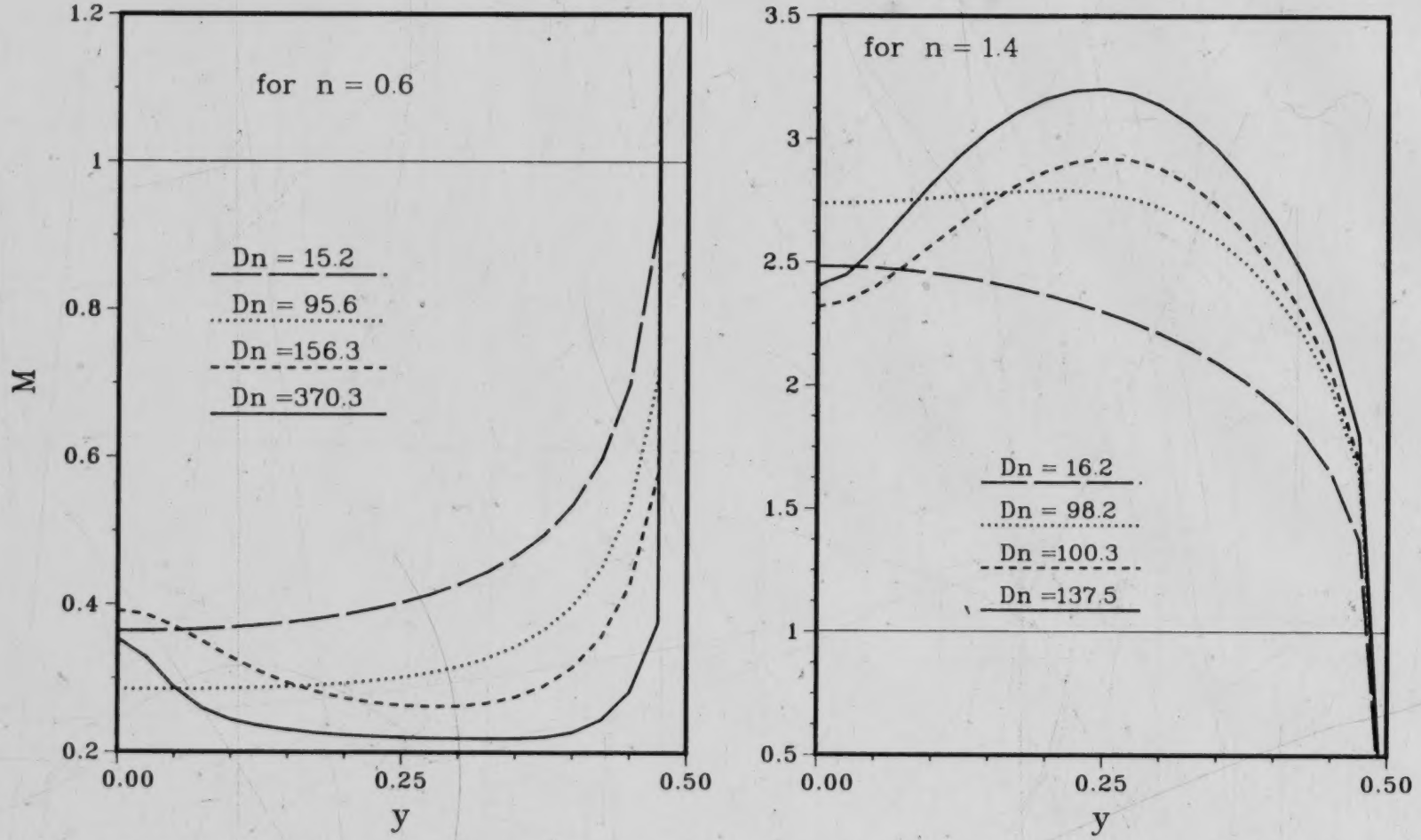

Fig. 5.12d The dimensionless viscosity (M) at the outer wall (x = 0.5) for $\gamma = 1$ & r = 100

experiences a higher resistance than the corresponding Newtonian fluid flow. The viscosity of the pseudoplastic fluid is less than that of the Newtonian fluid and hence it tends to decrease the frictional resistance. In pseudoplastic fluids, the contributions of these opposing phenomena, the local apperant viscosity and the secondary flow intensity, towards the frictional resistance must be annihilating each other at low enough Dn^+. As Dn^+ is increased further, the intensity of the secondary flow increases so much that the contribution of the lowering viscosity becomes less significant. As a result the $f\text{-}Re^+$ starts departing from the corresponding straight pipe $f\text{-}Re^+$.

It is interesting to note the works of Savins and Wallick(1965) and Tomcej and Nandakumar(1984) in which the helical flow has been found to decrease the frictional resistance experienced by the pseudoplastic fluids, significantly, below the corresponding purely axial flow. Savins and Wallick observed the same effect in a viscometric helical flow in the annulus of two long concentric cylinders. They generated the secondary flow by rotating one or both of the cylinders, independently. Tomcej and Nandakumar observed it in a non-viscometric helical flow in a straight square channel. They generated the secondary flow by heating the fluid by an axially uniform heat flux with peripherally uniform temperature conditions. In both these cases the driving forces of the secondary flow can be manipulated, to a certain extent, independent to the axial

flow. Whereas the secondary flow in a curved pipe is strongly dependent on the axial flow field. Also the secondary flow field in a curved pipe is comparatively much stronger at low flow conditions than the secondary flow field generated in the other two works under the corresponding flow conditions. These observations may explain the observed behaviour of the pseudoplastic fluid at low Dn^{+} in curved pipe. However experimental verification may be needed to strengthen it.

CHAPTER 6

CONCLUSIONS

- There exists a continuous but complex surface which represents the equilibrium solutions for flow in curved rectangular pipes. In this study, only the regions of symmetric 2 and 4 vortex solutions are mapped, but partially.

- The intensity of the centrifugal force, measured by Dn, has critical control on this equilibrium surface. In the direction of increasing Dn, this surface exhibits at least one fold which is typical of the models in catastrophe theory.

- The equilibrium surface is critically influenced by γ, the length scale. The behaviour surface repeats its nature at almost regular intervals of γ. Further investigations about this repetitive nature may provide one with a better understanding of the stability characteristics of curved flow.

- The bifurcation set in the Dn-γ space appears to follow a tilted cusp. However further search on asymmetric solutions and marginally stable solutions may reveal a more complicated equilibrium surface.

- Despite the non-linearity associated with the power-law fluids, the power-law index, n, does not have any critical control on the stability characteristics of the curved flow. The bifurcation set in the Dn-n space describes a fold-catastrophe.

- The effects of curvature is incorporated reasonably well in Dn. A slight shift of the critical Dn in the increasing direction of Dn is observed. This shift is significant at small enough radius of curvature, r.

- The effects of the parameters n and r on the equilibrium surface is merely shifting and/or stretching it. The bifurcation set determined in the Dn-γ space would remain qualitatively the same for any values of r or n.

- A unified view of what seems to be a complicated process is possible when directed by the models in Catastrophe theory.

BIBLIOGRAPHY

ADLER, M. 1934 Strömung in gekrümmten Rohren. Z. Angew. Math. Mech. 14, 257-275.

AKIYAMA, M. and CHENG, K.C. 1971 Boundary Vorticity Method for Laminar Forced Convection Heat Transfer in Curved Pipes. Int. J. Heat Mass Transfer 14, 1659-1675.

AUSTIN, L.R. and SEADER, J.D. 1973 Fully Developed Viscous Flow in Coiled Pipes. AIChE J 19, 85-94.

BARUA, S.N. 1963 On Secondary Flow in Stationary Curved Pipes. Q. Jour. Mech. Appl. Math. 16, 61-77.

BAYLIS, J.A. 1971 Experiments on Laminar Flow in Curved Channels of Square Section. J. Fluid Mech. 48, 417-422.

BENJAMIN, T.B. 1976 Application of Leray-Schauder degree Theory to problems of hydrodynamic stability. Math. Proc. Camb. Phil. Soc. 79, 373-392.

BENJAMIN, T.B. 1978a Bifurcation phenomena in steady flows of a viscous liquid, I. Theory. Proc. R. Soc. Lond. A359, 1-26.

BENJAMIN, T.B. 1978b Bifurcation phenomena in steady flows of a viscous liquid, II. Experiments. Proc. R. Soc. Lond. A359, 27-43.

BENJAMIN, T.B. 1978c Applications of generic bifurcation theory in fluid mechanics. In Contemporary Developments in continuum Mechanics and Partial Differential Equations (ed. G.M. de La Penha & L.A.J. Madeiros), Mathematical studies 30, North-Holland.

BENJAMIN, T.B. and MULLIN, T. 1981 Anamalous modes in the Taylor experiment. Proc. R. Soc. Lond. A377, 221-249.

BENJAMIN, T.B. and MULLIN, T. 1982 Notes on the Multiplicity of flows in the Taylor experiment. J. Fluid Mech. 121, 219-230.

BERGER, S.A., TALBOT, L. & YAO, L.-S. 1983 Flow in Curved Pipes. Ann. Rev. Fluid Mech. 15, 461-512

BIRD, R.B., ARMSTRONG, R.B. & HASSAGER, O. 1977 Dynamics of Polymeric Liquids, Vol.I Fluid Mechanics John Wiley & Sons, Inc., New York.

CHENG, K.C. and AKIYAMA, M. 1970 Laminar Forced Convection Heat Transfer in Curved Rectangular Channels. Int. J. Heat Mass Transfer 13, 471-490.

CHENG, K.C., LIN, R.-C. and OU, J.W. 1976 Fully Developed Laminar Flow in Curved Rectangular Channels. Trans. ASME, J. Fluid Eng 98, 41-48.

CHENG, K.C., NAKAYAMA, J. and AKIYAMA, M. 1977 Effect of Finite and Infinite Aspect Ratios of Flow Patterns in Curved Rectangular Channels. Proc. Int. Symp. on Flow Visualization Tokyo, Japan, 109-114.

CHENG, K.C., INABA, T. and AKIYAMA, M. 1983 Sept. Flow visualization studies of Secondary flow patterns and Centrifugal instability in curved circular and semicircular pipes. Third Int. Symp. on Flow Visualization Ann Arbor, Michigan.

COLLINS, W.M. and DENNIS, S.C.R. 1975 The Steady Motion of a Viscous Fluid in a Curved Tube. Q. J. Mech. & Appl. Math. 28, 133-156.

COLLINS, W.M. and DENNIS, S.C.R. 1976a Steady Flow in a Curved Tube of Triangular Cross-Section. Proc. Roy. Soc. Lond. A352, 189-211.

COLLINS, W.M. and DENNIS, S.C.R. 1976b Viscous Eddies Near a 90° and a 45° Corner in Flow Through a Curved Tube of Triangular Cross-Section. J. Fluid Mech. 76, 417-432.

CUMING, H.G. 1952 The Secondary Flow in Curved Pipes. Aeronautical Research Council Reports and Memoranda No. 2880.

DAVIES, A.R., WALTERS, K. & WEBSTER, M.F. 1979 Long-range memory effects in flows involving abrupt changes in geometry, Part 3. Moving boundaries. J. Non-Newt. Fluid Mech. 4, 325-344.

DEAN, W.R. 1927 Note on the Motion of Fluid in a Curved Pipe. Phil. Mag. 4, 208-233.

DEAN, W.R. 1928a The Stream Line Motion of Fluid in a Curved Pipe. Phil. Mag. 5, 673-695.

DEAN, W.R. 1928b Fluid Motion in a Curved Channel. Proc. Roy. Soc. A121, 402-420.

DEAN, W.R. and HURST, J.M. 1959 Note on the Motion of Fluid in a Curved Pipe. Mathematika 6, 77-85.

DENNIS, S.C.R. 1980 Calculation of the Steady Flow Through a Curved Tube Using a New Finite Difference Method. J. Fluid Mech. 99, 449-467.

DENNIS, S.C.R. and NG, M. 1982 Dual Solutions for Steady Laminar Flow Through a Curved Tube. to appear in Q. J. Mech. Appl. Math.

DETRA, R.W. 1953 The Secondary Flow in Curved Pipes. Mitt. Inst. Aerodyn. Zurich, Nr. 20.

DRAZIN, P.G. & REID, W.H. 1981 Hydrodynamic Stability Cambridge University Press, Cambridge.

EUSTICE, J. 1910 Flow of Water in Curved Pipe. Proc. Roy. Soc. A84, 107-118.

EUSTICE, J. 1911 Experiments on Stream-Line Motion in Curved Pipes. Proc. Roy. Soc. A85, 119-131.

EUSTICE, J. 1925 Flow of Water in Curved Passages. Engineering 13, 604-605.

FUNG, L., NANDAKUMAR, K. & MASLIYAH, J.H. 1985 Nov. Profuse Multiplicity in Mixed Convection Flow in Ducts. to be presented at the 106th ASME Winter Annual Meeting Miami Beach.

GREENSPAN, D. 1973 Secondary Flow in a Curved Tube. J. Fluid Mech. 57, 167-176.

GRINDLEY, J.H. and GIBSON, A.H. 1908 On the Frictional Resistance to the Flow of Air Through a Pipe. Proc. Roy. Soc. A80, 114-139.

GUPTA, S.N. and MISHRA, P. 1975 Isothermal laminar flow of Non-Newtonian fluid through helical coils. Indian J. of Technology 13, 245.

HAPPEL, J. and BRENNER, H. 1965 Low Reynolds Number Hydrodynamics Prentice-Hall, Inc., Englewood Cliffs, N.J.

HAWTHORNE, W.R. 1951 Secondary Circulations in Fluid Flow. Proc. Roy. Soc. A206, 374-387.

HSU, C.-H. and PATANKAR, S.V. 1982 Analysis of Laminar Non-Newtonian Flow and Heat Transfer in Curved Tubes. AIChE J 28, 610-616.

ITO, H. 1951 Theory of Laminar Flows Through Curved Pipes of Elliptic and Rectangular Cross Section. The Reports of the Institute of High Speed Mechanics Tohoku Univ., Sendai, Japan, 1, 1-16.

ITO, H. 1959 Friction Factors for Turbulent Flow in Curved Pipes. Trans. ASME, J. Basic Eng 81, 123-134.

ITO, H. 1969 Laminar Flow in Curved Pipes. Z. Angew. Math. Mech. 11, 653-663.

JONES, J.R. 1960 Flow of a Non-Newtonian Liquid in a Curved Pipe. J. Mech. Appl. Math. 13, 428-443.

JOSEPH, B., SMITH, E.P. and ADLER, R.J. 1975 Numerical Treatment of Laminar Flow in Helically Coiled Tubes of Square Cross Section, Part I. Stationary Helically Coiled Tubes. AIChE J 21, 965-974.

KERLEGAN, G.H. and BERJ, G.H. 1937 Pressure Losses for Fluid Flow in Curved Pipes. J. Res. Nat. Bur. Stand. 18, 89-114.

KUBAIR, V. and VARRIER, C.B.S. 1961/62 Pressure Drop for Liquid Flow in Helical Coils. Trans. Indian Institute of Chemical Engineers 14, 93-97.

LARRAIN, J. and BONILLA, C.F. 1970 Theoretical Analysis of Pressure Drop in the Laminar Flow of a Fluid in a Coiled Pipe. Trans. Soc. Reol. 14, 135-147.

LUDWIEG, H. 1951 Die Ausgebildete Kanalstromung in einem rotierenden System. Ingenieur-Archiv 19, 296-308.

MANLAPAZ, R.L. and CHURCHILL, S.W. 1980 Fully Developed Laminar Flow in a Helically Coiled Tube of Finite Pitch. Chem. Eng. Commun 7, 57-78.

MASHELKAR, R.A. and DEVARAJAN, G.V. 1976a Secondary Flow of Non-Newtonian Fluids: 2. Frictional Losses in Laminar Flow of Purely Viscous and Viscoelastic Fluids Through Coiled Tubes, Part I. Trans. Instn. Chem. Engrs 54, 100-107.

MASHELKAR, R.A. and DEVARAJAN, G.V. 1976b Secondary Flow of Non-Newtonian Fluids: 2. Frictional Losses in Laminar Flow of Purely Viscous and Viscoelastic Fluids Through Coiled Tubes, Part II. Trans. Instn. Chem. Engrs 54, 108-114.

MASHELKAR, R.A. and DEVARAJAN, G.V. 1977 Secondary Flows of Non-Newtonian Fluids: Part III - Turbulent Flow of Visco-inelastic Fluids in Coiled Tubes: A Theoretical Analysis and Experimental Verification. Trans. Instn. Chem. Engrs 55, 29-37.

MASLIYAH, J.H. 1980 On Laminar Flow in Curved Semicircular Ducts. J. Fluid Mech. 99, 469-479.

MASLIYAH, J.H. and NANDAKUMAR, K. 1979 Fully Developed Viscous Flow and Heat Transfer in Curved Semicircular Sectors. AIChE J 25, 478-487.

McCONALOGUE, D.J. and SRIVASTAVA, R.S. 1968 Motion of a Fluid in a Curved Tube. Proc. Roy. Soc. A307, 37-53.

MISHRA, P. & GUPTA, S.N. 1979a Momentum Transfer in Curved Pipes. 1. Newtonian Fluids. Ind. Eng. Chem. Process Des. Dev. 18-1, 130-137.

MISHRA, P. & GUPTA, S.N. 1979b Momentum Transfer in Curved Pipes. 2. Non-Newtonian Fluids. Ind. Eng. Chem. Process Des. Dev. 18-1, 137-142.

MORI, Y. and NAKAYAMA, W. 1965 Study on Forced Convective Heat Transfer in Curved Pipes, Part I. Int. J. Heat Mass Transfer 8, 67-82.

MORI, Y., UCHIDA, Y. and UKON, J. 1971 Forced Convective Heat Transfer in a Curved Channel with a Square Cross Section. Int. J. Heat Mass Transfer 14, 1787-1805.

MUJAWAR, B.A. and RAJA RAO, M. 1978 Flow of Non-Newtonian Fluids Through Helical Coils. Ind. Eng. Chem. Proc. Des. Dev. 17, 22-27.

MULLIN, T. 1982 Mutuations of Steady Cellular flows in the Taylor Experiment. J. Fluid Mech. 121, 207-218.

NANDAKUMAR, K. and MASLIYAH, J.H. 1982 Bifurcation in Steady Laminar Flow Through Curved Tubes. J. Fluid Mech. 119, 475-490.

NANDAKUMAR, K. and MASLIYAH, J.H. 1984 Swirling Flow and Heat Transfer in coiled and Twisted Pipes. Advances in Transport Processes Vol. 3 (in press).

NANDAKUMAR, K., MASLIYAH, J.H. & LAW, H.S. 1985 Bifurcation in steady laminar mixed convection flow in horizontal rectangular tubes. communicated to J. Heat Transfer

NUNGE, R.J. and LIN, T.-S. 1973 Laminar Flow in Strongly Curved Tubes. AIChE J 19, 1280-1281.

RAJASEKARAN, S., KUBAIR, V. and KULOOR, N.R. 1964 Isothermal Laminar Flow of Non-Newtonian Fluids in Spiral Tube Coils. Indian J. Technology 2, 149-152.

RAJASEKARAN, S., KUBAIR, V. and KULOOR, N.R. 1966 Secondary Flow of Non-Newtonian Fluids in Helical Coils. Indian J. Technology 4, 33-35.

RAJASEKARAN, S., KUBAIR, V. and KULOOR, N.R. 1970a Heat Transfer to Non-Newtonian Fluids in Coiled Pipes in Laminar Flow, Int. J. Heat Mass Transfer 13, 1583-1594.

RAJASEKARAN, S., KUBAIR, V. and KULOOR, N.R. 1970b Flow of Non-Newtonian fluid through Helical Coils. Indian J. of Technology 8, 391.

REID, W.H. 1958 On the Stability of Viscous Flow in a Curved Channel. Proc. Roy. Soc. A244, 186-198.

SANKARAIAH, M. and RAO, Y.V.N. 1973 Analysis of Steady Laminar Flow of an Incompressible Newtonian Fluid Through Curved Pipes of Small Curvature. Trans ASME, J. Fluid Eng 95, 75-80.

SAUNDERS, P.T. 1980 An Introduction to Catastrophe Theory Cambridge University Press, Cambridge.

SAVINS, J.G. and WALLICK, G.C. 1965 Viscosity Profiles, — Discharge Rates, Pressures, and Torques for a Rheologically Complex fluid in Helical flow. AIChE J 12:2, 357-363.

SCHAEFFER, D.G. 1980 Qualitative Analysis of a model for boundary effects in the Taylor problem. Math. Proc. Camb. Phil. Soc. 87, 307-337.

SHAH, R.K. and LONDON, A.L. 1978 Laminar Flow forced Convection in Ducts Academic Press, Inc., New York.

SKELLAND, A.H.P. 1967 Non-Newtonian Flow and Heat Transfer John Wiley & Sons, Inc. New York.

SPARROW, E.M. 1964 On the Onset of Flow Instability in a Curved Channel of Arbitrary Height. Zeitschrift fuer Angewandte Mathematic und Physik 15, 638-642.

SRINIVASAN, P.S., NANDAPURKAR, S.S. and HOLLAND, F.A. 1970 Friction Factors for Coils. Trans. Instn. Chem. Engrs 48, T156-T161.

TABARROK, B. and LIN, R.C. 1978 Laminar Flow and Heat Transfer in Curved Ducts. 1st International Conference on Numerical Methods in Laminar and Turbulent Flow

TAYLOR, G.I. 1923 Stability of a viscous liquid contained between two rotating cylinders. Phil. Trans R. Soc. Lond. A223, 289-343.

TAYLOR, G.I. 1929 The Criterion for Turbulence in Curved Pipes. Proc. Roy. Soc. A124, 243-249.

THOMPSON, J.M.T. 1982 Instabilities and Catastrophes in Science and Engineering John Wiley & Sons Ltd., New York.

THOMPSON, J. 1876 On the Origin of Windings of Rivers in Alluvial Plains, with Remarks on the Flow of Water Round Bends in Pipes. Proc. Roy. Soc. A25, 5-8.

TOMCEJ, R. & NANDAKUMAR, K. 1984 Oct. Multiple Solutions in Mixed convection flow of a power law fluid in Horizontal ducts. presented at the 34th Canadian Society of Chem. Eng. Conference Quebec.

TOPAKOGLU, H.C. 1967 Steady State Laminar Flows of an Incompressible Viscous Fluid in Curved Pipes. J. Math. & Mech. 16, 1321-1337.

TRUESDELL, L.C. and ADLER, R.J. 1970 Numerical Treatment of Fully Developed Laminar Flow in Helically Coiled Tubes. AIChE J 16, 1010-1015.

VAN DYKE, M. 1978 Extended Stokes Series: Laminar Flow Through a Loosely Coiled Pipe. J. Fluid Mech. 86, 129-145.

WHEELER, J.A. & WISSELER, E.H. 1965 The Friction Factor Reynolds Number Relation for the Stedy flow of Pseudoplastic fluids through Rectangular Ducts. AIChE J 11:2, 207-216.

WHITE, C.M. 1929 Streamline Flow Through Curved Pipes. Proc. Roy. Soc. A123, 645-663.

WHITE, C.M. 1932 Fluid Friction and its Relation to Heat Transfer. Trans. Instn. Chem. Engrs 10, 66-86.

WILLIAMS, G.S., HUBBELL, C.W. and FINKELL, G.H. 1902 Experiments at Detroit, Michigan on the Effect of Curvature on the Flow of Water in Pipes. Trans. ASCE 47, 1.

WINTERS, K.H. AND BRINDLEY, R.C.G. 1984 Aug. Multiple Solutions for Laminar flow in Hellicaly-coiled Tubes. Internal Report No. AERE-R. 11373 AERE Harwell.

YIH, C.S. and SANGSTER, W.M. 1957 Stability of Laminar Flows in Curved Channels. Phil. Mag. 2, 305-310.

ZEEMAN, E.C. 1977 Catastrophe Theory Reading, Mass.: Addison-Wesley Publishing Company, Inc. (Consists of reprints of Zeeman's selected papers).

APPENDIX A

THE SOURCE CODE OF THE COMPUTER PROGRAM

The computer program, written in Fortran IV, is given in this appendix. The 'driver' program does the input/output in MTS and calls the 'number cruncher' subroutine. This routine executes on an array processor in double precision (8 bytes). The results are stored in single precision (4 bytes).

The units assigned to this program are as follows:

unit	assignment
5	the terminal for parameter input
6	the terminal for computer output
7	a file where formatted data to be written if needed
10	a file with which the initial guesses are provided; the results of a previous run is stored in this file in machine code with single precision
11	a file to which the results are written by the computer in machine code with single precision in the order specified by the program

```
C...  *** DRIVER PROGRAM ***
C...
      REAL N,R,AR,PGRAD,STOL,GTOL,WTOL,SRF,GRF,WRF,RE,DN
      REAL FFRE1,FFRE2,ERS,ERG,ERW,WAV,FF1,FF2,RN
      REAL X(81),Y(81),S(81,81),V(81,81),W(81,81),U(81,81)
      REAL G(81,81)
      INTEGER NX,NY,NIC,NSX,NSY,IC,I,J,JJ,NXO,NYO,ICO
      INTEGER IANS,IDT
      INTEGER YES/'Y'/
C...
C...  SPECIFY THE NECESSARY PARAMETERS
C...
      WRITE(6,11)
11    FORMAT(1X,'RUN NUMBER = ?')
      READ(5,31)RN
      WRITE(6,41)
41    FORMAT(1X,'POWER LAW INDEX = ?')
      READ(5,31)N
      WRITE(6,42)
42    FORMAT(1X,'GEOMETRY R, AR = ?')
      READ(5,32)R,AR
      WRITE(6,43)
43    FORMAT(1X,'PRESSURE GRADIENT = ?')
      READ(5,31)PGRAD
      WRITE(6,44)
44    FORMAT(1X,'NX,NY = ?   (both should be odd numbers) ')
      READ(5,34)NX,NY
      WRITE(6,45)
45    FORMAT(1X,'MAX. NUMBER OF ITERATION CYCLES  = ?')
      READ(5,35)NIC
      WRITE(6,46)
46    FORMAT(1X,'TOLERANCE STOL,GTOL,WTOL = ?')
      READ(5,36)STOL,GTOL,WTOL
      WRITE(6,47)
47    FORMAT(1X,'RELAXATION FACTOR SRF,GRF,WRF = ?')
      READ(5,36)SRF,GRF,WRF
      WRITE(6,48)
48    FORMAT(1X,'STEP LENGTH TO PRINT OUT NSX,NSY = ?')
      READ(5,38)NSX,NSY
      WRITE(6,55)
55    FORMAT(1X,'IF DATA TO BE READ FROM A FILE (ANSWER Y/N)')
      READ(5,56)IDT
C...
C...  INITIALISE THE VARIABLES S,U,V,W,G & F
C...
      IF (IDT.NE.YES) GO TO  4
      READ(10) NXO,NYO
      READ(10)WAV
      READ(10)((S(I,J),J=1,NYO),I=1,NXO)
      READ(10)((W(I,J),J=1,NYO),I=1,NXO)
      READ(10)((G(I,J),J=1,NYO),I=1,NXO)
      IF((NXO.EQ.NX).AND.(NYO.EQ.NY))GO TO 5
```

```
C...
C...  INTERPOLATE IF NXO.NE.NX & NYO.NE.NY
C...
      CALL INTRPL (S,NX,NY,NXO,NYO,81)
      CALL INTRPL (W,NX,NY,NXO,NYO,81)
      CALL INTRPL (G,NX,NY,NXO,NYO,81)
      DO 110 I=1,NX
        S(I,1)=0.
        S(I,NY)=0.
        W(I,NY)=0.
110   CONTINUE
      DO 111 J=1,NY
        S(1,J)=0.
        S(NX,J)=0.
        W(1,J)=0.
        W(NX,J)=0.
111   CONTINUE
      GO TO 5
4     DO 20 I=1,NX
        DO 20 J=1,NY
          S(I,J)=0.
          G(I,J)=0.
          W(I,J)=0.
          WAV=0.
20    CONTINUE
5     DO 26 I=1,NX
        DO 26 J=1,NY
          U(I,J)=0.
          V(I,J)=0.
26    CONTINUE
C...
C...  Assigning the number crunching to the array processor
C...
      ICO=0.
500   CALL APINIT(0,0,0,0,IAPNO,ISTAT)
      CALL CLCLN(N,R,AR,PGRAD,NX,NY,NIC,STOL,GTOL,WTOL,SRF,
     &           GRF,WRF,IC,S,U,V,W,G,X,Y,RE,DN,FFRE1,FFRE2,
     &           ERS,ERG,ERW,WAV,FF1,FF2)
      CALL APRLSE
      ICO=ICO+IC
      IC=ICO
      WRITE(6,72)RN,IC,RE,DN,ERS,ERW,FFRE1,ERG,FFRE2
      WRITE(6,71)
71    FORMAT(1X,'DO YOU NEED MORE ITERATIONS ?',
     &'       (ANSWER  Y/N )')
      READ(5,56)IANS
      IF (IANS.EQ.YES) GO TO 500
C...
C...  back to the driver
C...
      WRITE(6,101)NX,NY
      WRITE(6,102)SRF,WRF,FF1,GRF,FF2
```

```
105           WRITE(6,103)WAV
106           WRITE(6,104)N,AR,R,PGRAD
107           WRITE(7,12) RN
108           WRITE(7,50) IC,NX,NY
109           WRITE(7,49)N,AR,R,PGRAD
110           WRITE(7,37)RE,DN,WAV
111           WRITE(7,61)FFRE1,FF1,FFRE2,FF2
112           WRITE(7,39)SRF,ERS,(X(I),I=1,NX,NSX)
113           DO 21 JJ=1,NY,NSY
114             J=NY+1-JJ
115     21      WRITE(7,51) Y(J),(S(I,J),I=1,NX,NSX)
116           WRITE(7,52)WRF,ERW,(X(I),I=1,NX,NSX)
117           DO 23 JJ=1,NY,NSY
118             J=NY+1-JJ
119     23      WRITE(7,51) Y(J),(W(I,J),I=1,NX,NSX)
120           WRITE(7,69)
121           WRITE(7,40)GRF,ERG,(X(I),I=1,NX,NSX)
122           DO 22 JJ=1,NY,NSY
123             J=NY+1-JJ
124     22      WRITE(7,51) Y(J),(G(I,J),I=1,NX,NSX)
125           WRITE(7,53) (X(I),I=1,NX,NSX)
126           DO 24 JJ=1,NY,NSY
127             J=NY+1-JJ
128     24      WRITE(7,51) Y(J),(U(I,J),I=1,NX,NSX)
129           WRITE(7,54) (X(I),I=1,NX,NSX)
130           DO 25 JJ=1,NY,NSY
131             J=NY+1-JJ
132     25      WRITE(7,51) Y(J),(V(I,J),I=1,NX,NSX)
133     C...
134     C...  Writing to a file in machine code
135     C...
136           REWIND 11
137           WRITE(11) NX,NY
138           WRITE(11) WAV
139           WRITE(11)((S(I,J),J=1,NY),I=1,NX)
140           WRITE(11)((W(I,J),J=1,NY),I=1,NX)
141           WRITE(11)((G(I,J),J=1,NY),I=1,NX)
142           WRITE(11)((U(I,J),J=1,NY),I=1,NX)
143           WRITE(11)((V(I,J),J=1,NY),I=1,NX)
144           WRITE(11)N,AR,R,PGRAD
145           WRITE(11)RE,DN,WAV,FFRE1,FFRE2
146           WRITE(11)FF1,FF2,SRF,WRF,GRF,ERS,ERW,ERG
147     C...
148           STOP
149     C...
150     31    FORMAT(F30.5)
151     32    FORMAT(2F30.5)
152     34    FORMAT(I2,1X,I2)
153     35    FORMAT(I3)
154     36    FORMAT(3F20.2)
155     38    FORMAT(I1,1X,I1)
156     56    FORMAT(A1)
```

```
      72    FORMAT(5X,'RUN NUMBER = ',F12.4,/,
     &       5X,'IC = ',I4,/,
     &       5X,'RE = ',E13.5,/,34X,'DN = ',E13.5,/,
     &       5X,'ERS = ',E13.5,/,
     &       5X,'ERW = ',E13.5,14X,'FFRE1 = ',E13.5,/,
     &       5X,'ERG = ',E13.5,14X,'FFRE2 = ',E13.5,/)
     101    FORMAT(//,5X,'GRID SIZE IS      ',I2,'X ',I2)
     102    FORMAT(//,5X,'SRF = ',E13.5,/,
     &          5X,'WRF = ',E13.5,14X,'FF1 = ',E13.5,/,
     &          5X,'GRF = ',E13.5,14X,'FF2 = ',E13.5)
     103    FORMAT(//,5X,'WAV = ',E13.5)
     104    FORMAT(//,5X,'POWER LAW INDEX      = ',F7.3,/,
     &         5X,'ASPECT RATIO         = ',F7.3,/,
     &         5X,'RADIUS OF CURVATURE = ',E15.6,/,
     &         5X,'PRESSURE GRADIENT   = ',E15.6)
      51    FORMAT(6X,F5.3,6X,E12.4,5(E12.4,4X))
     551    FORMAT(6X,6X,E12.4,5(E12.4,4X))
      12    FORMAT(//,1X,'RUN NUMBER IS ',F12.4)
      50    FORMAT(//,1X,'NUMBER OF ITERATION CYCLES ARE ',I4,//,
     &          1X, 'GRID SIZE IS    ',I2,' X ',I2)
      49    FORMAT(//,1X,'POWER LAW INDEX      = ',F7.3,/,
     &         1X,'ASPECT RATIO         = ',F7.3,/,
     &         1X,'RADIUS OF CURVATURE = ',E15.6,/,
     &         1X,'PRESSURE GRADIENT   = ',E15.6)
      37    FORMAT(//,1X,'MODIFIED REYNOLDS NUMBER  = ',E13.5,/,
     &         1X,'MODIFIED DEANS NUMBER     = ',E13.5,//,
     &         /,1X,'WAV    =',E13.5)
      61    FORMAT(//,1X,'FFRE1 = ',E13.5,15X,'FF1 = ',E13.5,/,
     &         1X,'FFRE2 = ',E13.5,15X,'FF2 = ',E13.5,/)
      39    FORMAT(//,1X,'STREAM FUNCTION (S)',//,
     &          1X,'    RELAXATION FACTOR USED = ',F7.3,/,
     &          1X,'    AVERAGE ERROR          = ',E13.5,//,
     &          8X,'Y  \X',4X,F5.3,5(8X,F5.3,3X))
      40    FORMAT(//,1X,'VORTICITY (G)',//,
     &          1X,'    RELAXATION FACTOR USED = ',F7.3,/,
     &          1X,'    AVERAGE ERROR          = ',E13.5,//,
     &          8X,'Y  \X',4X,F5.3,5(8X,F5.3,3X))
      52    FORMAT(//,1X,'AXIAL VELOCITY COMPONENT (W)',//,
     &          1X,'    RELAXATION FACTOR USED = ',F7.3,/,
     &          1X,'    AVERAGE ERROR          = ',E13.5,//,
     &          8X,'Y  \X',4X,F5.3,5(8X,F5.3,3X))
      53    FORMAT(//,1X,'VELOCITY COMPONENT IN X-DIRECTION (U)',//,
     &          8X,'Y  \X',4X,F5.3,5(8X,F5.3,3X))
      54    FORMAT(//,1X,'VELOCITY COMPONENT IN Y-DIRECTION (V)',//,
     &          8X,'Y  \X',4X,F5.3,5(8X,F5.3,3X))
      69    FORMAT(1H1)
            END
C...
C...  ######      #######      #######      ########      ########
C...
C...  This routine converts the results of one grid to another
C...
```

```
      SUBROUTINE INTRPL(A,NX,NY,NXO,NYO,ND1)
      REAL A(1),B(81,81)
      DATA B/6561*0.0/
      NDX(I,J)=ND1*(J-1)+I
      DO 10 I=1,NXO
        DO 10 J=1,NYO
          B(I,J)=A(NDX(I,J))
10    CONTINUE
      DXO=1.0/FLOAT(NXO-1)
      DYO=1.0/FLOAT(NYO-1)
      DX=1.0/FLOAT(NX-1)
      DY=1.0/FLOAT(NY-1)
      XS=DX/DXO
      YS=DY/DYO
      DO 20 I=1,NX
        I1=INT(XS*(I-1))+1
        P=XS*(I-1)-(I1-1)
          DO 20 J=1,NY
            J1=INT(YS*(J-1))+1
            Q=YS*(J-1)-(J1-1)
            PH1=B(I1,J1)+P*(B(I1+1,J1)-B(I1,J1))
            PH2=B(I1,J1+1)+P*(B(I1+1,J1+1)-B(I1,J1+1))
            A(NDX(I,J))=PH1+Q*(PH2-PH1)
20    CONTINUE
      RETURN
      END
```

```
C...  *** NUMBER  CRUNCHER ***
C...
C...  This routine evaluates Stream function(S), vorticity(G), &
C...  axial velocity(W) using Gauss-Siedel point iteration with
C...  relaxation.
C...
      SUBROUTINE CLCLN(N,R,AR,PGRAD,NX,NY,NIC,STOL,GTOL,WTOL,
     &                 SRF,GRF,WRF,IC,S,U,V,W,G,X,Y,RE,DN,
     &                 FFRE1,FFRE2,ERS,ERG,ERW,WAV,FF1,FF2)
C...
      INTEGER NX,NY,NIC,NX1,NX2,NY1,NY2,I,J,IC,K
      REAL N,R,AR,PGRAD,STOL,GTOL,WTOL,SRF,GRF,WRF,DX,DX2,DY
      REAL DY2,S1,S2,S3,S4,S5,S6,B1,ERS,ERG,ERW,LT,FINT,WAV
      REAL DIF,G1,G2,G3,G4,G5,G6,W1,W2,W3,W4,W5,W6,M1,C,TN
      REAL FF1,FF2,FFRE1,FFRE2,ARX,ARYI,ARYO,SUM,SUMP,RE,DN
      REAL WB1,WB2,WB3,WB4,WB6,WBTMP,GTEMP,WTEMP,STEMP
      REAL S(81,81),U(81,81),V(81,81),W(81,81),G(81,81),X(81)
      REAL Y(81),F(81),YINT(81),FXX(81,81),FXY(81,81),FXT(81,81)
      REAL FYY(81,81),FYT(81,81),FTT(81,81),C2(81,81),C3(81,81)
```

```
      REAL C4(81,81),C5(81,81),DXX(81,81),DXY(81,81),DXT(81,81)
      REAL DYY(81,81),DYT(81,81),DTT(81,81),M(81,81)
C...
      NX1=NX-1
      NX2=NX1-1
      DX=1.0/FLOAT(NX1)
      DX2=DX*DX
      DO 20 I=1,NX
        X(I)=-0.5+DX*FLOAT(I-1)
20    CONTINUE
C...
      NY1=NY-1
      NY2=NY1-1
      DY=0.5*AR/FLOAT(NY1)
      DY2=DY*DY
      DO 21 J=1,NY
        Y(J)=DY*FLOAT(J-1)
21    CONTINUE
C...
C...  INITIALISE THE ITERATION CYCLES
C...
      IC=1
C...
C...  UPDATE STREAM FUNCTION(S) at the interior points
C...
      S1=(2.0/DX2)+(2.0/DY2)
      S4=1.0/DY2
      S5=S4
100   ERS=0.
      DO 600 K=1,3
      DO 61 I=2,NX1
        S2=(1.0/DX2)-(0.5/DX/(R+X(I)))
        S3=(1.0/DX2)+(0.5/DX/(R+X(I)))
        DO 61 J=2,NY1
          S6=(R+X(I))*G(I,J)
          STMP=(S2*S(I+1,J)+S3*S(I-1,J)+S4*S(I,J+1)+S5*S(I,J-1)
     &          +S6)/S1
          DIF=STMP-S(I,J)
          ERS=ERS+ABS(DIF)
          S(I,J)=S(I,J)+SRF*DIF
61    CONTINUE
600   CONTINUE
C...
C...  EVALUATE THE BOUNDARY VALUES OF VORTICITY(G) USING THE
C...  UPDATED STREAM FUNCTION(S)
C...
      DO 23 I=2,NX1
        G(I,1)=0.
        G(I,NY)=(S(I,NY2)-8.0*S(I,NY1))/2.0/DY2/(R+X(I))
C       G(I,NY)=-2.0*S(I,NY1)/DY2/(R+X(I))
23    CONTINUE
      DO 24 J=2,NY1
```

```
      G(1,J)=(S(3,J)-8.0*S(2,J))/2.0/DX2/(R-0.5)
      G(NX,J)=(S(NX2,J)-8.0*S(NX1,J))/2.0/DX2/(R+0.5)
C     G(1,J)=-2.0*S(2,J)/DX2/(R-0.5)
C     G(NX,J)=-2.0*S(NX1,J)/DX2/(R+0.5)
24    CONTINUE
C...
C...  EVALUATE THE VELOCITY COMPONENTS IN X DIRECTION(U) & IN
C...  Y DIRECTION(V) USING THE UPDATED STREAM FUNCTION(S)
C...
C...  U & V at the interior points
C...
      DO 25 I=2,NX1
        DO 25 J=2,NY1
          U(I,J)=(S(I,J+1)-S(I,J-1))/2.0/DY/(R+X(I))
          V(I,J)=-(S(I+1,J)-S(I-1,J))/2.0/DX/(R+X(I))
25    CONTINUE
C...
C...  U at the bottom boundary ,where Y=0 (J=1)
C...
      DO 26 I=2,NX1
        U(I,1)=(4.0*S(I,2)-S(I,3))/2.0/DY/(R+X(I))
26    CONTINUE
C...
      IF (N.EQ.1.0) GO TO 900
C...
C...  EVALUATE THE FOLLOWING FOR NON-NEWTONIAN FLUIDS
C...                              (i.e. WHEN N .NE. 1.0)
C...
C...  EVALUATE THE RATE OF STRAIN TENSOR COMPONENTS(D) ,
C...
C...  D at the interior points
C...
      DO 28 I=2,NX1
        DO 28 J=2,NY1
          DXX(I,J)=(U(I+1,J)-U(I-1,J))/DX
          DXY(I,J)=((V(I+1,J)-V(I-1,J))/2.0/DX)
     &            +((U(I,J+1)-U(I,J-1))/2.0/DY)
          DXT(I,J)=((W(I+1,J)-W(I-1,J))/2.0/DX)-(W(I,J)/(R+X(I)))
          DYY(I,J)=(V(I,J+1)-V(I,J-1))/DY
          DYT(I,J)=(W(I,J+1)-W(I,J-1))/2.0/DY
          DTT(I,J)=2.0*U(I,J)/(R+X(I))
28    CONTINUE
C...
C...  D at the inner wall, where X=-0.5 (I=1)
C...
      DO 29 J=1,NY
        DXX(1,J)=(4.0*U(2,J)-U(3,J))/DX
        DXY(1,J)=(4.0*V(2,J)-V(3,J))/2.0/DX
        DXT(1,J)=(4.0*W(2,J)-W(3,J))/2.0/DX
        DYY(1,J)=0.
        DYT(1,J)=0.
        DTT(1,J)=0.
```

```
124     29    CONTINUE
125     C...
126     C...  D at the outer wall, where X=0.5 (I=NX)
127     C...
128           DO 51 J=1,NY
129             DXX(NX,J)=(-4.0*U(NX1,J)+U(NX2,J))/DX
130             DXY(NX,J)=(-4.0*V(NX1,J)+V(NX2,J))/2.0/DX
131             DXT(NX,J)=(-4.0*W(NX1,J)+W(NX2,J))/2.0/DX
132             DYY(NX,J)=0.
133             DYT(NX,J)=0.
134             DTT(NX,J)=0.
135     51    CONTINUE
136     C...
137     C...  D at the top wall, where Y=0.5*AR (J=NY)
138     C...
139           DO 52 I=2,NX1
140             DXX(I,NY)=0.
141             DXY(I,NY)=(-4.0*U(I,NY1)+U(I,NY2))/2.0/DY
142             DXT(I,NY)=0.
143             DYY(I,NY)=(-4.0*V(I,NY1)+V(I,NY2))/DY
144             DYT(I,NY)=(-4.0*W(I,NY1)+W(I,NY2))/2.0/DY
145             DTT(I,NY)=0.
146     52    CONTINUE
147     C...
148     C...  D at the bottom boundary, where Y=0. (J=1)
149     C...
150           DO 53 I=2,NX1
151             DXX(I,1)=(U(I+1,1)-U(I-1,1))/DX
152             DXY(I,1)=0.
153             DXT(I,1)=((W(I+1,1)-W(I-1,1))/2.0/DX)-(W(I,1)/(R+X(I)))
154             DYY(I,1)=(4.0*V(I,2)-V(I,3))/DY
155             DYT(I,1)=0.
156             DTT(I,1)=2.0*U(I,1)/(R+X(I))
157     53    CONTINUE
158     C...
159     C...  D at the top corners
160     C...
161           DXX(1,NY)=0.0
162           DXY(1,NY)=0.0
163           DXT(1,NY)=0.0
164           DYY(1,NY)=0.0
165           DYT(1,NY)=0.0
166           DTT(1,NY)=0.0
167     C...
168           DXX(NX,NY)=0.0
169           DXY(NX,NY)=0.0
170           DXT(NX,NY)=0.0
171           DYY(NX,NY)=0.0
172           DYT(NX,NY)=0.0
173           DTT(NX,NY)=0.0
174     C...
175     C...  EVALUATE THE DIMENSIONLSS VISCOSITY(M) & THE STRESS
```

```
C...  TENSOR COMPONENTS(F)
C...
      IF (WAV.EQ.0.) WAV=1.0
      DO 63 I=1,NX
        DO 63 J=1,NY
          SUM=0.5*DXX(I,J)**2+0.5*DYY(I,J)**2+0.5*DTT(I,J)**2
     &           +DXY(I,J)**2+DXT(I,J)**2+DYT(I,J)**2
          SUMP=SUM/(WAV**2)
          IF((SUMP.LT.1.0E-6) .AND. (N.LT.1.0))SUMP=1.0E-6
          M(I,J)=SUMP**((N-1.0)/2.0)
          M1=M(I,J)-1.0
          FXX(I,J)=M1*DXX(I,J)
          FXY(I,J)=M1*DXY(I,J)
          FXT(I,J)=M1*DXT(I,J)
          FYY(I,J)=M1*DYY(I,J)
          FYT(I,J)=M1*DYT(I,J)
          FTT(I,J)=M1*DTT(I,J)
63    CONTINUE
      GO TO 800
C...
C...  IF THE FLUID IS NEWTONIAN (i.e. N .EQ. 1.0) , THEN...
C...
900   DO 73 I=1,NX
        DO 73 J=1,NY
          FXX(I,J)=0.0
          FXY(I,J)=0.0
          FXT(I,J)=0.0
          FYY(I,J)=0.0
          FYT(I,J)=0.0
          FTT(I,J)=0.0
          M(I,J)=1.0
73    CONTINUE
C...
C...  EVALUATE SOME OF THE COEFFICIENTS INVOLVED IN THE
C...  EVALUATION OF G & W
C...
800   DO 54 I=2,NX1
        DO 54 J=2,NY1
          C2(I,J)=(1.0/DX2)+(0.5/DX/(R+X(I)))-(U(I,J)/2.0/DX)
          C3(I,J)=(1.0/DX2)-(0.5/DX/(R+X(I)))+(U(I,J)/2.0/DX)
          C4(I,J)=(1.0/DY2)-(V(I,J)/2.0/DY)
          C5(I,J)=(1.0/DY2)+(V(I,J)/2.0/DY)
54    CONTINUE
C...
C...  UPDATE AXIAL VELOCITY(W)
C...
C...  W at the interior points
C...
      ERW=0.
      DO 56 I=2,NX1
        B1=S1+(1.0/(R+X(I))**2)
        DO 56 J=2,NY1
```

```
228               W1=B1+(U(I,J)/(R+X(I)))
229               W2=C2(I,J)
230               W3=C3(I,J)
231               W4=C4(I,J)
232               W5=C5(I,J)
233               W6=-PGRAD/(R+X(I))
234              &       +(FXT(I+1,J)-FXT(I-1,J))/2.0/DX
235              &       +(FYT(I,J+1)-FYT(I,J-1))/2.0/DY
236              &       +2.0*FXT(I,J)/(R+X(I))
237               WTMP=(W2*W(I+1,J)+W3*W(I-1,J)+W4*W(I,J+1)+W5*W(I,J-1)
238              &          +W6)/W1
239               DIF=WTMP-W(I,J)
240               ERW=ERW+ABS(DIF)
241               W(I,J)=W(I,J)+WRF*DIF
242     56     CONTINUE
243     C...
244     C...  W at the bottom boundary, where Y=0. (J=1)
245     C...
246           DO 57 I=2,NX1
247             WB1=S1+(1.0/(R+X(I))**2)+(U(I,1)/(R+X(I)))
248             WB2=(1.0/DX2)+(0.5/DX/(R+X(I)))-(U(I,1)/2.0/DX)
249             WB3=(1.0/DX2)-(0.5/DX/(R+X(I)))+(U(I,1)/2.0/DX)
250             WB4=(2.0/DY2)
251             WB6=(-PGRAD/(R+X(I)))
252            &        +((FXT(I+1,1)-FXT(I-1,1))/2.0/DX)
253            &        +(FYT(I,2)/DY)
254            &        +(2.0*FXT(I,1)/(R+X(I)))
255             WBTMP=(WB2*W(I+1,1)+WB3*W(I-1,1)+WB4*W(I,2)+WB6)/WB1
256             DIF=WBTMP-W(I,1)
257             W(I,1)=W(I,1)+WRF*DIF
258     57     CONTINUE
259     C...
260     C...  EVALUATE THE AVERAGE OF THE AXIAL VELOCITY COMPONENT(WAV)
261     C...  USING THE LOCAL AXIAL VELOCITY COMPONENT(W)
262     C...
263     C...  integrate W with respect to Y & store
264     C...
265           LT=0.5*AR
266           DO 27 I=1,NX
267             DO 68 J=1,NY
268               F(J)=W(I,J)
269     68        CONTINUE
270             CALL SIM(0.0,LT,NY,F,FINT)
271             YINT(I)=FINT
272     27     CONTINUE
273     C...
274     C...  integrate with respect to X
275     C...
276           CALL SIM(-0.5,0.5,NX,YINT,FINT)
277           WAV=2.0*(FINT/AR)
278     C...
279     C...  UPDATE VORTICITY(G) at the interior points
```

```
C...
      ERG=0.
      DO 55 I=2,NX1
        B1=S1+(1.0/(R+X(I))**2)
        DO 55 J=2,NY1
          G1=B1-(U(I,J)/(R+X(I)))
          G2=C2(I,J)
          G3=C3(I,J)
          G4=C4(I,J)
          G5=C5(I,J)
          G6=-W(I,J)*(W(I,J+1)-W(I,J-1))/DY/(R+X(I))
     &       +(FXY(I+1,J)-2.0*FXY(I,J)+FXY(I-1,J))/DX2
     &       -(FXY(I,J+1)-2.0*FXY(I,J)+FXY(I,J-1))/DY2
     &       +(FYY(I+1,J+1)+FYY(I-1,J-1)-FYY(I+1,J-1)
     &                     -FYY(I-1,J+1))/4.0/DX/DY
     &       -(FXX(I+1,J+1)+FXX(I-1,J-1)-FXX(I+1,J-1)
     &                     -FXX(I-1,J+1))/4.0/DX/DY
     &       +(FXY(I+1,J)-FXY(I-1,J))/2.0/DX/(R+X(I))
     &       -(FXX(I,J+1)-FXX(I,J-1))/2.0/DY/(R+X(I))
     &       +(FTT(I,J+1)-FTT(I,J-1))/2.0/DY/(R+X(I))
     &       -FXY(I,J)/(R+X(I))**2
          GTMP=(G2*G(I+1,J)+G3*G(I-1,J)+G4*G(I,J+1)+G5*G(I,J-1)
     &          +G6)/G1
          DIF=GTMP-G(I,J)
          ERG=ERG+ABS(DIF)
          G(I,J)=G(I,J)+GRF*DIF
55      CONTINUE
C...
C...  STOPPING CRITERION
C...
      TN=FLOAT(NX1*NY1)
      ERS=ERS/TN
      ERG=ERG/TN
      ERW=ERW/TN
      IF((ERS.LE.STOL).AND.(ERG.LE.GTOL).AND.(ERW.LE.WTOL))GO TO 2
      IF(IC.GE.NIC)GO TO 1
      IC=IC+1
      GO TO 100
1     CONTINUE
C...
C...  CALCULATE MODIFIED REYNOLDS NUMBER(RE) & MODIFIED DEANS
C...  NUMBER(DN)
C...
2     C=(8.0**(N-1.0))*(((1.0+3.0*N)/(4.0*N))**N)
      RE=(WAV/C)*((2.0*AR/(1.0+AR))**N)
C     RE=WAV*((2.0*AR/(1.0+AR))**N)
      DN=RE/(R**0.5)
C...
C...  CALCULATE FRICTION FACTOR(FF) BY TWO DIFFERENT METHODS
C...
C...  METHOD 1 - CONSIDERING THE OVERALL FORCE BALANCE FOR THE
C...             DIFFRENTIAL AXIAL LENGTH
```

```
C...
      FF1=-(AR/(1.0+AR))*(PGRAD/R)/(WAV**2)
      FFRE1=FF1*RE
C...
C...  METHOD 2 - CONSIDERING THE STRESS ALONG THE CHANNEL WALL
C...
      DO 58 I=1,NX
        F(I)=-M(I,NY)*((-4.0*W(I,NY1)+W(I,NY2))/2.0/DY)*(R+X(I))
58    CONTINUE
      CALL SIM(-0.5,0.5,NX,F,ARX)
      DO 59 J=1,NY
        F(J)=M(1,J)*(4.0*W(2,J)-W(3,J))/2.0/DX
59    CONTINUE
      CALL SIM(0.,LT,NY,F,ARYI)
      DO 60 J=1,NY
        F(J)=-M(NX,J)*(-4.0*W(NX1,J)+W(NX2,J))/2.0/DX
60    CONTINUE
      CALL SIM(0.,LT,NY,F,ARYO)
      FF2=(2.0/R/(1.0+AR)/(WAV**2))*(ARX+(R-0.5)*ARYI
     &                              +(R+0.5)*ARYO)
      FFRE2=FF2*RE
C...
      RETURN
      END
C...
C...  ##### ##### ##### ##### ##### ##### ##### ##### #####
C...
C...  ***  SIMPSON'S 1/3 rd RULE FOR NUMERICAL INTEGRATION ***
C...
      SUBROUTINE SIM(A,B,N,F,FINTG)
C...
C...  A  -  INITIAL DATA POINT
C...  B  -  FINAL DATA POINT
C...  N  -  NUMBER OF DATA POINTS (should always be odd)
C...  F  -  INTEGRAND
C...  FINTG  -  INTEGRAL VALUE (OUTPUT)
C...
      INTEGER NN,K,N
      REAL F(81),FN,H,SUM,FINTG,A,B
C...
      FN=FLOAT(N)-1.0
      H=(B-A)/FN
      NN=(N-1)/2
      SUM=0
      DO 3 K=1,NN
        SUM=SUM+4.0*F(2*K)+2.0*F(2*K+1)
3     CONTINUE
      FINTG=(H/3.0)*(F(1)+SUM-F(N))
      RETURN
      END
```

APPENDIX B

THE NUMERICAL RESULTS FOR NEWTONIAN FLUIDS

The numerical results for the newtonian fluid are presented in tabular form. They are in the increasing order of the aspect ratio, γ, with 2-cell and 4-cell solutions placed alternatively. Isolated 2-cell solutions are given for γ=1.28, 1.35 & 1.4. All these results are for r=100. At the end of this appendix, the results for square pipes of r=10 & 4 are given.

$\gamma = 0.3$ 2-cell solution

pgrad	<w>	Re	Dn	f_1-Re	f_2-Re	%df	β_1	β_2	%dβ	u(4.0)	grid
0.500000E+07	303.84	140.23	14.023	17.5271	17.4106	0.66	1.0001	1.0001	0.0	0.610	41×25
0.100000E+08	607.10	280.20	28.020	17.5440	17.4272	0.67	1.0011	1.0010	0.0	2.659	41×25
0.200000E+08	1198.63	553.21	55.321	17.7718	17.6592	0.63	1.0141	1.0144	-0.03	14.506	41×25
0.400000E+08	2209.57	1019.80	101.980	19.2814	19.3151	-0.17	1.1002	1.1095	-0.84	64.274	41×25
0.600000E+08	3047.76	1406.66	140.666	20.9680	21.2210	-1.21	1.1965	1.2190	-1.88	100.079	41×25
0.800000E+08	3810.12	1758.52	175.852	22.3634	22.7610	-1.78	1.2761	1.3074	-2.46	117.686	41×25
0.100000E+09	4529.12	2090.36	209.036	23.5165	24.0046	-2.08	1.3419	1.3788	-2.76	123.595	41×25
0.120000E+09	5216.43	2407.58	240.758	24.5016	25.0508	-2.24	1.3981	1.4389	-2.92	123.502	41×25
0.128000E+09	5483.89	2531.03	253.103	24.8603	25.4280	-2.28	1.4186	1.4606	-2.96	122.620	41×25
0.150000E+09	6200.81	2861.91	286.191	25.7649	26.3655	-2.33	1.4702	1.5145	-3.01	118.849	41×25
0.180000E+09	7143.15	3296.84	329.684	26.8392	27.4195	-2.16	1.5315	1.5750	-2.84	110.737	41×25
0.185000E+09	7297.63	3368.14	336.814	27.0008	27.5625	-2.08	1.5407	1.5832	-2.76	108.647	41×25
0.187000E+09	7359.41	3396.65	339.665	27.0636	27.6151	-2.04	1.5443	1.5862	-2.72	107.654	41×25
0.188000E+09	7390.32	3410.92	341.092	27.0945	27.6401	-2.01	1.5460	1.5877	-2.69	107.106	41×25
0.189000E+09	7421.26	3425.20	342.520	27.1250	27.6639	-1.99	1.5478	1.5890	-2.67	106.515	41×25
0.190000E+09	7452.26	3439.51	343.951	27.1551	27.6866	-1.96	1.5495	1.5903	-2.64	105.868	41×25
0.191000E+09	7483.33	3453.85	345.385	27.1847	27.7075	-1.92	1.5512	1.5915	-2.60	105.148	41×25
0.192000E+09	7514.53	3468.25	346.825	27.2136	27.7264	-1.88	1.5528	1.5926	-2.56	104.327	41×25
0.193000E+09	7545.93	3482.74	348.274	27.2415	27.7419	-1.84	1.5544	1.5935	-2.52	103.347	41×25
0.194000E+09	7577.71	3497.41	349.741	27.2678	27.7522	-1.78	1.5559	1.5941	-2.45	102.093	41×25
0.195000E+09	7610.71	3512.64	351.264	27.2895	27.7466	-1.67	1.5572	1.5938	-2.35	99.993	41×25

$\gamma = 0.3$ 4-cell solution

pgrad	<w>	Re	Dn	f_1-Re	f_2-Re	%df	β_1	β_2	%dβ	u(4.0)	grid
0.190000E+09	7444.88	3436.10	343.610	27.1821	28.5679	-5.10	1.5510	1.6410	-5.80	-184.182	41×25
0.180000E+09	7152.41	3301.12	330.112	26.8044	27.9716	-4.35	1.5295	1.6067	-5.05	-168.085	41×25
0.160000E+09	6549.58	3022.88	302.288	26.0191	26.7759	-2.91	1.4847	1.5380	-3.59	-134.831	41×25
0.140000E+09	5920.01	2732.31	273.231	25.1879	25.5803	-1.56	1.4372	1.4694	-2.23	-94.240	41×25
0.130000E+09	5595.57	2582.57	258.257	24.7448	24.9652	-0.89	1.4120	1.4340	-1.56	-49.263	41×25

$\chi = 0.4$ 2-cell solution

pgrad	<w>	Re	Dn	f_1-Re	f_2-Re	%df	β_1	β_2	%dβ	u(4,0)	grid
0.100000E+07	99.67	56.96	5.696	16.3799	16.2748	0.64	1.0000	1.0000	0.0	0.093	41x17
0.500000E+07	496.28	283.59	28.359	16.4488	16.3419	0.65	1.0042	1.0041	0.01	2.819	41x17
0.100000E+08	954.97	545.70	54.570	17.0963	16.9969	0.58	1.0438	1.0444	-0.06	15.877	41x17
0.200000E+08	1688.56	964.89	96.489	19.3378	19.3532	-0.08	1.1806	1.1892	-0.73	48.470	41x17
0.300000E+08	2315.88	1323.36	132.336	21.1495	21.2671	-0.56	1.2912	1.3068	-1.20	62.585	41x17
0.400000E+08	2899.79	1657.02	165.702	22.5210	22.6986	-0.79	1.3749	1.3947	-1.44	65.340	41x17
0.500000E+08	3453.86	1973.64	197.364	23.6351	23.8537	-0.92	1.4430	1.4657	-1.58	63.149	41x17
0.550000E+08	3721.34	2126.48	212.648	24.1300	24.3653	-0.98	1.4732	1.4971	-1.63	61.305	41x17
0.600000E+08	3983.15	2276.08	227.608	24.5934	24.8436	-1.02	1.5015	1.5265	-1.67	59.212	41x17
0.700000E+08	4491.92	2566.81	256.681	25.4425	25.7148	-1.07	1.5533	1.5801	-1.72	54.248	41x17
0.725000E+08	4616.51	2638.01	263.801	25.6400	25.9153	-1.07	1.5654	1.5924	-1.73	52.688	41x17
0.735000E+08	4666.12	2666.35	266.635	25.7173	25.9934	-1.07	1.5701	1.5972	-1.73	51.987	41x17
0.745000E+08	4715.62	2694.64	269.464	25.7935	26.0700	-1.07	1.5747	1.6019	-1.72	51.224	41x17
0.750000E+08	4740.34	2708.77	270.877	25.8312	26.1077	-1.07	1.5770	1.6042	-1.72	50.811	41x17
0.755000E+08	4765.05	2722.88	272.288	25.8687	26.1450	-1.07	1.5793	1.6065	-1.72	50.374	41x17
0.760000E+08	4789.74	2737.00	273.700	25.9057	26.1817	-1.07	1.5816	1.6087	-1.72	49.906	41x17
0.765000E+08	4814.43	2751.10	275.110	25.9424	26.2180	-1.06	1.5838	1.6110	-1.71	49.400	41x17
0.770000E+08	4839.13	2765.21	276.521	25.9787	26.2536	-1.06	1.5860	1.6132	-1.71	48.847	41x17
0.775000E+08	4863.84	2779.34	277.934	26.0146	26.2884	-1.05	1.5882	1.6153	-1.70	48.231	41x17
0.780000E+08	4888.59	2793.48	279.348	26.0498	26.3223	-1.05	1.5904	1.6174	-1.70	47.529	41x17
0.785000E+08	4913.43	2807.68	280.768	26.0842	26.3548	-1.04	1.5925	1.6194	-1.69	46.692	41x17
0.790000E+08	4938.44	2821.97	282.197	26.1175	26.3851	-1.02	1.5945	1.6212	-1.68	45.630	41x17
0.795000E+08	4963.91	2836.52	283.652	26.1479	26.4105	-1.00	1.5964	1.6228	-1.66	44.005	41x17

$\chi = 0.4$ 4-cell solution

pgrad	<w>	Re	Dn	f_1-Re	f_2-Re	%df	β_1	β_2	%dβ	u(4,0)	grid
0.850000E+08	5169.00	2953.71	295.371	26.8476	27.9139	-3.97	1.6391	1.7152	-4.64	-180.270	41x17
0.800000E+08	4945.82	2826.19	282.619	26.4086	27.3139	-3.43	1.6123	1.6783	-4.10	-164.972	41x17
0.750000E+08	4717.59	2695.76	269.576	25.9558	26.7020	-2.87	1.5846	1.6407	-3.54	-149.258	41x17
0.700000E+08	4483.73	2562.13	256.213	25.4890	26.0799	-2.32	1.5561	1.6025	-2.98	-132.935	41x17
0.600000E+08	3996.90	2283.95	228.395	24.5088	24.8134	-1.24	1.4963	1.5247	-1.90	-95.694	41x17

0.575000E+08	3871.02	2212.01	221.201	24.2514	24.4907	-0.99	1.4800	1.5091	-1.97	-83.087	41x17
0.570000E+08	3845.70	2197.54	219.754	24.1988	24.4250	-0.94	1.4767	1.5051	-1.92	-79.987	41x17
0.565000E+08	3820.37	2183.07	218.307	24.1455	24.3586	-0.88	1.4735	1.5010	-1.86	-76.490	41x17
0.560000E+08	3795.08	2168.62	216.862	24.0913	24.2907	-0.83	1.4708	1.4925	-1.48	-72.335	41x17
0.555000E+08	3770.00	2154.29	215.429	24.0350	24.2192	-0.77	1.4674	1.4882	-1.42	-66.669	41x17
0.550000E+08	3721.34	2126.48	212.648	24.1300	24.3653	-0.98	1.4732	1.4971	-1.63	61.305	41x17

γ = 0.5 2-cell solution

pgrad	<w>	Re	Dn	f_1-Re	f_2-Re	%df	β_1	β_2	%dβ	u(.4,0)	grid
0.100000E+07	142.81	95.21	9.521	15.5605	15.4748	0.55	1.0002	1.0002	0.0	0.257	41x21
0.300000E+07	423.95	282.63	28.263	15.7250	15.6368	0.56	1.0108	1.0106	0.01	2.955	41x21
0.600000E+07	792.51	528.34	52.834	16.8241	16.7460	0.46	1.0814	1.0823	-0.08	14.598	41x21
0.100000E+08	1195.06	796.71	79.671	18.5950	18.5661	0.16	1.1953	1.2000	-0.40	29.416	41x21
0.150000E+08	1642.99	1095.32	109.532	20.2883	20.3087	-0.10	1.3041	1.3126	-0.65	37.543	41x21
0.200000E+08	2062.91	1375.27	137.527	21.5445	21.5924	-0.22	1.3848	1.3956	-0.78	38.760	41x21
0.250000E+08	2462.25	1641.50	164.150	22.5629	22.6286	-0.29	1.4503	1.4625	-0.84	36.907	41x21
0.275000E+08	2654.96	1769.97	176.997	23.0177	23.0909	-0.32	1.4795	1.4924	-0.87	35.481	41x21
0.280000E+08	2692.97	1795.32	179.532	23.1054	23.1799	-0.32	1.4852	1.4982	-0.88	35.176	41x21
0.300000E+08	2843.41	1895.61	189.561	23.4460	23.5260	-0.34	1.5071	1.5205	-0.90	33.878	41x21
0.350000E+08	3208.98	2139.32	213.932	24.2375	24.3293	-0.38	1.5579	1.5725	-0.93	30.111	41x21
0.370000E+08	3351.60	2234.40	223.440	24.5322	24.6274	-0.39	1.5769	1.5917	-0.94	28.174	41x21
0.380000E+08	3422.30	2281.53	228.153	24.6747	24.7711	-0.39	1.5860	1.6010	-0.94	26.984	41x21
0.385000E+08	3457.54	2305.03	230.503	24.7446	24.8413	-0.39	1.5905	1.6056	-0.95	26.291	41x21
0.390000E+08	3492.74	2328.49	232.849	24.8134	24.9103	-0.39	1.5950	1.6100	-0.94	25.495	41x21
0.395000E+08	3527.92	2351.95	235.195	24.8808	24.9776	-0.39	1.5993	1.6144	-0.94	24.540	41x21
0.400000E+08	3563.20	2375.47	237.547	24.9463	25.0423	-0.38	1.6035	1.6186	-0.94	23.296	41x21
0.405000E+08	3598.89	2399.26	239.926	25.0077	25.1015	-0.38	1.6074	1.6224	-0.93	21.274	41x21

γ = 0.5 4-cell solution

pgrad	<w>	Re	Dn	f_1-Re	f_2-Re	%df	β_1	β_2	%dβ	u(.4,0)	grid
0.500000E+08	4137.25	2758.17	275.817	26.8563	27.7963	-3.50	1.7263	1.7966	-4.07	-159.970	41x21
0.450000E+08	3834.84	2556.56	255.656	26.0767	26.8139	-2.83	1.6762	1.7331	-3.39	-139.377	41x21
0.400000E+08	3520.74	2347.16	234.716	25.2472	25.7787	-2.11	1.6228	1.6661	-2.67	-117.646	41x21

0.350000E+08	3192.46	2128.31	212.831	24.3629	24.6935	-1.36	1.5660	1.5960	-1.92	-94.208	41×21
0.300000E+08	2847.66	1898.44	189.844	23.4110	23.5552	-0.62	1.5048	1.5224	-1.17	-65.311	41×21
0.290000E+08	2777.72	1851.81	185.181	23.2005	23.3048	-0.45	1.4913	1.5063	-1.00	-55.107	41×21

$\gamma = 0.6$ 2-cell solution

pgrad	<w>	Re	Dn	f_1-Re	f_2-Re	%df	β_1	β_2	%dβ	u(4,0)	grid
0.400000E+07	674.04	505.53	50.553	16.6904	16.6235	0.40	1.1136	1.1145	-0.08	12.176	41×25
0.100000E+08	1398.73	1049.05	104.905	20.1075	20.0931	0.07	1.3416	1.3471	-0.41	24.785	41×25
0.125000E+08	1672.85	1254.64	125.464	21.0157	21.0101	0.03	1.4022	1.4086	-0.46	24.305	41×25
0.150000E+08	1935.66	1451.75	145.175	21.7949	21.7956	-0.0	1.4542	1.4612	-0.49	22.640	41×25
0.165000E+08	2088.21	1566.15	156.615	22.2230	22.2271	-0.02	1.4827	1.4902	-0.50	21.356	41×25
0.200000E+08	2430.83	1823.13	182.313	23.1402	23.1516	-0.05	1.5439	1.5521	-0.53	17.762	41×25
0.225000E+08	2666.39	1999.79	199.979	23.7329	23.7484	-0.07	1.5835	1.5922	-0.55	13.773	41×25
0.230000E+08	2713.01	2034.76	203.476	23.8434	23.8591	-0.07	1.5908	1.5996	-0.55	12.326	41×25
0.235000E+08	2760.49	2070.36	207.036	23.9428	23.9572	-0.06	1.5975	1.6061	-0.54	8.882	41×25

$\gamma = 0.6$ 4-cell solution

pgrad	<w>	Re	Dn	f_1-Re	f_2-Re	%df	β_1	β_2	%dβ	u(4,0)	grid
0.350000E+08	3610.27	2707.70	270.770	27.2660	28.1216	-3.14	1.8192	1.8853	-3.64	-144.652	41×25
0.275000E+08	3036.33	2277.25	227.725	25.4727	25.9998	-2.07	1.6995	1.7431	-2.56	-108.511	41×25
0.245000E+08	2793.33	2094.99	209.499	24.6682	25.0556	-1.57	1.6459	1.6798	-2.06	-92.511	41×25
0.235000E+08	2710.11	2032.58	203.258	24.3878	24.7283	-1.40	1.6272	1.6578	-1.89	-86.929	41×25
0.225000E+08	2625.74	1969.30	196.930	24.1004	24.3940	-1.22	1.6080	1.6354	-1.71	-81.195	41×25
0.200000E+08	2409.11	1806.83	180.683	23.3489	23.5285	-0.77	1.5578	1.5774	-1.26	-65.892	41×25
0.175000E+08	2184.80	1638.60	163.860	22.5278	22.5956	-0.30	1.5031	1.5149	-0.79	-46.024	41×25

$\gamma = 0.8$ 2-cell solution

pgrad	<w>	Re	Dn	f_1-Re	f_2-Re	%df	β_1	β_2	%dβ	u(4,0)	grid
0.400000E+07	851.90	757.24	75.724	18.5498	18.4707	0.43	1.2893	1.2914	-0.16	11.691	41×17
0.500000E+07	1022.98	909.32	90.932	19.3092	19.2485	0.31	1.3421	1.3457	-0.27	11.534	41×21

0.600000E+07	1185.75	1054.00	105.400	19.9904	19.9310	0.30	1.3894	1.3934	-0.29	10.574	41x17
0.650000E+07	1265.24	1124.66	112.466	20.2957	20.2422	0.26	1.4106	1.4152	-0.32	9.915	41x17
0.700000E+07	1343.21	1193.96	119.396	20.5882	20.5413	0.23	1.4310	1.4361	-0.36	9.169	41x17
0.725000E+07	1381.64	1228.12	122.812	20.7304	20.6870	0.21	1.4409	1.4463	-0.38	8.766	41x17
0.800000E+07	1494.84	1328.75	132.875	21.1426	21.1106	0.15	1.4695	1.4759	-0.44	7.419	41x17
0.900000E+07	1641.42	1459.04	145.904	21.6615	21.6475	0.06	1.5056	1.5135	-0.52	5.056	41x17
0.950000E+07	1713.22	1522.86	152.286	21.9066	21.9032	0.02	1.5226	1.5313	-0.57	3.075	41x17
0.970000E+07	1741.94	1548.39	154.839	21.9990	22.0008	-0.01	1.5290	1.5382	-0.60	1.383	41x17
0.975000E+07	1749.36	1554.99	155.499	22.0186	22.0225	-0.02	1.5304	1.5397	-0.61	0.017	41x17

γ = 0.8 4-cell solution

pgrad	<w>	Re	Dn	f_1-Re	f_2-Re	%df	β_1	β_2	%dβ	u(.4,0)	grid
0.200000E+08	2856.81	2539.39	253.939	27.6575	28.2222	-2.04	1.9223	1.9731	-2.64	-110.777	41x17
0.150000E+08	2320.30	2062.49	206.249	25.5394	25.8708	-1.30	1.7751	1.8087	-1.89	-82.205	41x17
0.120000E+08	1976.09	1756.53	175.653	23.9904	24.1726	-0.76	1.6674	1.6900	-1.35	-62.238	41x17
0.110000E+08	1856.07	1649.84	164.984	23.4133	23.5464	-0.57	1.6273	1.6462	-1.16	-54.935	41x17
0.100000E+08	1732.83	1540.29	154.029	22.7987	22.8844	-0.38	1.5846	1.5999	-0.97	-47.184	41x17
0.900000E+07	1606.17	1427.71	142.771	22.1369	22.1781	-0.19	1.5386	1.5505	-0.78	-38.697	41x17
0.800000E+07	1478.45	1314.18	131.418	21.3771	21.3773	-0.0	1.4858	1.4946	-0.59	-27.402	41x17
0.800000E+07	1480.41	1315.92	131.592	21.3487	21.3490	-0.0	1.4838	1.4926	-0.59	-27.348	41x21
0.790000E+07	1468.59	1305.42	130.542	21.2515	21.2455	0.03	1.4771	1.4853	-0.56	-25.333	41x21

γ = 1.0 2-cell solution

pgrad	<w>	Re	Dn	f_1-Re	f_2-Re	%df	β_1	β_2	%dβ	u(.4,0)	grid
0.100000E+03	0.04	0.04	0.004	14.2349	-14.1657	0.49	1.0000	1.0000	0.0	0.0	41x21
0.100000E+04	0.35	0.35	0.035	14.2349	14.1657	0.49	1.0000	1.0000	0.0	0.0	41x21
0.100000E+05	3.51	3.51	0.351	14.2349	14.1657	0.49	1.0000	1.0000	0.0	0.0	41x21
0.100000E+06	35.12	35.12	3.512	14.2356	14.1663	0.49	1.0000	1.0000	0.0	0.033	41x21
0.400000E+06	139.66	139.66	13.966	14.3208	14.2491	0.50	1.0060	1.0059	0.01	0.574	41x21
0.900000E+06	295.66	295.66	29.566	15.2203	15.1425	0.51	1.0692	1.0689	0.03	2.877	41x21
0.190000E+07	551.35	551.35	55.135	17.2305	17.1513	0.46	1.2104	1.2108	-0.03	6.125	41x21
0.400000E+07	1019.27	1019.27	101.927	19.6219	19.5541	0.35	1.3784	1.3804	-0.14	4.369	41x21

0.450000E+07	1121.35	1121.35	112.135	20.0650	20.0026	0.31	1.4096	1.4120	-0.18	3.240	41×21
0.475000E+07	1171.27	1171.27	117.127	20.2771	20.2178	0.29	1.4245	1.4272	-0.19	2.524	41×21
0.500000E+07	1220.50	1220.50	122.050	20.4833	20.4277	0.27	1.4389	1.4420	-0.22	1.579	41×21
0.525000E+07	1269.14	1269.14	126.914	20.6833	20.6325	0.25	1.4530	1.4565	-0.24	-0.259	41×21

γ = 1.0 4-cell solution

pgrad	<w>	Re	Dn	f_1-Re	f_2-Re	%df	β_1	β_2	%dβ	u(4,0)	grid
0.200000E+08	3322.31	3322.31	332.231	30.0995	30.5891	-1.63	2.1145	2.1594	-2.12	-115.565	41×21
0.180000E+08	3064.33	3064.33	306.433	29.3702	29.8143	-1.51	2.0633	2.1047	-2.01	-104.541	41×21
0.160000E+08	2799.60	2799.60	279.960	28.5755	28.9719	-1.39	2.0074	2.0452	-1.88	-93.717	41×21
0.140000E+08	2528.01	2528.01	252.801	27.6898	28.0331	-1.24	1.9452	1.9789	-1.73	-82.939	41×21
0.110000E+08	2106.79	2106.79	210.679	26.1061	26.3519	-0.94	1.8339	1.8603	-1.43	-66.203	41×21
0.700000E+07	1508.46	1508.46	150.846	23.2025	23.2790	-0.33	1.6300	1.6433	-0.82	-40.037	41×21
0.600000E+07	1348.21	1348.21	134.821	22.2517	22.2819	-0.14	1.5632	1.5729	-0.62	-32.077	41×21
0.575000E+07	1307.28	1307.28	130.728	21.9921	22.0109	-0.09	1.5449	1.5538	-0.57	-29.927	41×21
0.550000E+07	1266.04	1266.04	126.604	21.7213	21.7287	-0.03	1.5259	1.5339	-0.52	-27.683	41×21
0.525000E+07	1224.54	1224.54	122.454	21.4365	21.4328	0.02	1.5059	1.5130	-0.47	-25.308	41×21
0.500000E+07	1182.99	1182.99	118.299	21.1329	21.1181	0.07	1.4846	1.4908	-0.42	-22.723	41×21
0.475000E+07	1141.98	1141.98	114.198	20.7972	20.7712	0.13	1.4610	1.4663	-0.36	-19.689	41×24
0.470000E+07	1134.01	1134.01	113.401	20.7228	20.6944	0.14	1.4558	1.4609	-0.35	-18.963	41×21
0.465000E+07	1126.24	1126.24	112.624	20.6439	20.6130	0.15	1.4502	1.4551	-0.34	-18.153	41×21
0.460000E+07	1118.82	1118.82	111.882	20.5573	20.5238	0.16	1.4441	1.4488	-0.32	-17.194	41×21
0.455000E+07	1112.27	1112.27	111.227	20.4536	20.4167	0.18	1.4369	1.4413	-0.31	-15.884	41×21

γ = 1.2 2-cell solution

pgrad	<w>	Re	Dn	f_1-Re	f_2-Re	%df	β_1	β_2	%dβ	u(4,0)	grid
0.100000E+07	367.04	400.40	40.040	16.2121	16.1105	0.63	1.1306	1.1312	-0.05	3.331	31×19
0.200000E+07	656.66	716.36	71.636	18.1232	18.0321	0.50	1.2639	1.2661	-0.18	3.534	31×19
0.300000E+07	917.52	1000.94	100.094	19.4559	19.3851	0.36	1.3568	1.3611	-0.32	1.738	31×19
0.350000E+07	1039.28	1133.76	113.376	20.0392	19.9870	0.26	1.3975	1.4033	-0.42	-0.554	31×19
0.350000E+07	1040.97	1135.60	113.560	20.0068	19.9448	0.31	1.3952	1.4004	-0.37	-0.253	41×25

γ = 1.2 4-cell solution

pgrad	<w>	Re	Dn	f_1-Re	f_2-Re	%df	β_1	β_2	%dβ	u(.4,0)	grid
0.600000E+07	1480.02	1614.56	161.456	24.1230	24.3992	-1.14	1.6823	1.7131	-1.84	-37.399	31×25
0.400000E+07	1091.10	1190.29	119.029	21.8144	21.8963	-0.38	1.5213	1.5374	-1.06	-22.302	31×19
0.375000E+07	1041.39	1136.07	113.607	21.4271	21.4831	-0.26	1.4943	1.5084	-0.95	-19.963	31×19
0.360000E+07	1011.53	1103.48	110.348	21.1774	21.2176	-0.19	1.4768	1.4897	-0.87	-18.472	31×19
0.360000E+07	1014.05	1106.24	110.624	21.1246	21.1030	0.10	1.4732	1.4817	-0.58	-18.124	41×25
0.350000E+07	991.67	1081.82	108.182	21.0014	21.0310	-0.14	1.4646	1.4766	-0.82	-17.423	31×19
0.350000E+07	994.06	1084.43	108.443	20.9510	20.9250	0.12	1.4611	1.4692	-0.56	-17.100	41×25
0.340000E+07	974.19	1062.75	106.275	20.7674	20.7371	0.15	1.4482	1.4560	-0.54	-16.011	41×25
0.320000E+07	935.65	1020.71	102.071	20.3509	20.3114	0.19	1.4192	1.4261	-0.49	-13.439	41×25
0.310000E+07	918.83	1002.36	100.236	20.0757	20.0303	0.23	1.4000	1.4064	-0.45	-11.487	41×25

γ = 1.28 2-cell solution

pgrad	<w>	Re	Dn	f_1-Re	f_2-Re	%df	β_1	β_2	%dβ	u(.4,0)	grid
0.100000E+06	43.71	49.07	4.907	14.4223	14.3444	0.54	1.0002	0.9998	0.05	0.055	31×25
0.200000E+06	87.26	97.98	9.798	14.4470	14.3744	0.50	1.0019	1.0018	0.01	0.229	41×21
0.500000E+06	210.13	235.93	23.593	14.9990	14.9167	0.55	1.0402	1.0396	0.06	1.404	31×25
0.350000E+06	150.87	169.40	16.940	14.6233	14.5479	0.52	1.0142	1.0139	0.02	0.726	41×21
0.100000E+07	383.19	430.25	43.025	16.4501	16.3688	0.49	1.1409	1.1409	0.0	3.033	31×25

γ = 1.28 2-cell solution (isolated)

pgrad	<w>	Re	Dn	f_1-Re	f_2-Re	%df	β_1	β_2	%dβ	u(.4,0)	grid
0.500000E+07	1438.62	1615.29	161.529	21.9080	21.8816	0.12	1.5649	1.5630	0.12	3.616	31×25
0.520000E+07	1482.82	1664.92	166.492	22.1052	22.0846	0.09	1.5789	1.5775	0.09	4.285	31×25
0.530000E+07	1504.74	1689.53	168.953	22.2021	22.1846	0.08	1.5859	1.5846	0.08	4.566	31×25
0.540000E+07	1526.54	1714.01	171.401	22.2980	22.2837	0.06	1.5927	1.5917	0.06	4.820	31×25
0.550000E+07	1548.22	1738.36	173.836	22.3928	22.3818	0.05	1.5995	1.5987	0.05	5.050	31×25
0.560000E+07	1569.80	1762.58	176.258	22.4866	22.4788	0.03	1.6062	1.6056	0.03	5.259	31×25
0.570000E+07	1591.27	1786.69	178.669	22.5792	22.5749	0.02	1.6128	1.6125	0.02	5.450	31×25
0.580000E+07	1612.65	1810.69	181.069	22.6709	22.6699	0.0	1.6193	1.6193	0.0	5.623	31×25

0.590000E+07	1633.92	1834.58	183.458	22.7615	22.7640	-0.01	1.6258	1.6260	-0.01	5.779	31×25
0.600000E+07	1655.10	1858.36	185.836	22.8511	22.8571	-0.03	1.6322	1.6326	-0.03	5.921	31×25
0.610000E+07	1676.19	1882.03	188.203	22.9397	22.9492	-0.04	1.6385	1.6392	-0.04	6.048	31×25
0.620000E+07	1697.18	1905.61	190.561	23.0273	23.0403	-0.06	1.6448	1.6457	-0.06	6.162	31×25
0.630000E+07	1718.09	1929.08	192.908	23.1139	23.1305	-0.07	1.6510	1.6522	-0.07	6.263	31×25
0.640000E+07	1738.92	1952.47	195.247	23.1996	23.2197	-0.09	1.6571	1.6585	-0.09	6.351	31×25
0.650000E+07	1759.66	1975.76	197.576	23.2843	23.3080	-0.10	1.6632	1.6649	-0.10	6.428	31×25
0.660000E+07	1780.33	1998.97	199.897	23.3681	23.3954	-0.12	1.6691	1.6711	-0.12	6.493	31×25
0.670000E+07	1800.92	2022.08	202.208	23.4510	23.4819	-0.13	1.6751	1.6773	-0.13	6.545	31×25

γ = 1.35 2-cell solution

pgrad	<w>	Re	Dn	f_1-Re	f_2-Re	%df	β_1	β_2	%dβ	u(.4,0)	grid
0.100000E+06	45.50	52.28	5.228	14.5057	14.4531	0.36	1.0002	1.0002	0.0	0.059	41×29
0.200000E+06	90.80	104.33	10.433	14.5372	14.4836	0.37	1.0024	1.0023	0.01	0.245	41×29
0.400000E+06	177.52	203.96	20.396	14.8719	14.8146	0.39	1.0255	1.0252	0.03	0.982	41×29
0.450000E+06	197.82	227.28	22.728	15.0144	14.9559	0.39	1.0353	1.0350	0.03	1.206	41×29
0.500000E+06	217.57	249.98	24.998	15.1680	15.1086	0.39	1.0459	1.0455	0.03	1.426	41×29
0.750000E+06	310.24	356.45	35.645	15.9560	15.8933	0.39	1.1002	1.0998	0.03	2.305	41×29
0.100000E+07	396.68	455.76	45.576	16.6388	16.5740	0.39	1.1473	1.1469	0.03	2.714	41×29
0.150000E+07	559.11	642.38	64.238	17.7074	17.6402	0.38	1.2210	1.2207	0.02	2.616	41×29
0.200000E+07	711.20	817.13	81.713	18.5608	18.4933	0.36	1.2798	1.2798	0.0	2.047	41×29
0.250000E+07	854.92	982.24	98.224	19.3009	19.2350	0.34	1.3308	1.3311	-0.02	1.308	41×29
0.260000E+07	882.78	1014.26	101.426	19.4394	19.3740	0.34	1.3404	1.3407	-0.02	1.129	41×29
0.270000E+07	910.37	1045.96	104.596	19.5752	19.5106	0.33	1.3498	1.3502	-0.03	0.925	41×29
0.280000E+07	937.68	1077.34	107.734	19.7090	19.6451	0.32	1.3590	1.3595	-0.04	0.682	41×29
0.290000E+07	964.71	1108.39	110.839	19.8409	19.7781	0.32	1.3681	1.3687	-0.04	0.333	41×29
0.295000E+07	978.08	1123.75	112.375	19.9072	19.8451	0.31	1.3727	1.3733	-0.05	0.045	41×29

γ = 1.35 2-cell solution (isolated)

pgrad	<w>	Re	Dn	f_1-Re	f_2-Re	%df	β_1	β_2	%dβ	u(.4,0)	grid
0.380000E+07	1111.74	1277.31	127.731	22.5602	22.6682	-0.48	1.5556	1.5687	-0.84	-22.638	31×25

0.395000E+07	1147.08	1317.93	131.793	22.7281	22.7373	-0.04	1.5672	1.5735	-0.40	-23.469	41x29
0.400000E+07	1247.59	1433.40	143.340	21.1617	21.1197	0.20	1.4592	1.4615	-0.16	1.542	31x25
0.450000E+07	1368.12	1571.88	157.188	21.7095	21.6802	0.14	1.4969	1.5003	-0.23	3.766	31x25
0.500000E+07	1484.64	1705.76	170.576	22.2285	22.2159	0.06	1.5327	1.5374	-0.30	4.873	31x25
0.520000E+07	1530.34	1758.27	175.827	22.4272	22.4219	0.02	1.5464	1.5516	-0.34	5.171	31x25
0.540000E+07	1575.59	1810.25	181.025	22.6211	22.6230	-0.01	1.5598	1.5655	-0.37	5.401	31x25
0.550000E+07	1599.99	1838.29	183.829	22.6886	22.6629	0.11	1.5644	1.5683	-0.25	5.271	41x29
0.555000E+07	1611.21	1851.17	185.117	22.7354	22.7108	0.11	1.5677	1.5716	-0.25	5.311	41x29
0.560000E+07	1622.40	1864.04	186.404	22.7820	22.7584	0.10	1.5709	1.5749	-0.26	5.348	41x29
0.565000E+07	1633.57	1876.87	187.687	22.8282	22.8057	0.10	1.5741	1.5782	-0.26	5.380	41x29
0.570000E+07	1644.72	1889.67	188.967	22.8742	22.8526	0.09	1.5772	1.5814	-0.27	5.409	41x29
0.575000E+07	1655.84	1902.45	190.245	22.9198	22.8993	0.09	1.5804	1.5847	-0.27	5.436	41x29
0.580000E+07	1666.94	1915.21	191.521	22.9652	22.9457	0.08	1.5835	1.5879	-0.28	5.459	41x29
0.590000E+07	1689.06	1940.63	194.063	23.0551	23.0378	0.08	1.5897	1.5942	-0.29	5.495	41x29
0.600000E+07	1711.09	1965.94	196.594	23.1440	23.1285	0.07	1.5958	1.6005	-0.29	5.507	41x29

γ = 1.35 4-cell solution

pgrad	<w>	Re	Dn	f_1-Re	f_2-Re	%df	β_1	β_2	%dβ	u(.4,0)	grid
0.800000E+07	2000.16	2298.06	229.806	26.3989	26.4921	-0.35	1.8203	1.8333	-0.72	-50.231	41x29
0.750000E+07	1899.52	2182.43	218.243	26.0602	26.1463	-0.33	1.7969	1.8094	-0.69	-47.053	41x29
0.700000E+07	1797.56	2065.28	206.528	25.7026	25.7811	-0.31	1.7723	1.7841	-0.67	-43.886	41x29
0.650000E+07	1694.28	1946.61	194.661	25.3216	25.3919	-0.28	1.7460	1.7572	-0.64	-40.716	41x29
0.600000E+07	1589.70	1826.46	182.646	24.9114	24.9725	-0.25	1.7177	1.7281	-0.61	-37.524	41x29
0.550000E+07	1483.83	1704.83	170.483	24.4647	24.5155	-0.21	1.6869	1.6965	-0.57	-34.282	41x29
0.500000E+07	1376.66	1581.70	158.170	23.9720	24.0110	-0.16	1.6529	1.6616	-0.52	-30.955	41x29
0.475000E+07	1322.57	1519.55	151.955	23.7048	23.7374	-0.14	1.6345	1.6427	-0.50	-29.246	41x29
0.450000E+07	1268.13	1457.00	145.700	23.4212	23.4469	-0.11	1.6150	1.6226	-0.47	-27.497	41x29
0.425000E+07	1213.33	1394.04	139.404	23.1191	23.1375	-0.08	1.5941	1.6011	-0.44	-25.701	41x29
0.400000E+07	1158.16	1330.66	133.066	22.7956	22.8064	-0.05	1.5718	1.5782	-0.41	-23.848	41x29
0.380000E+07	1111.74	1277.31	127.731	22.5602	22.6682	-0.48	1.5556	1.5687	-0.84	-22.638	31x25
0.375000E+07	1102.62	1266.84	126.684	22.4474	22.4501	-0.01	1.5478	1.5536	-0.37	-21.926	41x29
0.350000E+07	1046.73	1202.62	120.262	22.0697	22.0638	0.03	1.5218	1.5268	-0.33	-19.919	41x29
0.300000E+07	934.31	1073.47	107.347	21.1929	21.1688	0.11	1.4613	1.4649	-0.25	-15.527	41x29
0.280000E+07	889.69	1022.20	102.220	20.7722	20.7401	0.15	1.4323	1.4352	-0.21	-13.511	41x29

0.270000E+07	867.82	997.07	99.707	20.5350	20.4987	0.18	1.4159	1.4185	-0.18	-12.377	41x29
0.260000E+07	846.78	972.89	97.289	20.2659	20.2250	0.20	1.3974	1.3996	-0.16	-11.059	41x29
0.255000E+07	837.01	961.67	96.167	20.1082	20.0646	0.22	1.3865	1.3885	-0.14	-10.244	41x29
0.252500E+07	832.57	956.58	95.658	20.0170	19.9719	0.23	1.3802	1.3821	-0.13	-9.745	41x29
0.250000E+07	828.92	952.38	95.238	19.9062	19.8592	0.24	1.3726	1.3743	-0.12	-9.087	41x29

$\gamma = 1.4$ 2-cell solution

pgrad	<w>	Re	Dn	f_1-Re	f_2-Re	%df	β_1	β_2	%dβ	u(4,0)	grid
0.100000E+06	46.68	54.46	5.446	14.5798	14.4806	0.68	1.0002	1.0002	-0.0	0.062	31x19
0.300000E+06	138.48	161.56	16.156	14.7437	14.6416	0.69	1.0115	1.0114	0.01	0.589	31x19
0.400000E+06	181.67	211.94	21.194	14.9847	14.8808	0.69	1.0280	1.0279	0.01	1.012	31x19
0.500000E+06	222.48	259.56	25.956	15.2947	15.1895	0.69	1.0493	1.0492	0.01	1.441	31x19
0.700000E+06	298.81	348.61	34.861	15.9428	15.8366	0.67	1.0937	1.0939	-0.01	2.110	31x19
0.800000E+06	335.19	391.06	39.106	16.2428	16.1367	0.65	1.1143	1.1146	-0.03	2.320	31x19
0.900000E+06	370.73	432.52	43.252	16.5215	16.4158	0.64	1.1334	1.1339	-0.04	2.453	31x19
0.100000E+07	405.56	473.16	47.316	16.7805	16.6753	0.63	1.1512	1.1518	-0.05	2.521	31x19
0.130000E+07	506.61	591.04	59.104	17.4637	17.3616	0.58	1.1981	1.1992	-0.10	2.465	31x19
0.170000E+07	634.64	740.42	74.042	18.2298	18.1354	0.52	1.2506	1.2527	-0.16	2.090	31x19
0.200000E+07	726.43	847.50	84.750	18.7370	18.6514	0.46	1.2854	1.2883	-0.23	1.736	31x19
0.250000E+07	872.55	1017.98	101.798	19.4989	19.4337	0.33	1.3377	1.3424	-0.35	1.076	31x19
0.275000E+07	942.75	1099.88	109.988	19.8517	19.7999	0.26	1.3619	1.3677	-0.42	0.653	31x19
0.285000E+07	970.31	1132.03	113.203	19.9893	19.9438	0.23	1.3713	1.3776	-0.46	0.401	31x19
0.290000E+07	983.94	1147.93	114.793	20.0582	20.0163	0.21	1.3761	1.3826	-0.48	0.170	31x19
0.290000E+07	986.37	1150.76	115.076	20.0088	19.9478	0.30	1.3727	1.3779	-0.38	0.224	41x29

$\gamma = 1.4$ 2-cell solution (isolated)

pgrad	<w>	Re	Dn	f_1-Re	f_2-Re	%df	β_1	β_2	%dβ	u(4,0)	grid
0.355000E+07	1159.81	1353.11	135.311	20.8307	20.7816	0.24	1.4291	1.4355	0.45	1.345	31x25
0.360000E+07	1172.81	1368.28	136.828	20.8899	20.8417	0.23	1.4331	1.4396	0.45	1.661	31x25
0.365000E+07	1185.74	1383.36	138.336	20.9492	20.9021	0.22	1.4372	1.4438	-0.46	1.919	31x25
0.370000E+07	1198.59	1398.36	139.836	21.0084	20.9625	0.22	1.4413	1.4480	-0.47	2.147	31x25
0.380000E+07	1224.13	1428.15	142.815	21.1262	21.0829	0.20	1.4493	1.4563	-0.48	2.548	31x25
0.400000E+07	1274.56	1486.98	148.698	21.3582	21.3209	0.17	1.4653	1.4727	-0.51	3.213	31x25

0.450000E+07	1397.48	1630.39	163.039	21.9144	21.8941	0.09	1.5034	1.5123	-0.59	4.360	31×25
0.500000E+07	1516.70	1769.48	176.948	22.4354	22.4339	0.01	1.5392	1.5496	-0.68	4.983	31×25
0.520000E+07	1563.51	1824.09	182.409	22.6342	22.6405	-0.03	1.5528	1.5639	-0.71	5.111	31×25
0.525000E+07	1575.14	1837.67	183.767	22.6831	22.6913	-0.04	1.5562	1.5674	-0.72	5.132	31×25
0.530000E+07	1586.75	1851.21	185.121	22.7316	22.7419	-0.05	1.5595	1.5709	-0.73	5.150	31×25
0.535000E+07	1598.33	1864.72	186.472	22.7798	22.7921	-0.05	1.5628	1.5743	-0.74	5.164	31×25
0.540000E+07	1609.89	1878.20	187.820	22.8277	22.8419	-0.06	1.5661	1.5778	-0.75	5.173	31×25

γ = 1.4 4-cell solution

pgrad	<w>	Re	Dn	f_1-Re	f_2-Re	%df	β_1	β_2	%dβ	u(4.0)	grid
0.850000E+07	2144.38	2501.78	250.178	26.9761	27.2671	-1.08	1.8507	1.8835	-1.77	-55.750	31×25
0.800000E+07	2042.89	2383.37	238.337	26.6507	26.9295	-1.05	1.8283	1.8601	-1.74	-52.239	31×25
0.750000E+07	1939.95	2263.28	226.328	26.3107	26.5771	-1.01	1.8050	1.8358	-1.70	-48.778	31×25
0.700000E+07	1835.53	2141.45	214.145	25.9537	26.2068	-0.98	1.7805	1.8102	-1.67	-45.357	31×25
0.650000E+07	1729.60	2017.87	201.787	25.5759	25.8144	-0.93	1.7546	1.7831	-1.62	-41.965	31×25
0.600000E+07	1622.18	1892.54	189.254	25.1719	25.3939	-0.88	1.7269	1.7541	-1.57	-38.584	31×25
0.550000E+07	1513.28	1765.50	176.550	24.7346	24.9375	-0.82	1.6969	1.7225	-1.51	-35.192	31×25
0.500000E+07	1402.95	1636.77	163.677	24.2545	24.4348	-0.74	1.6640	1.6878	-1.43	-31.756	31×25
0.450000E+07	1291.17	1506.36	150.636	23.7188	23.8725	-0.65	1.6272	1.6490	-1.34	-28.232	31×25
0.400000E+07	1177.93	1374.26	137.426	23.1101	23.2324	-0.53	1.5854	1.6048	-1.22	-24.563	31×25
0.400000E+07	1173.99	1369.65	136.965	23.1878	23.3067	-0.51	1.5908	1.6099	-1.20	-24.874	31×19
0.350000E+07	1060.25	1236.96	123.696	22.4658	22.5420	-0.34	1.5412	1.5571	-1.03	-20.853	31×19
0.300000E+07	945.30	1102.85	110.285	21.5980	21.6282	-0.14	1.4817	1.4940	-0.83	-16.483	31×19
0.250000E+07	832.14	970.83	97.083	20.4459	20.4258	0.10	1.4027	1.4109	-0.59	-11.186	31×19
0.235000E+07	806.06	940.41	94.041	19.8409	19.7915	0.25	1.3612	1.3671	-0.43	-8.276	41×29

γ = 1.5 2-cell solution

pgrad	<w>	Re	Dn	f_1-Re	f_2-Re	%df	β_1	β_2	%dβ	u(4.0)	grid
0.100000E+06	48.90	58.68	5.868	14.7246	14.6471	0.53	1.0003	1.0002	0.0	0.066	31×25
0.300000E+06	144.75	173.69	17.369	14.9227	14.8423	0.54	1.0137	1.0136	0.02	0.612	31×25
0.500000E+06	231.94	278.33	27.833	15.5212	15.4382	0.53	1.0544	1.0543	0.01	1.395	31×25
0.700000E+06	311.55	373.87	37.387	16.1769	16.0929	0.52	1.0989	1.0990	0.0	1.904	31×25

0.900000E+06	386.81	464.17	46.417	16.7524	16.6679	0.50	1.1380	1.1382	-0.02	2.092	31×25
0.110000E+07	459.06	550.87	55.087	17.2527	17.1680	0.49	1.1720	1.1724	-0.03	2.078	31×25
0.130000E+07	528.88	634.66	63.466	17.6977	17.6134	0.48	1.2023	1.2028	-0.05	1.965	31×25
0.150000E+07	596.60	715.92	71.592	18.1025	18.0190	0.46	1.2298	1.2305	-0.06	1.812	31×25
0.170000E+07	662.46	794.95	79.495	18.4766	18.3946	0.44	1.2552	1.2562	-0.08	1.651	31×25
0.190000E+07	726.63	871.96	87.196	18.8265	18.7467	0.42	1.2789	1.2802	-0.10	1.499	31×25
0.210000E+07	789.28	947.14	94.714	19.1566	19.0797	0.40	1.3014	1.3029	-0.12	1.369	31×25
0.230000E+07	850.54	1020.64	102.064	19.4700	19.3967	0.38	1.3227	1.3246	-0.15	1.276	31×25
0.240000E+07	880.68	1056.81	105.681	19.6213	19.5500	0.36	1.3329	1.3351	-0.16	1.254	31×25
0.242000E+07	886.67	1064.00	106.400	19.6511	19.5803	0.36	1.3350	1.3371	-0.16	1.252	31×25
0.244000E+07	892.64	1071.17	107.117	19.6808	19.6104	0.36	1.3370	1.3392	-0.17	1.252	31×25
0.246000E+07	898.61	1078.33	107.833	19.7104	19.6404	0.36	1.3390	1.3412	-0.17	1.252	31×25
0.248000E+07	904.56	1085.48	108.548	19.7399	19.6703	0.35	1.3410	1.3433	-0.17	1.254	31×25
0.250000E+07	910.51	1092.61	109.261	19.7692	19.7001	0.35	1.3430	1.3453	-0.17	1.257	31×25
0.260000E+07	940.04	1128.05	112.805	19.9140	19.8472	0.34	1.3528	1.3554	-0.19	1.296	31×25
0.270000E+07	969.29	1163.15	116.315	20.0559	19.9916	0.32	1.3625	1.3652	-0.20	1.382	31×25
0.275000E+07	983.81	1180.58	118.058	20.1257	20.0628	0.31	1.3672	1.3701	-0.21	1.445	31×25
0.285000E+07	1012.64	1215.17	121.517	20.2638	20.2035	0.30	1.3766	1.3797	-0.23	1.614	31×25
0.300000E+07	1055.36	1266.43	126.643	20.4670	20.4108	0.27	1.3904	1.3938	-0.25	1.949	31×25
0.325000E+07	1125.20	1350.24	135.024	20.7963	20.7477	0.23	1.4128	1.4169	-0.29	2.586	31×25
0.350000E+07	1193.46	1432.45	143.215	21.1151	21.0750	0.19	1.4344	1.4392	-0.33	3.164	31×25
0.375000E+07	1260.34	1512.41	151.241	21.4228	21.3919	0.14	1.4553	1.4608	-0.38	3.626	31×25
0.400000E+07	1326.03	1591.23	159.123	21.7190	21.6981	0.10	1.4754	1.4818	-0.43	3.963	31×25
0.425000E+07	1390.63	1668.76	166.876	22.0044	21.9937	0.05	1.4948	1.5019	-0.48	4.168	31×25
0.475000E+07	1517.17	1820.60	182.060	22.5419	22.5533	-0.05	1.5313	1.5402	-0.58	4.194	31×25
0.480000E+07	1529.65	1835.58	183.558	22.5933	22.6071	-0.06	1.5348	1.5438	-0.59	4.164	31×25
0.500000E+07	1463.91	1756.69	175.669	24.5917	24.7447	-0.62	1.6706	1.6898	-1.15	-32.400	31×25

$\gamma = 1.6$ 2-cell solution

pgrad	<w>	Re	Dn	f_1-Re	f_2-Re	%df	β_1	β_2	%dβ	u(.4,0)	grid
0.100000E+06	50.89	62.63	6.263	14.8835	14.8058	0.52	1.0003	1.0003	0.0	0.068	31x25
0.250000E+06	126.19	155.31	15.531	15.0053	14.9252	0.53	1.0085	1.0084	0.02	0.436	31x25
0.400000E+06	196.74	242.14	24.214	15.3990	15.3163	0.54	1.0350	1.0348	0.02	0.994	31x25
0.600000E+06	282.69	347.93	34.793	16.0755	15.9908	0.53	1.0804	1.0803	0.01	1.545	31x25
0.800000E+06	362.95	446.71	44.671	16.6942	16.6085	0.51	1.1220	1.1221	-0.0	1.753	31x25
0.900000E+06	401.63	494.31	49.431	16.9723	16.8863	0.51	1.1407	1.1408	-0.01	1.771	31x25
0.100000E+07	439.52	540.94	54.094	17.2325	17.1464	0.50	1.1582	1.1584	-0.02	1.756	31x25
0.150000E+07	619.37	762.30	76.230	18.3427	18.2591	0.46	1.2328	1.2336	-0.06	1.537	31x25
0.170000E+07	687.63	846.31	84.631	18.7248	18.6437	0.43	1.2585	1.2596	-0.09	1.474	31x25
0.180000E+07	721.09	887.50	88.750	18.9063	18.8267	0.42	1.2707	1.2719	-0.10	1.459	31x25
0.190000E+07	754.13	928.16	92.816	19.0822	19.0044	0.41	1.2825	1.2839	-0.11	1.458	31x25
0.191000E+07	757.42	932.20	93.220	19.0995	19.0219	0.41	1.2837	1.2851	-0.11	1.459	31x25
0.192000E+07	760.69	936.24	93.624	19.1168	19.0393	0.41	1.2848	1.2863	-0.11	1.460	31x25
0.193000E+07	763.97	940.27	94.027	19.1340	19.0567	0.40	1.2860	1.2875	-0.12	1.461	31x25
0.194000E+07	767.24	944.29	94.429	19.1511	19.0741	0.40	1.2872	1.2887	-0.12	1.463	31x25
0.195000E+07	770.50	948.31	94.831	19.1682	19.0914	0.40	1.2883	1.2898	-0.12	1.465	31x25
0.200000E+07	786.78	968.34	96.834	19.2531	19.1773	0.39	1.2940	1.2956	-0.12	1.476	31x25
0.220000E+07	850.94	1047.32	104.732	19.5814	19.5101	0.36	1.3161	1.3181	-0.15	1.578	31x25
0.240000E+07	913.70	1124.55	112.455	19.8944	19.8285	0.33	1.3371	1.3396	-0.19	1.790	31x25
0.250000E+07	944.57	1162.55	116.255	20.0461	19.9830	0.31	1.3473	1.3501	-0.20	1.939	31x25
0.300000E+07	1094.24	1346.75	134.675	20.7650	20.7191	0.22	1.3956	1.3998	-0.30	2.836	31x25
0.400000E+07	1375.19	1692.54	169.254	22.0303	22.0288	0.01	1.4807	1.4883	-0.51	3.530	31x25
0.425000E+07	1442.71	1775.64	177.564	22.3117	22.3233	-0.05	1.4996	1.5082	-0.57	3.288	31x25
0.427500E+07	1449.43	1783.91	178.391	22.3390	22.3520	-0.06	1.5014	1.5101	-0.58	3.245	31x25
0.430000E+07	1456.14	1792.17	179.217	22.3660	22.3804	-0.06	1.5032	1.5120	-0.59	3.198	31x25
0.432500E+07	1462.85	1800.43	180.043	22.3929	22.4087	-0.07	1.5050	1.5139	-0.59	3.143	31x25
0.435000E+07	1469.55	1808.68	180.868	22.4196	22.4367	-0.08	1.5068	1.5158	-0.60	3.080	31x25

$\gamma = 1.6$ 4-cell solution

pgrad	<w>	Re	Dn	f_1-Re	f_2-Re	%df	β_1	β_2	%dβ	u(.4,0)	grid
0.500000E+07	1525.46	1877.48	187.748	24.8252	24.9516	-0.51	1.6685	1.6857	-1.03	-33.274	31x25

0.450000E+07	1400.00	1723.08	172.308	24.3449	24.4551	-0.45	1.6362	1.6522	-0.98	-29.567	31x25
0.400000E+07	1272.16	1565.74	156.574	23.8145	23.9065	-0.39	1.6006	1.6151	-0.91	-25.837	31x25
0.350000E+07	1142.16	1405.74	140.574	23.2094	23.2801	-0.30	1.5599	1.5728	-0.83	-22.026	31x25
0.200000E+07	749.99	923.06	92.306	20.1975	20.1652	0.16	1.3575	1.3624	-0.36	-8.390	31x25
0.197500E+07	744.58	916.40	91.640	20.0900	20.0545	0.18	1.3503	1.3549	-0.34	-7.969	31x25
0.195000E+07	739.80	910.53	91.053	19.9637	19.9243	0.20	1.3418	1.3461	-0.32	-7.450	31x25
0.192500E+07	737.60	907.81	90.781	19.7667	19.7209	0.23	1.3285	1.3324	-0.29	-6.532	31x25

γ = 1.8 2-cell solution

pgrad	<w>	Re	Dn	f_1-Re	f_2-Re	%df	β_1	β_2	%dβ	u(.4,0)	grid
0.162500E+07	706.36	908.17	90.817	19.0146	18.9408	0.39	1.2500	1.2504	-0.04	1.592	31x31
0.250000E+07	1006.97	1294.68	129.468	20.5202	20.4606	0.29	1.3489	1.3507	-0.13	2.604	31x31
0.275000E+07	1087.81	1398.61	139.861	20.8948	20.8412	0.26	1.3736	1.3759	-0.17	2.741	31x31
0.325000E+07	1244.60	1600.20	160.020	21.5830	21.5428	0.19	1.4188	1.4222	-0.24	2.552	31x31
0.350000E+07	1321.37	1698.91	169.891	21.8928	21.8604	0.15	1.4392	1.4432	-0.28	1.841	31x31

γ = 1.8 4-cell solution

pgrad	<w>	Re	Dn	f_1-Re	f_2-Re	%df	β_1	β_2	%dβ	u(.4,0)	grid
0.375000E+07	1300.34	1671.87	167.187	23.8359	23.8835	-0.20	1.5669	1.5767	-0.63	-25.101	31x31
0.360000E+07	1257.24	1616.45	161.645	23.6670	23.7113	-0.19	1.5558	1.5653	-0.61	-23.932	31x31
0.175000E+07	711.86	915.25	91.525	20.3189	20.2877	0.15	1.3357	1.3393	-0.27	-7.757	31x31
0.170000E+07	699.02	898.74	89.874	20.1009	20.0645	0.18	1.3214	1.3246	-0.24	-7.009	31x31
0.165000E+07	689.99	887.13	88.713	19.7652	19.7200	0.23	1.2993	1.3019	-0.20	-5.737	31x31

γ = 2.0 2-cell solution

pgrad	<w>	Re	Dn	f_1-Re	f_2-Re	%df	β_1	β_2	%dβ	u(.4,0)	grid
0.100000E+06	57.12	76.16	7.616	15.5608	15.4952	0.42	1.0004	1.0003	0.0	0.061	31x31
0.200000E+06	113.78	151.70	15.170	15.6249	15.5577	0.43	1.0045	1.0044	0.01	0.245	31x31
0.400000E+06	220.45	293.93	29.393	16.1288	16.0572	0.44	1.0369	1.0366	0.03	0.738	31x31
0.600000E+06	317.31	423.08	42.308	16.8080	16.7332	0.44	1.0806	1.0803	0.03	0.966	31x31

0.700000E+06	363.23	484.30	48.430	17.1304	17.0545	0.44	1.1013	1.1010	0.03	1.017	31×31
0.800000E+06	407.89	543.86	54.386	17.4337	17.3572	0.44	1.1208	1.1205	0.02	1.062	31×31
0.850000E+06	429.82	573.09	57.309	17.5785	17.5017	0.44	1.1301	1.1299	0.02	1.087	31×31
0.900000E+06	451.50	602.00	60.200	17.7188	17.6419	0.43	1.1391	1.1389	0.02	1.114	31×31
0.950000E+06	472.95	630.59	63.059	17.8550	17.7780	0.43	1.1479	1.1477	0.01	1.144	31×31
0.100000E+07	494.18	658.90	65.890	17.9872	17.9102	0.43	1.1564	1.1563	0.01	1.179	31×31
0.130000E+07	617.57	823.42	82.342	18.7114	18.6361	0.40	1.2029	1.2031	-0.01	1.465	31×31
0.170000E+07	773.19	1030.92	103.092	19.5437	19.4743	0.36	1.2565	1.2572	-0.06	1.957	31×31
0.200000E+07	884.49	1179.32	117.932	20.0994	20.0363	0.31	1.2922	1.2935	-0.10	2.229	31×31
0.250000E+07	1062.11	1416.15	141.615	20.9227	20.8741	0.23	1.3451	1.3476	-0.19	2.270	31×31
0.275000E+07	1147.93	1530.57	153.057	21.2944	21.2545	0.19	1.3690	1.3722	-0.23	2.040	31×31
0.285000E+07	1181.83	1575.77	157.577	21.4357	21.3997	0.17	1.3781	1.3815	-0.25	1.856	31×31
0.295000E+07	1215.66	1620.88	162.088	21.5703	21.5387	0.15	1.3867	1.3905	-0.27	1.443	31×31
0.295000E+07	1217.02	1622.69	162.269	21.5462	21.4992	0.22	1.3852	1.3879	-0.20	1.597	41×41
0.297500E+07	1225.51	1634.01	163.401	21.5783	21.5316	0.22	1.3873	1.3900	-0.20	1.438	41×41

$\gamma = 2.0$ 2-cell solution

pgrad	<w>	Re	Dn	f_1-Re	f_2-Re	%df	β_1	β_2	%dβ	u(.4,0)	grid
0.300000E+07	1152.50	1536.67	153.667	23.1380	23.1062	0.14	1.4875	1.4917	-0.28	-20.058	41×41
0.300000E+07	1149.73	1532.97	153.297	23.1939	23.2026	-0.04	1.4911	1.4979	-0.46	-20.490	31×31
0.200000E+07	823.70	1098.27	109.827	21.5828	21.5629	0.09	1.3875	1.3921	-0.33	-11.776	31×31
0.175000E+07	741.53	988.71	98.871	20.9775	20.9471	0.15	1.3486	1.3523	-0.27	-9.351	31×31
0.150000E+07	663.61	884.82	88.482	20.0920	20.0460	0.23	1.2917	1.2941	-0.19	-6.361	31×31
0.148000E+07	660.74	880.99	88.099	19.9102	19.8328	0.39	1.2800	1.2804	-0.03	-5.576	41×21
0.147000E+07	655.98	874.64	87.464	19.9193	19.8700	0.25	1.2806	1.2828	-0.17	-5.784	31×31
0.146000E+07	653.96	871.94	87.194	19.8450	19.7943	0.26	1.2758	1.2779	-0.16	-5.523	31×31

$\gamma = 2.4$ 2-cell solution

pgrad	<w>	Re	Dn	f_1-Re	f_2-Re	%df	β_1	β_2	%dβ	u(.4,0)	grid
0.100000E+05	6.15	8.68	0.868	16.2166	16.1601	0.35	1.0000	1.0000	0.0	0.0	31×37
0.500000E+05	30.72	43.38	4.338	16.2173	16.1606	0.35	1.0000	1.0000	0.0	0.011	31×37
0.100000E+06	61.43	86.73	8.673	16.2219	16.1647	0.35	1.0003	1.0003	0.0	0.044	31×37
0.200000E+06	122.44	172.85	17.285	16.2786	16.2195	0.36	1.0038	1.0037	0.01	0.173	31×37

0.300000E+06	181.68	256.49	25.649	16.4554	16.3939	0.37	1.0147	1.0145	0.03	0.343	31×37
0.500000E+06	291.96	412.18	41.218	17.0663	17.0003	0.39	1.0524	1.0520	0.04	0.584	31×37
0.750000E+06	418.25	590.47	59.047	17.8697	17.8007	0.39	1.1019	1.1015	0.04	0.859	31×37
0.900000E+06	490.00	691.76	69.176	18.3038	18.2342	0.38	1.1287	1.1283	0.03	1.067	31×37
0.100000E+07	536.54	757.46	75.746	18.5736	18.5042	0.37	1.1454	1.1451	0.03	1.210	31×37
0.115000E+07	604.66	853.64	85.364	18.9531	18.8845	0.36	1.1688	1.1686	0.01	1.409	31×37
0.135000E+07	692.79	978.05	97.805	19.4190	19.3525	0.34	1.1975	1.1976	-0.01	1.608	31×37
0.150000E+07	757.14	1068.90	106.890	19.7428	19.6785	0.33	1.2175	1.2177	-0.02	1.695	31×37
0.165000E+07	820.19	1157.92	115.792	20.0476	19.9859	0.31	1.2362	1.2367	-0.04	1.729	31×37
0.185000E+07	902.47	1274.07	127.407	20.4284	20.3707	0.28	1.2597	1.2606	-0.07	1.703	31×37
0.200000E+07	962.97	1359.49	135.949	20.6972	20.6429	0.26	1.2763	1.2774	-0.09	1.642	31×37
0.225000E+07	1061.75	1498.94	149.894	21.1181	21.0708	0.22	1.3023	1.3039	-0.12	1.486	31×37
0.250000E+07	1158.07	1634.92	163.492	21.5129	21.4740	0.18	1.3266	1.3288	-0.17	1.400	31×37
0.250000E+07	1157.02	1633.44	163.344	21.5324	21.5200	0.06	1.3278	1.3317	-0.29	1.390	31×31
0.265000E+07	1214.55	1714.66	171.466	21.7433	21.7101	0.15	1.3408	1.3434	-0.20	1.542	31×37
0.275000E+07	1250.45	1765.34	176.534	21.9160	21.9223	-0.03	1.3515	1.3566	-0.38	1.683	31×31
0.275000E+07	1251.70	1767.11	176.711	21.8940	21.8649	0.13	1.3501	1.3530	-0.22	1.679	31×37
0.300000E+07	1343.06	1896.09	189.609	22.2597	22.2417	0.08	1.3727	1.3763	-0.27	2.029	31×37
0.325000E+07	1432.50	2022.35	202.235	22.6091	22.6033	0.03	1.3942	1.3987	-0.32	2.324	31×37
0.335000E+07	1467.79	2072.17	207.217	22.7445	22.7439	0.0	1.4026	1.4074	-0.35	2.423	31×37
0.340000E+07	1485.34	2096.95	209.695	22.8112	22.8132	-0.01	1.4067	1.4117	-0.36	2.468	31×37

γ = 3.0 2-cell solution

pgrad	<w>	Re	Dn	f_1-Re	f_2-Re	%df	β_1	β_2	%dβ	u(-4,0)	grid
0.100000E+05	6.58	9.87	0.987	17.0947	17.0416	0.31	1.0000	1.0000	0.0	0.0	31×41
0.500000E+05	32.90	49.36	4.936	17.0951	17.0419	0.31	1.0000	1.0000	0.0	0.005	31×41
0.100000E+06	65.79	98.69	9.869	17.0986	17.0449	0.31	1.0002	1.0002	0.0	0.021	31×41
0.200000E+06	131.28	196.92	19.692	17.1388	17.0833	0.32	1.0026	1.0024	0.01	0.080	31×41
0.300000E+06	195.39	293.09	29.309	17.2730	17.2149	0.34	1.0104	1.0102	0.03	0.162	31×41
0.500000E+06	316.05	474.07	47.407	17.7978	17.7350	0.35	1.0411	1.0407	0.04	0.387	31×41
0.700000E+06	427.98	641.96	64.196	18.4006	18.3353	0.35	1.0764	1.0759	0.05	0.688	31×41
0.900000E+06	533.85	800.78	80.078	18.9659	18.9006	0.34	1.1095	1.1091	0.03	0.923	31×41
0.100000E+07	585.09	877.63	87.763	19.2278	19.1638	0.33	1.1248	1.1245	0.02	0.998	31×41
0.115000E+07	660.06	990.08	99.008	19.6006	19.5380	0.32	1.1466	1.1465	0.01	1.074	31×41
0.135000E+07	757.21	1135.81	113.581	20.0573	19.9984	0.29	1.1733	1.1735	-0.02	1.143	31×41

0.150000E+07	828.21	1242.31	124.231	20.3753	20.3200	0.27	1.1919	1.1924	-0.04	1.209	31×41
0.160000E+07	874.73	1312.09	131.209	20.5778	20.5253	0.26	1.2038	1.2044	-0.05	1.275	31×41
0.175000E+07	943.39	1415.09	141.509	20.8689	20.8211	0.23	1.2208	1.2218	-0.08	1.402	31×41
0.200000E+07	1055.09	1582.64	158.264	21.3251	21.2868	0.18	1.2475	1.2491	-0.13	1.635	31×41
0.225000E+07	1163.83	1745.75	174.575	21.7493	21.7222	0.12	1.2723	1.2747	-0.19	1.808	31×41
0.225000E+07	1164.03	1746.04	174.604	21.7456	21.7242	0.10	1.2721	1.2748	-0.21	1.792	41×41
0.250000E+07	1270.11	1905.17	190.517	22.1436	22.1296	0.06	1.2954	1.2986	-0.25	1.870	31×41
0.260000E+07	1312.06	1968.09	196.809	22.2932	22.2849	0.04	1.3041	1.3077	-0.27	1.849	31×41
0.275000E+07	1299.69	1949.54	194.954	23.8037	23.7878	0.07	1.3925	1.3959	-0.24	-22.013	31×41

γ = 3.0 4-cell solution

pgrad	<w>	Re	Dn	f_1-Re	f_2-Re	%df	β_1	β_2	%dβ	u(.4,0)	grid
0.275000E+07	1299.69	1949.54	194.954	23.8037	23.7878	0.07	1.3925	1.3959	-0.24	-22.013	31×41
0.200000E+07	991.72	1487.59	148.759	22.6877	22.6548	0.15	1.3272	1.3294	-0.16	-15.078	31×41
0.150000E+07	777.63	1166.45	116.645	21.7005	21.6578	0.20	1.2694	1.2709	-0.11	-10.363	31×41
0.100000E+07	556.83	835.25	83.525	20.2035	20.1494	0.27	1.1819	1.1824	-0.04	-5.166	31×41
0.900000E+06	514.14	771.20	77.120	19.6932	19.6359	0.29	1.1520	1.1522	-0.02	-3.794	31×41
0.880000E+06	506.57	759.86	75.986	19.5430	19.4847	0.30	1.1432	1.1434	-0.01	-3.384	31×41
0.870000E+06	503.58	755.36	75.536	19.4360	19.3767	0.31	1.1370	1.1370	-0.0	-3.068	31×41

γ = 5.0 2-cell solution

pgrad	<w>	Re	Dn	f_1-Re	f_2-Re	%df	β_1	β_2	%dβ	u(.4,0)	grid
0.100000E+06	72.80	121.33	12.133	19.0787	19.0146	0.34	1.0001	1.0001	0.0	0.001	21×51
0.400000E+06	287.87	479.79	47.979	19.2987	19.2305	0.35	1.0117	1.0114	0.02	0.033	21×51
0.500000E+06	356.85	594.74	59.474	19.4606	19.3909	0.36	1.0201	1.0199	0.03	0.026	21×51

γ = 5.0 4-cell solution

pgrad	<w>	Re	Dn	f_1-Re	f_2-Re	%df	β_1	β_2	%dβ	u(.4,0)	grid
0.100000E+07	644.87	1074.78	107.478	21.5375	21.5003	0.17	1.1290	1.1308	-0.16	-7.150	21×51
0.600000E+06	412.94	688.24	68.824	20.1803	20.1224	0.29	1.0579	1.0584	-0.05	-2.683	21×51

0.550000E+06	383.59	639.31	63.931	19.9142	19.8523	0.31	1.0439	1.0442	-0.02	-1.964	21x51
0.530000E+06	372.06	620.09	62.009	19.7849	19.7210	0.32	1.0371	1.0372	-0.01	-1.596	21x51
0.520000E+06	366.44	610.73	61.073	19.7091	19.6440	0.33	1.0332	1.0332	-0.0	-1.361	21x51

$\gamma = 1.0$ & $r = 10$ 2-cell solution

pgrad	<w>	Re	Dn	f_1-Re	f_2-Re	%df	β_1	β_2	%dβ	u(4,0)	grid
0.100000E+05	34.96	34.96	11.055	14.3034	14.2141	0.62	1.0048	1.0034	0.14	0.330	41×21
0.200000E+05	67.90	67.90	21.472	14.7281	14.6019	0.86	1.0346	1.0308	0.37	1.408	41×21
0.300000E+05	97.00	97.00	30.674	15.4639	15.3006	1.06	1.0863	1.0801	0.57	2.907	41×21
0.400000E+05	123.39	123.39	39.019	16.2081	16.0165	1.18	1.1386	1.1306	0.70	4.263	41×21
0.500000E+05	148.29	148.29	46.893	16.8593	16.6472	1.26	1.1844	1.1752	0.78	5.252	41×21
0.600000E+05	172.27	172.27	54.477	17.4147	17.1877	1.30	1.2234	1.2133	0.82	5.860	41×21
0.700000E+05	195.61	195.61	61.857	17.8929	17.6549	1.33	1.2570	1.2463	0.85	6.144	41×21
0.850000E+05	229.64	229.64	72.619	18.5072	18.2576	1.35	1.3001	1.2889	0.87	6.115	41×21
0.100000E+06	262.59	262.59	83.038	19.0409	18.7834	1.35	1.3376	1.3260	0.87	5.722	41×21
0.150000E+06	365.22	365.22	115.493	20.5353	20.2657	1.31	1.4426	1.4306	0.83	3.123	41×21
0.160000E+06	384.59	384.59	121.618	20.8015	20.5318	1.30	1.4613	1.4494	0.81	2.344	41×21
0.165000E+06	394.15	394.15	124.641	20.9313	20.6618	1.29	1.4704	1.4586	0.81	1.868	41×21
0.170000E+06	403.63	403.63	127.639	21.0589	20.7900	1.28	1.4794	1.4676	0.79	1.283	41×21
0.175000E+06	413.05	413.05	130.618	21.1840	20.9165	1.26	1.4882	1.4766	0.78	0.451	41×21
0.176000E+06	414.92	414.92	131.209	21.2088	20.9417	1.26	1.4899	1.4783	0.78	0.223	41×21
0.177000E+06	416.80	416.80	131.804	21.2334	20.9667	1.26	1.4916	1.4801	0.77	-0.060	41×21

$\gamma = 1.0$ & $r = 10$ 4-cell solution

pgrad	<w>	Re	Dn	f_1-Re	f_2-Re	%df	β_1	β_2	%dβ	u(4,0)	grid
0.700000E+06	1118.96	1118.96	353.846	31.2790	31.3483	-0.22	2.1973	2.2130	-0.71	-118.430	41×21
0.650000E+06	1057.35	1057.35	334.363	30.7372	30.7796	-0.14	2.1593	2.1728	-0.63	-110.291	41×21
0.600000E+06	994.55	994.55	314.504	30.1645	30.1804	-0.05	2.1190	2.1305	-0.54	-102.269	41×21
0.550000E+06	930.53	930.53	294.259	29.5531	29.5425	0.04	2.0761	2.0855	-0.45	-94.337	41×21
0.500000E+06	865.28	865.28	273.625	28.8925	28.8542	0.13	2.0297	2.0369	-0.35	-86.438	41×21
0.300000E+06	590.34	590.34	186.682	25.4093	25.2412	0.66	1.7850	1.7818	0.18	-52.684	41×21
0.250000E+06	516.57	516.57	163.354	24.1979	23.9968	0.83	1.6999	1.6940	0.35	-42.638	41×21
0.200000E+06	439.37	439.37	138.941	22.7599	22.5324	1.00	1.5989	1.5906	0.52	-31.204	41×21
0.175000E+06	399.34	399.34	126.282	21.9110	21.6757	1.07	1.5392	1.5301	0.59	-24.517	41×21
0.165000E+06	383.26	383.26	121.197	21.5257	21.2886	1.10	1.5122	1.5028	0.62	-21.348	41×21
0.160000E+06	375.37	375.37	118.702	21.3122	21.0745	1.12	1.4972	1.4877	0.63	-19.461	41×21
0.155000E+06	367.95	367.95	116.356	21.0624	20.8241	1.13	1.4796	1.4700	0.65	-16.925	41×21

0.154000E+06	366.71	366.71	115.964	20.9974	20.7589	1.14	1.4751	1.4654	0.65	-16.113	41×21
0.153000E+06	366.05	366.05	115.755	20.8990	20.6597	1.15	1.4682	1.4584	0.66	-14.586	41×21

γ = 1.0 & r = 4 2-cell solution

pgrad	<w>	Re	Dn	f_1-Re	f_2-Re	%df	β_1	β_2	%dβ	u(.4,0)	grid
0.100000E+04	8.78	8.78	4.390	14.2423	14.1352	0.75	1.0005	0.9978	0.27	0.046	41×21
0.500000E+04	42.08	42.08	21.040	14.8541	14.6314	1.50	1.0435	1.0329	1.02	1.231	41×21
0.100000E+05	76.21	76.21	38.105	16.4019	16.0235	2.31	1.1522	1.1311	1.83	3.777	41×21
0.200000E+05	134.41	134.41	67.205	18.5998	18.0733	2.83	1.3066	1.2758	2.36	5.883	41×21
0.400000E+05	236.22	236.22	118.110	21.1663	20.5358	2.98	1.4869	1.4497	2.51	3.311	41×21
0.430000E+05	250.19	250.19	125.095	21.4836	20.8435	2.98	1.5092	1.4714	2.51	2.692	41×21
0.500000E+05	281.79	281.79	140.895	22.1800	21.5243	2.96	1.5581	1.5195	2.48	0.495	41×21
0.510000E+05	286.20	286.20	143.100	22.2743	21.6182	2.95	1.5648	1.5261	2.47	-0.227	41×21
0.512500E+05	287.31	287.31	143.655	22.2976	21.6418	2.94	1.5664	1.5278	2.47	-0.512	41×21

γ = 1.0 & r = 4 4-cell solution

pgrad	<w>	Re	Dn	f_1-Re	f_2-Re	%df	β_1	β_2	%dβ	u(.4,0)	grid
0.380000E+06	1225.74	1225.74	612.870	38.7522	38.5051	0.64	2.7223	2.7182	0.15	-226.418	41×21
0.370000E+06	1202.18	1202.18	601.090	38.4717	38.1886	0.74	2.7026	2.6958	0.25	-220.298	41×21
0.360000E+06	1178.39	1178.39	589.195	38.1876	37.8697	0.83	2.6827	2.6733	0.35	-214.180	41×21
0.350000E+06	1154.36	1154.36	577.180	37.8997	37.5484	0.93	2.6625	2.6506	0.44	-208.064	41×21
0.347500E+06	1148.31	1148.31	574.155	37.8272	37.4676	0.95	2.6574	2.6449	0.47	-206.535	41×21
0.347250E+06	1147.71	1147.71	573.855	37.8199	37.4596	0.95	2.6568	2.6444	0.47	-206.382	41×21
0.347000E+06	1147.10	1147.10	573.550	37.8127	37.4515	0.96	2.6563	2.6438	0.47	-206.229	41×21
0.346000E+06	1144.68	1144.68	572.340	37.7835	37.4191	0.96	2.6543	2.6415	0.48	-205.618	41×21
0.342000E+06	1134.96	1134.96	567.480	37.6666	37.2894	1.00	2.6461	2.6324	0.52	-203.172	41×21
0.340000E+06	1130.08	1130.08	565.040	37.6080	37.2244	1.02	2.6420	2.6278	0.54	-201.950	41×21
0.280000E+06	978.63	978.63	489.315	35.7642	35.2181	1.53	2.5124	2.4861	1.05	-165.496	41×21
0.240000E+06	871.64	871.64	435.820	34.4180	33.7943	1.81	2.4179	2.3856	1.33	-141.695	41×21
0.200000E+06	759.20	759.20	379.600	32.9295	32.2503	2.06	2.3133	2.2766	1.58	-118.502	41×21
0.180000E+06	700.71	700.71	350.355	32.1102	31.4098	2.18	2.2557	2.2173	1.70	-107.171	41×21
0.160000E+06	640.62	640.62	320.310	31.2197	30.5018	2.30	2.1932	2.1532	1.82	-95.997	41×21
0.140000E+06	578.87	578.87	289.435	30.2311	29.4988	2.42	2.1237	2.0824	1.95	-84.887	41×21

0.120000E+06	515.41	515.41	257.705	29.1028	28.3603	2.55	2.0445	2.0020	2.08	-73.630	41×21
0.100000E+06	450.04	450.04	225.020	27.7754	27.0302	2.68	1.9512	1.9081	2.21	-61.841	41×21
0.800000E+05	382.14	382.14	191.070	26.1686	25.4365	2.80	1.8383	1.7956	2.32	-48.927	41×21
0.600000E+05	310.37	310.37	155.185	24.1644	23.4763	2.85	1.6975	1.6573	2.37	-33.987	41×21
0.520000E+05	280.22	280.22	140.110	23.1964	22.5406	2.83	1.6295	1.5912	2.35	-26.986	41×21
0.517500E+05	279.26	279.26	139.630	23.1638	22.5093	2.83	1.6273	1.5890	2.35	-26.750	41×21
0.500000E+05	272.56	272.56	136.280	22.9306	22.2850	2.82	1.6109	1.5732	2.34	-25.044	41×21
0.450000E+05	253.56	253.56	126.780	22.1841	21.5688	2.77	1.5584	1.5226	2.30	-19.191	41×21
0.445000E+05	251.75	251.75	125.875	22.0951	21.4835	2.77	1.5522	1.5166	2.29	-18.380	41×21
0.440000E+05	250.02	250.02	125.010	21.9983	21.3905	2.76	1.5454	1.5100	2.29	-17.421	41×21
0.435000E+05	248.49	248.49	124.245	21.8825	21.2791	2.76	1.5372	1.5021	2.28	-16.083	41×21

APPENDIX C

THE NUMERICAL RESULTS FOR POWER-LAW FLUIDS

The numerical results for the power-law fluids in square pipes of r=100 are presented in tabular form in the increasing order of the power-law index, n, with 2-cell and 4-cell solutions being placed alternatively. The results of the fluid with index n=0.7 in square pipes of r=10 & 4 are given at the end of this appendix. All the results given in this appendix have been obtained with a 41x21 grid.

n = 0.6 2-cell solution

pgrad	<w>	Re	Dn	f_1-Re	f_2-Re	%df	β_1	β_2	%dβ	u(3,0)	Dn'
0.100000E+06	72.79	72.79	7.28	14.3864	14.2297	1.09	1.0021	1.0021	0.01	0.653	15.25
0.200000E+06	142.59	142.59	14.26	14.6885	14.5333	1.06	1.0232	1.0235	-0.03	2.643	29.86
0.300000E+06	205.98	205.98	20.60	15.2526	15.1075	0.95	1.0625	1.0639	-0.13	4.978	43.14
0.400000E+06	264.95	264.95	26.49	15.8103	15.6799	0.82	1.1013	1.1042	-0.26	6.717	55.49
0.600000E+06	376.35	376.35	37.64	16.6952	16.5949	0.60	1.1630	1.1686	-0.49	8.580	78.82
0.750000E+06	456.45	456.44	45.64	17.2072	17.1288	0.46	1.1986	1.2062	-0.63	9.140	95.60
0.900000E+06	534.29	534.29	53.43	17.6403	17.5837	0.32	1.2288	1.2383	-0.77	9.239	111.90
0.100000E+07	585.07	585.07	58.51	17.8991	17.8573	0.23	1.2468	1.2575	-0.86	9.114	122.54
0.115000E+07	659.72	659.72	65.97	18.2548	18.2359	0.10	1.2716	1.2842	-0.99	8.717	138.17
0.130000E+07	732.73	732.73	73.27	18.5796	18.5850	-0.03	1.2942	1.3088	-1.12	8.128	153.47
0.132500E+07	744.76	744.76	74.48	18.6311	18.6407	-0.05	1.2978	1.3127	-1.15	8.011	155.99
0.140000E+07	780.61	780.61	78.06	18.7815	18.8037	-0.12	1.3083	1.3242	-1.21	7.622	163.49
0.150000E+07	828.00	828.00	82.80	18.9713	19.0108	-0.21	1.3215	1.3388	-1.31	6.937	173.42
0.160000E+07	875.07	875.07	87.51	19.1477	19.2066	-0.31	1.3338	1.3526	-1.41	5.764	183.28

n = 0.6 4-cell solution

pgrad	<w>	Re	Dn	f_1-Re	f_2-Re	%df	β_1	β_2	%dβ	u(3,0)	Dn'
0.400000E+07	1768.06	1768.06	176.81	23.6920	24.4547	-3.22	1.6504	1.7221	-4.35	-96.261	370.31
0.350000E+07	1584.41	1584.41	158.44	23.1334	23.8149	-2.95	1.6114	1.6771	-4.07	-82.567	331.84
0.300000E+07	1396.80	1396.80	139.68	22.4918	23.0780	-2.61	1.5668	1.6252	-3.73	-68.278	292.55
0.250000E+07	1204.53	1204.53	120.45	21.7350	22.2071	-2.17	1.5140	1.5639	-3.29	-53.554	252.28
0.200000E+07	1006.63	1006.62	100.66	20.8065	21.1422	-1.61	1.4494	1.4889	-2.73	-38.281	210.83
0.170000E+07	885.15	885.15	88.51	20.1126	20.3500	-1.18	1.4010	1.4331	-2.29	-28.410	185.39
0.150000E+07	803.75	803.75	80.38	19.5438	19.7024	-0.81	1.3614	1.3875	-1.92	-20.870	168.34
0.140000E+07	763.82	763.82	76.38	19.1945	19.3079	-0.59	1.3371	1.3597	-1.69	-15.796	159.98
0.135000E+07	746.11	746.11	74.61	18.9482	19.0300	-0.43	1.3199	1.3401	-1.53	-10.969	156.27

n = 0.7 2-cell solution

pgrad	<w>	Re	Dn	f_1-Re	f_2-Re	%df	β_1	β_2	%dβ	u(.3,0)	Dn'
0.100000E+06	60.57	60.57	6.06	14.3453	14.2186	0.88	1.0008	1.0008	0.01	0.413	10.52
0.400000E+06	226.68	226.68	22.67	15.3320	15.2093	0.80	1.0697	1.0705	-0.08	5.778	39.39
0.900000E+06	454.13	454.13	45.41	17.2193	17.1350	0.49	1.2014	1.2061	-0.39	10.350	78.92
0.140000E+07	661.71	661.71	66.17	18.3828	18.3382	0.24	1.2825	1.2907	-0.64	10.033	114.99
0.170000E+07	779.66	779.66	77.97	18.9452	18.9279	0.09	1.3218	1.3323	-0.79	8.889	135.48
0.175000E+07	798.90	798.90	79.89	19.0327	19.0204	0.06	1.3279	1.3388	-0.82	8.650	138.83
0.200000E+07	893.57	893.57	89.36	19.4472	19.4625	-0.08	1.3568	1.3699	-0.97	7.100	155.28
0.205000E+07	912.23	912.23	91.22	19.5256	19.5474	-0.11	1.3623	1.3759	-1.00	6.625	158.52
0.207500E+07	921.54	921.54	92.15	19.5640	19.5892	-0.13	1.3649	1.3788	-1.02	6.266	160.14

n = 0.7 4-cell solution

pgrad	<w>	Re	Dn	f_1-Re	f_2-Re	%df	β_1	β_2	%dβ	u(.3,0)	Dn'
0.500000E+07	1765.30	1765.30	176.53	24.6097	25.3464	-2.99	1.7170	1.7840	-3.91	-99.599	306.76
0.450000E+07	1623.25	1623.24	162.32	24.0870	24.7472	-2.74	1.6805	1.7419	-3.65	-88.887	282.08
0.400000E+07	1478.46	1478.46	147.85	23.5074	24.0840	-2.45	1.6401	1.6952	-3.36	-77.628	256.92
0.350000E+07	1330.57	1330.56	133.06	22.8553	23.3404	-2.12	1.5946	1.6428	-3.03	-65.810	231.22
0.300000E+07	1179.12	1179.12	117.91	22.1063	22.4906	-1.74	1.5423	1.5830	-2.64	-53.422	204.90
0.250000E+07	1023.71	1023.71	102.37	21.2186	21.4876	-1.27	1.4804	1.5124	-2.16	-40.375	177.89
0.230000E+07	960.35	960.35	96.04	20.8091	21.0268	-1.05	1.4518	1.4800	-1.94	-34.824	166.88
0.220000E+07	928.46	928.45	92.84	20.5881	20.7790	-0.93	1.4364	1.4625	-1.82	-31.900	161.34
0.210000E+07	896.47	896.47	89.65	20.3535	20.5166	-0.80	1.4200	1.4441	-1.69	-28.818	155.78
0.200000E+07	864.46	864.46	86.45	20.1021	20.2364	-0.67	1.4025	1.4244	-1.56	-25.502	150.22
0.190000E+07	832.63	832.63	83.26	19.8270	19.9310	-0.52	1.3833	1.4029	-1.42	-21.717	144.69
0.180000E+07	802.11	802.11	80.21	19.4982	19.5675	-0.36	1.3603	1.3773	-1.24	-16.395	139.39

n = 0.9 2-cell solution

pgrad	<w>	Re	Dn	f_1-Re	f_2-Re	%df	β_1	β_2	%dβ	u(.3,0)	Dn'
0.100000E+06	42.08	42.08	4.21	14.2720	14.1878	0.59	1.0001	1.0001	0.0	0.157	5.06
0.400000E+06	165.58	165.58	16.56	14.5087	14.4209	0.61	1.0167	1.0165	0.02	2.736	19.89
0.900000E+06	339.39	339.39	33.94	15.9262	15.8362	0.56	1.1160	1.1163	-0.02	9.729	40.77
0.140000E+07	490.80	490.80	49.08	17.1315	17.0469	0.49	1.2005	1.2016	-0.09	13.187	58.95
0.200000E+07	661.28	661.28	66.13	18.1642	18.0873	0.42	1.2729	1.2750	-0.17	13.781	79.43
0.250000E+07	796.45	796.45	79.64	18.8517	18.7828	0.37	1.3210	1.3240	-0.22	12.771	95.67
0.300000E+07	925.87	925.87	92.59	19.4600	19.4014	0.30	1.3637	1.3676	-0.29	11.176	111.21
0.320000E+07	976.16	976.15	97.61	19.6880	19.6344	0.27	1.3797	1.3840	-0.32	10.414	117.25
0.350000E+07	1050.21	1050.20	105.02	20.0154	19.9704	0.22	1.4026	1.4077	-0.37	8.930	126.15
0.360000E+07	1074.56	1074.56	107.46	20.1206	20.0789	0.21	1.4100	1.4154	-0.38	8.224	129.07
0.370000E+07	1098.78	1098.78	109.88	20.2237	20.1858	0.19	1.4172	1.4229	-0.40	7.229	131.98
0.375000E+07	1110.85	1110.84	111.08	20.2744	20.2389	0.17	1.4207	1.4266	-0.41	6.443	133.43

n = 0.9 4-cell solution

pgrad	<w>	Re	Dn	f_1-Re	f_2-Re	%df	β_1	β_2	%dβ	u(.3,0)	Dn'
0.150000E+08	3061.60	3061.60	306.16	29.4247	30.1866	-2.59	2.0620	2.1279	-3.20	-189.160	367.75
0.125000E+08	2657.04	2657.04	265.70	28.2541	28.9063	-2.31	1.9799	2.0376	-2.91	-164.672	319.15
0.100000E+08	2235.76	2235.76	223.58	26.8624	27.3851	-1.95	1.8824	1.9304	-2.55	-136.606	268.55
0.950000E+07	2149.25	2149.25	214.92	26.5464	27.0398	-1.86	1.8603	1.9060	-2.46	-130.415	258.16
0.900000E+07	2061.91	2061.91	206.19	26.2145	26.6770	-1.76	1.8370	1.8805	-2.37	-123.994	247.67
0.800000E+07	1884.54	1884.54	188.45	25.4950	25.8911	-1.55	1.7866	1.8251	-2.15	-110.391	226.36
0.700000E+07	1703.07	1703.07	170.31	24.6851	25.0078	-1.31	1.7298	1.7628	-1.91	-95.677	204.57
0.600000E+07	1516.61	1516.61	151.66	23.7600	24.0020	-1.02	1.6650	1.6919	-1.62	-79.741	182.17
0.550000E+07	1421.10	1421.10	142.11	23.2438	23.4427	-0.86	1.6288	1.6525	-1.45	-71.266	170.70
0.500000E+07	1323.81	1323.81	132.38	22.6836	22.8381	-0.68	1.5896	1.6099	-1.28	-62.396	159.01
0.450000E+07	1224.54	1224.54	122.45	22.0703	22.1786	-0.49	1.5466	1.5634	-1.08	-53.024	147.09
0.400000E+07	1123.20	1123.20	112.32	21.3882	21.4495	-0.29	1.4988	1.5120	-0.88	-42.841	134.91
0.380000E+07	1082.17	1082.17	108.22	21.0891	21.1314	-0.20	1.4778	1.4896	-0.79	-38.360	129.99

0.350000E+07	1020.70	1020.70	102.07	20.5939	20.6073	-0.06	1.4431	1.4526	-0.66	-30.514	122.60
0.340000E+07	1000.65	1000.65	100.06	20.4064	20.4096	-0.02	1.4300	1.4387	-0.61	-27.217	120.19
0.330000E+07	981.81	981.81	98.18	20.1862	20.1778	0.04	1.4146	1.4223	-0.55	-22.627	117.93

n = 1.2 2-cell solution

pgrad	<w>	Re	Dn	f_1-Re	f_2-Re	%df	β_1	β_2	%dβ	u(.3,0)	Dn'
0.100000E+06	24.51	24.51	2.45	14.1633	14.1153	0.34	1.0000	1.0000	0.0	0.035	1.70
0.300000E+06	73.52	73.52	7.35	14.1665	14.1182	0.34	1.0002	1.0002	0.0	0.316	5.10
0.500000E+06	122.38	122.38	12.24	14.1838	14.1347	0.35	1.0015	1.0014	0.01	0.900	8.50
0.700000E+06	170.73	170.73	17.07	14.2341	14.1839	0.35	1.0050	1.0049	0.01	1.812	11.85
0.100000E+07	240.90	240.90	24.09	14.4112	14.3587	0.36	1.0175	1.0172	0.03	3.789	16.73
0.115000E+07	274.40	274.40	27.44	14.5494	14.4956	0.37	1.0273	1.0269	0.03	4.997	19.05
0.135000E+07	317.22	317.22	31.72	14.7741	14.7185	0.38	1.0431	1.0427	0.04	6.735	22.03
0.150000E+07	348.03	348.02	34.80	14.9628	14.9059	0.38	1.0565	1.0560	0.04	8.075	24.16
0.200000E+07	444.20	444.20	44.42	15.6307	15.5702	0.39	1.1036	1.1031	0.05	12.339	30.84
0.300000E+07	618.78	618.78	61.88	16.8312	16.7660	0.39	1.1884	1.1878	0.05	18.348	42.96
0.400000E+07	781.76	781.76	78.18	17.7631	17.6955	0.38	1.2542	1.2536	0.04	20.813	54.28
0.500000E+07	937.71	937.71	93.77	18.5111	18.4423	0.37	1.3070	1.3065	0.03	20.897	65.11
0.600000E+07	1087.60	1087.60	108.76	19.1520	19.0829	0.36	1.3522	1.3519	0.02	19.746	75.51
0.700000E+07	1231.70	1231.70	123.17	19.7299	19.6610	0.35	1.3930	1.3929	0.01	18.080	85.52
0.800000E+07	1370.42	1370.42	137.04	20.2661	20.1981	0.34	1.4309	1.4309	-0.0	16.236	95.15
0.850000E+07	1437.91	1437.91	143.79	20.5220	20.4546	0.33	1.4490	1.4491	-0.01	15.268	99.84
0.900000E+07	1504.26	1504.26	150.43	20.7708	20.7041	0.32	1.4665	1.4668	-0.02	14.242	104.44
0.100000E+08	1633.80	1633.80	163.38	21.2487	21.1841	0.30	1.5003	1.5008	-0.03	11.664	113.44
0.105000E+08	1697.17	1697.17	169.72	21.4781	21.4148	0.29	1.5165	1.5171	-0.04	9.236	117.84
0.107500E+08	1728.46	1728.45	172.84	21.5915	21.5293	0.29	1.5245	1.5252	-0.05	7.450	120.01

n = 1.2 4-cell solution

pgrad	<w>	Re	Dn	f_1-Re	f_2-Re	%df	β_1	β_2	%dβ	u(.3,0)	Dn'
0.200000E+08	2597.95	2597.95	259.79	26.7258	26.7474	-0.08	1.8870	1.8949	-0.42	-156.879	180.38
0.175000E+08	2359.75	2359.74	235.97	25.7457	25.7481	-0.01	1.8178	1.8241	-0.35	-136.147	163.84
0.150000E+08	2113.41	2113.41	211.34	24.6400	24.6219	0.07	1.7397	1.7443	-0.27	-113.398	146.74
0.125000E+08	1855.68	1855.68	185.57	23.3851	23.3473	0.16	1.6511	1.6540	-0.18	-88.066	128.84
0.120000E+08	1802.51	1802.51	180.25	23.1119	23.0704	0.18	1.6318	1.6344	-0.16	-82.534	125.15
0.110000E+08	1694.53	1694.53	169.45	22.5359	22.4878	0.21	1.5912	1.5932	-0.13	-70.696	117.65
0.100000E+08	1584.91	1584.90	158.49	21.9043	21.8502	0.25	1.5466	1.5480	-0.09	-57.044	110.04
0.950000E+07	1530.69	1530.69	153.07	21.5461	21.4895	0.26	1.5213	1.5224	-0.08	-48.165	106.28
0.930000E+07	1509.79	1509.79	150.98	21.3844	21.3267	0.27	1.5099	1.5109	-0.07	-43.596	104.83
0.910000E+07	1492.20	1492.20	149.22	21.1712	21.1125	0.28	1.4948	1.4957	-0.06	-35.506	103.61

n = 1.4 2-cell solution

pgrad	<w>	Re	Dn	f_1-Re	f_2-Re	%df	β_1	β_2	%dβ	u(.3,0)	Dn'
0.100000E+06	17.13	17.13	1.71	14.0938	14.0595	0.24	1.0000	1.0000	0.0	0.012	0.83
0.500000E+06	85.64	85.64	8.56	14.0960	14.0615	0.25	1.0002	1.0001	0.0	0.313	4.14
0.750000E+06	128.40	128.40	12.84	14.1028	14.0678	0.25	1.0006	1.0006	0.01	0.714	6.20
0.100000E+07	170.99	170.99	17.10	14.1194	14.0838	0.25	1.0018	1.0017	0.01	1.289	8.26
0.200000E+07	335.41	335.41	33.54	14.3962	14.3568	0.27	1.0215	1.0211	0.03	5.376	16.20
0.300000E+07	481.89	481.89	48.19	15.0303	14.9861	0.29	1.0665	1.0659	0.05	11.241	23.27
0.400000E+07	612.48	612.48	61.25	15.7675	15.7191	0.31	1.1188	1.1180	0.06	16.976	29.57
0.500000E+07	733.52	733.52	73.35	16.4569	16.4053	0.31	1.1677	1.1668	0.07	21.600	35.42
0.600000E+07	848.82	848.82	84.88	17.0658	17.0117	0.32	1.2109	1.2100	0.07	24.885	40.99
0.700000E+07	960.28	960.28	96.03	17.5992	17.5431	0.32	1.2487	1.2478	0.08	26.834	46.37
0.800000E+07	1068.81	1068.81	106.88	18.0710	18.0134	0.32	1.2822	1.2812	0.08	27.729	51.61
0.100000E+08	1278.50	1278.50	127.85	18.8839	18.8242	0.32	1.3399	1.3389	0.07	27.556	61.73
0.120000E+08	1479.14	1479.14	147.91	19.5868	19.5258	0.31	1.3898	1.3888	0.07	25.902	71.42
0.150000E+08	1764.44	1764.44	176.44	20.5247	20.4626	0.30	1.4563	1.4554	0.06	22.664	85.20
0.180000E+08	2033.28	2033.28	203.33	21.3731	21.3105	0.29	1.5165	1.5157	0.05	19.354	98.18
0.187500E+08	2098.25	2098.25	209.82	21.5743	21.5116	0.29	1.5308	1.5300	0.05	18.490	101.32

0.200000E+08	2204.75	2204.75	220.47	21.9010	21.8382	0.29	1.5539	1.5533	0.04	16.899	106.46
0.220000E+08	2370.84	2370.84	237.08	22.4034	22.3408	0.28	1.5896	1.5890	0.04	13.623	114.48
0.230000E+08	2451.96	2451.96	245.20	22.6468	22.5845	0.27	1.6069	1.6063	0.03	11.477	118.40
0.235000E+08	2492.03	2492.03	249.20	22.7671	22.7050	0.27	1.6154	1.6149	0.03	9.494	120.33

n = 1.4 4-cell solution

pgrad	<w>	Re	Dn	f_1-Re	f_2-Re	%df	β_1	β_2	%dβ	u(.3,0)	Dn'
0.300000E+08	2847.33	2847.33	284.73	25.4376	25.3718	0.26	1.8049	1.8046	0.02	-153.883	137.49
0.240000E+08	2435.20	2435.20	243.52	23.7941	23.7272	0.28	1.6883	1.6876	0.04	-112.236	117.59
0.220000E+08	2291.44	2291.44	229.14	23.1797	23.1133	0.29	1.6447	1.6440	0.04	-95.803	110.64
0.210000E+08	2218.67	2218.67	221.87	22.8517	22.7860	0.29	1.6214	1.6207	0.04	-86.606	107.13
0.200000E+08	2145.92	2145.92	214.59	22.5014	22.4363	0.29	1.5965	1.5958	0.05	-76.012	103.62
0.190000E+08	2076.59	2076.59	207.66	22.0900	22.0265	0.29	1.5674	1.5667	0.04	-60.267	100.27

n = 0.7 & r = 10 2-cell solution

pgrad	<w>	Re	Dn	f_1-Re	f_2-Re	%df	β_1	β_2	%dβ	u(.3,0)	Dn'
0.100000E+03	0.61	0.61	0.19	14.3322	14.1997	0.92	0.9999	0.9995	0.05	0.0	0.33
0.100000E+04	6.06	6.06	1.92	14.3343	14.2010	0.93	1.0001	0.9996	0.05	0.039	3.33
0.100000E+05	57.85	57.85	18.29	15.0193	14.8284	1.27	1.0479	1.0437	0.40	3.839	31.79
0.250000E+05	127.40	127.40	40.29	17.0498	16.8159	1.37	1.1895	1.1836	0.50	9.625	70.01
0.500000E+05	229.43	229.43	72.55	18.9355	18.7202	1.14	1.3211	1.3176	0.26	9.546	126.08

n = 0.7 & r = 10 4-cell solution

pgrad	<w>	Re	Dn	f_1-Re	f_2-Re	%df	β_1	β_2	%dβ	u(.3,0)	Dn'
0.750000E+05	308.29	308.29	97.49	21.1375	21.1105	0.13	1.4747	1.4859	-0.76	-33.896	169.41
0.900000E+05	354.43	354.43	112.08	22.0630	22.1171	-0.25	1.5393	1.5567	-1.13	-46.213	194.77
0.200000E+06	665.16	665.16	210.34	26.1250	26.6259	-1.92	1.8227	1.8741	-2.82	-118.727	365.52
0.250000E+06	796.28	796.28	251.81	27.2790	27.9124	-2.32	1.9032	1.9646	-3.23	-144.230	437.57

n = 0.7 & r = 4 2-cell solution

pgrad	<w>	Re	Dn	f_1-Re	f_2-Re	%df	β_1	β_2	%dβ	u(.3,0)	Dn'
0.100000E+02	0.15	0.15	0.07	14.3269	14.1595	1.17	0.9996	0.9966	0.29	0.0	0.13
0.100000E+03	1.52	1.52	0.76	14.3277	14.1600	1.17	0.9996	0.9967	0.29	0.006	1.31
0.100000E+04	15.06	15.06	7.53	14.4267	14.2279	1.38	1.0065	1.0014	0.50	0.588	13.08
0.250000E+04	35.85	35.85	17.93	15.1469	14.8351	2.06	1.0568	1.0442	1.19	3.403	31.15
0.500000E+04	65.14	65.14	32.57	16.6736	16.2319	2.65	1.1633	1.1425	1.79	7.734	56.60
0.750000E+04	91.74	91.74	45.87	17.7590	17.2602	2.81	1.2390	1.2149	1.95	9.692	79.71
0.100000E+05	117.00	117.00	58.50	18.5657	18.0405	2.83	1.2953	1.2698	1.97	10.108	101.65
0.125000E+05	141.19	141.19	70.60	19.2307	18.6935	2.79	1.3417	1.3158	1.93	9.651	122.68
0.150000E+05	164.44	164.44	82.22	19.8148	19.2747	2.73	1.3824	1.3567	1.86	8.781	142.88
0.160000E+05	173.50	173.50	86.75	20.0317	19.4928	2.69	1.3976	1.3720	1.83	8.356	150.75
0.170000E+05	182.45	182.45	91.22	20.2400	19.7037	2.65	1.4121	1.3869	1.79	7.869	158.52

0.180000E+05	191.29	191.29	95.64	20.4398	19.9078	2.60	1.4260	1.4012	1.74	7.261	166.20
0.190000E+05	200.06	200.06	100.03	20.6299	20.1054	2.54	1.4393	1.4151	1.68	6.247	173.82
0.192000E+05	201.81	201.81	100.90	20.6660	20.1442	2.52	1.4418	1.4179	1.66	5.825	175.34
0.193000E+05	202.69	202.69	101.35	20.6832	20.1637	2.51	1.4430	1.4192	1.65	5.439	176.11
0.193500E+05	203.14	203.14	101.57	20.6909	20.1743	2.50	1.4436	1.4200	1.63	4.887	176.51

n = 0.7 & r* = 4 4-cell solution

pgrad	<w>	Re	Dn	f_1-Re	f_2-Re	%df	β_1	β_2	%dβ	u(.3,0)	Dn*
0.161000E+05	172.20	172.20	86.10	20.3090	19.8384	2.32	1.4169	1.3963	1.45	-12.255	149.62
0.162000E+05	172.53	172.53	86.26	20.3957	19.9279	2.29	1.4230	1.4026	1.43	-14.414	149.91
0.163000E+05	173.11	173.11	86.55	20.4530	19.9866	2.28	1.4270	1.4068	1.41	-15.570	150.41
0.164000E+05	173.75	173.75	86.88	20.5031	20.0375	2.27	1.4305	1.4104	1.40	-16.481	150.96
0.170000E+05	177.97	177.97	88.99	20.7488	20.2875	2.22	1.4476	1.4280	1.36	-20.228	154.64
0.165000E+05	174.42	174.42	87.21	20.5485	20.0839	2.26	1.4336	1.4136	1.40	-17.243	151.55
0.180000E+05	185.39	185.39	92.69	21.0903	20.6349	2.16	1.4714	1.4524	1.29	-24.633	161.08
0.200000E+05	200.40	200.40	100.20	21.6782	21.2355	2.04	1.5124	1.4947	1.17	-31.637	174.13
0.300000E+05	273.14	273.14	136.57	23.8575	23.5005	1.50	1.6645	1.6541	0.62	-59.939	237.32
0.350000E+05	308.00	308.00	154.00	24.6839	24.3756	1.25	1.7221	1.7157	0.37	-72.656	267.61
0.400000E+05	342.05	342.05	171.03	25.4019	25.1427	1.02	1.7722	1.7697	0.14	-84.639	297.19
0.500000E+05	408.24	408.24	204.12	26.6043	26.4374	0.63	1.8561	1.8608	-0.25	-106.501	354.70
0.550000E+05	440.54	440.54	220.27	27.1189	26.9938	0.46	1.8920	1.9000	-0.42	-116.488	382.77
0.600000E+05	472.39	472.39	236.19	27.5893	27.5029	0.31	1.9249	1.9358	-0.57	-125.933	410.45
0.650000E+05	503.85	503.85	251.93	28.0226	27.9719	0.18	1.9551	1.9688	-0.70	-134.900	437.78
0.700000E+05	534.96	534.96	267.48	28.4231	28.4053	0.06	1.9830	1.9993	-0.82	-143.435	464.81
0.750000E+05	565.80	565.80	282.90	28.7932	28.8056	-0.04	2.0088	2.0275	-0.93	-151.568	491.61
0.800000E+05	596.50	596.50	298.25	29.1320	29.1721	-0.14	2.0325	2.0533	-1.02	-159.291	518.28
0.850000E+05	627.37	627.37	313.69	29.4302	29.4955	-0.22	2.0533	2.0761	-1.11	-166.478	545.10